UNIVERSITAT DE VALÈNCIA
FACULTAT DE FÍSICA
DEPARTAMENTO DE FÍSICA TEÓRICA

NEUTRINO MASSES AND THEIR IMPLICATIONS FOR LOW ENERGY EXPERIMENTS AND THE LHC

Tesis doctoral para optar al título académico de Doctor por la Universidad de Valencia, en el marco de los estudios del Programa de Doctorado en Física

Autor: Julien Alcaide de Wandeleer
Director: Dr. Arcadi Santamaria i Luna
Director: Dr. Mikael Rodríguez Chala

Mayo 2020

Contents

Agradecimientos

Creo que nada de lo que es importante se construye en soledad, sino que los mayores avances se alcanzan con el apoyo de muchísimas personas. Y la ciencia sigue el mismo programa. Me parece por tanto imprescindible reconocer y valorar a quienes han contribuido y acompañado en este proyecto.

Me gustaría comenzar por agradecer a quienes más influencia tuvieron para que el desarrollo de esta tesis fuera posible: a mis directores, Arcadi y Miki. Ambos son magníficos físicos, y me han guiado y enseñado en incalculable cantidad. Aun más importante: también son grandísimas personas. Nunca dejaré de valorar la importancia de la calidez humana de mis directores durante todo este período.

También me gustaría reconocer el trabajo y la paciencia de mis otros colaboradores, de los que he aprendido enormemente. Ellos fueron Dipankar, Jordi, Nicolás, Alejandro, Arsenii y Shankha.

Por supuesto quiero mencionar a las personas más importantes de mi vida, quienes han estado y estarán siempre, enseñando, jugando, motivando, apoyando, preocupándose por cada decisión. A mi madre y a mi padre, Carine y Olcar; a mis hermanos, Lucas y Pablo. A mi tia abuela, Marta, que me ha dado siempre todo el cariño propio de una abuela. No puedo dejar de pensar tampoco en las personas que ya no están y que habrían estado orgullosas de presenciar este momento.

Quiero agradecer y felicitar a mis amigos y compañeros del doctorado, quienes también han vivido en carne propia todos los placeres y desgracias de esta etapa. En orden alfabético ellos son: Ana, Chris, Clara, Fer, Flopa, Jesús, Joan, Judith, Luismi, Marti, Sergi.

En todos estos años, muchísimas otras personas también han influido mi camino. Pienso por ejemplo en mis amigos de Valencia: Julia, Davide, Lucio y Quique, Candido, Javi, Javi J., Sebas, Mar, Lorena, Ferran y Morales.

Por último, quiero recordar a aquellas personas con las que me hubiera gustado poder compartir los últimos años de manera presencial. Ellos son mis amigos de la infancia: Pablo, Kevin, Damian, Luli, Dani. También mis tios, tias, primos y primas de Málaga y Buenos Aires. A pesar de la distancia, siempre han estado ahí.

A todas estas personas dedico esta tesis.

Resumen

Quien lee estas páginas podría preguntarse qué es un neutrino y cuál es el interés que presenta la confirmación de que el neutrino es masivo. El neutrino es una partícula fermiónica, eléctricamente neutra, que viaja casi a la velocidad de la luz y que es muy difícil de detectar debido a que interacciona muy débilmente con la materia. De hecho, aunque el neutrino fue propuesto en 1929 por Wolfgang Pauli, hubo que esperar 23 años para su primera observación experimental. Ahora sabemos que el neutrino inunda todo el universo; de hecho, es la segunda partícula más numerosa, solo después del fotón. Entonces, si todavía no había sido observado, ¿qué motivó a Pauli a proponer el neutrino?

A principios de siglo pasado, los científicos estaban dando sus primeros pasos para comprender el mundo microscópico. Uno de los procesos físicos en el que centraban sus esfuerzos era la desintegración beta. Este proceso consiste en la transición espontánea de un elemento inestable de la tabla periódica en otro con número atómico una unidad más grande, pero manteniendo el número de nucleones. Dentro del núcleo, esta desintegración implica que un neutrón se convierte en un protón, cuya carga es una unidad mayor. La carga eléctrica es una cantidad conservada y por tanto en el camino ha de emitirse una partícula de carga negativa que compense el aumento positivo de carga; esta partícula es el electrón, y era observada en cada desintegración beta. Sin embargo, había un gran problema relacionado con la energía de los electrones emitidos. Debido a que es una partícula mucho más ligera que el protón, el electrón se lleva casi toda la energía cinética liberada en la desintegración. Además debería estar fijada a un valor T_e determinado por la conservación de la energía. Pero al momento de realizar el experimento, se observaba que el electrón tenía una energía diferente en cada desintegración; en otras palabras, la distribución de la energía del electrón era continua. Es más, en todos los casos la energía medida era menor que T_e, por lo que aparentemente la energía total no se conservaba. La solución fue imaginar que el producto de la desintegración incluía una tercera partícula que escapaba de los detectores. Esta partícula se llevaría la energía perdida, por lo que la conservación de la energía quedaría protegida. Además debería ser eléctricamente neutra y tener espín 1/2 para no romper la invariancia

electromagnética y de momento angular. Con el tiempo, esta partícula llegaría a ser conocida como neutrino.

Además, la distribución continua de la energía de los electrones mostraba otro aspecto interesante: la energía liberada en las desintegraciones beta era de orden 1 MeV y algunos de los electrones emitidos se observaban con energías cinéticas muy próximas a este valor (aunque siempre menor). La conclusión es que la masa del neutrino debía ser muy pequeña, o incluso nula. Años más tarde se produjo un sorprendente descubrimiento que reforzaría la idea de que los neutrinos podrían ser partículas sin masa. Los neutrinos parecían interaccionar con la materia de una forma en la que la paridad no se conservaba; dicho de otra forma, solo se observaban neutrinos cuyo momento tenía una dirección opuesta a la de su espín (estados de helicidad levógira) y antineutrinos para los que su momento y su espín estaban alineados (helicidad dextrógira). Con únicamente estos dos objetos no es posible formar Lagrangianos que describan masas sin romper la invariancia bajo transformaciones de Lorentz. Por ejemplo, si el neutrino tiene masa, se podría imaginar un observador que viaje más rápido que un neutrino levógiro; en estas condiciones el observador vería que el neutrino se mueve en dirección opuesta a su espín y por tanto su helicidad es dextrógira. Sin embargo, no existían neutrinos dextrógiros. La conclusión es que la hipótesis original de neutrinos masivos no podía ser cierta. Por tanto, los neutrinos experimentalmente parecían tener masa nula y teóricamente este modelo encajaba. El modelo estándar de las partículas elementales, que le da un marco teórico a las interacciones electrodébiles, incluye esta idea y predice neutrinos sin masa.

Sin embargo, había voces dentro de la comunidad científica que sugerían la posibilidad de que los neutrinos tuvieran masas no nulas (aunque muy pequeñas) y que por tanto pudieran mezclar sus sabores, en semejanza con la idea de mezclas de quarks, bien establecida en el modelo estándar. Así, por ejemplo, algunos de los neutrinos provenientes de una fuente de neutrinos electrónicos (es decir, el neutrino que es producido en asociación con un electrón en una desintegración beta) podrían ser detectados con un sabor muónico o tauónico. Este tipo de fenómenos obtiene el nombre de oscilación de neutrinos. Varios experimentos se pusieron en marcha para examinar esta posibilidad hasta que finalmente, en 1998, fue observada por primera vez por la colaboración Super-Kamiokande. Este descubrimiento constituyó la primera confirmación de la existencia de masas de neutrinos, cambiando por completo el paradigma de la física de partículas elementales. A día de hoy, gran cantidad de datos sobre oscilaciones de neutrinos han sido recogidos, dando lugar a nuevas posibilidades alrededor de las masas de neutrinos.

En primer lugar, la cuestión sobre el mecanismo responsable de la generación de las masas de neutrinos debe ser abordada. Antes hemos dicho que la generación de

masas con un neutrino levógiro y un antineutrino dextrógiro no es posible porque rompe la invariancia bajo transformaciones de Lorentz. Pero si además de estas dos componentes existieran un neutrino dextrógiro y un antineutrino levógiro, sería posible inducir masas de neutrinos manteniendo la simetría Lorentz. Así, el observador viajando a más velocidad que el neutrino levógiro, no entraría en ninguna paradoja al interpretarlo como dextrógiro. Entonces una posibilidad es darle al neutrino dos nuevos grados de libertad, correspondientes al nuevo neutrino dextrógiro y su antipartícula. En este caso, los neutrinos tienen el mismo número de grados de libertad que el resto de los fermiones del modelo estándar, y sus masas reciben la denominación de *masas de Dirac*. Sin embargo, debido a que los neutrinos son fermiones eléctricamente neutros (a diferencia del resto de los fermiones del modelo estándar), existe una segunda posibilidad que consiste en que el neutrino y el antineutrino sean en realidad un mismo objeto. En otras palabras, el neutrino sería su propia antipartícula. Entonces, cuando el observador acelerado observa un objeto que se comporta de manera dextrógira podría afirmar que se trata nada más y nada menos que del antineutrino dextrógiro. En este caso, no sería necesario agregar nuevos neutrinos: los neutrinos descritos por solo dos grados de libertad se llaman *neutrinos de Majorana*. No obstante, los Lagrangianos de masas construidos con neutrinos de Majorana todavía rompen las simetrías locales del modelo estándar, por lo que es necesario introducir nuevos mecanismos que generen sus masas. En el Capítulo 2 revisamos algunos de los mecanismos más simples y famosos, tanto con nuevos campos escalares y fermiónicos como con teorías efectivas del modelo estándar.

Sin embargo, diseñar modelos de masas de neutrinos presenta una gran dificultad añadida, que consiste en la falta de un conocimiento completo de los parámetros que entran en la matriz de masas. Estos parámetros pueden ser escritos en términos de aquellos que describen las oscilaciones de neutrinos. Para neutrinos de Dirac hay seis parámetros de oscilaciones (tres ángulos de mezcla, dos cuadrados de diferencias de masas y una fase *de Dirac*) además de la escala absoluta de los neutrinos, dada por la masa del neutrino más ligero. En el caso de que los neutrinos sean de Majorana, hay un total de nueve variables: las siete de los neutrinos de Dirac sumadas a dos fases denominadas *de Majorana*. A día de hoy solo dos ángulos de mezcla y una diferencia de masas han sido medidos con precisión. El valor absoluto de la segunda diferencia de masas también es conocido, mientras que su signo relativo permanece oculto (aunque en los últimos años se está logrado un notable avance en sus medidas). Pese a que el restante ángulo de mezcla y la fase de Dirac todavía presentan grandes incertidumbres experimentales, se espera que en los años venideros estas puedan ser reducidas. Por otro lado, las fases de Majorana, a las que los experimentos de oscilaciones de neutrino-neutrino no tienen acceso, y la masa del neutrino más ligero se

mantienen sin (casi) restricciones experimentales. Es decir, no conocemos los valores numéricos de la matriz de masas de neutrinos. Si todas estas variables estuvieran bien medidas podríamos intentar predecir con mejor éxito qué tipo de ingredientes necesitamos añadir a nuestros modelos de masas de neutrinos. Lo contrario también es posible: uno siempre puede evaluar cuáles serían las predicciones de un modelo en concreto y compararlas con los resultados experimentales. No obstante este es un programa de trabajosa realización, dado el enorme número de modelos disponible. Otra posibilidad, siguiendo esta idea, es sondear diferentes estructuras o patrones comunes a una variedad de modelos. Por ejemplo, entre otras razones, podría ser que detrás de estos modelos exista una simetría. En este caso, los posibles patrones darían lugar a relaciones entre las variables de la matriz de masas, reduciendo el número de parámetros independientes a través de correlaciones que pueden ser investigadas en el laboratorio. De esta forma es posible imaginar diferentes patrones y, si alguno de ellos es compatible con los datos experimentales, podrían indicar el camino hacia la descripción de la masa de neutrinos.

En este sentido, patrones de ceros, llamados comúnmente *texturas de ceros*, pueden ser de mucha utilidad. Puesto que la matriz de masas es compleja, cada cero implica dos ligaduras que relacionan los diferentes parámetros. De hecho, en el caso en concreto de neutrinos de Majorana, descrita por nueve parámetros, fijar solo dos elementos de matriz a cero permitiría realizar predicciones de estos parámetros, incluyendo aquellos cuyos valores son hasta ahora desconocidos. En la literatura se ha trabajado bastante en esta dirección, tanto a través de métodos analíticos como numéricos.

En el capítulo 3 damos continuidad a esta línea de investigación. Primero introducimos una nueva técnica numérica que no necesita de trabajo analítico previo y que es aplicable a cualquier tipo de patrones. Luego, por medio de dicha técnica, revisamos el caso de texturas con dos ceros en la matriz de masas de neutrinos de Majorana. Utilizando técnicas numéricas (simulaciones Montecarlo y rutinas numéricas de minimización) exploramos las texturas compatibles con los datos experimentales, obtenidos a partir de los más recientes análisis globales de datos de experimentos de oscilaciones. Así, encontramos predicciones de los parámetros cuyos valores son aún desconocidos. Nuestro método además permite estudiar patrones aproximados. Por ejemplo, en el caso de las texturas, se podría imaginar que los elementos de matriz de masas a los que se les ha fijado valores igual a cero sufrieran pequeñas perturbaciones de tal forma que ahora presenten valores pequeños. Esto tiene interesantes implicaciones, relacionadas con la estabilidad de los resultados obtenidos y con la posibilidad de que patrones incompatibles con los resultados experimentales pasen a ser compatibles. Para estudiar este fenómeno, primero revisamos el caso de una textura cuyo espacio de parámetros permitido es pequeño; en este caso,

encontramos que las conclusiones principales no desaparecen a la vez que el espacio de parámetros permitido aumenta de tamaño. Por otro lado, en el caso de las texturas excluidas, estudiamos qué conclusiones se pueden obtener si exigimos que las texturas solo sean aproximadas. En este contexto, encontramos que la mayoría de ellas continúan siendo incompatibles con los datos experimentales. Sin embargo, una de ellas pasa a ser compatible bajo ciertas condiciones; finalmente presentamos sus predicciones.

En los últimos párrafos hemos hablado bastante de neutrinos de Majorana. Es de central interés remarcar que si los neutrinos son de tipo Majorana, es decir que neutrino y antineutrino son el mismo concepto, el número leptónico no puede ser una simetría del sistema. En el modelo estándar, a un leptón puede asignársele por convención número leptónico -1 de tal forma que si un antileptón tiene número leptónico $+1$, el número leptónico se conserva siempre. Pero esta no es más que una simetría global que se cumple por mero accidente. En cambio, no es posible asignar un número leptónico a neutrinos de Majorana de forma consistente. Abandonar la idea de conservación de número leptónico no supone ningún drama desde el punto de vista teórico. De hecho, observar violación de número leptónico en el sector de neutrinos podría implicar que los neutrinos son de Majorana, con importantes consecuencias de nueva física. Hasta la fecha no hay ninguna evidencia experimental que sugiera que este es el caso, pero existe la posibilidad de que simplemente los procesos con violación de número leptónico ocurran de manera muy poco probable en la naturaleza. Es entonces menester hacer grandes esfuerzos para investigar experimentalmente este tipo de procesos.

El más importante de estos procesos recibe el nombre de *doble desintegración beta sin neutrinos*. Este proceso es una variación de la doble desintegración beta, que tiene lugar cuando se producen dos desintegraciones beta de manera simultánea. En su forma más simple, llamada *mecanismo de largo alcance*, el neutrino emitido por una desintegración beta es reabsorbido como un antineutrino por la segunda desintegración beta. Obviamente este proceso solo puede ocurrir cuando los neutrinos son de Majorana. El producto final consiste en los nuevos núcleos atómicos y dos electrones, por lo que se viola el número leptónico.

Existen otros mecanismos (típicamente incluyen nuevas partículas pesadas y por ello se conocen como *mecanismos de corto alcance*) que pueden dar lugar a nuevas contribuciones de doble desintegración beta sin neutrinos. Sin embargo, todas ellas implican que el número leptónico no es una cantidad conservada y que los neutrinos son de Majorana. En algunos casos, estas nuevas contribuciones pueden ser más importantes que aquella con intercambio de neutrinos, descrita más arriba. Esto es importante, porque la contribución con intercambio de neutrinos es proporcional a la matriz de masas de neutrinos. Si esta última toma valores muy pequeños, existe

la posibilidad de que la tasa de desintegración de la doble desintegración beta sin neutrinos se mantenga experimentalmente inaccesible durante mucho tiempo.

En el Capítulo 4 desarrollamos un modelo de masas de neutrinos capaz de inducir estos dos mecanismos de doble desintegración beta sin neutrinos. Para ello, nos basamos en las predicciones de operadores efectivos de una teoría efectiva del modelo estándar (es decir sin incluir nuevas simetrías locales y considerando solo los campos del modelo estándar) de dimensión nueve que incluyen dos electrones dextrógiros y varios dobletes de Higgs. Estos operadores, correspondientes a una escala de nueva física del orden de 1 TeV, generan masas de neutrinos naturalmente pequeñas a través de diagramas a tres lazos (normalmente conocidos como *loops* en inglés), y nuevos mecanismos de doble desintegración beta sin neutrinos por medio de diagramas a nivel árbol (el correspondiente mecanismo con intercambio de neutrinos siempre puede generarse insertando la masa generada a tres lazos en el propagador del neutrino).

El desarrollo del modelo empieza con encontrar un conjunto de escalares capaz de inducir los operadores de dimensión nueve descritos arriba. En primer lugar consideramos un escalar doblemente cargado que acople con los dos electrones dextrógiros a través de un vértice renormalizable. Adicionalmente introducimos un triplete escalar con hipercarga +2 y un escalar real. Luego, el conjunto irreducible de estos tres escalares prohíbe la asignación consistente de número leptónico, como es necesario para generar masas de neutrinos de Majorana y la doble desintegración beta sin neutrinos. Adicionalmente, los elementos de la matriz de masas de neutrinos, $(M_\nu)_{ab}$, son proporcionales al producto de masas de leptones cargados $m_a m_b$, siendo $a, b = e, \mu, \tau$. Por este motivo, el mecanismo de largas distancias está suprimido en nuestro modelo, para masas de los correspondientes escalares de nueva física en la escala del TeV, es decir, accesibles en búsquedas del LHC. Además, esta proporcionalidad implica una jerarquía entre los elementos de la matriz de masas: en concreto los elementos ee y $e\mu$ son mucho más pequeños que el resto de entradas de la matriz. En la práctica pueden tomarse iguales a cero de tal forma que esta jerarquía genera una textura de dos ceros para la matriz de masas de neutrinos que es compatible con los datos experimentales de oscilaciones de neutrinos y que se estudia en el Capítulo 3.

De esta forma, en el Capitulo 4, desarrollamos todos estos conceptos. Asimismo, con el uso de técnicas analíticas y numéricas, calculamos las integrales provenientes de los diagramas de doble desintegración beta sin neutrinos y de la matriz de masas de neutrinos. Por último, calculamos las contribuciones del modelo a procesos con violación de sabor leptónico y a búsquedas de materia oscura. El modelo presentado en el Capítulo 4, al igual que cualquier otro marco teórico, tiene que ser capaz de explicar los datos experimentales. Al ser un modelo de masas de neutrinos, debe

ser compatible con los datos de oscilaciones de neutrinos. Si no fuera así, el modelo es descartado por no poder describir la naturaleza, aunque todavía pudiera tener interés teórico. En cualquier caso, es el experimento quien marca el camino. Otros experimentos también pueden ser imprescindibles para poner límites a los posibles valores que toman los parámetros del modelo, o incluso para excluirlo. Algunos de estos experimentos incluyen búsquedas de doble desintegración beta sin neutrinos, medidas de precisión del modelo estándar, búsquedas de materia oscura, búsquedas de procesos con violación de sabor leptónico o búsquedas directas de escalares en el LHC. Excepto la última, todas ellas son abordadas en el Capítulo 4. Nos centramos a continuación, por tanto, en las búsquedas de escalares en el LHC.

Un ingrediente frecuentemente utilizado a la hora de construir marcos teóricos motivados por diferentes propiedades físicas, como son las masas de neutrinos, son nuevos campos escalares no incluidos en el modelo estándar. De hecho, muchos de estos escalares son comunes a una amplia variedad de modelos de física de partículas por lo que, independientemente de su motivación particular, es imprescindible realizar búsquedas directas en colisionadores de alta energía, como es el LHC. Volviendo a la generación de masas de neutrinos de Majorana, especialmente importantes son los escalares que inducen procesos con violación de número leptónico. Estas partículas suelen tener acoplamientos renormalizables a pares de leptones, de tal forma que se les asigne un número leptónico. Luego es posible añadir nuevos campos y por tanto nuevos términos en el Lagrangiano que rompan explícitamente la simetría de número leptónico. En estos casos, la asignación de número leptónico al escalar cargado no es consistente y decimos que estos escalares rompen el número leptónico.

Estos escalares se espera que se encuentren en la escala del TeV (porque típicamente aparecen en modelos de masas inducidas a nivel lazo) y se producen en interacciones electrodébiles dando lugar posteriormente a desintegraciones en leptones. Por tanto, las colisiones de protones del LHC son un buen lugar donde buscarlos. En el Capítulo 5 discutimos y proponemos nuevas búsquedas de escalares simple y doblemente cargados en el LHC.

Búsquedas de escalares doblemente cargados (llamados simplemente k) con acoplamientos a pares de leptones cargados, han sido realizadas en la literatura. Suelen están basadas en modelos de masas de neutrinos denominados normalmente como *seesaw tipo-II*, en cuyo caso k solo se desintegra leptónicamente. Así, la masa invariante de k es fácilmente reconstruible por lo que constituye un buen observable. No obstante, en cuanto k tenga otro tipo de interacciones que puedan repercutir en nuevos canales de desintegración, especialmente con fuentes de energía perdida, la distribución de su masa invariante se aplana y es más difícil obtener resultados concluyentes. Para remediar dicha situación, proponemos nuevas estrategias de

búsqueda con diferentes regiones de señal y distintos observables. A continuación demostramos la utilidad de esta estrategia en la búsquedas de escalares cargados, por medio de la aplicación a modelos concretos de masas de neutrinos de Majorana como son el Zee-Babu y el modelo desarrollado en el Capítulo 4. En concreto, utilizando simulaciones numéricas, generamos tanto la señal que dichos modelos producirían en el LHC como el fondo dado por el modelo estándar. Finalmente, estudiamos cómo de compatible serían la señal de nueva física con el fondo del modelo estándar y obtenemos perspectivas de restricciones a los parámetros de los modelos estudiados para las energías y luminosidades de las fases actuales y futuras del LHC.

Además, también se han realizado varias búsquedas de nuevos escalares simplemente cargados (que denominaremos h por brevedad) en el LHC. Típicamente, están motivadas en contextos de supersimetría, o en modelos para los que el canal de desintegración dominante incluye un tau y un neutrino (como el modelo de dos dobletes de Higgs); sin embargo no existen búsquedas con leptones ligeros (electrones y muones) como productos de desintegración de h. A diferencia de los τ, estas partículas no hadronizan y pueden ser directamente observadas en los detectores del LHC. En la segunda parte del Capítulo 5 proponemos una búsqueda de h con leptones cargados ligeros y energía perdida en el LHC, que incluye la estrategia planteada en la primera parte del capítulo. Finalmente, evaluamos las posibilidades que tendrían estas búsquedas de restringir los valores permitidos de los parámetros que aparecen en el Lagrangiano de h.

Por otro lado, una manera diferente de atacar el problema de generación de masas de neutrinos, y de hecho cualquier problema de física de partículas, es por medio del uso de *teorías efectivas*. Este tipo de enfoque asume que procesos a una energía dada reciben efectos de física a una escala de energía mucho mayor. Sin embargo, no es necesario conocer los detalles de la física de altas energías (es decir, qué campos hay exactamente) sino que estos efectos pueden ser descritos por una serie de *operadores efectivos* con dimensiones de energía mayores a cuatro. Esta serie incluye todos los posibles operadores que están construidos utilizando todos los campos menos masivos que la escala de nueva física, y que son compatibles con las simetrías del sistema. Para que esto sea posible, es necesario que exista un salto de energía entre los procesos a bajas energías y los campos de nueva física. Finalmente, los detalles de la nueva física quedan ocultos en los coeficientes que preceden a cada operador efectivo y en la escala de nueva física.

La teoría efectiva más simple que es capaz de generar masas de neutrinos incluye únicamente a los campos del modelo estándar. Entonces, el operador efectivo de menor dimensión, de dimensión cinco, genera masas de neutrinos de Majorana. En este contexto, operadores de dimensión mayor también dan contribuciones a las masas de neutrinos de Majorana. El operador de dimensión cinco dará la contribu-

ción más importante, pero pueden encontrarse modelos cuyos campos sean tales que el operador de dimensión cinco no exista; en dicho caso, uno tiene que buscar el operador de menor dimensión que genere las masas de neutrinos.

Sin embargo, también existe la posibilidad de que existan partículas aún desconocidas por debajo de la escala de nueva física. Este sería el caso de, por ejemplo, un neutrino dextrógiro masivo, necesario para inducir masas de Dirac. En tal situación, cabe imaginar una teoría efectiva que incluya tanto los campos del modelo estándar así como el nuevo neutrino. A esta teoría efectiva se la conoce como νSMEFT, por sus siglas en inglés. Igual que antes, los operadores de esta teoría darían nuevas contribuciones a procesos a bajas energías. Aunque en general estas contribuciones estarán suprimidas por la escala de nueva física, en muchos casos pueden compararse con los experimentos. Esto es muy importante porque serviría para buscar señales de nueva física. Con este objetivo, en el Capítulo 6 ponemos límites a los posibles valores que pueden tomar los coeficientes de los operadores efectivos y la escala de nueva física. Los operadores débilmente restringidos (o incluso sin restringir en absoluto) podrían indicar nuevas direcciones en donde hallar nueva física. En particular, nos centramos en los operadores de dimensión seis con cuatro fermiones. Este tipo de operadores son muy interesantes porque pueden inducir observables que pueden ser comparados con los resultados experimentales obtenidos en el LHC a partir de búsquedas de un leptón y energía perdida, búsquedas con solo un jet, además de en desintegraciones de piones y taus. Para alcanzar dicha finalidad, utilizamos tanto cálculos analíticos como simulaciones numéricas. Además, algunos de estos operadores también darían nuevas contribuciones a desintegraciones de quarks top. Sin embargo, estas contribuciones implicarían nuevas señales que no pueden ser analizadas con la metodología hasta ahora utilizada por las colaboraciones del LHC. Así, proponemos una nueva estrategia, más adecuada para estudiar dichas señales. Finalmente, utilizando todos los procesos hasta ahora descritos, efectuamos un análisis global con el objetivo de obtener los límites más restrictivos de los parámetros considerados de la νSMEFT.

En todos estos temas se centra la tesis que sucede a las presentes páginas. En ella se discuten variadas implicaciones de las masas de neutrinos, con procesos con violación de número leptónico jugando un rol predominante, y de la figura del neutrino en general.

List of publications

This Ph.D. thesis is based on the following publications:

1. Fitting flavour symmetries: the case of two-zero neutrino mass textures

Julien Alcaide, Jordi Salvado and Arcadi Santamaria.
Published in: JHEP 07 (2018) 164, e-Print: 1806.06785

2. A model of neutrino mass and dark matter with large neutrinoless double beta decay

Julien Alcaide, Dipankar Das and Arcadi Santamaria.
Published in: JHEP 04 (2017) 049, e-Print: 1701.01402

3. LHC signals of radiatively-induced neutrino masses and implications for the Zee–Babu model

Julien Alcaide, Mikael Chala and Arcadi Santamaria.
Published in: Phys.Lett.B 779 (2018) 107-116, e-Print: 1710.05885

4. LHC sensitivity to singly-charged scalars decaying into electrons and muons

Julien Alcaide and Nicolas Mileo.
Sent for publication in PRD, e-Print: 1906.08685

5. Probes of the Standard Model effective field theory extended with a right-handed neutrino

Julien Alcaide, Shankha Banerjee, Mikael Chala and Arsenii Titov.
Published in: JHEP 08 (2019) 031, e-Print: 1905.11375

Abstract

Neutrino oscillations constitute the first experimental evidence of new physics. Contrary to the prediction of the Standard Model, neutrinos are now well-established as particles with mass. In this thesis we study four topics related to neutrino masses. We examine a class of patterns of Majorana neutrino mass matrices, called two-zero textures, that could lead to the building of the underlying flavour theory. Using a purely numerical technique, we compare the constraints given by the textures with the most updated data of oscillation parameters. We find that the most promising textures are those of class A with normal ordering. Further, we revisit the case of excluded textures and study the stability of the results when the textures are only approximate. Then, we present a new model of neutrino masses that is able to generate an A class texture. Due to the form of the mass matrix, the standard neutrino exchange mechanism is suppressed; however, a neutrinoless double beta decay rate large enough to be tested in the near future is induced through a short range mechanism. Moreover, this model belongs to a broad variety of frameworks that are based on the interaction of a lepton number violating charged scalar with light leptons. The signatures of such scalars, often accompanied by missing energy, are not currently being probed at high-energy accelerators. We propose a search strategy and examine the prospects for their signatures at the Large Hadron Collider. Finally, we consider the possibility that neutrinos are Dirac particles. In this context, right-handed neutrinos need to be properly included in the effective field theory of the Standard Model. Some of the resulting effective operators would show interesting phenomenological impact that can be addressed with current experimental data. Furthermore, our results would indicate how further investigations should be designed in the future in order to test the unbounded operators to shed light on possible new physics. Accordingly, we propose a new search in the context of rare top decays.

CHAPTER 1

Introduction

At the beginning of the 19th century, the Maxwell theory of electrodynamics was well-established and physicists were taking the first steps towards a quantum description of the atom and the subatomic particles. The discovery of radioactivity was originally made by Becquerel in 1896. At first, only two types of radioactive processes were known. The first one consists of an excited atom that decays into a state of lower energy by the emission of a gamma particle, which then came to be established as an energetic photon. The second type occurs when a given atomic element transits into a more stable element, through the emission of some particle. Rutherford realised that there were two of these processes, and he classified them based on the penetration of the emitting particle into target objects: they were called alpha and beta decays. In alpha decays, the unstable atom emits a particle (by the time called alpha particle and then identified as the He^{2+} ion) consisting of two neutrons and two protons, and hence electrically charged. This process releases a large amount of energy carried by the alpha particle, making it short-lived and very ionising. On the other hand, in beta decays there is a nuclear transition from an element of atomic number Z to one with atomic number $Z + 1$. In the process, a so-called beta particle is emitted by the unstable nucleus. Now we know that the beta particle is no other than an electron or a positron, and thus is more penetrating and less ionising than the alpha particle.

The beta decay has had a central role in the development of the theory of particle physics. When experimentalists began measuring the energy of the particles resulting from a beta decay they found something they did not expect: a continuous spectrum. Owing to energy conservation, the energy of the daughter particles adds up to the energy of the original atom. Provided there are only two particles, the energy of the electron would then be well-defined, and measurements of its distribution should show a peak. In order to explain this discrepancy, in 1930 Pauli proposes the existence of a mysterious electrically neutral particle of spin 1/2 that would carry

this extra energy. A couple of years later this particle was named neutrino.

Particle physicists had to wait until 1956 for the first experimental confirmation of the existence of the eluding neutrino. But it was not until 1957 that another shocking discovery took place [1]. Interactions involving neutrinos do not conserve parity! In other words, only the left-handed component of the neutrino was observed. Moreover, a right-handed neutrino remains unobserved nowadays.

With these considerations, the four-fermion Fermi theory describing beta decays was constructed. Earliest versions involved electrons (e), neutrinos (ν), protons (p) and neutrons (n). The modern expression of the four-fermion interaction involves quark fields (where u and d are the up-type and down-type quarks, respectively), which are fundamental particles, in contrast to neutrons and protons, which are hadronic states. Additionally, in order to describe left-handed fields, it includes both vector (V) and axial (A) currents.

$$-\mathcal{L}_{V-A} = \frac{G_F}{\sqrt{2}}[\overline{e}\gamma^{\mu}(1-\gamma_5)\nu_e][\overline{u}\gamma_{\mu}(1-\gamma_5)d]. \tag{1.1}$$

G_F is the Fermi coupling constant, whose expression will be described in the upcoming sections. In 1955, Gershtein and Zeldovich proposed that the Fermi interaction should also work for explaining the muon decay into electrons and neutrinos [2], and this is indeed what experiments have found. Subsequent experiments reported the same behaviour for the tau decay [3]. The universality of the Fermi constant led physicists to believe there is an underlying symmetry involving the interactions of these particles. Over time, the mechanism responsible for beta decays and other processes at subatomic distances became to be known as the theory of the weak interactions.

The observation of the half-life of the muon decay gives the most precise measurement of the Fermi coupling constant [4]

$$G_F = 1.1663787(6) \times 10^{-5}\ \text{GeV}^{-2} \simeq \frac{1}{(293\ \text{GeV})^2}, \tag{1.2}$$

which reveals that the Fermi interaction works for physics up to a scale of ~ 300 GeV. Nevertheless, despite describing low-energy physics with great accuracy, this model breaks down at high-energy scales. Within the Fermi theory, the cross section of weak processes like $e^-\bar{\nu}_e \longrightarrow \mu^-\bar{\nu}_\mu$ grows with the energy, $\sigma \sim (p_e + p_\nu)^2 G_F^2$, where p_e and p_ν are the four-momenta of the electron and the neutrino, respectively. The reason for this behaviour is purely dimensional, since G_F has dimensions of E^{-2}. However the cross section describes the probability of a process to happen and it cannot grow arbitrarily. In other words, the cross section needs to satisfy unitarity bounds or otherwise the theory falls apart. This became a problem. Thus, in the

sixties, physicists began a journey to try to find a solution for this puzzle, until they came up with the gauge theories.

The idea is as follows. When considering the kinetic Lagrangian of some fermionic field, it can be easily seen that this Lagrangian is invariant under some redefinition of the field under the action of some symmetry. This redefinition is induced by some arbitrary phase with no physical meaning. In principle, it can be anything but, in order for the Lagrangian to remain invariant, it must depend on the space-time coordinates so that its values in different points are related. We often say that this transformation is local or *gauge*. To do so, we must add some new gauge boson field that carries the information of the phase from some point in space-time to others. Mathematically, one adds a new term to the derivative of the field and the shape of this addition is completely determined by the gauge transformation. The new derivative, called covariant derivative, is invariant under the gauge transformation and induces the interactions of the gauge bosons with the fermions.

Physicists promptly realised that $U(1)$ was a symmetry of the Dirac Lagrangian that describes electrons. They understood that, within this model, the equations of motion are no others than the Maxwell equations of the electromagnetic interactions. This allowed them to identify the gauge field as the photon. Furthermore, Noether Theorem tells us that whenever there is a symmetry of the equations of motion, a quantity is conserved. This is the electric charge. Of course one needs to include a kinetic term for the photon field in order for it to be able to propagate, but, remarkably, a mass term would break gauge invariance. Therefore, a massless photon is a consequence of the symmetry of the theory.

Despite the success of the quantum description of the electromagnetism (QED), a larger symmetry was still needed to explain weak interactions and the beta decay. In 1961, Glashow proposed an $SU(2) \times U(1)$ local symmetry, which would unify the weak interactions with the electromagnetism [5]. Along with the photon of the electromagnetism, the model introduces two charged vector bosons $W^{\pm}$ and a neutral one, Z. These new additions are the mediators of the weak interactions among left-handed fields. On the downside, this model predicted the fermions to be exactly massless, as a mass term would break the gauge invariance.

It was not until 1965 that this problem was resolved, when Higgs, Brout, Englert, Guralnik, Hagen and Kibble [6–10] introduced a mechanism that spontaneously breaks the symmetry allowing for the generation of masses. This mechanism has come to be known as the Higgs mechanism. We will further talk about it at the end of this chapter. Weinberg in 1967, and Salam in 1968 applied the Higgs mechanism to Glashow's model [11]. The extension that includes quarks came a couple of years later [12]. This concludes the modern version of the Glashow-Weinberg-Salam

theory of the electroweak interactions.

Yet, gauge theories with spontaneous symmetry breaking have ultraviolet divergences. This was an important burden for the electroweak theory and the scientific community was reluctant to accept the Glashow-Weinberg-Salam model until, in 1971, t'Hooft solved the problem of renormalisation [13]. It became clear that operators with dimension four or less were renormalizable, while those with larger dimensions had problems at high-energies scales. This clarified the problems with the Fermi theory and allowed for radiative calculations.

Regarding the theory of hadrons, the first consistent description was the quark model, proposed independently by Gell-Mann and Zweig in 1964 [14–16]. This classification implies that quarks, that come in three flavours, carry a new quantum number called colour. Accordingly, baryons and mesons are combinations of quarks that make color singlets states. In 1973, Fritzsch, Leutwyler and Gell-Mann developed the $SU(3)_c$ theory of the strong interactions based on new non-abelian gauge fields (known as gluons) and governed by an universal strong coupling constant [17]. Finally, that same year, Gross, Wilczek and Politzer discovered the asymptotic freedom, meaning that strong interactions decreases at short distances (and hence allowing for perturbation calculations) and increases at long distances (confinement of quarks within hadrons) [18, 19]. This completed the theoretical basis for the Standard Model (SM) of the electroweak and strong interactions.

At that point, the theoretical predictions of the Standard Model started to guide the experimental work. The discovery of the muon neutrino [20] was made in 1962, leaving no doubts about the existence of more than one type of neutrinos. Moreover, the discovery of the tau lepton in 1975 [21] as well as measurements of the Z boson decay suggested the existence of a third neutrino [22]. Finally, in 2000, the discovery of the tau neutrino was announced by Fermilab [23], which allowed to dispose of three families (also called generations) with the charged leptons and quarks:

$$\begin{aligned} &(u, d, e, \nu_e) \\ &(c, s, \mu, \nu_\mu) \\ &(t, b, \tau, \nu_\tau). \end{aligned} \tag{1.3}$$

Each generation is a copy of the original family, with the same quantum numbers, but with heavier masses. Finally, in 2012, with the discovery of the Higgs boson, predicted more than 40 years in advance, the Standard Model was completed.

1.1 The theory of electroweak interactions

Let us start building the theory of electroweak interactions. A theory of fermions that is invariant under an $U(1)$ gauge symmetry is perfectly able to describe the electromagnetism, but is not enough for also explaining the weak interactions. On the other hand, an $SU(2)$ theory would give no massless gauge boson, and we need one (the photon). So we use the product of these two symmetries, $SU(2)_L \times U(1)_Y$. Under the action of the group, a field φ transforms as:

$$\varphi(x) \longrightarrow U_L(x) U_Y(x) \varphi(x), \tag{1.4}$$

where

$$U_L(x) = \exp\left(i\theta^i(x) T_i\right) \tag{1.5}$$

$$U_Y(x) = \exp\left(i\theta^0(x) Y\right) \tag{1.6}$$

are the matrix representations of the $SU(2)_L$ and $U(1)_Y$ groups, respectively. The index i runs on $i = 1, 2, 3$, and we expect a sum among them when repeated. The parameters θ^0 and θ^i are unphysical phases, while T_i and Y are the generators of the gauge groups[1].

The kinematic part of a renormalizable Lagrangian describing a fermion field, ψ, follows the Dirac equation and reads:

$$\mathcal{L} = i\bar{\psi}\gamma^\mu \partial_\mu \psi. \tag{1.8}$$

However, this Lagrangian is not invariant under gauge transformations. Indeed, from Eq. (1.4), one can see that the derivative of the field gives two additional contributions:

$$\partial_\mu \psi(x) \longrightarrow \exp\left(iY\theta^0\right) \exp\left(i\theta^i T_i\right) \left(\partial_\mu + iY\partial_\mu\theta^0 + iT_i\partial_\mu\theta^i\right) \psi(x). \tag{1.9}$$

So we need to introduce some new terms that cancel these extra pieces. Because we have a Lorentz index coming from the partial derivative, the new terms involve new vector fields, B_μ and W^i_μ, transforming as

$$B_\mu \longrightarrow B_\mu - \frac{1}{g'}\partial_\mu\theta^0 \tag{1.10}$$

[1]The generators of $SU(2)$ in the $1/2$ representation can be defined as $T_i = \sigma_i/2$, in terms of the three Pauli matrices

$$\sigma_1 = \begin{pmatrix} 0 & 1 \\ 1 & 0 \end{pmatrix}, \quad \sigma_2 = \begin{pmatrix} 0 & -i \\ i & 0 \end{pmatrix}, \quad \sigma_3 = \begin{pmatrix} 1 & 0 \\ 0 & -1 \end{pmatrix}. \tag{1.7}$$

and

$$W_\mu \longrightarrow U_L W_\mu U_L^\dagger - \frac{1}{ig}(\partial_\mu U_L)U_L^\dagger, \tag{1.11}$$

where we have defined

$$W_\mu = \frac{\sigma^i}{2} W_\mu^i. \tag{1.12}$$

The parameters g and g' are called the weak coupling constants and, since they control the strength of the interactions, are a property of the gauge fields. Now we can construct a covariant derivative

$$D_\mu = \partial_\mu + igW_\mu^i T_i + ig'YB_\mu, \tag{1.13}$$

which transforms under $SU(2)_L \times U(1)_Y$ in the same way as ψ in Eq. (1.4). Therefore, after replacing the partial derivative in Eq. (1.8) with the covariant derivative in Eq. (1.13), the renormalizable Lagrangian becomes invariant under $SU(2)_L \times U(1)_Y$ transformations.

Having the covariant derivative in our toolbox, we still need to define the gauge charges of the fermionic fields. As said above, charged gauge bosons only couple to left-handed fermions. By making use of the chirality projectors[2] we can decompose the fermion field in its left-handed and right-handed chiral components

$$\psi = \psi_L + \psi_R. \tag{1.18}$$

We will simply call them the LH and RH components of the fermionic field. Each of them will correspond to different representations of the gauge group, with definite quantum numbers. We can then group fields with similar properties together into multiplets of $SU(2)_L$. In particular, we demand the left-handed fields to be members of doublets (which requires $T_3 = 1/2$) and the right-handed fields to be singlets ($T_3 = 0$). Likewise, we let the hypercharge Y take the value that reproduces the

[2]The chirality projectors are defined as

$$P_{L,R} = \frac{1 \mp \gamma_5}{2} \tag{1.14}$$

and follows the usual properties of projectors:

$$P_L\psi = \psi_L, \quad P_R\psi = \psi_R, \tag{1.15}$$

$$\mathbb{1} = P_L + P_R, \tag{1.16}$$

$$P_{L,R}^2 = P_{L,R}, \quad P_L P_R = 0, \quad P_R P_L = 0. \tag{1.17}$$

correct electric charge of each field after the relationship[3]

$$Q = T_3 + Y. \tag{1.19}$$

There are five fermionic multiplets in the Standard Model. The lepton fields transform under the $SU(2)_L \times U(1)_Y$ gauge group as follows:

$$\ell_L = \begin{pmatrix} \nu \\ e \end{pmatrix}_L \sim (1/2, -1/2), \qquad e_R \sim (0, -1), \tag{1.20}$$

while the quark fields as

$$q_L = \begin{pmatrix} u \\ d \end{pmatrix}_L \sim (1/2, 1/6), \qquad u_R \sim (0, 2/3), \qquad d_R \sim (0, -1/3). \tag{1.21}$$

When coupling to gauge fields, each fermion multiplet has a specific covariant derivative, controlled by the corresponding quantum numbers.

At this point we have everything we need to begin working out the interactions of the leptons with the weak gauge bosons. To start with, we separate the Lagrangian into its purely left- and right-handed parts, which for the case of the leptons gives

$$\mathcal{L} = \mathcal{L}_{LL} + \mathcal{L}_{RR} = i(\bar{\ell}_L \gamma^\mu D_\mu \ell_L) + i(\overline{e_R} \gamma^\mu D_\mu e_R). \tag{1.22}$$

We then plug the expression of the covariant derivative in Eq. (1.22) and expand. The Lagrangian with the left-handed leptons gives

$$\begin{aligned} -\mathcal{L}_{LL} = {} & \frac{1}{2}\bar{\nu}_L \gamma^\mu (g W_{3\mu} - g' B_\mu) \nu_L - \frac{1}{2}(g W_{3\mu} + g' B_\mu) \bar{e}_L \gamma^\mu e_L \\ & + g \frac{1}{\sqrt{2}} (\bar{\nu}_L \gamma^\mu e_L) \frac{W_{1\mu} - i W_{2\mu}}{\sqrt{2}} + g \frac{1}{\sqrt{2}} (\bar{e}_L \gamma^\mu \nu_L) \frac{W_{1\mu} + i W_{2\mu}}{\sqrt{2}}. \end{aligned} \tag{1.23}$$

Neutrinos carry no electric charge and thus cannot couple to photons. Hence, in the first term, neither $W_{3\mu}$ nor B_μ can be identified as the photon field, A_μ. The only way out is to define a new neutral field, Z_μ, to which neutrinos can indeed couple:

$$Z_\mu = \frac{1}{\sqrt{g^2 + g'^2}} (g W_{3\mu} - g' B_\mu). \tag{1.24}$$

The fields $W_{3\mu}$ and B_μ in the neutral sector are connected with the fields Z_μ and

[3] This equation follows from an straightforward rearrangement of the covariant derivative in the Dirac Lagrangian and then identifying the electric charge Q as the quantum number associated to the interactions of the fermions with the photon.

A_μ through a rotation:

$$W_{3\mu} = \cos\theta_W Z_\mu + \sin\theta_W A_\mu, \tag{1.25}$$

$$B_\mu = -\sin\theta_W Z_\mu + \cos\theta_W A_\mu, \tag{1.26}$$

where θ_W is the weak mixing angle that changes the basis. We will see that Z_μ and A_μ are actually the mass eigenstates. Combining Eq. (1.25) and Eq. (1.26) with Eq. (1.24) and identifing the coefficients, we find:

$$g\sin\theta_W = g'\cos\theta_W, \tag{1.27}$$

so that the interaction of the neutrinos with the Z gauge boson is:

$$-\mathcal{L}_{\nu\nu Z} = \frac{1}{2}\frac{g}{\cos\theta_W}(\bar{\nu}_L\gamma^\mu\nu_L)Z_\mu. \tag{1.28}$$

Now, we can investigate the interactions of the electron-positron pair in the purely left-handed Lagrangian, Eq. (1.23). Plugging in Eq. (1.25) and Eq. (1.26) we find after some rearranging:

$$\frac{1}{2}(gW_{3\mu} + g'B_\mu) = A_\mu\frac{g\sin\theta_W + g'\cos\theta_W}{2} + Z_\mu\frac{g\cos\theta_W - g'\sin\theta_W}{2}. \tag{1.29}$$

The electromagnetic interaction of the electon-positron pair with the photon happens via the electric charge, e. So we can redefine the coupling constants:

$$e = g\sin\theta_W = g'\cos\theta_W \tag{1.30}$$

and hence the interactions of the left-handed electrons with the gauge bosons become

$$-\mathcal{L}_{e_Le_L} = (\bar{e}_L\gamma^\mu e_L)\left[Z_\mu\frac{g}{\cos\theta_W}\left(-\frac{1}{2} + \sin^2\theta_W\right) - eA_\mu\right]. \tag{1.31}$$

On the other hand, the interactions of the right-handed electrons with the gauge bosons are

$$\mathcal{L}_{RR} = i(\bar{e}_R\gamma^\mu D_\mu e_R) = i\bar{e}_R(\partial_\mu - ig'B_\mu)e_R. \tag{1.32}$$

After changing basis and using the redefinition of the coupling constants, Eq. (1.30), the interaction terms are

$$-\mathcal{L}_{RR} = \bar{e}_R\gamma^\mu e_R\left(\frac{g\sin^2\theta_W}{\cos\theta_W}Z_\mu - eA_\mu\right), \tag{1.33}$$

which of course sets the same electric charge for both chiralities of electrons, as ex-

pected since electromagnetic interactions are not chiral. This completes the neutral currents for the leptons.

Finally, let us build up the charged current interactions. From Eq. (1.23) we see that the last two terms are just the conjugate version of each other. Moreover, they involve electrons (or positrons) which are electrically charged particles. For these reasons, we can redefine the fields W_1 and W_2 into charged gauge bosons, in the following way

$$W_\mu^\pm = \frac{W_{1\mu} \mp i W_{2\mu}}{\sqrt{2}}, \tag{1.34}$$

so that the terms in the Lagrangian do not break the electric charge. With this, the interactions of the leptons with the charged gauge bosons read

$$-\mathcal{L}_{e\nu W} = \frac{g}{\sqrt{2}}(\bar{\nu}_L \gamma^\mu e_L) W_\mu^+ + \frac{g}{\sqrt{2}}(\bar{e}_L \gamma^\mu \nu_L) W_\mu^-. \tag{1.35}$$

We can repeat the complete procedure for the quarks, obtaining

$$-\mathcal{L}_{quarks} = \frac{g}{\sqrt{2}}(W_\mu^+ j_+^\mu + W_\mu^- j_-^\mu) + \frac{g}{\cos\theta_W} Z_\mu j_Z^\mu + e A_\mu j_A^\mu, \tag{1.36}$$

with the charged currents being

$$j_+^\mu = \bar{u}_L \gamma^\mu d_L, \qquad j_-^\mu = \bar{d}_L \gamma^\mu u_L, \tag{1.37}$$

and the neutral currents

$$\begin{aligned} j_Z^\mu = [&\bar{u}_L \gamma^\mu \left(\frac{1}{2} - \frac{2}{3}\sin^2\theta_W\right) u_L + \bar{u}_R \gamma^\mu \left(-\frac{2}{3}\sin^2\theta_W\right) u_R \\ &+ \bar{d}_L \gamma^\mu \left(-\frac{1}{2} + \frac{1}{3}\sin^2\theta_W\right) d_L + \bar{d}_R \gamma^\mu \left(\frac{1}{3}\sin^2\theta_W\right) d_R], \end{aligned} \tag{1.38}$$

$$j_A^\mu = \frac{2}{3}\bar{u}\gamma^\mu u - \frac{1}{3}\bar{d}\gamma^\mu d. \tag{1.39}$$

1.2 The mass of the gauge bosons

Certainly, we would like the gauge boson fields to propagate and for that we need to add the corresponding kinetic terms. These are completely fixed by the gauge invariance. The only quadratic structure available reads

$$\mathcal{L}_{kin} = -\frac{1}{4} B_{\mu\nu} B^{\mu\nu} - \frac{1}{4} W_{\mu\nu}^i W_i^{\mu\nu}, \tag{1.40}$$

where

$$B_{\mu\nu} = \partial_\mu B_\nu - \partial_\nu B_\mu \tag{1.41}$$

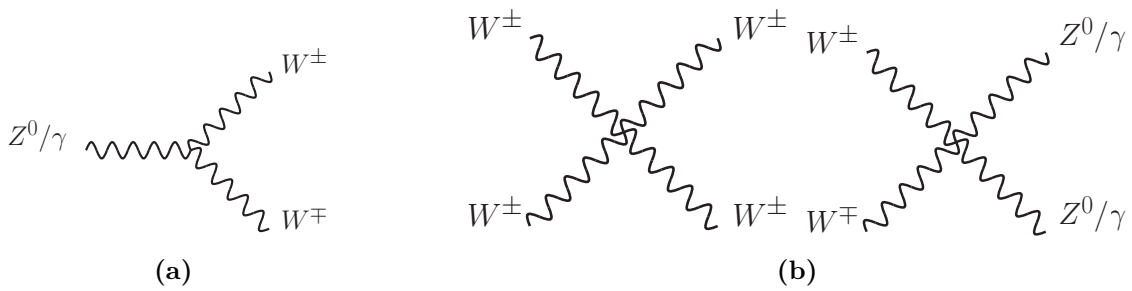

(a) **(b)**

Figure 1.1: (a) Triple and (b) quartic gauge boson self interactions

is the tensor invariant under $U(1)_Y$ and

$$W^i_{\mu\nu} = \partial_\mu W^i_\nu - \partial_\nu W^i_\mu - g\epsilon_{ijk} W^j_\mu W^k_\nu \tag{1.42}$$

is the object covariant under $SU(2)_L$ transformations. After expanding this kinetic Lagrangian, the gauge boson self-interactions are found (see Figure 1.1). These can be triple interactions, which always include a W pair and a photon or a Z boson. No triplet interaction involves only photons and Z bosons, as photons only couple to charged particles. Finally, there can also be quartic interactions, involving all types of gauge bosons.

However, a gauge boson mass term would break the gauge invariance. Hence the gauge bosons seem to be massless. This is a problem, as we know that the weak interactions are short range interactions.

In order to generate a mass for the gauge bosons we need to somehow break the symmetry that forbids the mass terms. Let us begin with a set of scalar fields ϕ_i that transforms under a continuous gauge group G as

$$\begin{aligned} \phi_i \longrightarrow U_{ij}\phi_j &= \exp[i\theta^a (T_a)_{ij}]\phi_j \\ &\simeq [1 + i\theta^a T_a]_{ij}\phi_j \\ &\simeq \phi_i + i\theta^a (T_a)_{ij}\phi_j, \end{aligned} \tag{1.43}$$

where there is generator T_a for each symmetry of the model. In the second line we have expanded the transformation for the infinitesimal parameter θ^a and kept only the leading terms. In other words, the field ϕ_i gets transformed by a small shift.

Now consider a potential, $V(\phi)$, with a minimum v given by the condition

$$\left.\frac{\partial V}{\partial \phi^i}\right|_{\phi=v} = 0. \tag{1.44}$$

Whenever there are more than one minimum, the arbitrary choice of one of them as the ground state makes the symmetry to be spontaneously broken. The selected ground state v is then called vacuum expectation value (VEV) and may not be

invariant under the gauge transformation G.

We expect the potential to be invariant under gauge transformations, and then, for small perturbations, it reads

$$\begin{aligned} V(\phi_i) = V(U_{ij}\phi_j) &= V(\phi_i + i\theta^a (T_a)_{ij}\phi_j) \\ &\simeq V(\phi_i) + i\theta^a (T_a)_{ij}\phi_j \frac{\partial}{\phi_i} V(\phi) \quad \Longrightarrow \quad (T_a)_{ij}\phi_j \frac{\partial}{\partial \phi_i} V(\phi) = 0. \end{aligned} \tag{1.45}$$

Expanding around the minimum $\phi = v$:

$$(T_a)_{ij} \frac{\partial \phi_j}{\partial \phi_k} \cancelto{0}{\frac{\partial V}{\partial \phi_i}\bigg|_{\phi=v}} + [(T_a)_{ij} v_j] \frac{\partial^2}{\partial \phi_i \partial \phi_k} V(\phi) = 0 \tag{1.46}$$

The first term vanishes because of the minimisation condition. Note that an expression of the form

$$m_{ij}^2 = \frac{\partial^2 V}{\partial \phi_i \partial \phi_j} \tag{1.47}$$

would generate a mass term and thus the second term is the product of the action of the group on the vacuum and a squared mass. When $T^a v = 0$, the selected ground state is still invariant under the gauge transformation and the mass m_{ij} is not necessarily zero. Otherwise, whenever $T^a v \neq 0$, the symmetry is spontaneously broken by the vacuum and a set of massless scalar modes, called Goldstone bosons, appears. The number of Goldstone bosons is the same as the number of generators broken by the vacuum. The unbroken generators are left as the generators of a remaining symmetry of the theory.

Now we promote the derivative in the kinetic term of the scalar Lagrangian to be covariant, and upon expansion, it reads

$$\mathcal{L}_{kin} = \frac{1}{2}(\partial_\mu \phi_i)^2 + g A_\mu^a (\partial_\mu \phi_i T_{ij}^a \phi_j) + \frac{1}{2} g^2 A_\mu^a A^{b\mu} (T^a \phi_i)(T^b \phi_i), \tag{1.48}$$

where A_μ^a are the (vector) gauge bosons corresponding to the gauge transformation G. After spontaneous symmetry breaking, the field ϕ_i acquires a VEV, v_i, and the last term of the previous Lagrangian becomes a mass term for the gauge bosons,

$$\mathcal{L}_{mass} = \frac{1}{2} g^2 A_\mu^a A^{b\mu} (T^a v_i)(T^b v_i). \tag{1.49}$$

Thus, if the VEV does not respect the symmetry, or in other words, whenever a generator does not annihilates the vacuum, $T^a v \neq 0$, the corresponding gauge boson acquires a mass. In other words, only the gauge bosons associated with a generator spontaneously broken by the vacuum are massive.

As a result of the invariant nature of the scalar field under the group transformations, there is always a way to reabsorb the massless modes into a redefinition of the field. Then, the degrees of freedom apparently lost get eaten by the gauge bosons, giving them the longitudinal polarisation needed to be massive.

Nevertheless, the unphysical Goldstone modes still affect the physical observables. At high energy, as a consequence of the gauge invariance of the theory, the amplitude for a scattering of a gauge boson is equivalent to the amplitude of emission of absorption of the Goldstone boson eaten by the gauge boson. This is the *Goldstone equivalence theorem*.

So let us apply this formalism to the case of the Standard Model. So far we only had a fermion sector that got accompanied by a set of gauge bosons when the derivative was promoted to be covariant. We now add a scalar sector with only a complex doublet,

$$\phi = \begin{pmatrix} \phi^+ \\ \phi^0 \end{pmatrix}, \tag{1.50}$$

having four degrees of freedom. Under $SU(2)_L \times U(1)_Y$ transformations the scalar doublet has the following quantum numbers:

$$\phi \sim \left(\frac{1}{2}, \frac{1}{2}\right). \tag{1.51}$$

The gauge invariant Lagrangian describing the scalar sector, up to dimension four, is given by

$$\mathcal{L} = \partial_\mu \phi^\dagger \partial^\mu \phi - V(\phi), \qquad V(\phi) = m_\phi^2 |\phi|^2 + \lambda_\phi |\phi|^4. \tag{1.52}$$

In order to avoid a potential not bounded from below, we let the parameter λ_ϕ take only positive values. On the other hand, the parameter with dimensions of mass, m_ϕ, may be of either sign. If $m_\phi^2 > 0$ the potential has a single ground state at $\phi = 0$ and the system describes a scalar field of mass m_ϕ. Conversely, when $m_\phi^2 < 0$, the potential has an infinite number of possible degenerate ground states, which are apart from the origin by a distance

$$|\langle\phi\rangle| = \frac{v}{\sqrt{2}} = \sqrt{\frac{-m_\phi^2}{2\lambda}}. \tag{1.53}$$

In this case, there are three fields describing excitations into states with the same energy as the ground state.

The next step is to spontaneously break the symmetry, which will make the field ϕ develop a VEV. Due to the freedom of $SU(2)$ rotations, there are multiple ways

to do this. We want to break the symmetry in the following manner

$$SU(2)_L \times U(1)_Y \longrightarrow U(1)_{QED}, \tag{1.54}$$

leaving the electromagnetic group as a symmetry of the vacuum and the electric charge as a conserved quantity. Only the neutral part of the scalar doublet can get a VEV, or otherwise QED would also be broken by the vacuum, and then

$$\langle \phi \rangle = \frac{1}{\sqrt{2}} \begin{pmatrix} 0 \\ v \end{pmatrix}, \tag{1.55}$$

where v is given by Eq. (1.53).

In general, we can parametrise the scalar doublet in terms of a neutral field h shifted from the origin by the VEV, and three real Goldstone bosons, θ^i, as follows

$$\phi = \exp\left(i\frac{\sigma_i}{2}\theta^i\right) \frac{1}{\sqrt{2}} \begin{pmatrix} 0 \\ v+h \end{pmatrix}. \tag{1.56}$$

In this parametrisation, it is straightforward to see that, after expanding the potential in Eq. (1.52), the field h is the only one that gets a quadratic term and hence become massive, while the three Goldstone bosons remain massless. Moreover, because the Lagrangian is invariant under local $SU(2)_L$ transformations, we can reabsorb the three massless Goldstone bosons into a redefinition of ϕ:

$$\phi \longrightarrow \exp\left(-i\frac{\sigma_i}{2}\theta^i\right) \phi = \frac{1}{\sqrt{2}} \begin{pmatrix} 0 \\ v+h \end{pmatrix}. \tag{1.57}$$

The remaining physical field, h, is the so-called *Higgs boson*. When using this particular parametrisation of ϕ after spontaneous symmetry breaking, we say that we are working in the *unitary gauge*. As described above, the three degrees of freedom, θ^i, now become the longitudinal polarisation of $W^\pm$ and Z, allowing the gauge bosons to get a mass.

We can now see how this affects the physical states of the gauge bosons associated with the gauge symmetries. We promote the derivatives in the kinetic term of the scalar Lagrangian to be covariant derivatives, and take into account the quantum numbers of ϕ. After spontaneous symmetry breaking, the piece of the Lagrangian

describing the masses of the gauge bosons reads

$$\begin{aligned}\mathcal{L} &= \frac{1}{2}\begin{pmatrix}0 & v\end{pmatrix}\left(-\frac{ig}{2}W_\mu^i\sigma_i - \frac{ig'}{2}B_\mu\mathbb{1}\right)\left(\frac{ig}{2}W_i^\mu\sigma^i + \frac{ig'}{2}B^\mu\mathbb{1}\right)\begin{pmatrix}0\\ v\end{pmatrix} \\ &= \frac{v^2}{8}\left[g^2(W_1^\mu - iW_2^\mu)(W_\mu^1 + iW_\mu^2) + (g'B_\mu - gW_\mu^3)^2\right] \\ &= \frac{v^2}{4}\left[g^2W^{+\mu}W_\mu^- + (g^2+g'^2)Z_\mu Z^\mu\right].\end{aligned} \tag{1.58}$$

In the second step, we have used the change of basis in Eq. (1.24) and Eq. (1.34). To this extent, we find the masses of the gauge bosons

$$m_W^2 = \frac{v^2g^2}{4} \tag{1.59}$$

and

$$m_Z^2 = \frac{v^2(g^2+g'^2)}{4} = \frac{m_W^2}{\cos^2\theta_W}. \tag{1.60}$$

Hence, the Z boson is slightly heavier than the W boson. Specifically, the observed values of their masses are $m_W = 80.379 \pm 0.012$ GeV and $m_Z = 91.1876 \pm 0.0021$ GeV [4]. On the other hand, the photon remains massless, as expected.

In addition, from the expression of the Fermi constant, Eq. (1.79), and the mass of the charged gauge boson, we find the value of the VEV of the scalar field, which defines the so-called *electroweak scale*, $v \simeq 246$ GeV.

Finally, the interactions of the Higgs boson with the gauge bosons can be found from Eq. (1.58) and the expression of the scalar field ϕ in the unitary gauge, i.e., Eq. (1.57). Provided the interacting Lagrangian involves products of the form $(v+h)^2$ and pairs of gauge bosons, all the following interactions occur: hWW, hZZ, $hhWW$, $hhZZ$.

Moreover, we can plug Eq. (1.57) in Eq. (1.52) and find the Higgs boson self-interactions, as well as the form of the mass of the Higgs boson. In terms of physical parameters, the Higgs Lagrangian reads

$$\mathcal{L}_h = \frac{1}{2}(\partial_\mu h)(\partial^\mu h) - \frac{1}{2}m_h^2h^2 - \frac{m_h^2}{2v}h^3 - \frac{m_h^2}{8v^2}h^4, \tag{1.61}$$

where the mass of the Higgs boson is given by

$$m_h^2 = -2m_\phi^2 = 2\lambda_\phi v^2. \tag{1.62}$$

In 2012, the LHC reported the discovery of the Higgs boson [24]. The most updated value for its mass is $m_h = 125.10 \pm 0.14$ GeV [4].

1.3 Fermion masses

We now move on to describe the mass of the fermions. The most straightforward idea one might try is to write a mass term for the electrons as

$$\begin{aligned} -m_e\bar{e}e &= -m_e\bar{e}(P_L+P_R)(P_L+P_R)e \\ &= -m_e\bar{e}(P_L^2+P_R^2)e \\ &= -m_e(\overline{e_R}e_L+\overline{e_L}e_R). \end{aligned} \tag{1.63}$$

However, both terms break the gauge invariance, as e_R and e_L belong to different representation of $SU(2)_L$. Moreover, they carry different $U(1)_Y$ charges. Quark mass terms suffer the same obstacle. Thus we are not allowed to explicitly write fermion mass terms.

Another possibility is to generate them dynamically. In the previous section we have introduced a scalar doublet ϕ with just the correct quantum numbers to couple to a fermion doublet and a fermion singlet. Indeed, for the case of the leptons,

$$\mathcal{L}_Y = -y_e\bar{\ell}_L\phi\, e_R. \tag{1.64}$$

Since this is a trilinear interaction, it is called the Yukawa interaction of the electrons with the Higgs doublet. After spontaneous symmetry breaking, the Yukawa Lagrangian reads

$$\mathcal{L}_Y = -y_e\frac{v}{\sqrt{2}}\overline{e_L}e_R - y_e\frac{1}{\sqrt{2}}h\overline{e_L}e_R. \tag{1.65}$$

The second term gives the interaction of the Higgs boson with the pair of electrons. On the other hand, the first term results in a mass term for the electrons, whose expression is

$$m_e = y_e\frac{v}{\sqrt{2}}. \tag{1.66}$$

This allows to actually measure the Yukawa couplings in terms of the fermion masses.

Additionally, since the Standard Model has no right-handed neutrinos, we cannot write a Yukawa interaction that give mass to neutrinos in the same fashion as to electrons and quarks. So the Standard Model predicts neutrinos to be massless.

We note that, generating fermion masses in this fashion, the Dirac Lagrangian for the leptons,

$$\mathcal{L} = \bar{\ell}(i\gamma^\mu\partial_\mu - m)\ell, \tag{1.67}$$

remains invariant under an $U(1)$ symmetry:

$$\ell(x) \longrightarrow \exp(-iL\theta)\ell(x), \qquad \bar{\ell}(x) \longrightarrow \exp(+iL\theta)\bar{\ell}(x). \tag{1.68}$$

The associated conserved charge is L and is simply called *lepton number*. With this convention, leptons carry $L = -1$ and antileptons $L = 1$, while the rest of the SM particles, $L = 0$.

Up until now, we have worked with only one generation of quarks and fermions. But we know there are at least three families. Every member of a new generation is an exact copy of those of the first family, with the same gauge charges, but with larger mass. In order to implement this modification we let the fields carry an index that runs over the three families. With this, the mass terms of the three charged leptons and the three families of quarks read

$$\mathcal{L}_m = -(\bar{e}_{La} M^e_{ab} e_{Rb} + \bar{u}_{La} M^u_{ab} u_{Rb} + \bar{d}_{La} M^d_{ab} d_{Rb}), \tag{1.69}$$

where a and b are the indexes running on the three families. Thus, the mass matrices are not necessarily diagonal and the fields may not be the mass eigenstates. In order to diagonalise the mass matrix we need to change the basis of the fields with some unitary transformation. Since the left- and right-handed components are actually different fields, they will typically transform differently. In general, they follow

$$\psi_R \longrightarrow U^\psi_R \psi_R, \qquad \bar{\psi}_L \longrightarrow \bar{\psi}_L U^{\psi\dagger}_L, \tag{1.70}$$

where ψ are either leptons or quarks. After this change of basis, we obtain a diagonal mass matrix upon the following transformation:

$$M^D_\psi = U^\psi_L M_\psi U^{\psi\dagger}_R. \tag{1.71}$$

There is some freedom to select an appropriate lepton and quark basis, but ultimately the form of the unitary transformations depend on the interactions among different fields, which are mediated by the $W^\pm$ gauge boson. Recalling Eq. (1.35),

$$-\mathcal{L}_I = \frac{g}{\sqrt{2}} (\bar{\nu}_L \gamma^\mu e_L + \bar{u}_L \gamma^\mu d_L) W^+_\mu + h.c. \tag{1.35}$$

For instance, let us first focus on the unitary transformation for the charged leptons. We can always choose the mass of the charged leptons to be described by a diagonal matrix. Then, the lepton bilinear in the first term in Eq. (1.35) gets transformed by

$$\overline{\nu_L} e_L \longrightarrow \overline{\nu_L} U^e_L e_L. \tag{1.72}$$

However, as there is no neutrino mass term in the Standard Model, we can always redefine the neutrinos so that they reabsorb the unitary transformation and the interactions become diagonal in flavour, $\overline{\nu_L} e_L \longrightarrow \overline{\nu_L} e_L$. This situation changes

when there is new physics describing the mass of neutrinos. We will see more about this in the next chapters when we address neutrino mixing.

The case of the quarks is different, as in the Standard Model both u- and d-type quarks are massive. Like for the charged leptons, we are free to choose the u-type quarks to have a diagonal mass matrix. Then the quarks part of the interaction in Eq. (1.35) transforms following

$$\bar{u}_L d_L \longrightarrow \bar{u}_L U_L^{u\dagger} U_L^d d_L. \tag{1.73}$$

But now we are not able to reabsorb the transformation with a redefinition of the d_L field and the mass matrix of the d-type quarks remains complex and non-diagonal. Moreover, because in general $U_L^{u\dagger} U_L^d \neq \mathbb{1}$, the change of basis remains as a residue in the interaction in Eq. (1.35). So we define a new mixing matrix

$$V_{\text{CKM}} = U_L^{u\dagger} U_L^d = \begin{pmatrix} V_{ud} & V_{us} & V_{ub} \\ V_{cd} & V_{cs} & V_{cb} \\ V_{td} & V_{ts} & V_{tb} \end{pmatrix} \tag{1.74}$$

called after Cabibbo, Kobayashi and Maskawa [25, 26]. The CKM matrix is unitary and gives information about the transitions of quarks with different flavours in the interaction with the W boson:

$$\mathcal{L}_I = \frac{g}{\sqrt{2}} (\bar{\nu}_{La} \gamma^\mu e_{La} + \bar{u}_{La} \gamma^\mu V_{\text{CKM}}^{ab} d_{Lb}) W_\mu^+ + h.c. \tag{1.75}$$

An $n \times n$ unitary matrix has n^2 real parameters: $n(n-1)/2$ moduli and $n(n+1)/2$ phases. However, many of these phases can be reabsorbed into a redefinition of the fields. Ultimately, there are $(n-1)(n-2)/2$ phases. With $n = 2$ families of quarks and leptons, the CKM matrix is described by only one module, called the Cabibbo angle. In this case, there is no CP-violating phase. This led physicists to think there are more than two generations of quarks. After introducing a third family, the CKM matrix is characterised with three moduli and one phase.

There are several ways of parametrising the CKM matrix. The standard

parametrisation is in terms of three Euler angles and one phase, and reads

$$V_{\text{CKM}} = \begin{pmatrix} 1 & 0 & 0 \\ 0 & c_{23} & s_{23} \\ 0 & -s_{23} & c_{23} \end{pmatrix} \begin{pmatrix} c_{13} & 0 & s_{13}e^{-i\delta_{CP}} \\ 0 & 1 & 0 \\ -s_{13}e^{i\delta_{CP}} & 0 & c_{13} \end{pmatrix} \begin{pmatrix} c_{12} & s_{12} & 0 \\ -s_{12} & c_{12} & 0 \\ 0 & 0 & 1 \end{pmatrix}$$
$$= \begin{pmatrix} c_{12}c_{13} & s_{12}c_{13} & s_{13}e^{-i\delta_{CP}} \\ -s_{12}c_{23} - c_{12}c_{23}s_{13}e^{i\delta_{CP}} & c_{12}c_{23} - s_{12}s_{23}s_{13}e^{i\delta_{CP}} & s_{23}c_{13} \\ s_{12}s_{23} - c_{12}c_{23}s_{13}e^{i\delta_{CP}} & -c_{12}s_{23} - s_{12}c_{23}s_{13}e^{i\delta_{CP}} & c_{23}c_{13} \end{pmatrix}, \tag{1.76}$$

where $c_{ij} = \cos\theta_{ij}$ and $s_{ij} = \sin\theta_{ij}$ are trigonometric functions of the three angles, and δ_{CP} is the only complex phase in the Standard Model, and thus the only source of CP violation. The values of the parameters are collected by various experiments and make use of the unitarity properties of the CKM matrix. The particle data group collaboration [27] gives the following values for the entries of the CKM matrix:

$$V_{\text{CKM}} = \begin{pmatrix} 0.97420(21) & 0.2243(5) & 0.00394(36) \\ 0.218(4) & 0.997(17) & 0.00422(8) \\ 0.0081(5) & 0.00394(23) & 1.019(25) \end{pmatrix}, \tag{1.77}$$

where values in parentheses are uncertainties in the significant figures. We see that the elements of the main diagonal are much larger than the off-diagonal entries.

Finally, the interactions of the leptons remain diagonal and there is no term in the Lagrangian connecting different flavours of leptons. For this reason, we often say that lepton flavour is a global symmetry of the Standard Model. Indeed, lepton flavour conservation is observed with great precision [4], but it is imperative to note that this symmetry is no more than an accident of the theory and there is no strong theoretical argument that leads us to think it cannot be broken by heavier new physics.

So far, we have been considering neutrinos to be massless. This is a prediction of the Standard Model and, owing to the elusive nature of neutrinos, a suggestion of the experiments for long time. But in recent years, there has been plenty of experimental evidence of neutrino oscillations, which implies not only that neutrinos are massive but also that they are not degenerated. This opens up a window for processes that change lepton flavor, the most significant instance of which is the generation of neutrino masses. We will talk about all this in the next chapter.

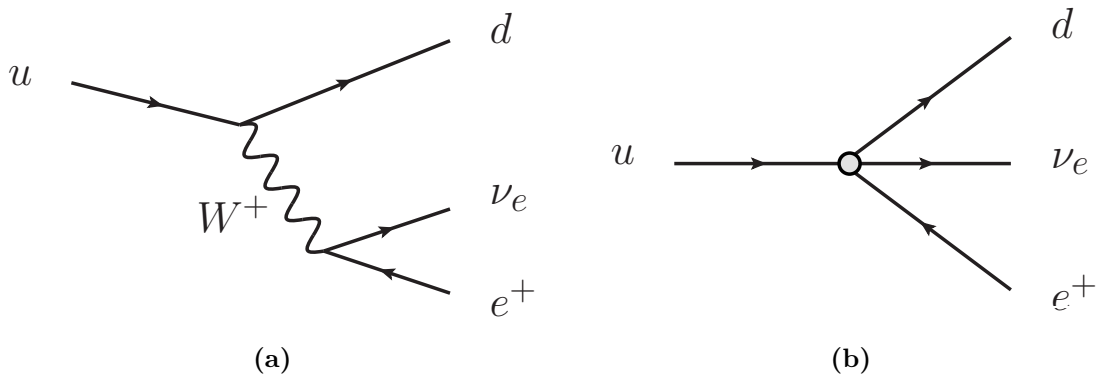

Figure 1.2: Feynman diagrams describing the beta decay within the Standard Model (a) and the Fermi theory (b). In the second case, the propagator of W^+ shrinks to a point, and the process becomes a contact interaction.

1.4 The Standard Model as an effective field theory

Having outlined the interactions of the fermions with the gauge bosons in the Standard Model, we can revisit the study of the beta decay. We know that the Fermi theory describes this type of processes with great precision by means of a four-fermion operator. However, for large enough energies, this simple model breaks. The obvious questions are whether the Standard Model is able to handle the beta decay and if so, what is the connection between the two pictures. Feynman diagrams within both the Standard Model and the Fermi theory are displayed in Figure 1.2. In the Standard Model, the relevant piece of the Lagrangian reads

$$-\mathcal{L}_W = \frac{g}{2\sqrt{2}} W_\mu^- (\bar{e}\gamma^\mu(1-\gamma_5)\nu_e) + \frac{g}{2\sqrt{2}} W_\mu^+ (\bar{u}\gamma^\mu(1-\gamma_5)d) + h.c. \tag{1.35}$$

The total energy of the beta decay is driven by the mass of the neutron, which lies around 1 GeV. The mass of the charged gauge boson $W^\pm$ is much heavier than this value and indeed than the momentum $q^2 = (p_u - p_d)^2 = (p_e - p_\nu)^2$ transferred between the two fermionic currents. Then, the propagator of $W^\pm$ reduces to a point:

$$\frac{1}{q^2 - M_W^2} = -\frac{1}{M_W^2} + \mathcal{O}(q^2/M_W^4). \tag{1.78}$$

Keeping only the leading term in the $1/M_W^2$ expansion, the resulting Lagrangian is the $V-A$ four-fermion contact interaction of the Fermi theory,

$$\mathcal{L}_F = -\frac{G_F}{\sqrt{2}} [\bar{e}\gamma^\mu(1-\gamma_5)\nu_e][\bar{u}\gamma^\mu(1-\gamma_5)d], \tag{1.1}$$

where we have reformulated the weak coupling constant in terms of the Fermi constant as

$$\frac{G_F}{\sqrt{2}} = \frac{g^2}{8M_W^2}. \tag{1.79}$$

The Lagrangian in Eq. (1.1) represents a contact interaction among light fields (in this case, the quarks and leptons) that approximately replaces the non-local exchanges of a heavy particle (e.g. the W gauge boson) in the complete picture.

The conclusion is that the Fermi theory is what is called an *effective field theory* (EFT) of the Standard Model at low energies. The idea is that whenever we are interested in phenomena at a certain energy, there are objects at much heavier scales and we might get an approximate but useful picture of the low-energy physics by ignoring the details of such objects. In particle physics terms, the explicit dependence of those particles too heavy to be produced can be left out of the Lagrangian describing long-distance physics, and we often say that in an effective field theory they have been *integrated out*. However, the influence of the removed heavy degrees of freedom remains hidden in the new coupling constants, as seen in Eq. (1.79).

So far we were focusing on one specific effective operator, namely, the Fermi interaction. We can generalise this framework and list all possible operators constructed with a set of fields and respecting some chosen symmetries, at any energy dimension d. For a field theory in four dimensions, the general effective Lagrangian reads

$$\mathcal{L} = \sum_{n=2}^{\infty} \frac{1}{\Lambda^{n-4}} \sum_i \alpha_i \mathcal{O}_i^{(n)}, \tag{1.80}$$

where Λ is a heavy scale associated with the operator $\mathcal{O}$, and α is some coupling constant that is taken to be dimensionless. For every dimension, these operators will have different influence on physical phenomena, depending on the energy scale E of the process described by these operators.

First, operators of dimension $d = 4$, like some interactions in the Standard Model, are equally relevant at all energy scales. For dimension less than four, like mass terms, the corresponding operators are relevant at scales similar to the mass of the particles involved; at high energies their influence rapidly become negligible.

For $d > 4$, the effects of the contact interactions are suppressed by the scale of the heavy physics, which makes them weak at low energies. If the energy gap between Λ and the energy scale E is arbitrarily large, their effects would be negligible. In fact, the great success of the Fermi theory is only due to the lightness of the W gauge boson; if M_W was much heavier, beta decay would remain unobserved.

In fact, when Λ is much larger than E and the influence of higher dimensional operators are suppressed by powers of E/Λ, we can build an EFT that is renormalizable using only operators of dimension less or equal to four.

Following this idea, we can describe the Standard Model as an EFT constructed out of all operators of dimension four or less, invariant under $SU(3)_c \times SU(2)_L \times U(1)_Y$, with the fermion fields of Eq. (1.3), the gauge bosons associated with these symmetries, and the Higgs boson. The Standard Model has become a remarkably successful EFT describing physics below the TeV scale. However, we know it is not the complete picture because it fails to provide a theoretical interpretation for the experimental evidence regarding dark matter and neutrino masses.

In order to tackle these problems in the context of an EFT, we can go further and consider operators of higher dimensions. If we restrain to a framework with the same local symmetries and field content of the Standard Model, the EFT that generalise the Standard Model is called the Standard Model Effective Field Theory (SMEFT). The fundamental assumption is that there is some degree of decoupling of the new physics particles with the SM fields. Then, the relevant scale of new physics will be above the electroweak scale, given by the VEV of the SM Higgs doublet. In fact, this decoupling is strongly suggested by the increasingly large data set collected by the LHC and other experiments.

A complete basis of independent operators of the SMEFT can be found in Ref. [28] for dimension five (in fact, there is only one dimension-five operator, often called Weinberg operator), in Ref. [29] for dimension six and in Ref. [30] for dimension seven. It is important to note that when looking for these operators, one can come upon redundancies, which can be handled with the aid of equations of motion, integration by parts or Fierz transformations. In recent years a systematic approach was developed to find all operators at a given order [31–34]. Of particular interest is Ref. [34], in which authors obtained that this algorithm can be programmed, making it very appealing for practical uses.

To sum up, unless a new particle lighter than the electroweak scale is found, the SMEFT is a powerful framework for approximately describing low energy phenomena. The great amount of empirical information obtained by the LHC, along with current and future precision measurements, can be used for setting bounds on the parameters of the effective operators. Moreover, if any of these local interactions is found to be consistent with data, it could become a building block of an ultraviolet completion of the Standard Model. The SMEFT will play an important role in the development of this thesis.

CHAPTER 2

Neutrino masses

Before the development of the Standard Model, the following main characteristics of neutrinos were known:

- Neutrinos interact very weakly with matter. This makes observations of neutrinos extremely hard.
- Neutrinos are very light, so light that for long time they were thought to be massless.
- Only two degrees of freedom of neutrinos were ever observed: one particle-state that behaves like a left-handed object and an antiparticle counterpart corresponding to a right-handed object.

So it was natural that, when building the Standard Model, physicists included solely a left-handed neutrino and its antiparticle counterpart. Within this framework, neutrinos do not have a mass, in agreement with the experimental knowledge at the time. From a purely theoretical perspective, however, this was cumbersome because there is no strong reason (e.g. a fundamental symmetry, like in the case of the photon) to force neutrinos to be massless. But then neutrino oscillations were observed, and this is only possible if neutrinos are massive: now neutrino mass is a fact, with no controversy among the scientific community. This opened up plenty of new physics possibilities.

The first attempt to explain neutrino masses consisted in considering neutrinos to have four degrees of freedom, in similarity with the electron. The two extra degrees of freedom would correspond to an additional right-handed neutrino. Then, just as in the Standard Model, the Higgs mechanism would make neutrinos massive. Moreover, this would put neutrinos in a similar footing to the rest of the fermions in the Standard Model. Not only they would have the same number of degrees of freedom, but also the generation of masses would be given by the same mechanism

for all fermions. However, there is still an important difference that makes physicists struggle: neutrinos seem to be much lighter than the other fermions. Any theory that is proud of generating neutrino masses needs to explain the smallness of neutrino masses in a convincing way, and a model that adds only a right-handed neutrino fails to do so without proper fine-tuning.

Another possibility for generating neutrino masses consists in giving up on demanding neutrinos to have four degrees of freedom. Neutrinos are fundamentally different from the charged leptons and quarks, as they are electrically neutral particles. Because of this reason, it is possible to generate Majorana neutrino masses without the inclusion of new neutrino degrees of freedom. However, further ingredients are still needed. In any case, and irrespective of the mechanism inducing the Majorana masses, it is worth pointing out that lepton number would no longer be a good symmetry. This would have interesting consequences regarding lepton number violating (LNV) processes.

In this chapter, we will briefly review some of the implications of the mass of neutrinos.

2.1 Dirac or Majorana nature?

The lowest-dimensional faithful irreducible representations of the Lorentz group, $SU(2) \times SU(2)$ are the two-dimensional ψ_L chiral field and its conjugate counterpart ψ_L^c [1]. They are called Weyl spinors and describe massless fermions. The goal is to build Lorentz invariant mass terms using chiral fields.

One possibility is to consider only one independent chiral field. Then, we can construct only one type of mass terms, called *Majorana mass terms*, following:

$$\text{Majorana:} \qquad \overline{\psi_L^c}\psi_L + \overline{\psi_L}\psi_L^c. \tag{2.1}$$

The bilinears in the previous equation relate two particle states (or two antiparticle states), forbidding the conservation of any global symmetry. For this reason, only electrically neutral fermions, such as neutrinos, can have Majorana masses. Furthermore, following the same argument, we see that fermion number cannot be conserved either. This feature is expected: an observer travelling faster than a ψ_L will see it as its right-handed counterpart, ψ_L^c, which is an antiparticle state. In this scenario, fermion number, which is the only symmetry that could help distinguishing ψ_L from ψ_L^c, cannot be established. The conclusion is that Majorana fermions are their own antiparticle. Finally, the mass eigenstates are two-component fields,

[1] The conjugate of a field ψ is defined as $\psi^c = C\bar{\psi}^t$, where $C = i\gamma^2\gamma^0$ is the charge conjugation operator.

called *Majorana fields*, given by $\psi = \psi_L + \psi_L^c$.

The second possibility is that the mass terms are built using two independent chiral fields, ψ_L and ψ_R. Then, two sets of mass terms can arise: those obtained with only one chiral field (and its conjugate), which are Majorana mass terms, and those realised using the two distinct chiral fields. The latter are called *Dirac mass terms* and read:

$$\text{Dirac:} \qquad \overline{\psi_L}\psi_R + \overline{\psi_R}\psi_L. \tag{2.2}$$

If only Dirac masses are present, global symmetries can be conserved. Then, fermion number can be assigned to fermions in a consistent way. In this case, the mass eigenstates are four-component fermions, defined by $\psi = \psi_L + \psi_R$. They are called *Dirac fields.*

Either of these two formalisms allows a description of neutrino masses. However, in similarity to quarks and charged leptons, the addition of neutrino mass terms (both Dirac and Majorana) breaks the gauge invariance of the Standard Model. Dirac neutrino masses can be generated by the Higgs mechanism, and thus including a right-handed neutrino that acts as the right-handed component of the SM neutrino would be enough to induce neutrino masses. However, Majorana masses cannot be obtained in the same way, and new ingredients are needed (for instance, the inclusion of additional heavy fields that at low energies generate effective Majorana mass terms after spontaneous symmetry breaking).

2.2 Flavours in the neutrino mass matrix

In this section we describe the implications of the existence of three families of neutrinos for the neutrino mass matrix. Let us begin with the general Lagrangian involving charged leptons and neutrinos:

$$\mathcal{L} = -(M_\ell)_{ab}\bar{\ell}_a\ell_b - (M_\nu)_{ab}\bar{\nu}_a\nu_b - \frac{g}{\sqrt{2}}\left[W_\mu^-\left(\sum_{ab}\overline{\ell_a}\gamma^\mu P_L\nu_b\right) + h.c.\right]. \tag{2.3}$$

where M_ℓ and M_ν are the 3×3 lepton and neutrino mass matrices, respectively. Throughout the text, sometimes when referring to specific matrix elements of the neutrino mass matrix we will simply write M_{ab} (instead of $(M_\nu)_{ab}$).

The subindices a, b denote interaction eigenstates and need not correspond to the mass eigenstates, as there is no reason for M_ℓ or M_ν to be diagonal matrices. However, one can diagonalise the lepton mass matrix without loss of generality. This transformation can then be reabsorbed in a redefinition of the ν field, in the weak interaction terms. But then there is no longer freedom to diagonalise M_ν as in general the two mass matrices are different; it seems M_ℓ and M_ν cannot be

simultaneously diagonal and one of them will introduce mixing among its fields. (Of course one could always choose to make the neutrino mass matrix diagonal at the expense of charged lepton mixing. The convention is to keep the lepton basis diagonal and let neutrinos mix. Here we follow this approach.)

In order to find the physical basis for neutrinos, we rotate them with

$$\nu_a = \sum_i U_{ai}\nu_i. \tag{2.4}$$

The neutrinos ν_a (with $a = e, \mu, \tau$) are expressed in the flavour basis (also called interaction basis) whereas ν_i (with $i = 1, 2, 3$) correspond to the mass basis. The matrix $U \equiv U_{PMNS}$ is often called Pontecorvo–Maki–Nakagawa–Sakata matrix. Then, the weak interaction terms in Eq. (2.3) become:

$$\mathcal{L}_{int} = \frac{g}{\sqrt{2}} W_\mu^- \begin{pmatrix} \overline{e} & \overline{\mu} & \overline{\tau} \end{pmatrix} \gamma^\mu P_L \, U_{PMNS} \begin{pmatrix} \nu_1 \\ \nu_2 \\ \nu_3 \end{pmatrix} + h.c. \tag{2.5}$$

From here we can start to find a parametrisation for the leptonic mixing matrix U_{PMNS}. With $n = 3$ lepton flavours, U_{PMNS} is a 3×3 unitary matrix and, as such, it has $n^2 = 9$ real parameters, with $n(n-1)/2 = 3$ Euler angles and $n(n+1)/2 = 6$ phases. Then, it can be described by

$$U_{PMNS} = P_\ell \, V \, P_\nu, \tag{2.6}$$

where $P_\ell = \mathrm{diag}(e^{i\phi_e}, e^{i\phi_\mu}, e^{i\phi_\tau})$ carries three phases and $P_\nu = \mathrm{diag}(e^{i\alpha/2}, e^{i\beta/2}, 1)$, two phases. The form of the last matrix will be obvious in a moment. Also, assuming unitarity, the V matrix can be parametrised by rotations in three planes:

$$\begin{aligned} V &= \begin{pmatrix} 1 & 0 & 0 \\ 0 & c_{23} & s_{23} \\ 0 & -s_{23} & c_{23} \end{pmatrix} \begin{pmatrix} c_{13} & 0 & s_{13}e^{-i\delta} \\ 0 & 1 & 0 \\ s_{13}e^{-i\delta} & 0 & c_{13} \end{pmatrix} \begin{pmatrix} c_{12} & s_{12} & 0 \\ -s_{12} & c_{12} & 0 \\ 0 & 0 & 1 \end{pmatrix} \\ &= \begin{pmatrix} c_{12}c_{13} & c_{13}s_{12} & s_{13}e^{-i\delta} \\ c_{23}s_{12} + s_{23}s_{13}c_{12}e^{-i\delta} & c_{23}c_{12} + s_{23}s_{12}s_{13}e^{-i\delta} & c_{13}s_{23} \\ c_{23}c_{12}e^{-i\delta} - s_{23}s_{12} & c_{23}s_{13}s_{12}e^{-i\delta} - c_{12}s_{23} & c_{13}c_{23} \end{pmatrix}, \end{aligned} \tag{2.7}$$

where δ is a CP-violating phase and $s_{23} \equiv \sin\theta_{23}$, $s_{13} \equiv \sin\theta_{13}$ and $s_{12} \equiv \sin\theta_{12}$ are three Euler angles.

Now, if we go back to the interaction term of the Lagrangian in Eq. (2.3) and plug in the expression for U_{PMNS} we see that P_ℓ can be rotated away by a redefinition of

the charged lepton fields,

$$\begin{cases} e & \longrightarrow e^{-i\phi_e}\, e \\ \mu & \longrightarrow e^{-i\phi_\mu}\, \mu \\ \tau & \longrightarrow e^{-i\phi_\tau}\, \tau. \end{cases} \tag{2.8}$$

so that the PMNS matrix becomes

$$U_{PMNS} = V\, P_\nu. \tag{2.9}$$

The Dirac or Majorana nature of neutrinos did not play any role in this discussion yet. If neutrinos are Dirac, then the two phases in P_ν can also be reabsorbed by the ν fields in the same way as in P_ℓ, leaving three angles and only one CP-violating phase. In this case, U_{PMNS} is identically equal to V. However, if neutrinos are Majorana, the phases in P_ν cannot be rotated away. This is because the effective Majorana mass term is not invariant under a redefinition of the phase, $\nu \longrightarrow e^{-i\phi}\nu$:

$$M_\nu \overline{\nu^c}\nu \longrightarrow e^{-i2\phi} M_\nu \overline{\nu^c}\nu. \tag{2.10}$$

Because of this reason, for Majorana neutrinos there are still three phases. Now, $U_{PMNS} = VP_\nu$ with three angles, one Dirac phase, δ, and two Majorana phases, α and β[2].

Finally, δ cannot be included in P_ν. This is because a redefinition of all the phases by a constant will leave the U_{PMNS} matrix invariant; one of them is not independent and can be always eliminated by a redefinition. Indeed, imagine we let the Dirac phase δ to be part of P_ν. Then U_{PMNS} is written as

$$U_{PMNS} = \begin{pmatrix} e^{i\phi_e} & 0 & 0 \\ 0 & e^{i\phi_\mu} & 0 \\ 0 & 0 & e^{i\phi_\tau} \end{pmatrix} V \begin{pmatrix} e^{-i\alpha} & 0 & 0 \\ 0 & e^{-i\beta} & 0 \\ 0 & 0 & e^{-i\delta} \end{pmatrix}. \tag{2.11}$$

But if we shift all the phases by the same constant, U_{PMNS} remains the same. We

[2]Note that δ is called 'Dirac phase' because it is the only phase remaining if neutrinos are Dirac; similarly, α and β are the 'Majorana phases' as they are only present when neutrinos are Majorana.

can choose this constant to be one of the six phases, in this case δ:

$$U_{PMNS} = \begin{pmatrix} e^{i(\phi_e-\delta)} & 0 & 0 \\ 0 & e^{i(\phi_\mu-\delta)} & 0 \\ 0 & 0 & e^{i(\phi_\tau-\delta)} \end{pmatrix} e^{+i\delta} V e^{-i\delta} \begin{pmatrix} e^{-i(\alpha-\delta)} & 0 & 0 \\ 0 & e^{-i(\beta-\delta)} & 0 \\ 0 & 0 & e^{-i(\delta-\delta)} \end{pmatrix}$$
$$= \begin{pmatrix} e^{i\phi'_e} & 0 & 0 \\ 0 & e^{i\phi'_\mu} & 0 \\ 0 & 0 & e^{i\phi'_\tau} \end{pmatrix} V \begin{pmatrix} e^{-i\alpha'} & 0 & 0 \\ 0 & e^{-i\beta'} & 0 \\ 0 & 0 & 1 \end{pmatrix}. \tag{2.12}$$

One of the phases is now gone and we redefine the remaining five phases which are now independent. But a 3×3 unitary matrix is parametrised with six independent phases, and hence one of them has to be inside V, which reduces to three Euler angles and one CP-violating phase.

We have constructed the mixing matrix for neutrinos. Now we can again focus our attention on the mass matrix. We need to distinguish two different scenarios: Dirac and Majorana masses. For Dirac neutrinos the two chiral fields are different degrees of freedom. In order to build a mass term using Dirac neutrinos one needs both right- and left-handed neutrinos. Then:

$$\mathcal{L} = -(M_\nu)_{ab}\, \overline{\nu_{aL}} \nu_{bR}, \tag{2.13}$$

where neutrinos are in the flavor basis, and of course M_ν is not diagonal. Now we want to find the physical eigenstates of neutrinos so we change basis with Eq. (2.4). The mass matrix transforms as

$$M_\nu \longrightarrow U_{PMNS} M_\nu^D U_{PMNS}^\dagger, \tag{2.14}$$

where M_ν^D is a diagonal matrix. For Dirac neutrinos, the mass matrix is hermitian.

What happens when neutrinos are Majorana? In this case, RH neutrinos are not independent degrees of freedom. The mass Lagrangian is built using the neutrino ν and its charge conjugate counterpart, ν^c:

$$\mathcal{L} = -\frac{1}{2}(M_\nu)_{ab} \overline{\nu_a} \nu_b^c + h.c. \tag{2.15}$$

If we plug the transformation (2.4) in the last equation we find that the mass matrix is diagonalised by

$$M_\nu \longrightarrow U_{PMNS} M_\nu^D U_{PMNS}^t. \tag{2.16}$$

Now it is clear that the Majorana mass matrix is not hermitian. However M_ν is

symmetric, $(M_\nu)^t = M_\nu$, and out of its 9 complex parameters (18 real parameters), only 6 are independent (12). After rotating away the three charged-lepton Dirac phases we are left with 9 real parameters; they are those of the Majorana neutrino PMNS mixing matrix (three angles, one Dirac phase and two Majorana phases) and the three physical masses.

Experimentally, neutrino masses are not easy to measure. Instead, via neutrino oscillation, neutrino mass differences ($\Delta m^2_{ij} = m^2_i - m^2_j$) are observed so a good idea is to change the independent parameters of the diagonal mass matrix to be the mass of the lightest neutrino (hereafter called m_ℓ for *lightest*) and two mass differences. Another experimental issue is that we are still missing information regarding the correct hierarchy among the masses. One of the mass differences (Δm^2_{21}) is currently well known, while for the other (Δm^2_{3i}) only the modulus is constrained but not its sign. Two different scenarios arise. When $m_1 < m_2 < m_3$ holds, the mass ordering is called normal (NO, with $\Delta m^2_{32} > 0$), while if neutrino masses are such that $m_3 < m_1 < m_2$, then they have an inverted ordering (IO, with $\Delta m^2_{31} < 0$).

2.3 Implications of neutrino masses

The existence of non-vanishing neutrino masses has interesting phenomenological implications. Here we review some of the most important ones.

Neutrino oscillations

This is the most obvious consequence of neutrinos being massive, and the first (and only) experimental confirmation of this feature. As a result of the charged current weak interactions, three flavour states of neutrinos interact with the charged leptons. Each of these flavour states is a superposition of different mass eigenstates. As the neutrino propagates through space, the physical states evolve with different frequencies so that the probability of detecting a given neutrino flavour changes with time.

The time evolution of the flavour state ν_a, which is superposition of the physical states ν_i, reads:

$$|\nu_a(t)\rangle = \sum_i e^{-iE_i t}\, U_{ai} |\nu_i\rangle, \tag{2.17}$$

where the energy of the i mass eigenstate is given by

$$E_i = \sqrt{|\vec{p}_i|^2 + m_i^2} \approx |\vec{p}_i| + \frac{m_i^2}{2|\vec{p}_i|} \approx E + \frac{m_i^2}{2E}. \tag{2.18}$$

We have made the approximation for relativistic neutrinos, $|\vec{p}_i| \gg m_i$, and $|\vec{p}_i| = E$, where E is the total energy of the neutrino. With this, the evolution of ν_a after a time $t = T$ is

$$|\nu_a(t=T)\rangle = \sum_i e^{-i\frac{m_i^2 T}{2E}} U_{ai}|\nu_i\rangle, \tag{2.19}$$

where the phase e^{-iET} has been dropped that is common to all ν_i, because observables are not sensitive to it. Then, the probability for a neutrino with original flavour a to be detected with flavour b, after a time $t = T$, reads

$$P_{ab} = |\langle\nu_b(t=T)|\nu_a\rangle|^2 = \sum_{ij} U_{bj}U_{aj}^* U_{bi}^* U_{ai} e^{-i\frac{(m_i^2-m_j^2)T}{2E}}. \tag{2.20}$$

It depends on the parameters entering the neutrino mixing matrix and the differences of squared masses which, for three families of neutrinos, there are only two. Moreover, in P_{ab} the Majorana phases disappear; neutrino-neutrino oscillations give no information regarding Majorana phases.

Currently, there are several neutrino oscillation experiments. Some of them look for disappearance of ν_e neutrinos produced in nuclear reactions in the sun (e.g. Super-Kamiokande [35]). Other experiments detect the probability of ν_μ disappearance from neutrinos originated after collisions of cosmic rays with atmospheric particles (for instance Super-Kamiokande [36], IceCube [37]). Finally, there are experiments that use neutrinos obtained from nuclear reactors (Daya Bay [38], RENO [39], Double Chooz [40]) and particle accelerators (T2K [41], MINOS [42], NOνA [43]). In Table 2.1 we present the current experimental status of three-flavour neutrino oscillation parameters.

	Normal Ordering	*Inverted Ordering* ($\Delta\chi^2 = 10.4$)
$\sin^2\theta_{12}$	$0.31^{+0.013}_{-0.012}$	$0.31^{+0.013}_{-0.012}$
$\sin^2\theta_{23}$	$0.563^{+0.018}_{-0.024}$	$0.565^{+0.017}_{-0.022}$
$\sin^2\theta_{13}$	$0.02237^{+0.00066}_{-0.00065}$	$0.02259^{+0.00065}_{-0.00065}$
$\delta/^\circ$	221^{+39}_{-28}	282^{+23}_{-25}
$\frac{\Delta m^2_{21}}{10^{-5}\text{ eV}}$	$7.39^{+0.21}_{-0.20}$	$7.39^{+0.21}_{0.20}$
$\frac{\Delta m^2_{3\ell}}{10^{-3}\text{ eV}}$	$+2.528^{+0.029}_{-0.031}$	$-2.510^{+0.030}_{-0.031}$

Table 2.1: Best fit values of the oscillation parameters and their $\pm1\sigma$ uncertainties obtained with the global analysis performed by the nuFIT collaboration [44]. In the last row, $\Delta m^2_{3\ell} = \Delta m^2_{31} > 0$ for NO while $\Delta m^2_{3\ell} = \Delta m^2_{32} < 0$ for IO. Values of IO are disfavoured respect to those of NO with $\Delta\chi^2 = 10.4$.

Neutrinoless double beta decay

Similar to conventional double beta decay, neutrinoless double beta decay ($0\nu\beta\beta$) involves a simultaneous conversion of two neutrons into two protons and the emission of two electrons. However, in this case, the neutrinos emitted by the two beta decays are reabsorbed. Then,

$$0\nu\beta\beta: \qquad n + n \longrightarrow p + p + e + e. \tag{2.21}$$

This is only possible if neutrinos are Majorana as, in this case, particle and antiparticle are the same object. Further, because the final products of this process involve two electrons, it breaks lepton number in two units, which is forbidden for Dirac neutrinos. For this reason, an observation of $0\nu\beta\beta$ would undoubtedly lead to the confirmation of the Majorana nature of neutrinos.

This process could also shed light on the scale of neutrino masses. Because it involves interactions of electrons and the three families of neutrinos, this processes is also sensitive to the following observable:

$$m_{\beta\beta} = \left| \sum_i U_{ei}^2 \, m_i \right|. \tag{2.22}$$

This observable can also be identified with M_{ee}, the ee matrix element of the neutrino mass matrix. But the form of this matrix entry receives restrictions from oscillation data, so that, for a given range of values, it correlates with the mass of the lightest neutrino. The conclusion is that detecting $0\nu\beta\beta$ could also give information about the mass of the lightest neutrino.

Neutrino decays

In the Standard Model, neutrinos are massless and hence stable particles. As soon as neutrinos become massive, they start to decay into lighter particles, given that there is no symmetry that forbids it. Heavier neutrinos would decay into lighter particles, while only the lightest neutrino would be stable. Depending on the particular framework considered, different decay modes could occur in nature. One possibility is a loop-mediated decay channel with a two-body final state involving a photon and a light neutrino:

$$\nu_a \longrightarrow \nu_b \gamma. \tag{2.23}$$

In some contexts, in which heavier neutrinos are included, three-body final states also become possible, including:

- two light jets and a light neutrino:

$$\nu_a \longrightarrow \nu_b u\bar{u},\ \nu_b d\bar{d}, \tag{2.24}$$

- two light jets and a charged lepton:

$$\nu_a \longrightarrow e u\bar{d}, \tag{2.25}$$

- and three lighter neutrinos:

$$\nu_a \longrightarrow \nu_b \nu_c \nu_d. \tag{2.26}$$

2.4 Generation of neutrino masses

With the purpose of illustrating how neutrino masses can be generated, we will restrict to scenarios preserving the local symmetries of the Standard Model, provided so far there is no evidence of new fundamental forces. The SM local group fixes only the gauge bosons of the framework, while the fermion and scalar contents have to be chosen somewhat arbitrarily. Then, one can conjecture extra fermions or Higgs bosons so that the new physics model predicts massive neutrinos.

2.4.1 Right-handed neutrinos

The Standard Model contains left- and right-handed components of all fermions except neutrinos. One can choose to include right-handed neutrinos N (with n families), so that the chirality of neutrinos behaves in a similar manner as for the rest of the SM particles. Only left-handed particles take part of the weak interactions, and thus N must be a singlet under $SU(2)_L$. Moreover, because neutrinos are chargeless, N would also be a singlet under $U(1)_Y$. In summary, N has no renormalizable interactions with the SM gauge bosons; we say that it is a *sterile* neutrino (accordingly, the SM neutrinos are also known as *active* neutrinos).

The main aspect of insisting on treating N in the same footing as the rest of the SM fermions is that it allows us to generate neutrino mass terms through the Higgs mechanism. Indeed, when N is included in the field content, the following Yukawa interaction takes place:

$$\mathcal{L} = -f\, \overline{\ell_L} \widetilde{\phi}\, N + h.c., \tag{2.27}$$

where families indices have been omitted for simplicity, f is a Yukawa coupling matrix and $\widetilde{\psi} = i\sigma_2 \psi^*$. After spontaneous symmetry breaking, the SM doublet

develops a VEV and a Dirac mass term for the neutrinos is dynamically induced:

$$M_D = fv. \tag{2.28}$$

Moreover, we can also write a Majorana mass term, that reads:

$$\mathcal{L}_{bare} = -\frac{1}{2} M_M \, \overline{N} N^c, \tag{2.29}$$

where M_M is a bare mass matrix. Once again we have omitted families indices. Consequently, the neutrino mass matrix becomes

$$\mathcal{L}_{mass} = -\frac{1}{2} \begin{pmatrix} \overline{\nu_L} & \overline{N^c} \end{pmatrix} \begin{pmatrix} 0 & M_D \\ M_D^t & M_M \end{pmatrix} \begin{pmatrix} \nu_L^c \\ N \end{pmatrix}. \tag{2.30}$$

After diagonalisation, $3+n$ Majorana eigenvalues appear[3]. In the particular case in which $M_M \gg M_D$, the masses of the active neutrinos are given by $m_1 \approx M_D^2/M_M$, which of course is very suppressed, while heavy neutrinos have a mass $m_2 \approx M_M$. Because a heavy M_M pulls down the masses of the active neutrinos while rising the masses of the sterile neutrinos, this mechanism is commonly known as *seesaw*. (There are several seesaw models; the one just described is referred as *type-I* [45–47]).

Depending of the values of the Majorana mass matrix, several scenarios arise. $M_M \sim 10^{14}$ GeV leads to very heavy sterile neutrinos, but the mass of the active neutrinos (which should be below the eV scale) are obtained with M_D at the electroweak scale (that is, Yukawa couplings of order 1).

On the other hand, M_M can also lie at or below the electroweak scale if the Yukawa couplings f are very fine-tuned (for instance, $M_M = 100$ GeV would require $f \sim 10^{-7}$). In that case, the sterile neutrinos could be at the reach of the LHC or even low energy experiments. In fact, several anomalies in short-baseline oscillation experiments have been reported (see Ref. [48] for a review), which could lead to the existence of a sterile neutrino in the eV range [49].

Finally, M_M could be zero. Then, if $n = 3$, neutrinos are Dirac particles because the right-handed neutrinos could be combined with the left-handed neutrinos to form Dirac spinors. This means that there are no additional particles in the model, but rather N constitute the right-handed components of the SM neutrinos. There would be only three neutrinos and M_D would describe their mass. In this scenario, the Yukawa couplings f need to be very suppressed ($f \sim 10^{-12}$) so that the eigenvalues

[3] Each N gives mass to a left-handed neutrino, which implies that at least $n = 2$ families of N are needed in order to reproduce the observed values of the neutrino mass splittings. In that case, the lightest active neutrino would be massless.

of M_D are lighter than 0.1 eV. However, for the moment there is no fundamental reason, like a gauge symmetry, forbidding an explicit Majorana mass term.

2.4.2 Adding scalar fields

Without adding new fermionic degrees of freedom, we cannot generate Dirac neutrino masses, and only Majorana masses are possible.

Let us begin studying this scenario within an EFT framework. In Chapter 1 we constructed an effective theory with the SM field content and local symmetries, called SMEFT. However, in the Standard Model there is no actual theoretical argument to enforce the global symmetries, like lepton or baryon number; they were there just by accident. So, unless someday we come upon a strong reason for keeping global symmetries, we might as well avoid them when considering the possible operators of the SMEFT. As a matter of fact, the only dimension-five effective interaction given by the SMEFT breaks lepton number in two units [28]. This operator, now called Weinberg operator, involves a lepton bilinear and two units of the SM Higgs doublet:

$$\mathcal{O}_W^{(5)} = (\overline{\widetilde{\ell_L}\phi})(\widetilde{\phi}^\dagger \ell_L). \tag{2.31}$$

More importantly, the Weinberg operator generates a neutrino mass. In this context, neutrinos are predicted to be Majorana-type.

Of course, this effective Lagrangian can be realised with an appropriate enlargement of the scalar sector. Just as an illustration, here we restrict to simple models introducing only one scalar that breaks lepton number. In order to give the scalars some lepton number, we need them to couple to a lepton bilinear. But the only lepton bilinears with a net quantum number are those composed by either two leptons or by two antileptons, otherwise they will carry a vanishing lepton number. Hence, there are two possibilities. First, by making use of left-handed leptons, transforming under $SU(2)_L \times U(1)_Y$ as

$$\ell_L \ell_L \sim (1/2, -1/2) \times (1/2, -1/2) = (0, -1) + (1, -1), \tag{2.32}$$

we see that we can couple a singly-charged singlet or a triplet, both with hypercharge +1. On the other hand, if we consider right-handed charged leptons we get a lepton bilinear that transforms as

$$e_R e_R \sim (0, -1) \times (0, -1) = (0, -2). \tag{2.33}$$

This lepton bilinear can couple with a doubly-charged singlet.

For instance, the addition of a triplet leads to the scenario commonly known as

seesaw type-II [50–54]. The Yukawa interactions with leptons reads

$$\mathcal{L} = -f_{ab}\,\overline{\widetilde{\ell}_{La}}\,\chi\,\ell_{Lb} + h.c., \tag{2.34}$$

where the triplet χ is in its 2×2 matrix representation and the Yukawa coupling f_{ab} is symmetric. Because of this interaction, χ carries a net lepton number. The potential is given by:

$$\begin{aligned} V = -m_\phi^2|\phi|^2 + m_\chi^2\mathrm{Tr}(\chi^\dagger\chi) + \lambda_\phi|\phi|^4 + \lambda_\chi\mathrm{Tr}(\chi^\dagger\chi)^2 + \lambda'_\chi\mathrm{Tr}[(\chi^\dagger\chi)^2] \\ +\lambda_{\phi\chi}|\phi|^2\mathrm{Tr}(\chi^\dagger\chi) + \lambda'_{\phi\chi}\phi^\dagger\chi\chi^\dagger\phi + (\mu\phi^\dagger\chi i\sigma_2\phi^* + h.c.). \end{aligned} \tag{2.35}$$

After spontaneous symmetry breaking, not only the SM scalar acquires a VEV, but also does χ; we denote the VEV of the triplet by v_χ. In particular, v_χ breaks lepton number in two units and induces a Majorana mass term through Eq. (2.34):

$$M = f_{ab}\frac{v_\chi}{\sqrt{2}}. \tag{2.36}$$

Interestingly enough, because of the trilinear term in the potential, v_χ can be expressed in terms of v with $v_\chi = \mu v^2/m_\chi^2$. Accordingly, this simple model would explain the smallness of neutrino masses when the triplet is massive enough. For $\mu \sim 1$ TeV and $f_{ab} \sim 1$, the mass of the triplet should be above the 10^8 GeV scale, but this would make it well beyond the reach of current experiments.

2.5 Open questions regarding neutrino masses

The thesis presented in these pages attempts to account for several implications of the massive nature of neutrinos.

The most straightforward topic is related to the mechanism responsible for giving a mass to neutrinos. A great amount of models have been designed for this purpose but they typically include new fields or fundamental symmetries of nature; so far none of them has been experimentally confirmed. Moreover, although we *know* neutrinos are massive, we are still lacking of a precise numerical characterisation of the variables of the neutrino mass matrix, namely the neutrino mixing parameters. While measurements of some of these parameters are rapidly being improved, others still show large uncertainties or are even completely undetermined. Such is the case of the mass of the lightest neutrino and, if neutrinos are Majorana, the two Majorana phases.

A more complete knowledge of the numerical values of the entries of the neutrino mass matrix would lead to possible realisations of the underlying flavour theory. Therefore, instead of building new models, one could adopt a more modest approach

and look for patterns of neutrino masses; these would then give relations among the neutrino mixing parameters that could be tested in the laboratory. Among the various patterns one could imagine, Majorana mass matrices with some vanishing entries, called textures zeros, show interesting prospects. We study the case of textures with two zeros in Chapter 3.

Another fundamental question that needs to be addressed is whether neutrinos are Majorana particles. The experiment that is able to test this possibility searches for neutrinoless double beta decay. In its simplest realisation (within the SMEFT framework), the neutrino emitted by one beta decay is reabsorbed as an antineutrino by the other beta decay; this is only possible if the chirality is flipped in mid flight, and this implies that the process is proportional to the neutrino mass, which might be very suppressed. In fact, the inverse relation is also true: if neutrinoless double beta decay is observed, a Majorana mass term can always be generated at the quantum level with a $0\nu\beta\beta$-like diagram [55]. In Chapter 4 we build a model of neutrino masses, with the aim of inducing a testable neutrinoless double beta decay rate. The new ingredients, introduced by the model, consist of additional scalars, one of which is responsible for breaking lepton number.

In fact, multiple models of Majorana neutrino masses are based on new LNV scalars. The simplest instances of these models, like seesaw scenarios or the Zee-Babu model, require scalars whose quantum numbers are determined by how they couple to the SM lepton bilinears. In some cases, these interactions give signatures so far not explored at particle colliders. In Chapter 5 we study the prospects for new strategies designed for probing singly- and doubly-charged LNV scalars at the LHC.

Finally, we address the possibility that neutrino masses are of Dirac type, induced by the inclusion of right-handed neutrinos. Moreover, one can motivate different scenarios in which additional heavy fields are introduced. If there is a decoupling of the heavy fields, the resulting EFT describing low energy physics is the SMEFT extended with the right-handed neutrino. This new EFT is called νSMEFT and would help us gain a broader knowledge of possible new physics descriptions. In Chapter 6 we study how to set constraints to the parameters of different operators within this framework. Some operators remain unbounded and, accordingly, new strategies are to be designed in order to look for new physics in those directions. As an illustration, we propose one such analysis in searches of new rare top decays.

CHAPTER 3

Texture zeros

In the recent years, significant progress has been achieved in measuring the neutrino oscillation parameters. For instance, $\sin^2\theta_{13}$ is known with good accuracy only nine years after the first observation of its non-vanishing value [56]. Moreover, the absolute values of the neutrino mass splittings are well determined, and so is $\sin^2\theta_{12}$. Current open questions include the neutrino mass ordering, the octant problem regarding the atmospheric angle and the value of the Dirac CP phase, δ. However, the latest global analyses on oscillation parameters suggest that the first two of these issues are on the verge of being solved, while δ is gradually being constrained [57]. Other type of experiments could shed light on the parameters of the neutrino mass matrix in the upcoming years. For instance, great efforts have been made in the direction of measuring neutrinoless double beta decay. Although so far there has been no more than null results, if neutrinoless double beta decay is observed in the near future, we will obtain a great deal of information regarding the scale of the neutrino masses. However, and despite all these great achievements, the two remaining phases, provided neutrinos are Majorana-type, seem to be hardly measurable. Indeed, Majorana phases can be looked for in CP violating processes, such as neutrino-anti neutrino oscillation. However, this process is very rare [58]. Thus a complete numerical description of the Majorana neutrino mass matrix is not expected to be achieved in the imminent future.

Traditionally, physicists would try to find models that succeed in explaining the mechanism responsible for neutrino masses. They typically include several new massive fields or symmetries, like a S_3 permutation or a $\mu - \tau$ symmetry [59–61]. In some cases these symmetries are further dynamically broken, as it would be the case if one desires to predict a small non-zero $\sin^2\theta_{13}$ [62, 63]. However, until experimental data give us a more complete knowledge of the neutrino parameters, we can look for patterns that help to arrive to a better theoretical comprehension of the neutrino mass matrix. These patterns would give relations between the parameters

that can be confronted with experimental data. Moreover, they might have a hidden fundamental origin which would lead to the building of the flavor theory.

In this chapter we will discuss patterns of zeros in the neutrino mass matrix, which are simply called texture zeros [64]. There are several ways to implement texture zeros. For instance, one could imagine an underlying theory whose additional symmetries are such that impose zero values in some entries of the neutrino mass matrix. Typically, these symmetries are based on Abelian groups. For instance, in Refs. [65, 66], the different textures were realised with discrete Z_n cyclic symmetry, where the dimension n depends on the specific texture considered. In Ref. [67] the authors constructed the minimal Abelian symmetry realisations of two-zero textures. Continuous Abelian symmetries were also considered, as in Ref. [68] where a $L_\mu - L_\tau$ symmetry was softly broken in the context of a seesaw model with three right-handed neutrinos. Other possible symmetry realisations were obtained with A_4 [69–71] or S_3 permutation groups [72].

In the following section we will present the details of textures with two zeros.

3.1 Two-zero textures

Texture zeros are matrices with some number of vanishing matrix elements. Here we will concentrate on the Majorana neutrino mass matrix with only three families of light neutrinos, and use the parametrisation of the neutrino mixing matrix in Eq. (2.9) and Eq. (2.7). Then, the matrix is symmetric with six independent complex matrix elements. Zeros in pairs of symmetric elements are counted only once. For a generic n-zero texture, there are $\binom{6}{n} = \frac{6!}{n!(6-n)!}$ possible ways of placing n zeros in six matrix entries. Since the neutrino mass matrix is a complex matrix, each texture gives two phenomenological relations among the parameters of the model. In fact, when $M_{ab} = 0$ holds, we get the following complex constraint:

$$U_{a1}\, U_{b1}\, m_1\, e^{i\alpha/2} + U_{a2}\, U_{b2}\, m_2\, e^{i\beta/2} + U_{a3}\, U_{b3}\, m_3 = 0. \tag{3.1}$$

We can then use these relationships to explore the parameter space. For instance, the case of one-zero textures has been studied in the literature [73, 74]. All of the six possible matrices are compatible with data. But, as a matter of fact, two conditions give too weak constraints. For a Majorana neutrino mass matrix that depends on nine parameters, five of which are well measured, one-zero textures leave two parameters unbounded. So, should we be interested in making predictions in the context of one-zero textures, we will need to introduce more constraints. One such approach would be to additionally consider a vanishing trace [75, 76] or

determinant [77]. In this chapter, though, we take a different approach.

Here, we consider textures with two zeros. Two complex constraints allow us to make predictions for the still unobserved non-oscillation parameters, namely the mass of the lightest neutrino and the two Majorana phases. Hence, two-zero textures are of much interest.

There are 15 possible textures, which are grouped in classes A, B, C, D, E and F. Within each class, we can go from one texture to another by means of some transformation. For this reason, textures belonging to the same category give related constraints. Depending on the experimental data, they could also lead to similar phenomenological implications.

By the time two-zero textures were proposed [64], only classes A, B and C were allowed by experimental data. Hereafter these textures will be denoted by the term 'allowed'. They are defined as

$$\text{A1}: \begin{pmatrix} 0 & 0 & \times \\ 0 & \times & \times \\ \times & \times & \times \end{pmatrix}, \qquad \text{A2}: \begin{pmatrix} 0 & \times & 0 \\ \times & \times & \times \\ 0 & \times & \times \end{pmatrix}, \tag{3.2}$$

$$\text{B1}: \begin{pmatrix} \times & \times & 0 \\ \times & 0 & \times \\ 0 & \times & \times \end{pmatrix}, \quad \text{B2}: \begin{pmatrix} \times & 0 & \times \\ 0 & \times & \times \\ \times & \times & 0 \end{pmatrix}, \quad \text{B3}: \begin{pmatrix} \times & 0 & \times \\ 0 & 0 & \times \\ \times & \times & \times \end{pmatrix}, \quad \text{B4}: \begin{pmatrix} \times & \times & 0 \\ \times & \times & \times \\ 0 & \times & 0 \end{pmatrix}, \tag{3.3}$$

$$\text{C}: \begin{pmatrix} \times & \times & \times \\ \times & 0 & \times \\ \times & \times & 0 \end{pmatrix}. \tag{3.4}$$

As stated above, textures within the same category are connected by some kind of transformation [78]. For instance, it is straightforward to see that the A2 texture is obtained from A1 by interchanging rows 2 and 3 (and hence, because the neutrino mass matrix is symmetric, also columns 2 and 3). The same happens for textures B1 with B2, and B3 with B4. This transformation can be described by a permutation matrix[1]

$$P_{23} = \begin{pmatrix} 1 & 0 & 0 \\ 0 & 0 & 1 \\ 0 & 1 & 0 \end{pmatrix}, \text{ with } \qquad M_\nu^{\text{A2}} = P_{23} M_\nu^{\text{A1}} P_{23}. \tag{3.5}$$

Then the PMNS matrix associated with texture A2 is obtained from that of texture A1 following $U^{A2}_{PMNS} = P_{23} U^{A1}_{PMNS}$. Using the standard parametrisation of the neutrino mass matrix, outlined in Chapter 2, the following transformation for the

[1] We have written the transformation in terms of A1 and A2 just to illustrate this computation with the aid of labels. The transformation for textures B is completely equivalent.

oscillation parameters is easily obtained:

$$\sin^2\theta_{23} \longrightarrow 1-\sin^2\theta_{23}, \qquad \delta \longrightarrow \delta + 180^\circ, \tag{3.6}$$

while the rest of the oscillation parameters remains invariant. We will see in the upcoming sections the impact of this transformation on the textures of the same category.

On the other hand, the textures incompatible with data, which we are going to denote by the term 'excluded', are

$$\text{D1}: \begin{pmatrix} \times & \times & \times \\ \times & 0 & 0 \\ \times & 0 & \times \end{pmatrix}, \qquad \text{D2}: \begin{pmatrix} \times & \times & \times \\ \times & \times & 0 \\ \times & 0 & 0 \end{pmatrix}, \tag{3.7}$$

$$\text{E1}: \begin{pmatrix} 0 & \times & \times \\ \times & 0 & \times \\ \times & \times & \times \end{pmatrix}, \qquad \text{E2}: \begin{pmatrix} 0 & \times & \times \\ \times & \times & \times \\ \times & \times & 0 \end{pmatrix}, \qquad \text{E3}: \begin{pmatrix} 0 & \times & \times \\ \times & \times & 0 \\ \times & 0 & \times \end{pmatrix}, \tag{3.8}$$

$$\text{F1}: \begin{pmatrix} \times & 0 & 0 \\ 0 & \times & \times \\ 0 & \times & \times \end{pmatrix}, \qquad \text{F2}: \begin{pmatrix} \times & 0 & \times \\ 0 & \times & 0 \\ \times & 0 & \times \end{pmatrix}, \qquad \text{F3}: \begin{pmatrix} \times & \times & 0 \\ \times & \times & 0 \\ 0 & 0 & \times \end{pmatrix}. \tag{3.9}$$

Significant efforts have been made to find analytical solutions to the constraints given by each texture in terms of the oscillation parameters. For instance, in Ref. [78] the authors found, after expanding for small values of $\sin^2\theta_{13}$, the scale of the neutrino mass in textures A to be of order $\sqrt{\Delta m^2_{31}} \sim$ meV. Furthermore, textures of category B would give very degenerated neutrino masses and Majorana phases highly correlated with the Dirac phase, following $\alpha \sim \beta \sim \delta - 90^\circ$. For the case of texture C-NO, the authors in Ref. [66] found $\sin^2\theta_{23} = 0.5$ with extremely high degree of accuracy, using the experimental information on $\sin^2\theta_{13}$. Moreover, they predicted the lightest neutrino to show a weaker mass or, in other words, a degenerated neutrino mass spectrum. In the case of the 'excluded' textures it is easy to find solutions, all of which are incompatible with data. For instance, textures F1 and F2 can be obtained by setting $\sin\theta_{13} = 0$. Likewise, $\sin\theta_{23} = 0$ leads to textures F2 and F3. Textures of category D cannot simultaneously give small $\sin^2\theta_{13}$ and large $\sin^2\theta_{23}$ [79].

Here we will solve the equations in a numerical and systematic manner.

3.2 Fitting the constraints

As said in Chapter 2, several collaborations have fitted all available neutrino oscillation data. Some of them, like nuFIT [80] and Neutrino Global Fit [44], have released their 1D and 2D χ^2 profiles, as function of the Dirac δ phase and the five oscillation parameters, $\sin^2\theta_{13}$, $\sin^2\theta_{12}$, $\sin^2\theta_{23}$, Δm^2_{21} and Δm^2_{31} (Δm^2_{32}). Here we will make use of the most updated χ^2 functions provided by the nuFIT collaboration [81]. They give their results with or without the inclusion of the atmospheric neutrino data provided by the Super-Kamiokande collaboration [82]. In the study presented here[2], we will take into consideration the Super-Kamiokande results.

As things stand, there is a great preference for normal mass ordering over inverted ordering. In fact, the minimum value of the χ^2 function in the IO relative to the NO is $\Delta\chi^2_{\text{min}} = 10.4$. We have also looked at all 2D profiles and concluded that all correlations are small except in the $\sin^2\theta_{23} - \delta$ plane, for which the octant ambiguity has not been resolved yet. Hence, we are safe to consider the rest of the parameters described by their 1D profiles and to approximately construct the χ^2 function describing data as

$$\chi^2_{\text{data}} \approx \Delta\chi^2(s^2_{23}, \delta) + \Delta\chi^2(s^2_{13}) + \Delta\chi^2(s^2_{12}) + \Delta\chi^2(\Delta m^2_{21}) + \Delta\chi^2(\Delta m^2_{31}) - 4\chi^2_{\text{min}}. \tag{3.10}$$

in NO, and substituting $\Delta\chi^2(\Delta m^2_{31})$ for $\Delta\chi^2(\Delta m^2_{32})$ in IO. Each profile gives its values relative to χ^2_{min}; there are five profiles so we needed to subtract four times the minimum value of χ^2 so that the global function is relative to only one unit of χ^2_{min}.

We have the data and now we would like to impose the constraints. We can do so with Lagrange multipliers. In the particular context of two-zero textures, this is realised by

$$\chi^2 = \chi^2_{\text{data}} + \frac{1}{\lambda_1^2}|M_{ab}|^2 + \frac{1}{\lambda_2^2}|M_{cd}|^2, \tag{3.11}$$

where the two entries of the neutrino mass matrix, M_{ab} and M_{cd} are forced to be zero for values of $\lambda_{1,2} \longrightarrow 0$. In practice, one cannot exactly set $\lambda = 0$, but as long as $\lambda_1 \ll |M_{ab}|$ (and $\lambda_2 \ll |M_{cd}|$), the new terms give sizeable contributions and the results are guaranteed. On the other hand, when $\lambda \longrightarrow \infty$ the new terms vanish, no condition is enforced, and we are left with just the original data.

Furthermore, when the values of the Lagrange multipliers are just below those of the matrix elements, $\lambda_1 < |M_{ab}|$ and $\lambda_2 < |M_{cd}|$, the constraints are only approximately enforced. This will permit us to revisit the case of the excluded two-zero textures and study whether they show interesting prospects in those cases in which

[2]The work described in this chapter was originally published by the author of this thesis and collaborators in Ref. [83].

	data	A1	A2	B1	B2	B3	B4	C
NO	0	2.7	1.9	3.6	1.5	3.7	1.3	3
IO	10.4	-	-	10.7	15.7	10.7	15.4	12.4

Table 3.1: Minimum value of the complete χ^2 function obtained for the data (first column) and for each 'allowed' texture (columns $2-8$). Values in the IO row include $\chi^2_{data} = 10.4$ and therefore are typically larger.

the textures are not exact.

Before moving on to obtaining results, it is important to note that this technique is completely general and can be applied to any interesting constraint on the neutrino mass matrix elements. For instance, we could demand the neutrino mass matrix to be traceless by adding a term $\frac{1}{\lambda^2}|M_{ee}+M_{\mu\mu}+M_{\tau\tau}|^2$, which would give two additional conditions on the neutrino parameters. Moreover, the method needs no previous algebraic work, which makes it very appealing for numerical calculations.

3.3 Allowed textures

We are going to work with textures that can accommodate the experimental data on the oscillation parameters. The first thing to check is the value at the global minimum of the complete χ^2 function involving data along with the theoretical condition. For this, we vary all oscillation parameters in their 3σ values, the Majorana phases for all possible angles and with the mass of the lightest neutrino being $m_\ell < 1$ eV. In Table 3.1 we show the values obtained for the 'allowed' textures, while in Table 3.2 we give the same but for the 'excluded' textures. In those cases where χ^2_{min} is larger than 9 relative to the minimum χ^2 of the data alone (from now on called simply χ^2_{data}), the predictions of the constraint are at least 3σ away from the best fit of the data *in the ordering in consideration*, and hence texture and data are not compatible. For instance, texture C-IO shows a $\chi^2_{min} - \chi^2_{data} = 2.4$ which indicates that is $\sim 1.5\sigma$ away from the best value of the data alone. In this section we will study the 'allowed' textures, all of which still meet the previous condition. However, note that, when also performing the minimisation respect to the ordering, almost all textures in the IO become incompatible with data, because of the stringent value $(\chi^2_{data})_{\text{IO}} = 10.4$.

Notice that the texture F1 shows small values of χ^2_{min} in both orderings. However, these results correspond to the limit $m_\ell \longrightarrow 1$ eV, the highest value of the range considered for the mass of the lightest neutrino, which is in tension with cosmological data. As soon as we demand m_ℓ to take lower values, $(\chi^2_{min})_{F1}$ grows abruptly and texture F1 becomes incompatible with the experimental data again. We will study

	data	D1	D2	E1	E2	E3	F1	F2	F2
NO	0	> 100	> 100	> 100	> 100	> 100	3.4	~ 60	~ 40
IO	10.4	> 100	> 100	> 100	> 100	> 100	13.8	~ 50	~ 50

Table 3.2: Minimum value of the complete χ^2 function obtained for the data (first column) and for each 'excluded' texture (columns $2-9$). As before, values in the IO row include $\chi^2_{data} = 10.4$.

the case of texture F1 in more detail in the next section.

Next off, we compare the constraints with the nuFIT data, which will assist to estimate the size of the resulting parameter space. In the present circumstances, the less bounded parameters are $\sin^2\theta_{23}$ and, in particular, δ. Thus, we will show the constraints as a superposition over the data in the $\sin^2\theta_{23}-\delta$ plane. Furthermore, we will compute the predictions on the unknown parameters against δ. In order to build the superposition plots we turn off the pieces of the χ^2 functions regarding data and scan the $\sin^2\theta_{23}-\delta$ plane using the constraints alone. For each point $(\sin^2\theta_{23}, \delta)$ we minimise the χ^2 function with respect to the rest of the parameters. For this we make use of homemade routines in python with the differential evolution minimisation function of the `scipy` library. In order to get reliable results it is enough to take $\lambda_1 = \lambda_2 = 0.1$ meV, while using lower values does not improve the results. We have checked this by redoing some of our calculations with $\lambda_1 = \lambda_2 = 0.05$ meV. Consequently, we plot 1σ contours over the nuFIT data. The overlapping regions describe those points for which the constraint is compatible with the data.

Finally, we obtain the fit with the complete χ^2 function in the $\sin^2\theta_{23}-\delta$ plane, along with the predictions for the mass of the lightest neutrino and the two Majorana phases. Contours correspond to regions with 68%, 95% and 99.7% confidence level (CL). In two dimensions, this means $\chi^2-\chi^2_{min} = 2.3$, 5.99 and 11.83. Here, as stated before, χ^2_{min} denotes the global minimum obtained for the texture and ordering in consideration.

Before performing the explicit minimisation on every point of the plane of interest, it may be useful to carry out a scan of the complete parameter space with a nested sampling algorithm. This type of algorithms is very efficient in exploring the parameter space, and will give us information about what we should expect around the minimum. The particular code we have used for this purpose is `Multinest` [84, 85].

Textures A

Textures of class A require $M_{ee} = 0$ which is also the parameter that controls the standard neutrino exchange source of neutrinoless double beta decay. Any model

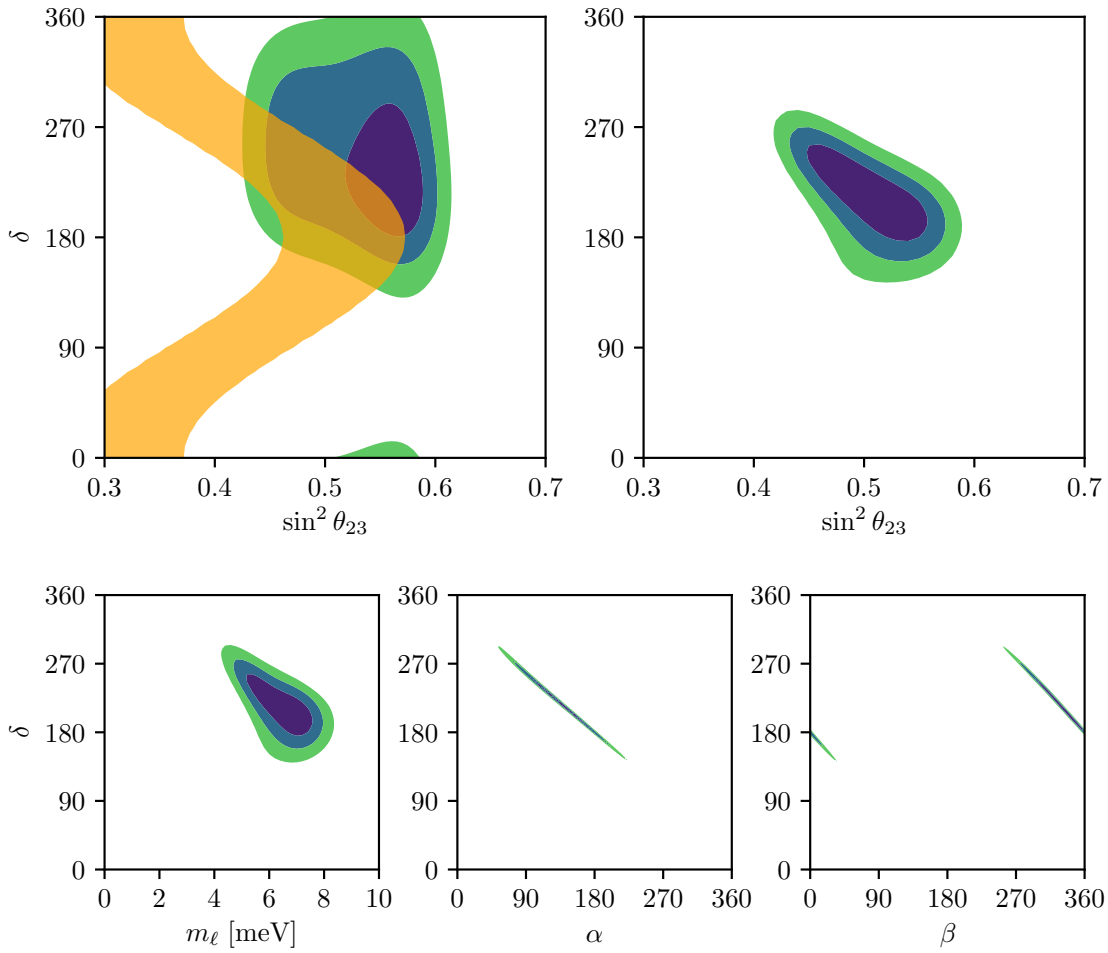

Figure 3.1: Results for the texture A1 in NO. Darker blue, blue and green colours correspond to 1σ, 2σ and 3σ contours. Upper left panel: 1σ contour of the constraint (yellow) superimposed over the contours of the data in the $\sin^2\theta_{23} - \delta$ plane. Upper right panel: contours of the fit, in the same plane as before. Lower left, central and right panels: contours of the fit for m_ℓ, α and β against δ.

whose neutrino mass matrix is described by a texture A will induce a very suppressed contribution to $0\nu\beta\beta$ through this mechanism. However this poses no problem as there could be other new physics mechanisms responsible for the production of a sizeable $0\nu\beta\beta$ decay rate.

Moreover, it is well known that M_{ee} in IO is bounded from below by neutrino oscillation data, with $M_{ee} > 10$ meV [86]. We have stated above that exact textures correspond to $M_{ab} < 0.1$ meV, which is clearly incompatible with this experimental bound. For this reason, class A is only allowed in the NO case.

In Figure 3.1 we present the results for the A1 texture following the methodology described above. The two upper plots depict the $\sin^2\theta_{23} - \delta$ plane. On the left we see what we expect to obtain when the constraint (yellow) is applied over the data and, on the right, the result after the minimisation of the complete χ^2. Darker blue, blue and green colours correspond to 1σ, 2σ and 3σ contours. Here, we are

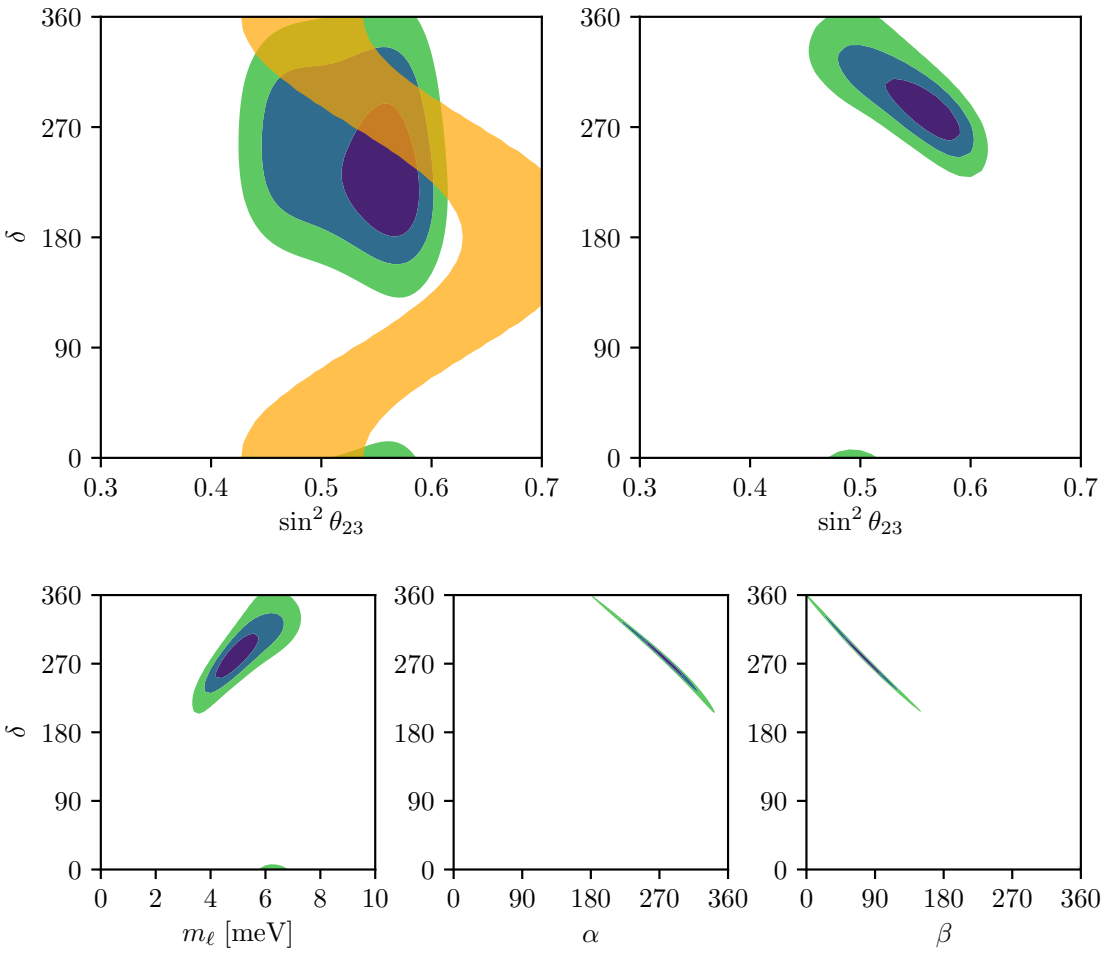

Figure 3.2: Same as Figure 3.1 but for the texture A2 in NO.

not performing a model comparison and therefore we always subtract the minimum value of the χ^2 obtained for the texture in consideration. For this reason, although $(\chi^2_{\text{min}})_{A1} = 2.7$, the plot still shows a 1σ region. Finally, the lower plots show the results for the mass of the lightest neutrino and the two Majorana phases. We see a large available parameter space, as the constraints from this class of textures show a great overlapping area respect to the data. In particular, m_ℓ takes values of order 1 meV while the three phases are strongly correlated.

Results for A2 texture are shown in Figure 3.2. In general, the predictions regarding the unknown parameters are qualitatively similar to those of A1. The values of $\sin^2\theta_{23}$ allowed by the constraint of the texture are shifted to the right, as suggested by the transformation in Eq. (3.6). Moreover, when compared with experimental data, the shift in the atmospheric angle translates into a prediction of δ closer to 270°, for which CP violation is maximal. The mass of the lightest neutrino remains of order 1 meV and the phases highly correlated.

Both textures give a low minimum value of χ^2. In particular, A2 has the lowest value of all textures. Moreover, when comparing to the model with no texture

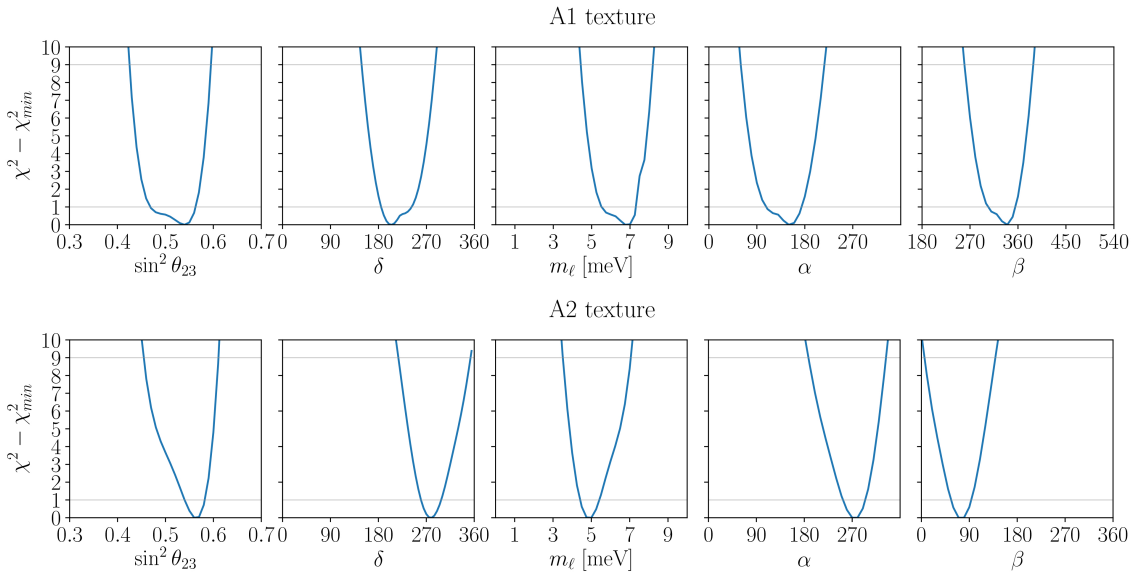

Figure 3.3: χ^2 profiles of $\sin^2\theta_{23}$, δ, m_ℓ, α and β for textures A1 (upper panel) and A2 (lower panel). Grey grid lines correspond to $\chi^2 = 1$ (1σ CL) and $\chi^2 = 9$ (3σ CL).

(only data) A2 is the only texture that still returns a 1σ region. Older versions of the global analyses of the data showed an octant problem [87], which consisted in the existence of two minimums, for $\sin^2\theta_{23} < 0.5$ and $\sin^2\theta_{23} > 0.5$. Since the constraints from A1 and A2 respectively lie on those regions, both textures were fairly as favoured (although A1 gave a somewhat smaller value of χ^2_{min}). As things stands regarding present data, the octant problem is starting to become resolved, with a preference for $\sin^2\theta_{23} > 0.5$. For these reasons, A2 is currently the most promising texture.

In Figure 3.3 we show χ^2 profiles for $\sin^2\theta_{23}$ and δ along with the unknown parameters. As in the 2D contour plots, the minimum value of χ^2 has been subtracted. The best fit values and intervals of 1σ and 3σ CL correspond to those points of the profile for which $\chi^2 = 0$, $\chi^2 = 1$ and $\chi^2 = 9$, respectively.

Textures B

All B textures show very similar predictions, as suggested by the overlap of the constraints over the data seen in Figure 3.4. In general, the results split into two main cases: those for which the constraint allows for values with $\sin^2\theta_{23} > 0.5$, and those where $\sin^2\theta_{23} < 0.5$ holds. When comparing to data, the former take smaller overall values of χ^2, while the latter ones give larger χ^2. In Figure 3.5 we show the results for texture B4-NO only, which has the lowest χ^2, as a paradigmatic case of textures B. The parameter space is highly constrained, as values of the phases are essentially fixed to $\delta = 270°$ and $\alpha = \beta = 180°$ in every class B texture. There are more subtle differences regarding the phases, but they only imply tiny deviations

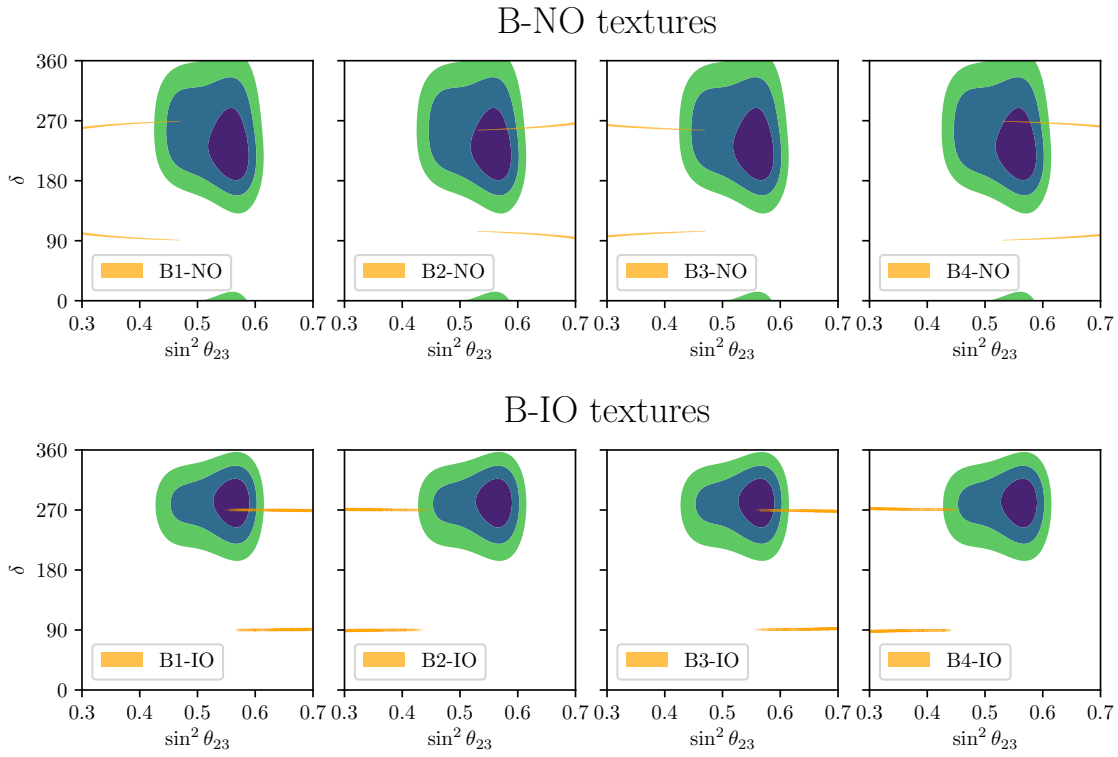

Figure 3.4: Constraints imposed by the B textures on the $\sin^2\theta_{23} - \delta$ plane. The upper panel correspond to textures B1, B2, B3 and B4 for NO, while in the lower panel we show the same but in the IO.

from these values and are expected by the transformation in Eq. (3.6).

Finally, the best value for the mass of the lightest neutrino can take values as low as $\sim$ 50 meV for textures B2-NO, B4-NO, B1-IO and B3-IO (see Figures 3.6 and 3.7). This is because the constraint from these textures overlaps well near the best fit of the data. At a scale of $\sim$ 50 meV, the mass splittings Δm^2_{21} and Δm^2_{31} are negligible compared to the mass of the lightest neutrino so that the three neutrinos are very degenerated.

On the other hand, the χ^2_{min} in the remaining B textures is obtained in the vicinity of $\sin^2\theta_{23} \approx 0.5$ which, in turn, correspond to large values of m_ℓ. For this reason, textures B1-NO, B3-NO, B2-IO and B4-IO show a larger lower bound on the mass of the lightest neutrino. Moreover, they might be in tension with Cosmology measurements of the absolute neutrino mass scale, defined as the sum of the masses of the mass of the three light neutrinos. Indeed, the authors of Ref. [88], combining CMB and baryonic acoustic oscillation data, obtained a 95% CL upper bound on the sum of the three neutrinos to be 0.151 eV. At this scale we can approximate the upper bound of the mass of the lightest neutrino to be $m_\ell \lesssim (m_1 + m_2 + m_3)/3 \lesssim 50$ meV, which lies below the preferred values of m_ℓ in B1-NO, B3-NO, B2-IO and B4-IO.

In summary, the predictions from class B are practically identical which makes textures within this class almost experimentally indiscernible.

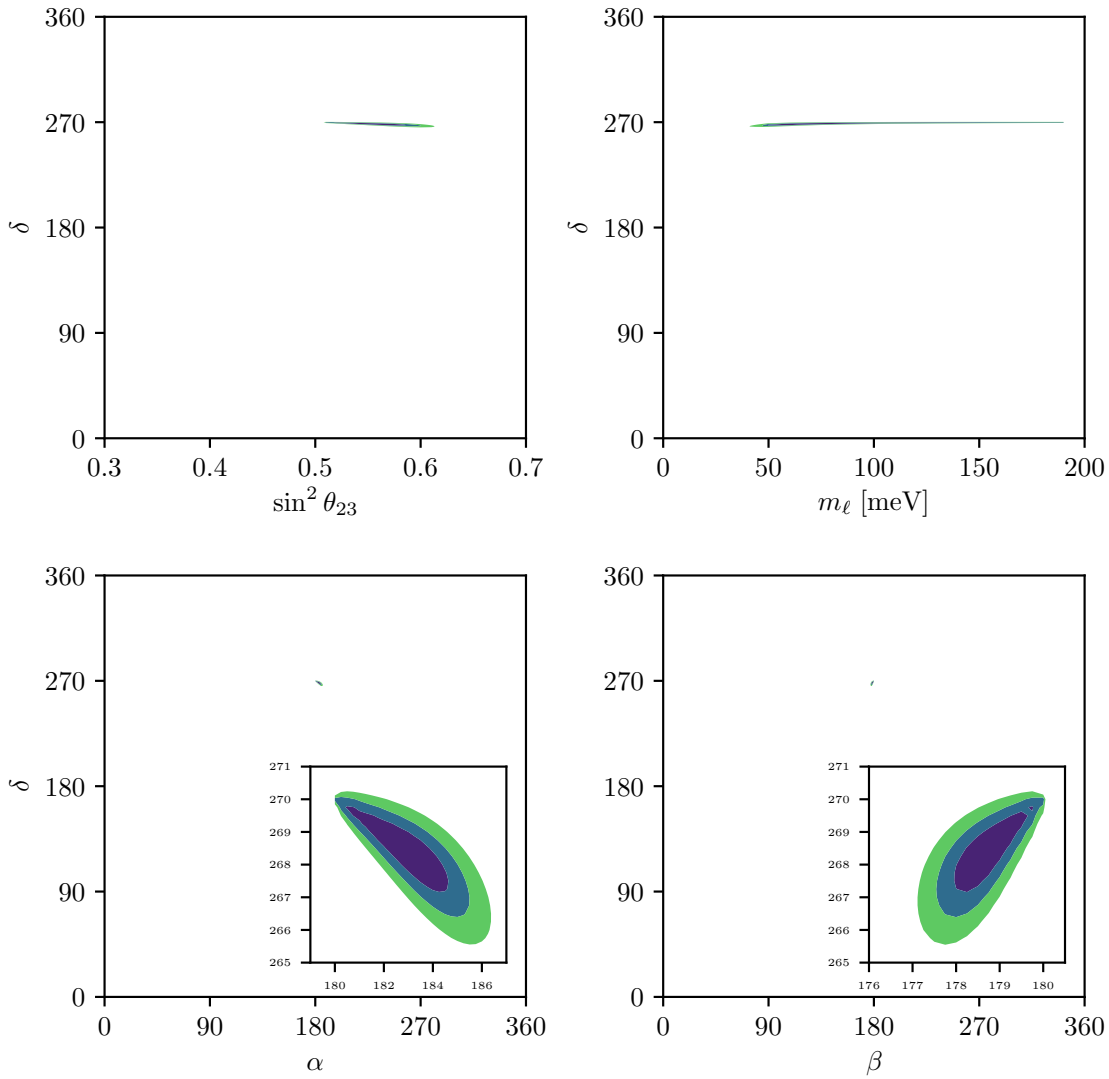

Figure 3.5: Results for the texture B4-NO, for $\sin^2\theta_{23}$, m_ℓ, α and β against δ.

Textures C

There is only one texture in this class. In NO, depicted in Figure 3.8, we see that the constraint demands $\sin^2\theta_{23} = 0.5$ with extremely high precision, as anticipated in Ref. [66]. Despite exhibiting relative low values of χ^2, the results avoid values near $\delta = 270°$ which is reached only for increasingly larger values of m_ℓ. This is the general behaviour, making texture C-NO to possibly be in tension with Cosmology data (see textures B). Finally, this texture fixes the values of the Majorana phases to be very closed to 180°.

On the other hand, C-IO shows an available parameter space slightly larger. For this reason, the predictions of the unknown parameters are somewhat less constrained. Results are collected in Figure 3.9. Another important improvement with respect to C-NO is that the mass of the lightest neutrino could take smaller values, as low as ~ 40 meV, so that it escapes from the bounds of Cosmology data. However

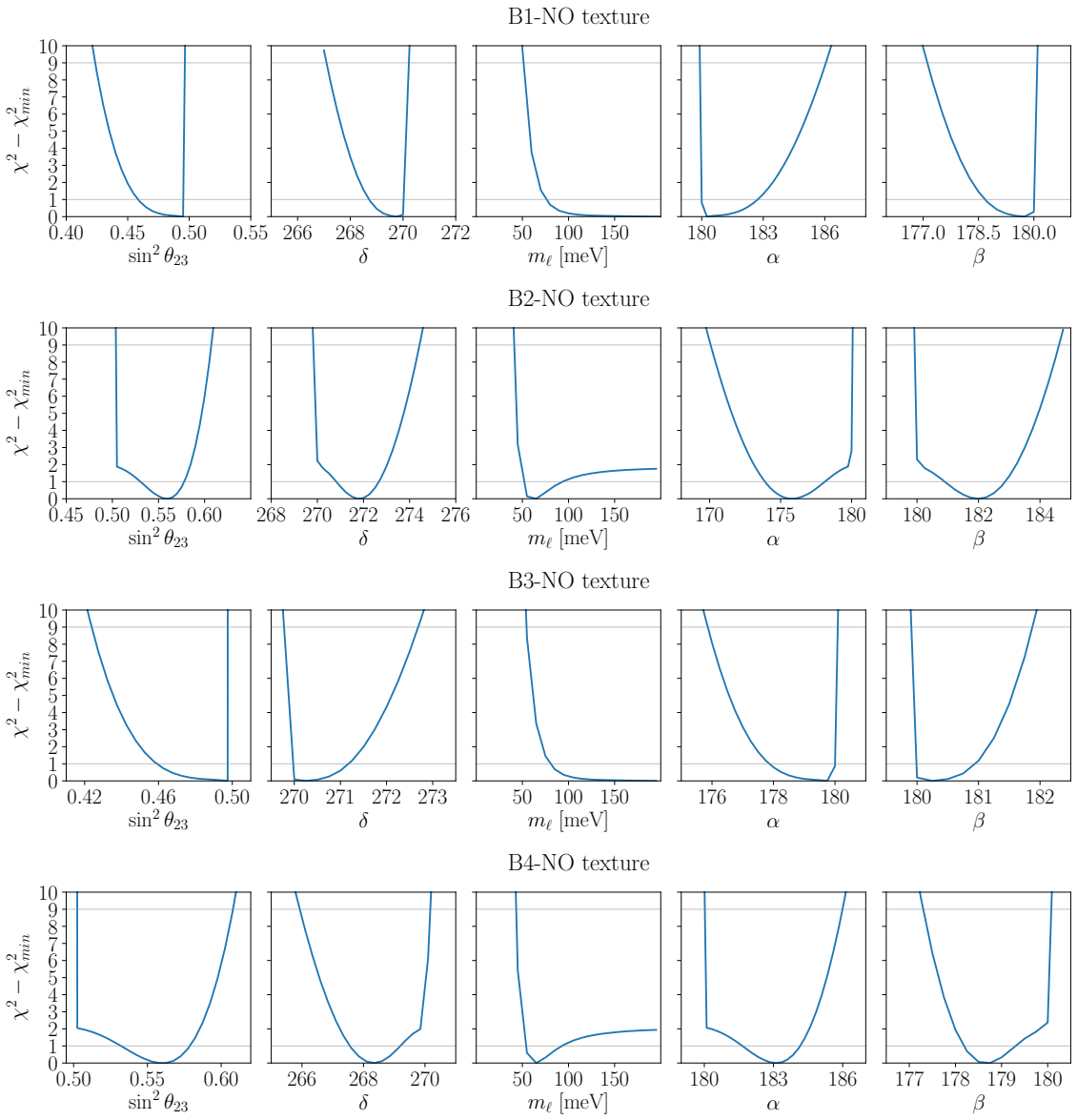

Figure 3.6: χ^2 profiles of $\sin^2\theta_{23}$, δ, m_ℓ, α and β for textures B1-NO, B2-NO, B3-NO and B4-NO. Grey grid lines correspond to $\chi^2 = 1$ (1σ CL) and $\chi^2 = 9$ (3σ CL).

it is important to keep in mind that, belonging to the inverted mass ordering, this texture still shows a large value of $\chi^2_{min} \approx 12$ when compared to the model with null hypothesis (only data).

3.4 Approximate textures

Exact texture zeros are very interesting from a theoretical point of view as they allow us to learn things about the neutrino mass matrix without developing any specific model. However, the details of an underlying theory could be such that the texture is not exact. For instance, this could happen if the symmetry that induces the texture is slightly broken, or when the neutrino mass matrix is proportional

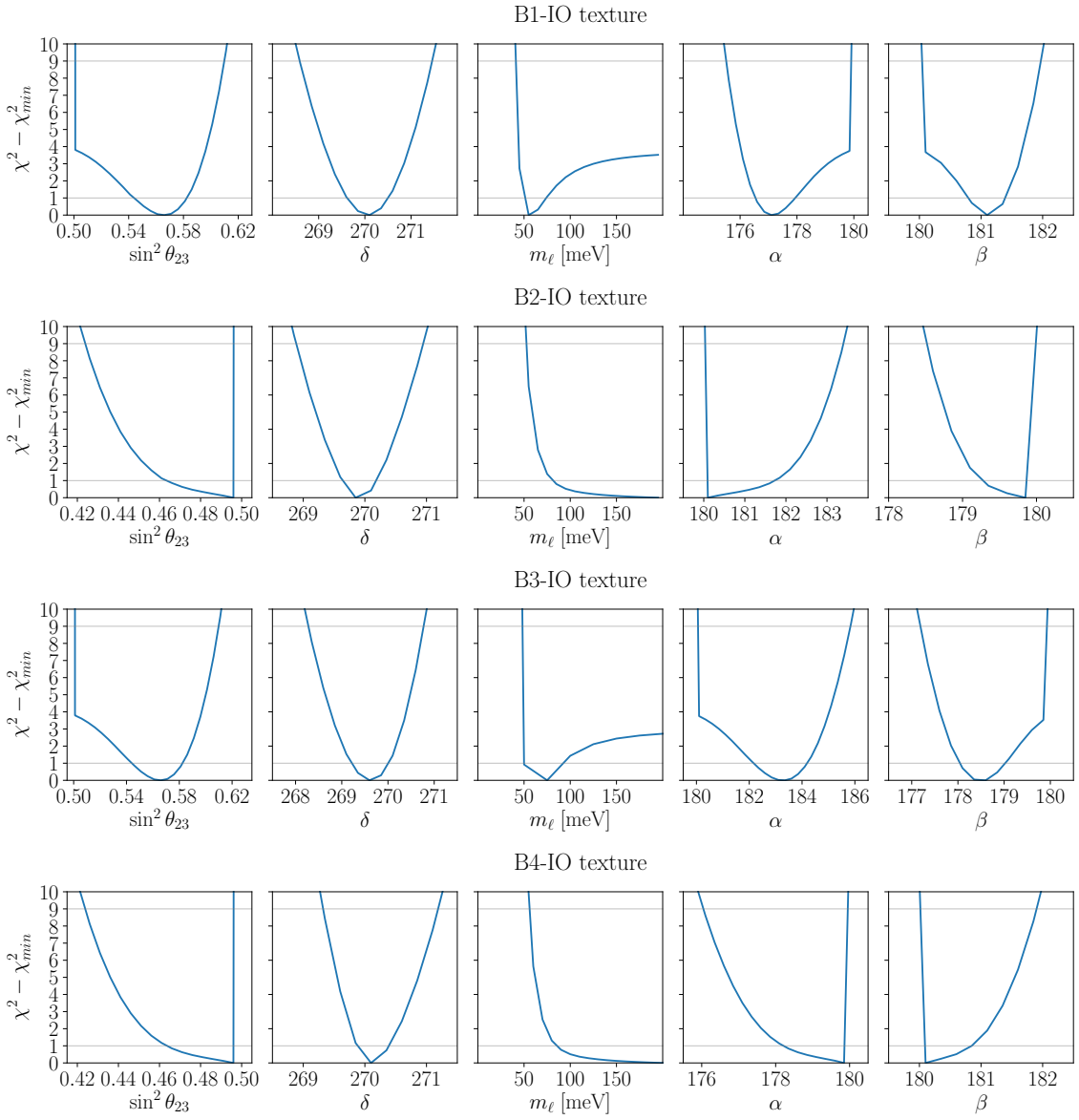

Figure 3.7: χ^2 profiles of $\sin^2\theta_{23}$, δ, m_ℓ, α and β for textures B1-IO, B2-IO, B3-IO and B4-IO. Grey grid lines correspond to $\chi^2 = 1$ (1σ CL) and $\chi^2 = 9$ (3σ CL).

to tiny non-vanishing couplings. The model presented in the next chapter is an illustration of this last case. Moreover, exact textures could get filled to some degree by radiative corrections [89]. Here we will study whether the results are stable even when textures are only approximate.

In the context of exact textures we have worked with $\lambda = 0.1$ meV which, in turn, only implied that $|M_{ab}|, |M_{cd}| < 0.1$ meV. We can relax this condition and demand $\lambda = 1$ meV. In order to check whether the main predictions of the textures survive we examine the paradigmatic case of class B textures, for which the available parameter space is highly constrained. In Figure 3.11 we compare the results obtained for the two different values of λ, concerning the B4-NO texture. It is clear that the parameter space is greatly enlarged, while the predictions are kept stable. Another

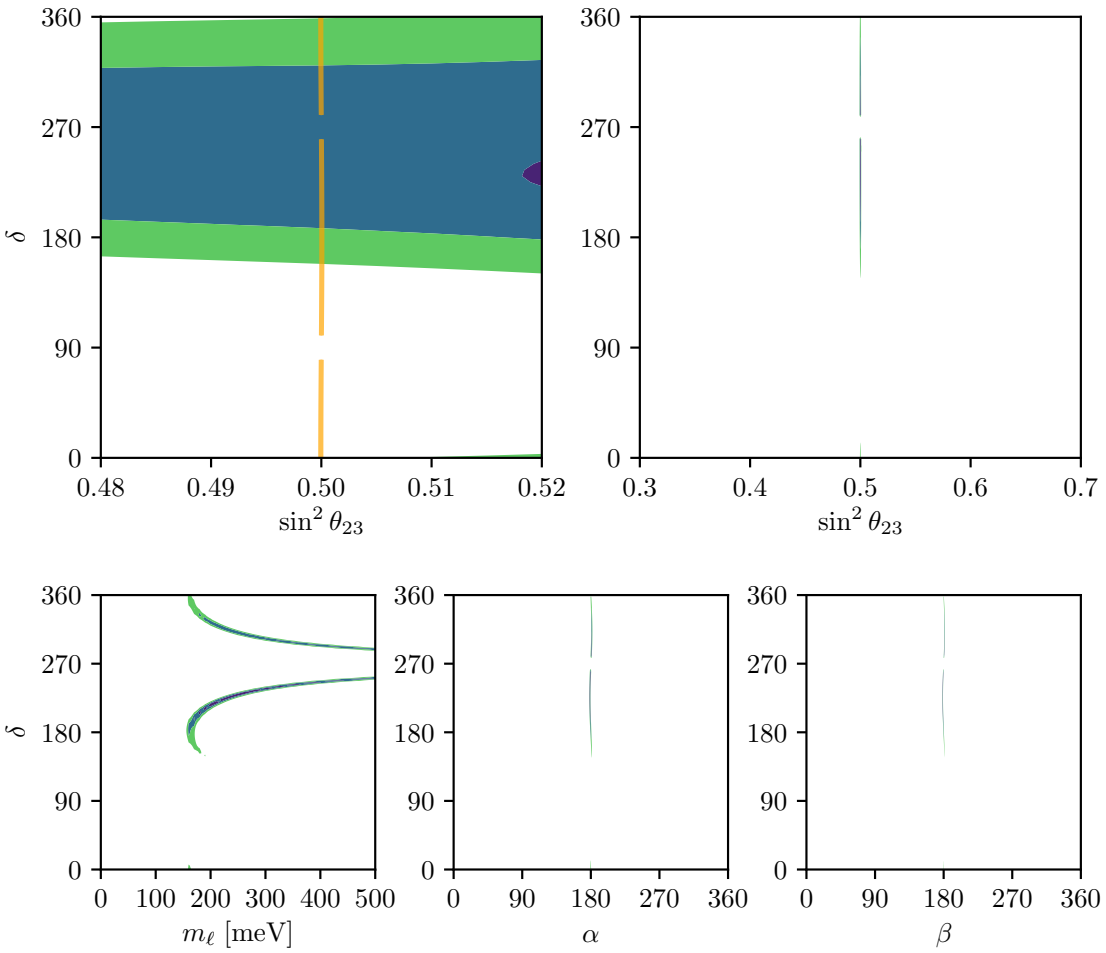

Figure 3.8: Same as Figure 3.1 but for the texture C in NO.

interesting feature one can check is the change of χ^2_{min} when the textures are only approximate. In such a case, the constraint overlaps with larger regions of the original data and one may expect that these regions could show lower values of χ^2. As an illustration, we have computed the values of χ^2_{min} (with $\lambda = 1$ meV) in the cases of A1 and A2 textures, and obtained 0.29 and 0.46, respectively. This is a great improvement respect to the scenario of exact textures and implies that both textures are still very promising.

Furthermore, by using the formalism of approximate texture, we can investigate what happens to the 'excluded' textures when the constraint gets relaxed. Because F1-NO has the lowest χ^2_{min} of all 'excluded' textures, it is only natural to consider it as a paradigmatic case of study. When applying the procedure described above to the texture F1-NO, with a relaxed condition ($\lambda = 1$ meV), we find that the constraint covers the whole oscillation parameter space. The constraint from the texture does not favour any particular values and hence the information about the oscillation parameters is given completely by the experimental data. Notwithstanding, the texture does give predictions on the unknown parameters. In Figure 3.12 we show

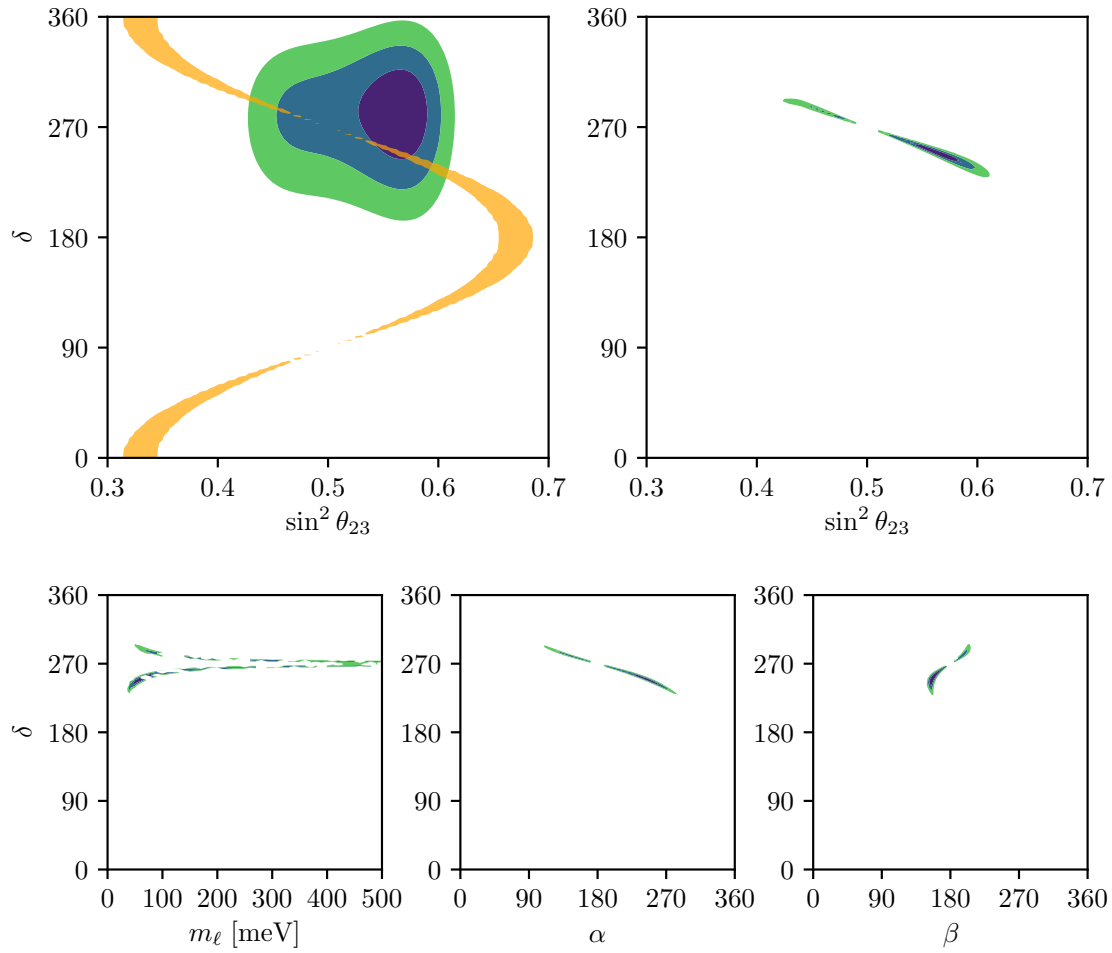

Figure 3.9: Same as Figure 3.1 but for the texture C in IO.

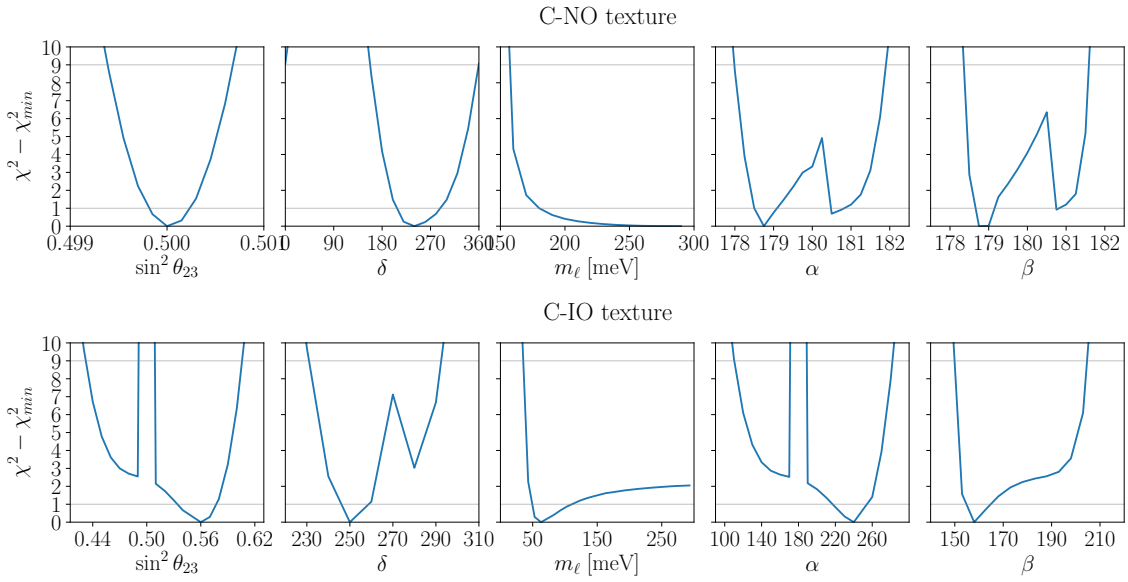

Figure 3.10: χ^2 profiles of $\sin^2\theta_{23}$, δ, m_ℓ, α and β for textures C-NO and C-IO. Grey grid lines correspond to $\chi^2 = 1$ (1σ CL) and $\chi^2 = 9$ (3σ CL).

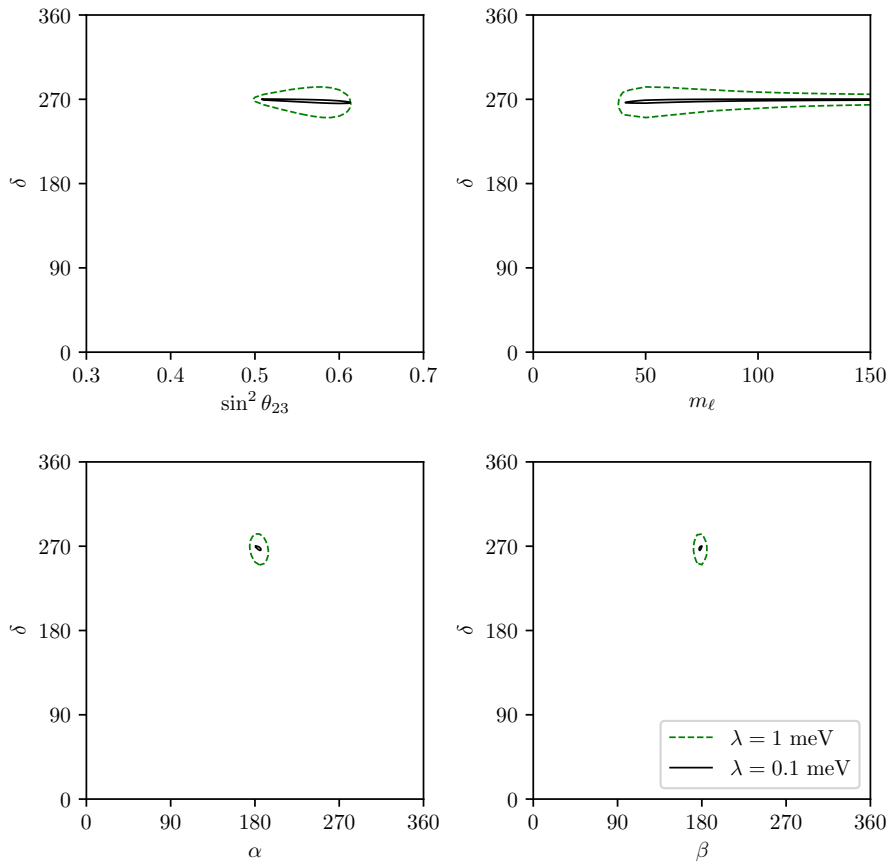

Figure 3.11: Predictions of the B4-NO case when the texture is only approximate. Contours represent the 3σ values. In black we show the results when the constraint is maximally enforced with $\lambda = 0.1$ meV, while in green the constraint is more relaxed, with $\lambda = 1$ meV.

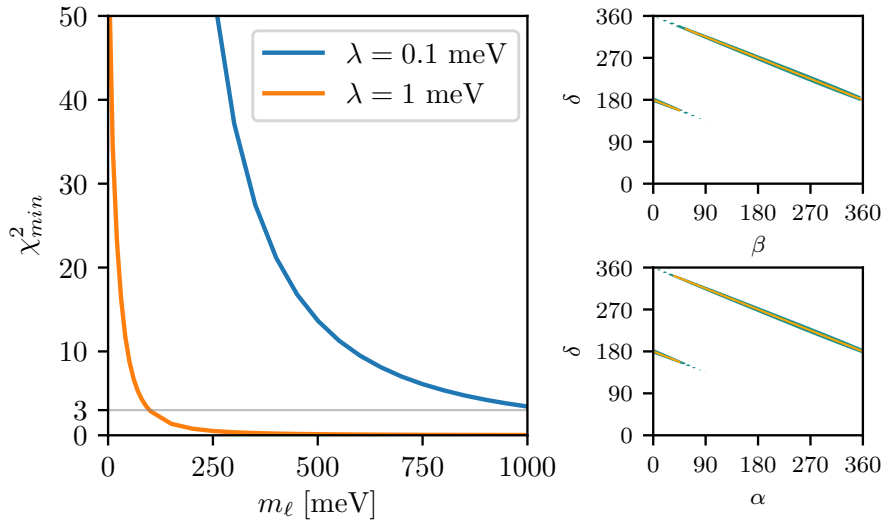

Figure 3.12: Predictions of the mass of the lightest neutrino along with the Majorana phases for texture F1-NO. We show the results in two different cases, for which the constraints have been applied for different values of the Lagrange multiplier λ.

the predictions on the mass of the lightest neutrino and the two Majorana phases given by texture F1-NO. For the sake of evaluating the impact of a relaxed constraint, we depicted the results for two different values of λ. We see that the phases are highly correlated, even when the constraint is weakened. More importantly, the goodness of the fit strongly depends on the mass of the neutrinos. For an exact texture, χ^2_{min} takes small values only in the limit of massive neutrinos. This implies that neutrinos are also degenerated, a possibility rejected by data. Therefore, an exact F1-NO texture is forbidden. From Figure 3.12 we also observe that as soon as the texture becomes approximate, small values of χ^2_{min} are obtained, while also keeping the mass of the lightest neutrino low. For this reason, texture approximate F1-NO texture has interesting prospects.

3.5 Summary

- Constraints on the neutrino mass matrix give relationships among the neutrino parameters. These conditions can be motivated by different theoretical frameworks, and among them, two-zero textures allow us to make predictions on the parameters that remain unmeasured.

- The most promising texture is A2, giving the lowest χ^2_{min} and the largest available parameter space. The A1 texture gives a slightly worse χ^2_{min} (less than 1σ away from the best value of A2) and in fact when the constraints from the textures are relaxed, both textures are almost as favoured.

- B and C textures have very constrained parameter space and give larger values of χ^2_{min}.

- As things stand with current data, the case of inverted mass ordering is disfavoured by more than 3σ. This translates to a larger complete χ^2 obtained with the textures in IO.

- Approximate textures could be a more real-world scenario. They could be induced by the dynamics of the model or when the symmetry that enforced the texture is slightly broken. With the method of Lagrange multipliers, approximate texture can be easily addressed. In particular, we see that the predictions of the textures do not change much but the parameter space is highly enhanced.

- 'Excluded' textures were also revisited, in the framework of approximate textures. In particular, we have studied the case of the F1-NO texture. For strong constraints, the solutions giving the lowest values of χ^2_{min} imply that

the neutrino masses are very degenerated, which is in tension with experimental data. However, when the texture is approximate, it gives interesting results with lower values of m_ℓ.

CHAPTER 4

Implications for neutrinoless double beta decay

In the Standard Model, the following reaction can take place within a nucleus:

$$\beta\beta : n + n \longrightarrow p + p + e + e + \bar{\nu} + \bar{\nu}. \tag{4.1}$$

This process implies the simultaneous occurrence of two beta decays, as shown in Figure 4.1a, and consequently it is called *double beta decay*. The probability of this process is proportional to G_F^4, making it a very suppressed decay. Despite being a very rare process, the double beta decay was observed many times for different nuclei since it was first suggested by Maria Goeppert-Mayer in 1935 [90]. It should be noted that the $\beta\beta$ decay conserves lepton number and portrays another confirmation of the predictions of the Standard Model.

Consider now the possibility that neutrinos are of Majorana type. Then, neutrinos and antineutrinos are the same object, and the neutrino emitted by a nucleon could be reabsorbed by another nucleon. At the end, we are left with a double beta decay with no neutrinos in the final state:

$$0\nu\beta\beta : n + n \longrightarrow p + p + e + e \tag{4.2}$$

or, simpler, a *neutrinoless double beta decay*. In contrast with the $\beta\beta$ decay, the absence of emitted antineutrinos leads to a total lepton number violation in two units. In Figure 4.1b we show the *(light) neutrino exchange mechanism* of the $0\nu\beta\beta$ decay, responsible for the process described above. Owing to the propagator of the virtual neutrino, the decay rate is proportional to $m_{\beta\beta}$, defined as

$$m_{\beta\beta} \equiv \left| \sum_{i=1}^{3} U_{ei}^2 \, m_i \right| = |M_{ee}|, \tag{4.3}$$

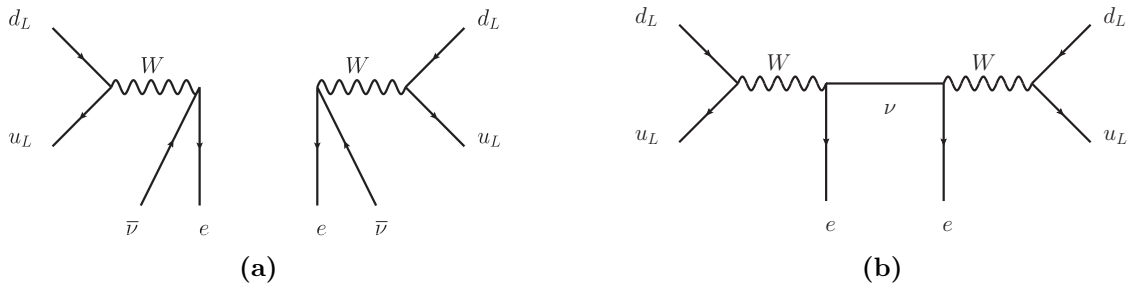

Figure 4.1: Feynman diagrams representing mechanisms of $\beta\beta$ (subfigure a) and $0\nu\beta\beta$ (subfigure b) decays.

where the sum runs over the three light neutrinos of the Standard Model, U_{ei} are elements of the PMNS matrix describing neutrino mixing and defined in Chapter 3, and m_i are the masses of the neutrinos. We see that $m_{\beta\beta}$ can be identified with M_{ee}, the ee element of the neutrino mass matrix. This feature will have a central role in the development of the current chapter.

Moreover, the PMNS matrix is a complex matrix and there might be extensions of the Standard Model for which the terms in Eq. (4.3) cancel and $m_{\beta\beta}$ vanishes, even when the masses of the neutrinos take non-zero values. Such scenarios pose no problem for the prospects for observation of the $0\nu\beta\beta$ decay, as the neutrino exchange mechanism might not be its only source. Lepton number violation is still a requirement but it might be induced by the couplings of the SM extension, giving another source of $0\nu\beta\beta$ with no intervention of Majorana neutrino masses. However, these couplings will still generate Majorana neutrino masses at a higher loop level, as stated by the black box theorem [55]. This assures the connection between Majorana neutrino masses and $0\nu\beta\beta$, irrespective of the mechanism that induces the latter.

Several experiments have searched for $0\nu\beta\beta$, so far with null results. The Heidelberg-Moscow collaboration [91] took data until the year 2001, using ^{76}Ge isotopes. Current experiments include, among others, GERDA in the same isotope [92], EXO-200 [93], KamLAND-Zen [94] and NEXT [95], using ^{136}Xe. Such experiments typically set bounds on the allowed values of $m_{\beta\beta}$, as shown in Figure 4.2

4.1 Effective Lagrangian approach

We proceed to start building models that explain neutrino masses and $0\nu\beta\beta$. As a result of being low energy processes, we can describe them by making use of effective Lagrangians, following the work by del Aguila, Aparici, Bhattacharya, Santamaria and Wudka [96]. Hereafter, we assume that the new physics does not couple to the quark sector, so that quark interactions are only mediated by electroweak gauge bosons. In addition, we restrain to the field content and the local symmetries of

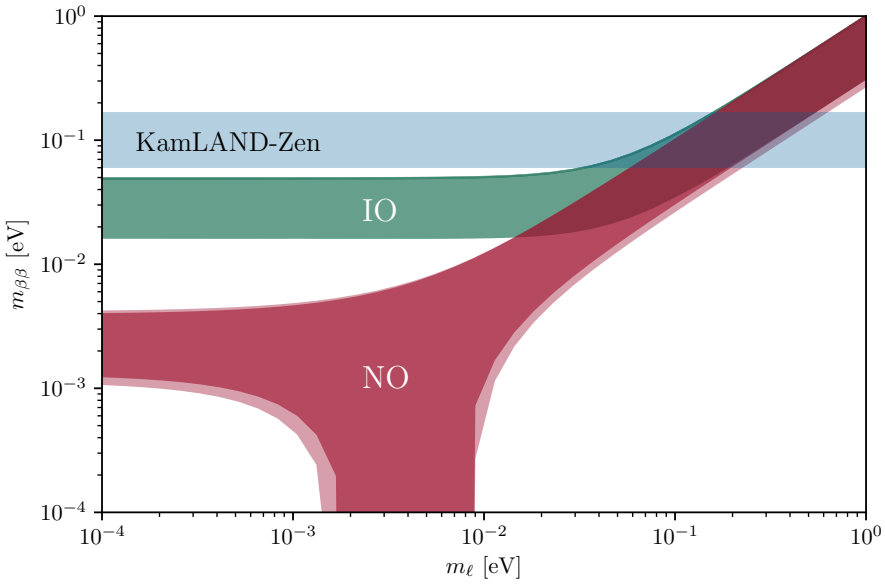

Figure 4.2: Bounds on $m_{\beta\beta}$ as a function of the mass of the lightest neutrino m_ℓ, set by $0\nu\beta\beta$ experiments. For this plot, limits obtained by the KamLAND-Zen collaboration are shown in blue ($m_{\beta\beta} < 61 - 165$ meV) [86]. Regions with 1σ and 3σ CL (darker and lighter colours) for normal and inverted neutrino mass ordering allowed by neutrino oscillation data [81] are depicted for comparison.

the Standard Model; in this context, our EFT is just the SMEFT. LNV operators giving contributions to $0\nu\beta\beta$ must involve two leptons of either chirality, a certain number of the SM scalar doublet to preserve the gauge symmetry and some covariant derivatives. Restricting to operators with the lowest possible dimension, only three arise: $\mathcal{O}_{LL}^{(5)}$, $\mathcal{O}_{LR}^{(7)}$ and $\mathcal{O}_{RR}^{(9)}$, where the subindices represent the chirality of the leptons they involve.

With these considerations in mind and in order to illustrate the process, we start with the LL operator. Left-handed charged leptons belong to a lepton doublet of $SU(2)_L$. Then, a bilinear with two left-handed charged leptons transforms as

$$\ell_L \ell_L \sim (1/2, -1/2) \times (1/2, -1/2) = (0, -1) + (1, -1). \tag{4.4}$$

For the sake of keeping all interactions gauge invariant, the LL bilinear needs to couple with objects that are either a singlet or a triplet under $SU(2)_L$, with hypercharge $Y = 1$. This can be achieved by means of some even number of SM scalar doublets. In particular and restricting to the lowest possible dimension, we need two of them, since the hypercharges add. The only possibility with dimension five is the Weinberg operator, given by

$$\mathcal{O}_{LL}^{(5)} = (\overline{\widetilde{\ell}_L \phi})(\widetilde{\phi}^\dagger \ell_L). \tag{4.5}$$

After spontaneous symmetry breaking, $\mathcal{O}_{LL}^{(5)}$ induces a neutrino mass matrix with the insertion of two VEVs and a $0\nu\beta\beta$ with a standard neutrino exchange mechanism, as seen in Figure 4.3. Note that the Weinberg operator generates the seesaw mechanisms of neutrino masses.

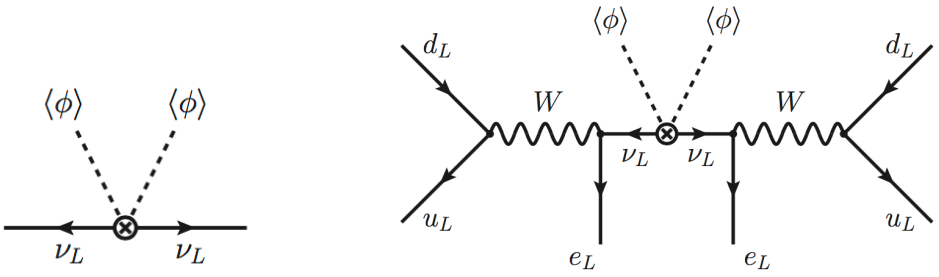

Figure 4.3: Neutrino mass (left) and $0\nu\beta\beta$ (right) generated with the dimension-five Weinberg operator.

Let us now concentrate on the RR operator[1]. The lepton bilinear has the following net gauge quantum numbers:

$$e_R e_R \longrightarrow (0,-1)\times(0,-1) = (0,-2). \tag{4.6}$$

In other words, the bilinear with two right-handed charged leptons couples with four SM scalar doublets. This combination of fields leads to a dimension-seven operator. However, it turns out that said operator vanishes as it includes the scalar product $\phi^\dagger\widetilde{\phi} = 0$. Adding a covariant derivative between the scalars, which does not change the quantum numbers, remedies this problem, at the expense of rising the dimension of the operator. There are two scalar products, hence two covariant derivatives are needed. The lowest operator then has dimension nine and reads

$$\mathcal{O}_{RR}^{(9)} = \overline{e_R} e_R^c (\phi^\dagger D^\mu \widetilde{\phi})(\phi^\dagger D_\mu \widetilde{\phi}). \tag{4.7}$$

The RR operator induces a $0\nu\beta\beta$ at tree level (see left panel of Figure 4.4), which is a very low energy process. Thus, the use of a high dimension operator is justified, and it translates into a description with a scale of new physics, Λ, of the order of the TeV. In contrast with the LL and LR operators, the TeV scale arises naturally. Moreover, $\mathcal{O}_{RR}^{(9)}$ generates neutrino masses at the two-loop level (right panel of Figure 4.4). Because it involves two chirality flips, the neutrino mass matrix will be proportional to the mass of the charged leptons, $m_{a,b}$. Indeed,

$$M_{ab} \propto \frac{1}{(4\pi)^4\Lambda} C_{ab}^{(9)} m_a m_b, \tag{4.8}$$

[1] Additionally, there is a LR operator of dimension seven, constructed in a similar way than the LL and RR operators.

which will let us make predictions of the neutrino oscillation parameters in terms of the A1 texture of Chapter 3.

Owing to its interesting implications for neutrino masses and $0\nu\beta\beta$, in this chapter we will build an ultraviolet completion of the dimension-nine operator.

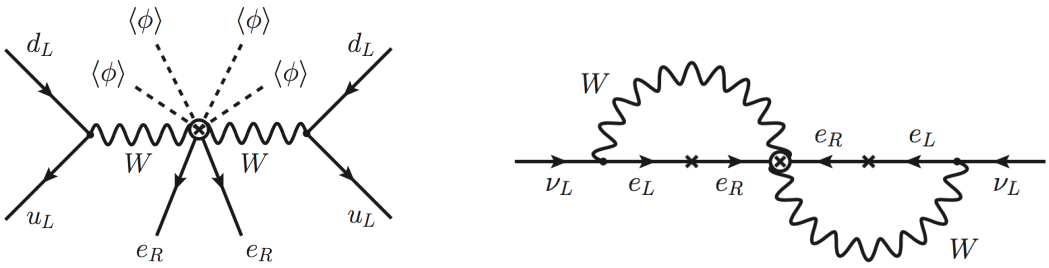

Figure 4.4: $0\nu\beta\beta$ (left) and neutrino masses (right) generated with the dimension-nine operator.

4.2 The model

The model presented here[2] extends the scalar field content of the Standard Model without adding new local symmetries. The enlarged scalar sector includes a doubly charged scalar singlet $k^{\pm\pm}$, a scalar triplet χ with hypercharge $+1$ and a real scalar singlet σ. For the sake of keeping the Yukawa interactions restricted to those with right-handed charged leptons, we impose a discrete Z_2 parity symmetry, under which the doubly charged singlet is even while the triplet and the real singlet are odd. The singlet σ will be responsible for preventing the discrete symmetry from breaking spontaneously, which would allow the triplet to couple to SM fermions, and will have a central role in inducing lepton number violation.

Under $SU(2)_L \times U(1)_Y$ the fields in the scalar sector have the following quantum numbers:

$$\phi \sim (1/2, 1/2), \qquad \chi \sim (1, 1), \qquad k^{\pm\pm} \sim (0, 2), \qquad \sigma \sim (0, 0), \tag{4.9}$$

where, as usual, ϕ is the SM Higgs doublet.

The Yukawa interactions are given by

$$\mathcal{L}_Y = -y_a \bar{\ell}_{La} \phi e_{Ra} + f_{ab} \overline{e^c_{Ra}} e_{Rb} k^{++} + h.c., \tag{4.10}$$

where $e^c_R = C e_R$ and C is the charge conjugation operator. The first term is the Yukawa interactions of the Standard Model, where the Yukawa matrix y_a is diagonal

[2]The model was published by the author of this thesis and collaborators in Ref. [97]. In the following, it will be referred as 'the three-loop model' for reasons that will be clear later on.

in flavour. The new physics is represented in the second term. As a result of the Z_2 symmetry, only $k^{\pm\pm}$ is allowed to couple to the SM fermions. The form of this interaction is governed by the gauge quantum numbers of $k^{\pm\pm}$ in Eq. (4.9), and this makes the fermion bilinear to necessary be composed of two right-handed charged leptons. Finally, the Yukawa matrix f_{ab} is a symmetric complex matrix. There are two e_R and for this reason the entire combination must obey Fermi statistics and thus be antisymmetric. The charge conjugation operator is antisymmetric which requires the generation indices a and b to be symmetric. Hence $f_{ab} = f_{ba}$.

The gauge invariant potential reads

$$\begin{aligned} V =& -m_\phi^2|\phi|^2 + m_\chi^2 \mathrm{Tr}(\chi^\dagger\chi) + m_k^2|k|^2 + \frac{1}{2}m_\sigma^2\sigma^2 + \lambda_\phi|\phi|^4 + \lambda_\chi \mathrm{Tr}(\chi^\dagger\chi)^2 \\ &+ \lambda'_\chi \mathrm{Tr}[(\chi^\dagger\chi)^2] + \lambda_k|k|^4 + \lambda_\sigma\sigma^4 + \lambda_{\phi\chi}|\phi|^2\mathrm{Tr}(\chi^\dagger\chi) + \lambda'_{\phi\chi}\mathrm{Tr}(\phi^\dagger\chi^\dagger\chi\phi) \\ &+ \lambda_{\phi k}|k|^2|\phi|^2 + \lambda_{\phi\sigma}\sigma^2|\phi|^2 + \lambda_{k\chi}|k|^2\mathrm{Tr}(\chi^\dagger\chi) + \lambda_{\sigma\chi}\sigma^2\mathrm{Tr}(\chi^\dagger\chi) \\ &+ \lambda_{\sigma k}\sigma^2|k|^2 + \Big[\mu_k k^{++}\mathrm{Tr}(\chi^\dagger\chi^\dagger) + \lambda_6\sigma\phi^\dagger\chi\widetilde{\phi} + h.c.\Big], \end{aligned} \tag{4.11}$$

where $\widetilde{\phi} = i\sigma_2\phi^*$. We choose to use the 2×2 matrix representation of the triplet,

$$\chi = \begin{pmatrix} \chi^+/\sqrt{2} & \chi^{++} \\ \chi^0 & -\chi^+/\sqrt{2} \end{pmatrix} \tag{4.12}$$

where $\chi^0 = (\chi_R^0 + iA)/\sqrt{2}$. Then 'Tr' represents the trace over a matrix. All parameters in the potential are set to be real without any loss of generality.

It is important to note that this model breaks lepton number, in particular, by the combined presence of the following terms:

$$y_a\overline{\ell_{La}}\phi e_{Ra}, \qquad f_{ab}e_{Ra}e_{Rb}k^{++}, \qquad \mu_k k^{++}\mathrm{Tr}(\chi^\dagger\chi^\dagger), \qquad \lambda_6\sigma\phi^\dagger\chi\widetilde{\phi}. \tag{4.13}$$

As said in Chapter 1, the Standard Model conserves lepton number. This allows us to define the lepton number of the leptons to be -1, and, due to the SM Yukawa interactions (first term in the list above), to set the lepton number of the SM scalar doublet to zero. Then, from the second and third terms, the lepton number of $k^{\pm\pm}$ and χ are $+2$ and $+1$. Had the potential conserved lepton number, σ would have had lepton number -1, but it is impossible to assign to it a lepton number different than zero, as it is a *real* scalar. In other words, lepton number is broken in one unit. Furthermore, whenever any of these four couplings vanishes, lepton number is automatically conserved, which indicates that any process breaking lepton number within this model should be proportional to the joint combination of the four parameters. We will discuss more about this in the upcoming sections.

After spontaneous symmetry breaking, the particles in the extended scalar sector

get their masses shifted by some new term, due to their interactions with the SM scalar doublet. Starting with the doubly-charged particles, the mass of the singlet is

$$m_{k^{\pm\pm}}^2 = m_k^2 + \frac{1}{2}\lambda_{\phi k} v^2, \tag{4.14}$$

while the mass of $\chi^{\pm\pm}$ reads:

$$m_{\chi^{\pm\pm}}^2 = m_\chi^2 + \frac{1}{2}\lambda_{\phi\chi} v^2. \tag{4.15}$$

The mass of the singly-charged component of the triplet reads

$$m_{\chi^{\pm}}^2 = m_\chi^2 + \frac{1}{2}(\lambda_{\phi\chi} + \frac{1}{2}\lambda'_{\phi\chi}) v^2, \tag{4.16}$$

while the mass the pseudoscalar particle is:

$$m_A^2 = m_\chi^2 + \frac{1}{2}(\lambda_{\phi\chi} + \lambda'_{\phi\chi}) v^2. \tag{4.17}$$

Moreover, owing to the interaction with ϕ, the masses of $\chi^{\pm\pm}$, $\chi^{\pm}$ and A are correlated. The mass splittings are controlled by the parameter $\lambda'_{\phi\chi}$,

$$m_{\chi^{\pm}}^2 - m_{\chi^{\pm\pm}}^2 = m_A^2 - m_{\chi^{\pm}}^2 = \frac{1}{4}\lambda'_{\phi\chi} v^2, \tag{4.18}$$

which means that the three scalars become degenerated when setting $\lambda'_{\phi\chi} = 0$. We will see at the end of this chapter that these masses get further constrained by electroweak precision data. We can also rearrange the previous relation in the following way:

$$m_{\chi^{\pm}}^2 = \frac{1}{2}(m_A^2 + m_{\chi^{\pm\pm}}^2). \tag{4.19}$$

The CP-even neutral scalars mix through the following mass matrix:

$$\Delta V_{mass} = \frac{1}{2}\begin{pmatrix}\sigma & \chi_R^0\end{pmatrix}\begin{pmatrix} m_{\sigma\sigma}^2 & m_{\sigma\chi}^2 \\ m_{\sigma\chi}^2 & m_{\chi\chi}^2 \end{pmatrix}\begin{pmatrix}\sigma \\ \chi_R^0\end{pmatrix}, \tag{4.20}$$

where

$$m_{\sigma\sigma}^2 = m_\sigma^2 + \lambda_{\phi\sigma} v^2, \qquad m_{\sigma\chi}^2 = \frac{1}{\sqrt{2}}\lambda_6 v^2, \qquad m_{\chi\chi}^2 = m_\chi^2 + \frac{1}{2}(\lambda_{\phi\chi} + \lambda'_{\phi\chi}) v^2 = m_A^2. \tag{4.21}$$

When $\lambda_6 = 0$, the mass matrix is diagonal and there is no mixing between the

neutral scalars. Otherwise, we need to change basis with an orthogonal matrix,

$$\begin{pmatrix} S \\ H \end{pmatrix} = \begin{pmatrix} \cos\alpha & -\sin\alpha \\ \sin\alpha & \cos\alpha \end{pmatrix} \begin{pmatrix} \sigma \\ \chi_R^0 \end{pmatrix}, \tag{4.22}$$

so that the Lagrangian becomes diagonal:

$$\Delta V_{mass} = \frac{1}{2} \begin{pmatrix} S & H \end{pmatrix} \begin{pmatrix} m_S^2 & 0 \\ 0 & m_H^2 \end{pmatrix} \begin{pmatrix} S \\ H \end{pmatrix}. \tag{4.23}$$

Since we are arbitrarily defining S and H, there is no preferred hierarchy among them. Inserting Eq. (4.22) in the last expression we find the parameters $m_{\sigma\sigma}^2$, $m_{\sigma\chi}^2$ and $m_{\chi\chi}^2$ in terms of the physical masses and the mixing angle,

$$\begin{aligned} m_{\sigma\sigma}^2 &= m_H^2 \sin^2\alpha + m_S^2 \cos^2\alpha, \\ m_{\sigma\chi}^2 &= \frac{1}{2}\sin 2\alpha (m_H^2 - m_S^2), \\ m_{\chi\chi}^2 &= m_H^2 \cos^2\alpha + m_S^2 \sin^2\alpha. \end{aligned} \tag{4.24}$$

The last relation, combined with Eq. (4.21), gives

$$m_A^2 = m_H^2 \cos^2\alpha + m_S^2 \sin^2\alpha, \tag{4.25}$$

which makes the mass of A to lie between the masses of S and H. In particular, we choose S to be the lightest particle, and hence

$$m_S < m_A < m_H. \tag{4.26}$$

It is also useful to put λ_6 in terms of physical parameters. Joining the two expressions of $m_{\sigma\chi}^2$ together, we arrive at

$$\lambda_6 = \frac{\sin 2\alpha}{\sqrt{2}v^2}(m_H^2 - m_S^2), \tag{4.27}$$

which leads to an indispensable result: should S and H be degenerate, lepton number will remain unbroken and the model will not be able to generate neutrino masses.

4.3 The neutrino mass

The Lagrangian describing the mass of neutrinos reads

$$-\mathcal{L}_{mass} = \frac{1}{2}\overline{\nu_{La}^c} M_{ab} \nu_{Lb} + h.c. \tag{4.28}$$

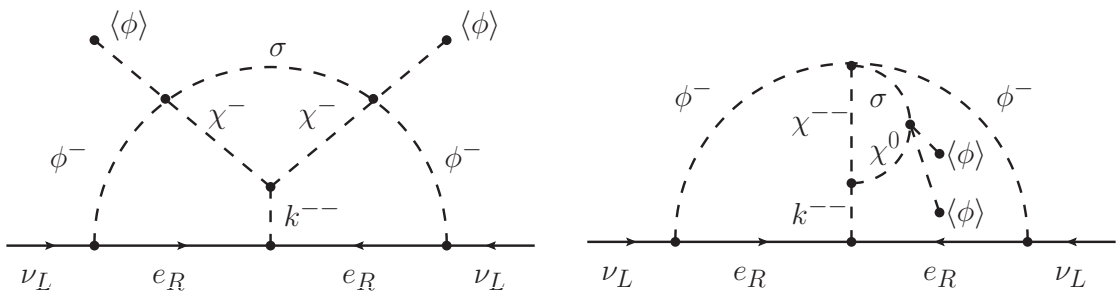

Figure 4.5: Three-loop flavour diagrams contributing to neutrino masses. There are two VEV insertions in each diagrams which, together with $y_{a,b}$, give rise to the charged lepton masses $m_{a,b}$.

and the problem consists in obtaining the form of M_{ab}.

In order to arrive at a better understanding of the generation of the mass and the topic of lepton number violation we will start by working within the *mass insertion approach* in the so-called *gaugeless limit*. This technique requires that we depict the Feynman diagrams using the fields in the gauge invariant Lagrangian, before symmetry breaking and diagonalisation into physical states. Accordingly, in this limit the gauge bosons are massless and have vanishing external momenta. Moreover, drawn this way, the diagrams are called *flavour diagrams*. Both left- and right-handed components of the fermions are shown explicitly and so do VEVs $\langle\phi\rangle$, whose insertion into the diagram represents the annihilation of ϕ into the vacuum. Then, one can easily estimate the main contribution to the amplitude of the process as the product of the couplings entering the diagram. Later on, we can check the goodness of the gaugeless limit approximation by setting $g \to 0$ (or equivalently $M_W \to 0$) in the complete calculation in the unitary gauge. Further, the inspection of lepton number violation becomes obvious in the flavor basis, as parameters and physical particles tend to hide their nature after diagonalisation. We will see this explicitly when working out the neutrino mass in the unitary gauge.

The model generates neutrino masses at the three-loop level. In the flavour basis, the two Feynman diagrams are shown in Figure 4.5. It is straightforward to realise that the only interactions entering the process are the following:

$$f_{ab}e_{Ra}e_{Rb}k^{++}, \qquad y_a\overline{\ell_{La}}\phi e_{Ra}, \qquad \mu_k k^{++}\mathrm{Tr}(\chi^\dagger\chi^\dagger), \qquad \lambda_6\sigma\phi^\dagger\chi\widetilde{\phi}. \tag{4.29}$$

As said above, the generation of neutrino mass revolves around the scalar interaction with the right-handed charged leptons, which is the first term. Next off, we need to introduce neutrinos into the mix. This is achieved with the second vertex. Finally, the connection to the doubly charged singlet is carried out through the interactions with the triplet and the real singlet.

More importantly, these are the same four interactions required for lepton num-

ber violation. In particular, the last term is included twice in both diagrams, making lepton number to be broken by two units, which is exactly what Majorana neutrinos mass terms need.

With this considerations, the neutrino mass matrix is given by

$$\begin{aligned} M_{ab} &= 8\frac{\mu_k \lambda_6^2 (y_a v)(y_b v) f_{ab}}{(4\pi)^6 m_k^2} I_\nu \\ &= 8\frac{\mu_k \lambda_6^2 m_a m_b f_{ab}}{(4\pi)^6 m_k^2} I_\nu \end{aligned} \tag{4.30}$$

with

$$I_\nu \equiv I_1 + I_2, \tag{4.31}$$

and where $m_{a,b} = y_{a,b} v$ are the masses of the charged leptons with flavours a and b. The integrals $I_{1,2}$ correspond to each diagram in Figure 4.5. The suppression by $(4\pi)^6$ is due to the three-loop topology and have been factorised out of the integrals. The mass m_k was included in the denominator to prevent the integrals from having dimensions of energy. Finally, the factor of 8 is common to the two diagrams and appears from the combination of all the relevant terms entering each diagram.

In Euclidean space the momentum gets rotated with $q^0 \to iq^0$, and then the integrals read

$$I_1 = -(4\pi)^6 m_k^2 \int_q \frac{q_1 \cdot q_2}{q_1^4 q_2^4 ((q_1+q_2)^2 + m_k^2)(q_3^2 + m_\sigma^2)((q_1+q_3)^2 + m_{\chi^\pm}^2)((q_2-q_3)^2 + m_{\chi^\pm}^2)} \tag{4.32}$$

and

$$I_2 = (4\pi)^6 m_k^2 \int_q \frac{q_1 \cdot q_2}{q_1^4 q_2^4 ((q_1+q_2)^2 + m_k^2)(q_3^2 + m_\sigma^2)(q_3^2 + m_{\chi^0}^2)((q_1+q_2+q_3)^2 + m_{\chi^{\pm\pm}}^2)}, \tag{4.33}$$

where

$$\int_q = \int \prod_{i=1}^{3} \frac{dq_i q_i^3}{(2\pi)^4} d\phi_i d\theta_i \sin\theta_i d\psi_i \sin^2\psi_i, \qquad \phi_i \in [0, 2\pi],\ \theta_i \in [0,\pi],\ \psi_i \in [0,\pi]. \tag{4.34}$$

There is a relative sign between the two integrals because each diagram involves a different term in the expansion of the λ_6 interactions:

$$\lambda_6 \sigma \phi^\dagger \chi \widetilde{\phi} = \lambda_6 \sigma (\chi^0 \phi^{0*} \phi^{0*} + \sqrt{2}\chi^+ \phi^{0*} \phi^- - \chi^{++} \phi^- \phi^-). \tag{4.35}$$

We note that in the limit in which the masses of the triplet are degenerated and much heavier than the masses of the singlets, the two integrals are identical and cancel exactly, because of the relative sign. In that limit one can integrate out

the triplet. Then, the interactions in both diagrams collapse to an unique effective vertex:

$$\begin{aligned}(k^{--}\chi^{+}\chi^{+})(\sigma\chi^{-}\phi^{\dagger}\widetilde{\phi})(\sigma\chi^{-}\phi^{\dagger}\widetilde{\phi}) &\longrightarrow k^{--}\sigma^{2}(\phi^{\dagger}\widetilde{\phi})^{2},\\ (k^{--}\chi^{++}\chi^{0})(\sigma\chi^{--}\phi^{\dagger}\widetilde{\phi})(\sigma\chi^{0*}\phi^{\dagger}\widetilde{\phi}) &\longrightarrow k^{--}\sigma^{2}(\phi^{\dagger}\widetilde{\phi})^{2}.\end{aligned} \tag{4.36}$$

However the combination $\phi^{\dagger}\widetilde{\phi}$ is exactly zero and the effective vertex vanishes. The conclusion is that, for the sake of keeping a non-vanishing neutrino mass, there cannot be a large gap between the scalar masses of the model.

Both integrals are convergent and expected to be of order 1. In order to perform the numerical evaluation, we take the momenta to be

$$\begin{aligned}q_3^{\mu} = q_3(1,0,0,0), \qquad q_2^{\mu} = q_2(\cos\psi_2, \sin\psi_2, 0, 0),\\ q_1^{\mu} = q_1(\cos\psi_1, \sin\psi_1\cos\theta_1, \sin\psi_1\sin\theta_1, 0).\end{aligned} \tag{4.37}$$

With this choice, the products of momenta will depend on only three of the angles:

$$\begin{aligned}q_1\cdot q_2 &= q_1\ q_2(\cos\psi_2\cos\psi_1 + \sin\psi_2\sin\psi_1\cos\theta_1),\\ q_1\cdot q_3 &= q_1\ q_3\cos\psi_1,\\ q_2\cdot q_3 &= q_2\ q_3\cos\psi_2.\end{aligned} \tag{4.38}$$

Then we can integrate the remaining angles, and thus Eq. (4.34) becomes

$$\int_q = (2\pi)^4 \int \frac{dq_1\ dq_2\ dq_3\ d\theta_1\ d\psi_1\ d\psi_2}{(2\pi)^{12}} q_1^3\ q_2^3\ q_3^3 \sin\theta_1 \sin^2\psi_1 \sin^2\psi_2. \tag{4.39}$$

With these manipulations, we numerically evaluate the integrals in the gaugeless limit. In Figure 4.6 we depict the results for some reference values of the masses. We see that, for the ranges of masses considered, we can safely take $I_\nu \approx 1$.

4.3.1 The effective propagator

Before proceeding to the complete calculation in the unitary gauge, we note that there are some contractions of the fields that cannot be straightforwardly performed. For instance, owing to the form of the Lagrangian, the following contraction between the χ^0 neutral fields is needed:

$$(W^{+}W^{+}\chi^{--}\chi^{0})(k^{--}\chi^{++}\chi^{0}). \tag{4.40}$$

However, χ^0 is a complex field and can only contract with its conjugate counterpart. Indeed, when decomposing into its real and imaginary part, the only possible

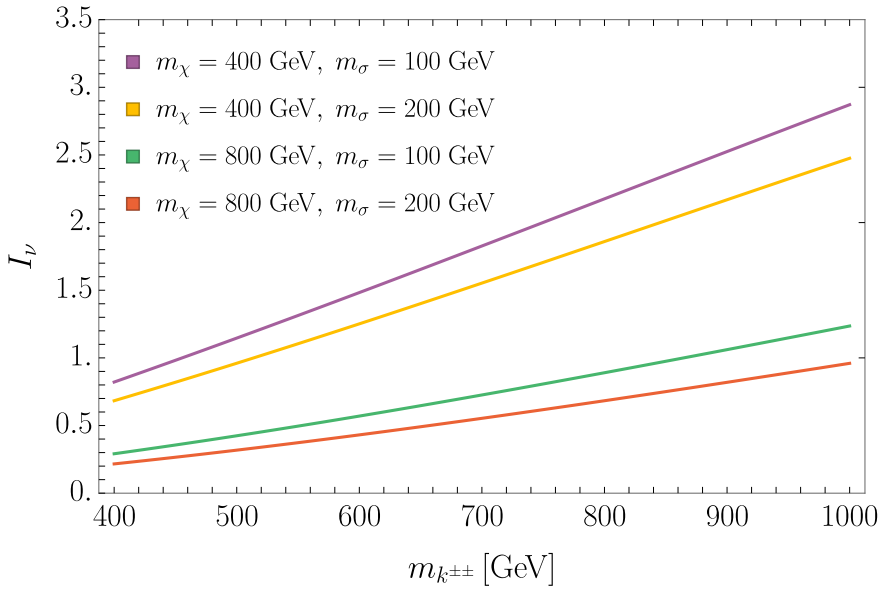

Figure 4.6: Numerical evaluation of the neutrino mass matrix integral I_ν calculated in the gaugeless limit for some representative points, and where we have taken $m_{\chi^\pm} = m_{\chi^{\pm\pm}} = m_{\chi^0} \equiv m_\chi$.

contractions go with

$$\overline{\chi^0(x)\chi^0(y)} = \frac{1}{2}\Big[\overline{\chi_R(x)\chi_R(y)} - \overline{A(x)A(y)}\Big]. \tag{4.41}$$

Without mixing, χ_R and A are degenerated and the propagator vanishes. This looks terrible, as this propagator enters each and every one of the diagrams; thus it seems impossible to generate neutrino masses. But mixing does happen within the model, the interaction with σ induces lepton number violation and neutrino masses should be guaranteed. Consider the mixing of χ_R in Eq. (4.22). Then, after diagonalisation, the contractions become

$$\overline{\chi^0(x)\chi^0(y)} = \frac{1}{2}\Big[\cos^2\alpha\ \overline{H(x)H(y)} + \sin^2\alpha\ \overline{S(x)S(y)} - \overline{A(x)A(y)}\Big], \tag{4.42}$$

and as long as H and S have different masses, the propagator survives. But there is another interesting point to make. When we insert the expression of the propagator of each physical particle, we get

$$\begin{aligned}\overline{\chi^0\chi^0} &= \frac{1}{2}\left(\cos^2\alpha\frac{1}{p^2-m_H^2} + \sin^2\alpha\frac{1}{p^2-m_S^2} - \frac{1}{p^2-m_A^2}\right)\\ &= \frac{1}{2}\frac{\sin^2\alpha\cos^2\alpha(m_H^2-m_S^2)^2}{(p^2-m_H^2)(p^2-m_S^2)(p^2-m_A^2)}\\ &= \frac{1}{4}\frac{\lambda_6^2 v^4}{(p^2-m_H^2)(p^2-m_S^2)(p^2-m_A^2)},\end{aligned} \tag{4.43}$$

where in the last step we have used Eq. (4.27). The conclusion is that the contraction of the χ^0 fields gives an effective operator that goes with $1/p^6$ which will allow all integrals to be finite, even in the unitary gauge. Moreover, because it is proportional to λ_6^2, the effective operator induces the breaking of lepton number in two units.

We can also understand the behaviour of the effective operator before symmetry breaking in terms of the propagator matrix, provided there is mixing with σ. Before diagonalisation, the propagator matrix reads

$$P_{\alpha\beta} = (p^2\delta_{\alpha\beta} - M^2_{\alpha\beta})^{-1}, \tag{4.44}$$

where M^2 is the mass matrix of the CP-even scalars in Eq. (4.20). Then,

$$\begin{aligned} P &= \begin{pmatrix} p^2 - m^2_{\sigma\sigma} & -m^2_{\sigma\chi} \\ -m^2_{\sigma\chi} & p^2 - m^2_{\chi\chi} \end{pmatrix}^{-1} \\ &= \frac{1}{(p^2 - m^2_{\sigma\sigma})(p^2 - m^2_{\chi\chi}) - m^4_{\sigma\chi}} \begin{pmatrix} p^2 - m^2_{\chi\chi} & m^2_{\sigma\chi} \\ m^2_{\sigma\chi} & p^2 - m^2_{\sigma\sigma} \end{pmatrix}. \end{aligned} \tag{4.45}$$

The factor before the resulting matrix is just the inverse of its determinant. The contraction $\overline{\chi_R\chi_R}$ in Eq. (4.41) is obtained from the $\chi\chi$ element of the matrix. With this, the contraction in Eq. (4.41) becomes

$$\overline{\chi^0\chi^0} = \frac{1}{2}\left(\frac{p^2 - m^2_{\sigma\sigma}}{(p^2 - m^2_{\sigma\sigma})(p^2 - m^2_{\chi\chi}) - m^4_{\sigma\chi}} - \frac{1}{p^2 - m^2_A}\right). \tag{4.46}$$

But because $m^2_{\chi\chi} = m^2_A$, we can combine the two terms in the following way:

$$\overline{\chi^0\chi^0} = \frac{1}{2}\left(\frac{m^4_{\sigma\chi}}{((p^2 - m^2_{\sigma\sigma})(p^2 - m^2_A) - m^4_{\sigma\chi})(p^2 - m^2_A)}\right), \tag{4.47}$$

making the effective operator to go with $1/p^6$. Finally we can write the effective operator in terms of the physical parameters. Using Eqs. (4.24) and the invariance of the determinant, which in the diagonal basis is simply $(p^2 - m^2_H)(p^2 - m^2_S)$, the propagator turns out to be

$$\begin{aligned} \overline{\chi^0\chi^0} &= \frac{1}{2}\frac{\sin^2\alpha\cos^2\alpha(m^2_H - m^2_S)^2}{(p^2 - m^2_H)(p^2 - m^2_S)(p^2 - m^2_A)} \\ &= \frac{1}{4}\frac{\lambda_6^2 v^4}{(p^2 - m^2_H)(p^2 - m^2_S)(p^2 - m^2_A)}, \end{aligned} \tag{4.48}$$

where once again the breaking of lepton number in two units has become explicit.

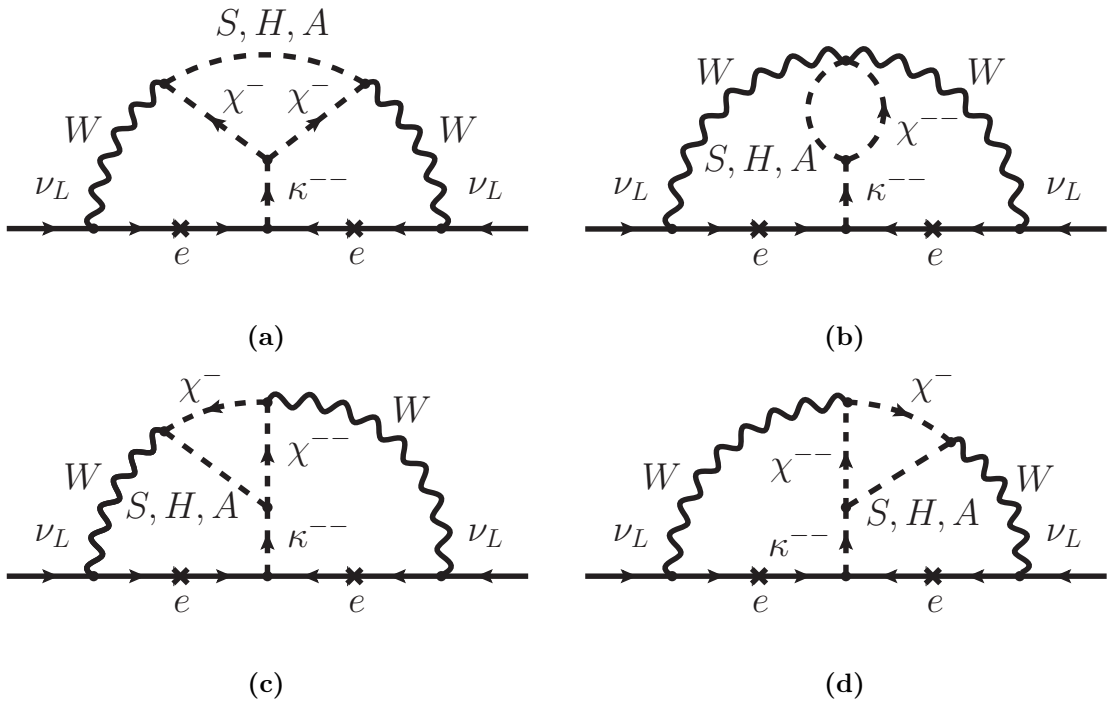

Figure 4.7: Three-loop diagrams contributing to neutrino masses in the unitary gauge.

4.3.2 The complete calculation

The generation of the neutrino mass revolves around the scalar interaction with the right-handed charged leptons,

$$f_{ab} e_{Ra} e_{Rb} k^{++}. \tag{4.49}$$

The connection to neutrinos is governed by the interactions involving gauge bosons coming from the covariant derivative of the SM Higgs doublet in Eq. (1.13) of Chapter 1. However, $k^{\pm\pm}$ has no interactions with the $W^{\pm}$ gauge bosons and there is no way to directly couple these two last vertices. The situation changes when considering the other scalars of the model. The triplet has the following relevant interactions with the gauge bosons:

$$\begin{gathered} -g^2 W^+_\mu W^{+\mu} \chi^{--} \chi^0, \qquad -igW^+_\mu (\chi^{--} \partial^\mu \chi^+ - \partial^\mu \chi^{--} \chi^+), \\ igW^+_\mu (\chi^- \partial^\mu \chi^0 - \partial^\mu \chi^- \chi^0), \end{gathered} \tag{4.50}$$

where, as in the last section, $\chi^0 = (-S \sin\alpha + H \cos\alpha + iA)/\sqrt{2}$. The breaking of lepton number in two units is guaranteed by the effective operator.

In Figure 4.7 we depict the four diagrams generating neutrino masses in the unitary gauge. Diagrams (c) and (d) can be obtained from each other by changing $q_1 \leftrightarrow q_2$. Using the same normalisation as in the gaugeless limit calculation, we get

$$M_{ab} = \frac{8 \mu_k \lambda_6^2 m_a f_{ab} m_b}{(4\pi)^6 m_k^2} I_\nu. \tag{4.51}$$

The loop functions associated with each diagram are:

$$I_\nu \equiv I_1^U + I_2^U + I_{34}^U, \tag{4.52}$$

with

$$I_1^U = (4\pi)^6 m_k^2 \int_q P_c \frac{V_1 \cdot V_2}{((q_1+q_3)^2 + m_{\chi^\pm}^2)((q_2-q_3)^2 + m_{\chi^\pm}^2)}, \tag{4.53}$$

$$I_2^U = -2(4\pi)^6 m_k^2 \int_q P_c \frac{4M_W^4 + M_W^2(q_1^2+q_2^2) + (q_1 q_2)^2}{(q_1+q_2+q_3)^2 + m_{\chi^{\pm\pm}}^2}, \tag{4.54}$$

$$I_{34}^U = 2(4\pi)^6 m_k^2 \int_q P_c \frac{V_1 \cdot V_3}{((q_1+q_2+q_3)^2 + m_{\chi^{\pm\pm}}^2)((q_1+q_3)^2 + m_{\chi^\pm}^2)}, \tag{4.55}$$

$$\tag{4.56}$$

where

$$P_c = \frac{1}{q_1^2 q_2^2 (q_1^2 + M_W^2)(q_2^2 + M_W^2)((q_1+q_2)^2 + m_{k^{\pm\pm}}^2)(q_3^2 + m_H^2)(q_3^2 + m_S^2)(q_3^2 + m_A^2)} \tag{4.57}$$

is a common factor of every loop function, and

$$V_1^\mu = M_W^2 (q_1 + 2q_3)^\mu + (q_1^2 + 2q_1 q_3) q_1^\mu, \tag{4.58}$$

$$V_2^\mu = M_W^2 (2q_3 - q_2)^\mu + (2q_2 q_3 - q_2^2) q_2^\mu, \tag{4.59}$$

$$V_3^\mu = M_W^2 (2q_1 + q_2 + 2q_3)^\mu + (2q_1 q_2 + q_2^2 + 2q_2 q_3) q_2^\mu. \tag{4.60}$$

Using the same methods discussed for the calculation in the gaugeless limit, we numerically evaluate the integrals. We have checked that in the limit $M_W \longrightarrow 0$, $m_H = m_A = m_{\chi^{\pm\pm}} = m_{\chi^\pm} \equiv m_\chi$ and $m_S \equiv m_\sigma$ we get the same results. Moreover, even in the complete result with $M_W \simeq 80$ GeV, we see in Figure 4.8 that the integrals in the unitary gauge are mainly dominated by the gaugeless part.

4.4 Neutrinoless double beta decay

In this section we will discuss the two mechanisms of $0\nu\beta\beta$. The standard source is induced by a Majorana neutrino exchange between two vector-axial SM vertices. This contribution, often called long-range mechanism, is proportional to the mass of the neutrinos. On the other hand, short-range mechanisms involve particles much heavier than the typical separation between the nucleons. For this reason, effective operators are a common approach for describing these new physics contributions.

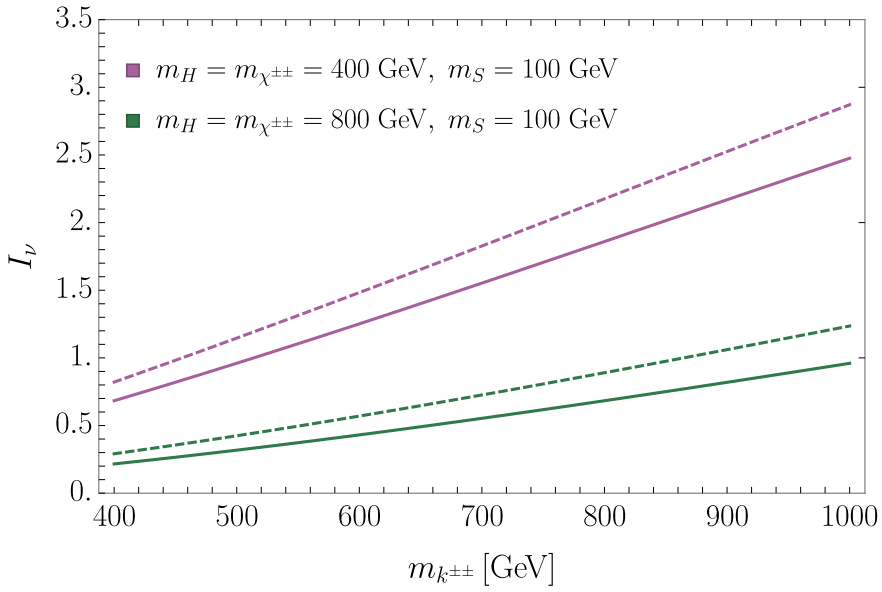

Figure 4.8: Comparison of the numerical evaluation of the integrals calculated in the unitary gauge (dashed lines) and in the gaugeless limit (solid lines) for two reference points.

4.4.1 Neutrino exchange contribution

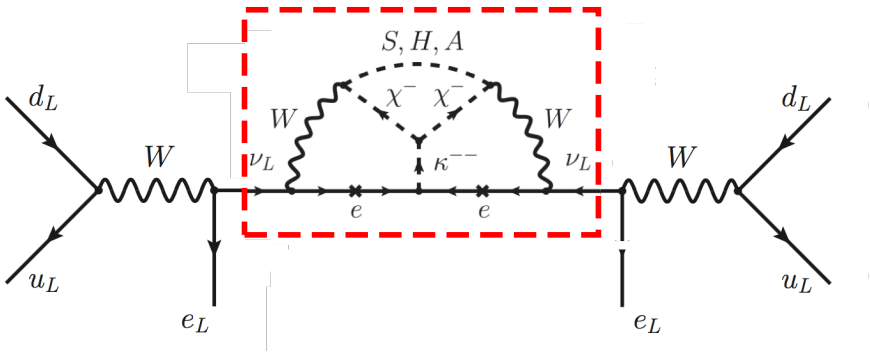

Figure 4.9: Contribution to the standard neutrino exchange mechanism for the generation of neutrinoless double beta decay with two left-handed electrons.

In this type of mechanisms, the $0\nu\beta\beta$ rate is proportional to M_{ee}, which depends on the details of the model (see Figure 4.9). Very often, as in the case of the model presented here, the description is such that M_{ee} takes small values. Then, the observation of $0\nu\beta\beta$ could be difficult, provided the long range mechanism is preferred. Indeed, in our model, the neutrino mass matrix is proportional to the mass of the charged leptons so it is natural that the ee and $e\mu$ entries are suppressed. Just to illustrate this behaviour, we can see the form of squared mass matrix of the

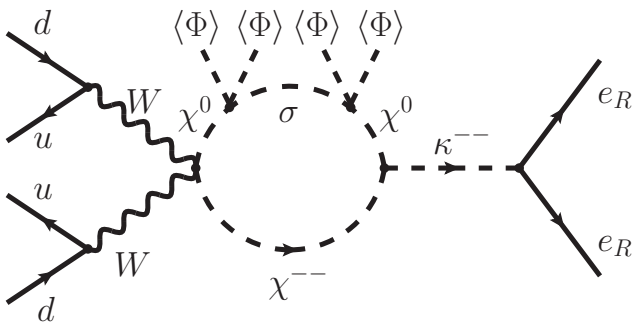

Figure 4.10: One-loop diagram contributing to the short-range source of neutrinoless double beta decay with two right-handed electrons.

charged leptons:

$$\sum_{a,b} m_a m_b \approx \begin{pmatrix} 10^{-7} & 10^{-4} & 10^{-3} \\ 10^{-4} & 10^{-2} & 10^{-1} \\ 10^{-3} & 10^{-1} & 1 \end{pmatrix} \text{ eV}, \tag{4.61}$$

where $m_e \approx 0.5 \times 10^{-3}$ GeV, $m_\mu \approx 0.1$ GeV and $m_\tau \approx 2$ GeV. Then, the previous matrix leads to the following hierarchy among the elements of the neutrino mass matrix:

$$M_{ee}, M_{e\mu} \ll M_{e\tau}, M_{\mu\mu}, M_{\mu\tau}, M_{\tau\tau}. \tag{4.62}$$

This will be sufficient to accommodate neutrino oscillation data in terms of texture zeros in the neutrino mass matrix, as seen in Chapter 3, but points to a difficult observation of $0\nu\beta\beta$ when the standard neutrino exchange mechanism is the dominant source of $0\nu\beta\beta$, as $M_{ee} \approx 0$. Fortunately, the model also provides a short-distance mechanism which is successful to give a large $0\nu\beta\beta$ rate, while keeping the ee neutrino mass matrix element small. Contrary to seesaw models [98], the short-range mechanism will be the dominant source of $0\nu\beta\beta$ for low scalar masses, as we will see.

4.4.2 New physics contribution

In Figure 4.10 we show one of the diagrams contributing to the short-range source of $0\nu\beta\beta$ with two right-handed electrons. When the scalars running in the loop are much heavier than all the momenta exchanged in the process, we can perform the calculation from the effective Lagrangian perspective described in Section 4.1. The effective operator responsible for the short-range contributions reads

$$\mathcal{O}_{kWW} = k^{--} W_\mu^+ W^{\mu +} + h.c., \tag{4.63}$$

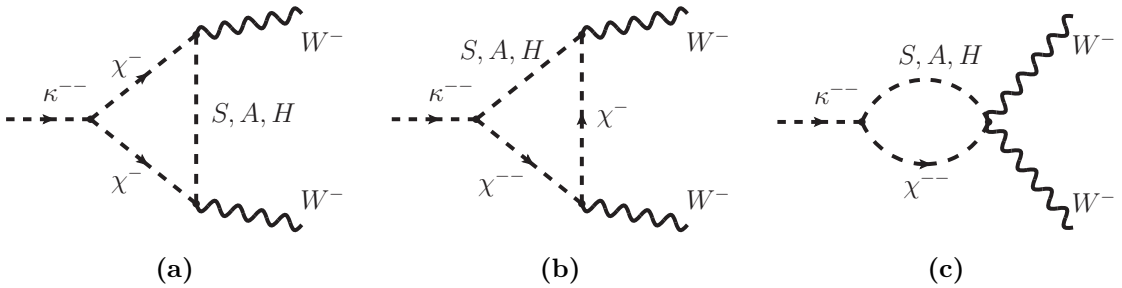

Figure 4.11: One-loop diagrams giving contributions to the kWW effective vertex in the unitary gauge.

which comes from the gauge invariant operator

$$\mathcal{O}_{k\phi^4} = k^{++}(\phi^\dagger D^\mu \widetilde{\phi})(\phi^\dagger D_\mu \widetilde{\phi}) + h.c. \tag{4.64}$$

Now, we can integrate out $k^{\pm\pm}$ and obtain

$$\mathcal{O}_{eeWW} = (\overline{e_R} e_R^c)(\phi^\dagger D^\mu \widetilde{\phi})(\phi^\dagger D_\mu \widetilde{\phi}) + h.c., \tag{4.65}$$

which is the dimension-nine RR operator of Section 4.1. Finally, we can further integrate out the gauge boson with the SM charged current interactions. The resulting effective operator describes the $0\nu\beta\beta$ within our model:

$$\mathcal{O}_{0\nu\beta\beta} = \Big[\bar{u}\gamma^\mu(1-\gamma_5)d\Big]\Big[\bar{u}\gamma^\mu(1-\gamma_5)d\Big]\Big[\bar{e}(1-\gamma_5)e^c\Big]. \tag{4.66}$$

We compute the effective kWW vertex at one-loop level with all external momenta set to zero. The reason for this choice is that all transferred momenta in $0\nu\beta\beta$ are typically around 100 MeV [98], which we assume to be much smaller than the masses of the exchanged particles in the diagram. In Figure 4.11 we show the three topologies that give contributions to the effective vertex.

As for the generation of neutrino masses, the computation in the unitary gauge hides the connection to lepton number violation in the effective neutral scalar propagator. What is more, when rudely inspecting each of the topologies in Figure 4.11, one might arrive at the conclusion that every diagram individually diverges and hope for huge cancellations between diagrams. Of course, one needs to remember that each topology actually involves three diagrams, one for each physical neutral scalar (S, H and A). Then, one would add the propagators of the three scalars and obtain the effective operator in Eq. (4.43), whose behaviour goes with $1/p^6$ and hence cancelling the divergences. Moreover, the effective propagator recovers the parameter λ_6, responsible for lepton number violation.

With these considerations, we obtain the following Wilson coefficient of the

kWW effective operator:

$$\mathcal{C}_{kWW} = \frac{g^2 v^4}{4} \frac{\mu_k \lambda_6^2}{(4\pi)^2 m_A^4} I_\beta, \tag{4.67}$$

where I_β is a dimensionless function of the masses of the scalar particles running in the loop.

As stated above, we can further integrate out $k^{\pm\pm}$ and $W^\pm$ using the equations of motion, leading to the six-fermion effective operator in Eq. (4.66). The Wilson coefficient describing $0\nu\beta\beta$ then becomes

$$\mathcal{C}_{0\nu\beta\beta} = 2 \frac{f_{ee}^*}{(4\pi)^2} \frac{\mu_k \lambda_6^2}{m_{k^{\pm\pm}}^2 m_A^4} I_\beta. \tag{4.68}$$

Regarding the function I_β, there are three contributions, corresponding to each of the diagrams in Figure 4.11:

$$I_\beta = I_\beta^1 + I_\beta^2 + I_\beta^3, \tag{4.69}$$

with

$$I_\beta^1 = m_A^4 \int_0^\infty dq q^3 \frac{q^2}{(q^2 + m_{\chi^\pm}^2)^2 (q^2 + m_S^2)(q^2 + m_H^2)(q^2 + m_A^2)}, \tag{4.70}$$

$$I_\beta^2 = -2 m_A^4 \int_0^\infty dq q^3 \frac{1}{(q^2 + m_{\chi^{\pm\pm}}^2)(q^2 + m_S^2)(q^2 + m_H^2)(q^2 + m_A^2)}, \tag{4.71}$$

$$I_\beta^3 = 2 m_A^4 \int_0^\infty dq q^3 \frac{q^2}{(q^2 + m_{\chi^{\pm\pm}}^2)(q^2 + m_{\chi^\pm}^2)(q^2 + m_S^2)(q^2 + m_H^2)(q^2 + m_A^2)}. \tag{4.72}$$

The integrals are represented in Euclidean space and the angular variables have already been integrated. At the end, the sum of the three integrals gives

$$I_\beta = m_A^4 \int_0^\infty dq\, q^3 \frac{q^4 + q^2(m_{\chi^{\pm\pm}}^2 - 2m_{\chi^\pm}^2) - 2m_{\chi^{\pm\pm}}^4}{(q^2 + m_{\chi^{\pm\pm}}^2)(q^2 + m_{\chi^\pm}^2)^2 (q^2 + m_S^2)(q^2 + m_H^2)(q^2 + m_A^2)}. \tag{4.73}$$

We have checked that we arrive at the same result when using the Goldstone boson equivalence theorem, in which the SM Golstone bosons before symmetry breaking are used instead of the gauge bosons.

In Figure 4.12 we present the numerical evaluations of the integral I_β for some representative cases. We have made use of Eq. (4.19) and Eq. (4.25) to write the integral only in terms of $\sin\alpha$, m_S, m_H, $m_{\chi^{\pm\pm}}$.

Finally, we can check the numerical results by evaluating the integral in two limits:

- In the limit of small mixing, and in which the masses satisfy

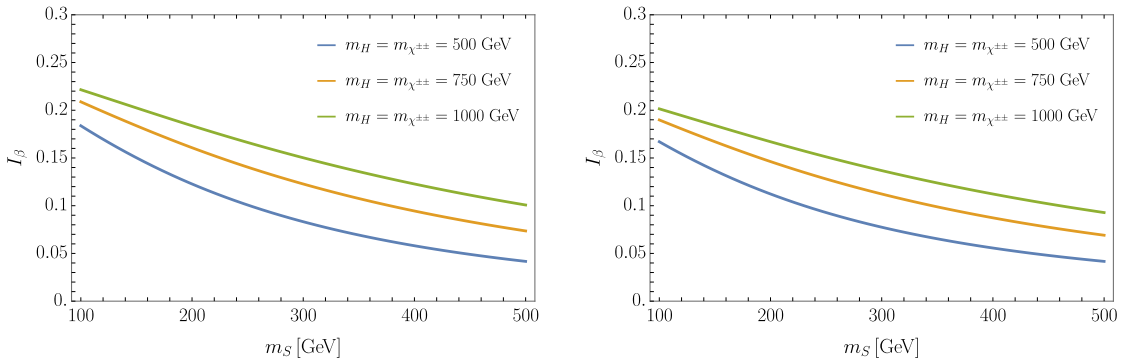

(a) $\sin\alpha = 0.05$ **(b)** $\sin\alpha = 0.25$

Figure 4.12: Numerical evaluation of the $0\nu\beta\beta$ integral, I_β, as a function of m_S. We have fixed $\sin\alpha$ for two representative values, and $m_H = m_{\chi^{\pm\pm}}$.

$m_{\chi^{\pm\pm}} \simeq m_{\chi^\pm} \simeq m_A \simeq m_H \equiv M$ and $m_S \equiv m$, the integral reduces to

$$\begin{aligned} I_\beta &= -M^4 \int_0^\infty dq\, q^3 \frac{q^4 - q^2M^2 - 2M^4}{(q^2+M^2)^5(q^2+m^2)} \\ &= -M^4 \int_0^\infty dq\, q^3 \frac{q^2 - 2M^2}{(q^2+M^2)^4(q^2+m^2)}. \end{aligned} \tag{4.74}$$

Now the integral is straightforward to calculate. In the limit in which the lightest scalar is much lighter than the other scalars, $m \ll M$, the function equals $I_\beta \approx 1/4$.

- When all the masses are degenerated, the integral becomes

$$I_\beta = -m^4 \int_0^\infty dq\, q^3 \frac{q^2 - 2m^2}{(q^2+m^2)^5} = \frac{1}{24}. \tag{4.75}$$

With this in mind, we will work in a regime of small mixing and in which S is somewhat lighter than all remaining scalars. The integral should give values between those of the cases above. In the following, we will take

$$I_\beta \simeq 1/8 \tag{4.76}$$

in our estimations.

4.4.3 Comparison with the experiment: long and short range bounds

The question remains regarding how to use experimental bounds on $0\nu\beta\beta$ rates to set limits on the parameters of the model. KamLAND-Zen reported two interchangeable

bounds on $0\nu\beta\beta$ [86]. First, in terms of the half-life of the decay:

$$T_{1/2}^{0\nu\beta\beta}(^{136}\text{Xe}) > 1.07 \times 10^{26} \text{ yrs}, \tag{4.77}$$

or, equivalently, in terms of the ee matrix element of the neutrino mass matrix:

$$M_{ee}^{max} < 0.1 \text{ eV}. \tag{4.78}$$

In the case that neutrino exchange is the dominant source of $0\nu\beta\beta$, we can use the above experimental limit to set bounds on the parameters of the model without any further manipulation.

To set bounds on short range mechanisms, such as the new physics contribution, is a more delicate task. We will follow an effective Lagrangian approach developed by Deppisch, Hirsch and Päs [99]. In their work, they have characterised all possible hadronic and leptonic currents entering the effective contact interaction that generates the $0\nu\beta\beta$. The most general six-fermion effective Lagrangian reads

$$\mathcal{L} = \frac{G_F^2}{2m_p}\Big\{\epsilon_1\ JJj + \epsilon_2\ J^{\mu\nu}J_{\mu\nu}j + \epsilon_3\ J^{\mu}J_{\mu}j + \epsilon_4\ J^{\mu}J_{\mu\nu}j^{\nu} + \epsilon_5\ J^{\mu}Jj_{\mu}\Big\}, \tag{4.79}$$

where the scalar, vector and tensor hadronic currents are given by

$$J = \bar{u}\ (1 \pm \gamma_5)\ d, \qquad J^{\mu} = \bar{u}\ \gamma^{\mu}(1 \pm \gamma_5)\ d, \qquad J^{\mu\nu} = \bar{u}\ \frac{i}{2}\ [\gamma^{\mu}, \gamma^{\nu}]\ (1 \pm \gamma_5)\ d, \tag{4.80}$$

while

$$j = \bar{e}\ (1 \pm \gamma_5)\ e^c, \qquad j^{\mu} = \bar{e}\ \gamma^{\mu}(1 \pm \gamma_5)\ e^c \tag{4.81}$$

are scalar and vector leptonic currents. The parameters ϵ_i encode the new physics information for each effective contribution.

In our particular model, we need the ϵ_3 term, with two vector-axial hadronic currents and two scalar leptonic currents describing right-handed electrons:

$$\mathcal{L}_{0\nu\beta\beta} = \frac{G_F^2}{2m_p}\epsilon_3\Big[\bar{u}\gamma^{\mu}(1-\gamma_5)d\Big]\Big[\bar{u}\gamma_{\mu}(1-\gamma_5)d\Big]\Big[\bar{e}(1-\gamma_5)e^c\Big]. \tag{4.82}$$

Rearranging Eq. (4.68), we get

$$\epsilon_3 = \frac{m_p}{2G_F^2}\frac{f_{ee}^*}{(4\pi)^2}\frac{\mu_k\lambda_6^2}{m_{k^{\pm\pm}}^2 m_A^4}I_{\beta}. \tag{4.83}$$

Using standard nuclear physics methods, the authors of Ref. [99] put limits on each ϵ_i by calculating the half-life of the $0\nu\beta\beta$ rate. For instance, regarding the parameter

we need for our model, they found the following expression

$$[T_{1/2}^{0\nu\beta\beta}]^{-1} = G_{01}|\epsilon_3 \mathcal{M}_3|^2, \tag{4.84}$$

where G_{01} is a phase space factor and $\mathcal{M}_3$ is a nuclear matrix element that depends on the isotope on which the experiment is based. The values of G_{01} and $\mathcal{M}_3$ can be obtained from [99] and [100] for different nuclei. Finally, they set upper limits on the ϵ_3 parameter, describing the new physics contributions to short range mechanisms, which makes the two equivalent bounds by KamLAND-ZEN to be

$$M_{ee}^{max} < 0.1 \text{ eV} \qquad \text{and} \qquad \epsilon_3^{max} < 4 \times 10^{-9} \qquad (90\% \text{ CL}) \tag{4.85}$$

for the long- and short-range mechanisms, respectively. One can compare both contributions and find the leading source of $0\nu\beta\beta$. Both sources compete when the following relation holds

$$x_3|\epsilon_3^{max}|^2 = x_{ee}|M_{ee}^{max}|^2, \tag{4.86}$$

where x_3 and x_{ee} include the phase factors and hadronic matrix elements corresponding to the short-range operator and the neutrino exchange mechanism. Obviously, one source of $0\nu\beta\beta$ will dominate when one is larger than the other. In particular, the short-range source is dominant when

$$x_3|\epsilon_3|^2 > x_{ee}|M_{ee}|^2. \tag{4.87}$$

Plugging the formulas for ϵ_3 and M_{ee} in the last expression, we find

$$m_A < 4\pi \left(\frac{0.1 \text{ eV}}{4 \times 10^{-9}} \frac{I_\beta}{I_\nu} \frac{m_p}{16 m_e^2 G_F^2} \right)^{1/4} \sim 15 \text{ TeV}, \tag{4.88}$$

where we have assumed $I_\beta / I_\nu \approx 0.1$. Since the masses of the heaviest scalars are correlated and very degenerated by electroweak precision data, this result suggests that all the scalars should be lighter than $\sim$ 15 TeV in order for the short-range mechanism to be the dominant source of $0\nu\beta\beta$. However, one needs to keep in mind that the model predicts M_{ee} to be much more suppressed. In practice, the short-range source of $0\nu\beta\beta$ could be tested provided the scalars are rather light.

Moreover, the next round of experiments are expected to be sensitive to half-lives of order $10^{27} - 10^{28}$ years [101]. Because of Eq (4.84), this traduces to a reduction of the bound on ϵ_3 by one to two orders of magnitude, making the expected limit by the upcoming experiments to be $\epsilon_3 < 4 \times 10^{-10}$. Taking $f_{ee} = 1$, $\lambda_6 = 1$, $\mu_k = m_A = m_{k^{\pm\pm}} = 1$ TeV and $I_\beta = 0.1$ in Eq. (4.83), we obtain $\epsilon_3 \sim 10^{-9}$ which would allow the observation of $0\nu\beta\beta$ in future experiments.

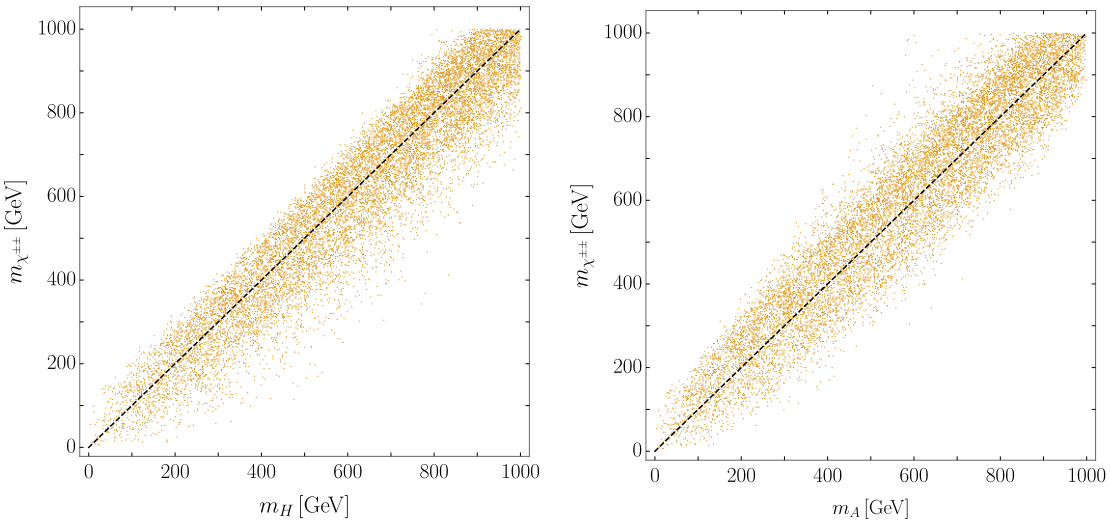

Figure 4.13: Correlation plots for $m_{\chi^{\pm\pm}} - m_H$ (left) and $m_{\chi^{\pm\pm}} - m_A$ (right) obtained from weak precision test data and scanning the complete range of values of the mixing angle and all the scalar masses between $0 - 1000$ GeV. The dashed line represents the case in which the scalars are completely degenerated. The splitting between the masses of the scalars is typically smaller than $\sim 100 - 200$ GeV.

4.5 Constraints from other processes

4.5.1 Electroweak precision data

The most obvious way to discover new phenomena is high-energy physics. However, precision measurements of low energy properties of electroweak bosons, such as decay rates and masses, can be also used to investigate new physics scenarios. There are several parameters encoding this information, but the most relevant ones are the oblique parameters S, T and U describing the self-energy of the gauge bosons [102, 103], along with the related parameter ρ. In the Standard Model, they are exactly zero ($\rho = 1$), and deviations from this value point towards new physics.

Here we will concentrate on the T parameter, which is proportional to the difference of the self-energies of the W and Z gauge bosons. Indeed, it is defined as

$$\Delta T = \frac{4\pi}{g^2 \sin^2\theta_W M_W^2}(\Pi_{WW} - \Pi_{33}), \tag{4.89}$$

where the self-energies of the W boson, Π_{WW}, and of the W_3 boson, Π_{33}, are calculated at $p^2 = 0$.

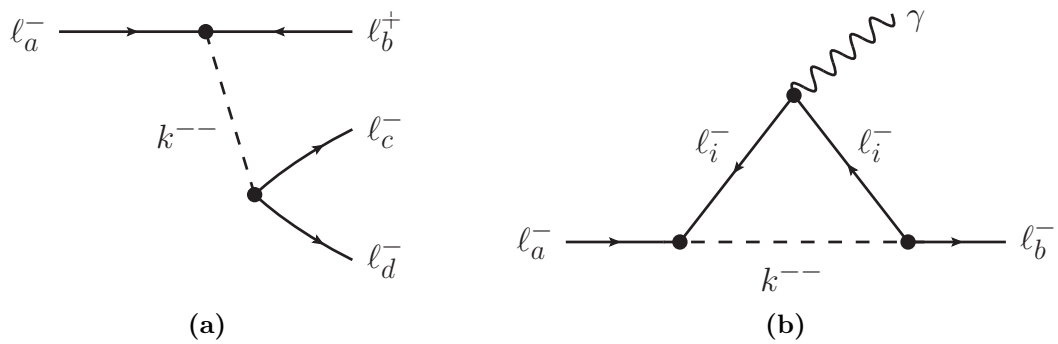

Figure 4.14: Feynman diagrams for the most relevant LFV processes. Subfigure (a) shows $\ell_a^\pm \longrightarrow \ell_b^\mp \ell_c^\pm \ell_d^\pm$, while $\ell_a^\pm \longrightarrow \ell_b^\pm \gamma$ is displayed in (b).

The new physics contribution to the T parameter, predicted by our model, reads

$$\begin{aligned}\Delta T = \frac{1}{4\pi \sin^2\theta_W M_W^2}\Bigg(& F(m^2_{\chi^{\pm\pm}}, m^2_{\chi^\pm}) + \frac{1}{2}F(m^2_{\chi^\pm}, m^2_A) \\ & + \frac{1}{2}\cos^2\alpha\Big[F(m^2_{\chi^\pm}, m^2_H) - 2F(m^2_A, m^2_H)\Big] \\ & + \frac{1}{2}\sin^2\alpha\Big[F(m^2_{\chi^\pm}, m^2_S) - 2F(m^2_A, m^2_S)\Big]\Bigg),\end{aligned} \tag{4.90}$$

where

$$F(A,B) = 8\pi^2 \int \frac{dk}{(2\pi)^4} k^2 \left(\frac{1}{k^2+A} - \frac{1}{k^2+B}\right)^2 = \frac{A+B}{2} - \frac{AB}{A-B}\log\left(\frac{A}{B}\right). \tag{4.91}$$

The measured value of the T parameter is $\Delta T = 0.05 \pm 0.12$ [104]. Using the 2σ uncertainty of this measurement we can explore the parameter space of the scalar masses. We allow the mixing angle to take any value and vary the masses between $0 - 1000$ GeV. In Figure 4.13 we show the correlation plots for $m_{\chi^{\pm\pm}} - m_H$ and $m_{\chi^{\pm\pm}} - m_A$. We see that in general the splitting is smaller than ~ 200 GeV, although for small mixing the splitting reduces to be smaller than ~ 100 GeV.

4.5.2 Lepton flavour violating processes

Until now we elaborated significantly on the breaking of total lepton number, but did not mention lepton flavour violation (LFV). Nothing in the model prevents the doubly-charged scalar from changing the lepton flavour of the charged leptons via their Yukawa interactions. Indeed, had the Yukawa couplings conserved lepton flavour, we would have generated a diagonal neutrino mass matrix, which is unable to accommodate neutrino oscillation data. We can use processes involving lepton flavour violation in order to further constrain the couplings and masses of the model. These processes will be associated with $k^{\pm\pm}$, and thus will set bounds on its mass and

the Yukawa couplings. The main LFV constraints in the model come from $\ell_a^\pm \longrightarrow \ell_b^\mp \ell_c^\pm \ell_d^\pm$ and $\ell_a^\pm \longrightarrow \ell_b^\pm \gamma$, displayed in Figure 4.14. While the latter is generated at the one-loop level, the former happen at tree-level via the exchange of a $k^{\pm\pm}$, which will make it more relevant for our case. These processes have been studied in Ref. [105] in the context of the Zee-Babu model, which has a doubly-charged singlet with the same quantum numbers and hence the same Yukawa interactions with the charged leptons. Table 4.1 summarises the experimental data and the corresponding bounds on the parameters of the model.

Experimental data (90% CL)	*Bounds* (90% CL)
$\mathrm{BR}(\mu^- \longrightarrow e^+e^-e^-) < 1.0 \times 10^{-12}$	$\lvert f^*_{ee} f_{e\mu}\rvert < 2.3 \times 10^{-5} \left(\frac{m_{k^{\pm\pm}}}{\mathrm{TeV}}\right)^2$
$\mathrm{BR}(\tau^- \longrightarrow e^+e^-e^-) < 2.7 \times 10^{-8}$	$\lvert f^*_{ee} f_{e\tau}\rvert < 0.009 \left(\frac{m_{k^{\pm\pm}}}{\mathrm{TeV}}\right)^2$
$\mathrm{BR}(\tau^- \longrightarrow e^+e^-\mu^-) < 1.8 \times 10^{-8}$	$\lvert f^*_{e\mu} f_{e\tau}\rvert < 0.005 \left(\frac{m_{k^{\pm\pm}}}{\mathrm{TeV}}\right)^2$
$\mathrm{BR}(\tau^- \longrightarrow e^+\mu^-\mu^-) < 1.7 \times 10^{-8}$	$\lvert f^*_{\mu\mu} f_{e\tau}\rvert < 0.007 \left(\frac{m_{k^{\pm\pm}}}{\mathrm{TeV}}\right)^2$
$\mathrm{BR}(\mu^- \longrightarrow e\gamma) < 5.7 \times 10^{-13}$	$\lvert f^*_{ee} f_{e\mu} + f^*_{e\mu} f_{\mu\mu} + f^*_{e\tau} f_{\mu\tau}\rvert^2 < 10^{-7} \left(\frac{m_{k^{\pm\pm}}}{\mathrm{TeV}}\right)^4$

Table 4.1: Relevant constraints from LFV processes. Only processes that give the most stringent bounds on the parameters of the model has been displayed. Experimental data is shown in the left column [106, 107]. Limits on the parameters of the model, in the right column, are obtained using Eq. (4.92) and Eq. (4.93).

The branching ratio of the process $l_a^\pm \longrightarrow l_b^\mp l_c^\pm l_d^\pm$, shown in Figure 4.14a, reads

$$\mathrm{BR}(\ell_a^- \longrightarrow \ell_b^+ \ell_c^- \ell_d^-) = \frac{1}{2(1+\delta_{cd})} \left| \frac{f_{ab} f^*_{cd}}{G_F m^2_{k^{\pm\pm}}} \right|^2 \mathrm{BR}(\ell_a^- \longrightarrow \ell_b^- \nu\bar{\nu}). \tag{4.92}$$

The branching ratio of a lepton decaying into a lighter lepton and a pair of neutrinos, $\mathrm{BR}(\ell_a^- \longrightarrow \ell_b^- \nu\bar{\nu})$, is well measured and gives $\mathrm{BR}(\mu \longrightarrow e\nu\bar{\nu}) = 1$, $\mathrm{BR}(\tau \longrightarrow e\nu\bar{\nu}) \approx 0.1784$ and $\mathrm{BR}(\tau \longrightarrow \mu\nu\bar{\nu}) \approx 0.1736$. When there are two identical particles in the final state, $1 + \delta_{cd}$ gives a factor of 2. For instance, despite of the weaker bound on the corresponding branching ratio, line 4 in Table 4.1 gives a stronger bound on the Yukawa couplings than line 3, because of the factor of the two identical muons.

Other low-energy processes give weaker bounds. In particular, $\mu \longrightarrow e\gamma$, displayed in Figure 4.14b, is generated at the one-loop level and is suppressed by the loop factor. The branching ratio of this process is given by

$$\mathrm{BR}(\ell_a \longrightarrow \ell_b \gamma) = \frac{\alpha}{3\pi G_F^2} \left| \frac{\sum_i f^*_{bi} f_{ia}}{m^2_{k^{\pm\pm}}} \right|^2 \mathrm{BR}(\ell_a \longrightarrow \ell_b \nu\nu), \tag{4.93}$$

where $\alpha \approx 1/137$ is the fine-structure constant of the electromagnetic interactions. In addition, $\mu - e$ conversion in nuclei does not generate tree-level amplitudes as

the doubly-charged scalar cannot couple to quarks. The amplitude of this type of processes is obtained by coupling the photon in $\mu \longrightarrow e\gamma$ to a quark neutral current. Finally, processes like $\mu^+e^- \longrightarrow \mu^-e^+$ also give less severe bounds. Here, we will restrict to the processes listed in Table 4.1.

Note that in order to have a sizeable $0\nu\beta\beta$ we need a somewhat large value of f_{ee}, which in turn will require $f_{e\mu}$ to be insignificantly small to keep the bounds from $\mu \longrightarrow eee$ under control.

Additionally, we can use the constraints on $\tau \longrightarrow e\mu\mu$ and the relations among the Yukawa couplings coming from the texture zeros to put bounds on $f_{\tau\tau}$ and, consequently, to $f_{e\tau}$ and $f_{\mu\tau}$. Indeed, the predictions of texture A1 imply

$$3M_{e\tau} \sim M_{\mu\mu} \sim M_{\mu\tau} \sim M_{\tau\tau} \sim 0.02 \text{ eV}, \tag{4.94}$$

which allows us to put the Yukawa couplings in terms of $f_{\tau\tau}$ as

$$f_{e\tau} \sim f_{\tau\tau}\left(\frac{m_\tau}{3m_e}\right), \qquad f_{\mu\mu} \sim f_{\tau\tau}\left(\frac{m_\tau}{m_\mu}\right)^2, \qquad f_{\mu\tau} \sim f_{\tau\tau}\left(\frac{m_\tau}{m_\mu}\right). \tag{4.95}$$

After the relevant substitutions, we get

$$|f_{\tau\tau}| < 1.1 \times 10^{-4}\left(\frac{m_{k^{\pm\pm}}}{\text{TeV}}\right). \tag{4.96}$$

For a $k^{\pm\pm}$ with mass of order 1 TeV and $|f_{\tau\tau}| = 10^{-4}$, the Yukawa matrix reads

$$f_{ab} \approx \begin{pmatrix} f_{ee} & 0 & 10^{-1} \\ 0 & 10^{-2} & 10^{-3} \\ 10^{-1} & 10^{-3} & 10^{-4} \end{pmatrix}, \tag{4.97}$$

where we have left f_{ee} unfixed as it gets limits also from the $0\nu\beta\beta$ data.

Moreover, we can use the bound on $f_{\tau\tau}$ in Eq. (4.96) to further constrain the parameters entering the neutrino mass matrix. Using $M_{\tau\tau} \simeq 0.02$ eV together with Eq. (4.96), this feature leads to a large μ_k and/or large somewhat splitting between m_S and m_H.

4.5.3 Dark matter

The model includes an unbroken Z_2 parity symmetry that divides the spectrum in two sectors. The even sector includes the Standard Model and the doubly charged scalar. The neutral scalars as well as $\chi^\pm$ and $\chi^{\pm\pm}$ are odd particles and hence constitute the so-called dark sector. Moreover, a good dark matter (DM) candidate will be stable as long as it is the lightest neutral particle of the dark sector. For our

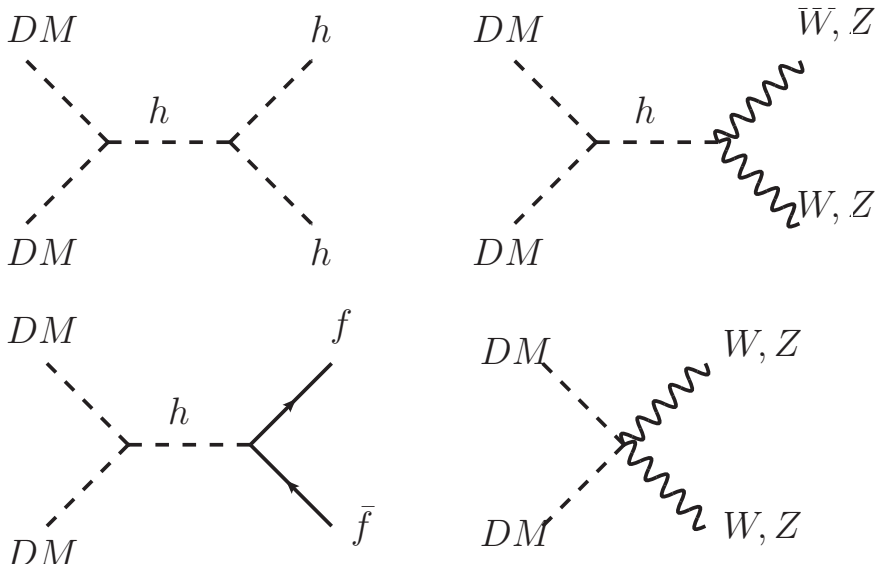

Figure 4.15: Some of the relevant annihilation channels. The first three diagrams correspond to the standard pure Higgs portal scenario. In the last diagram, the pair of DM particles annihilates into gauge bosons, provided the mixing angle between the singlet and the triplet scalars is larger than zero.

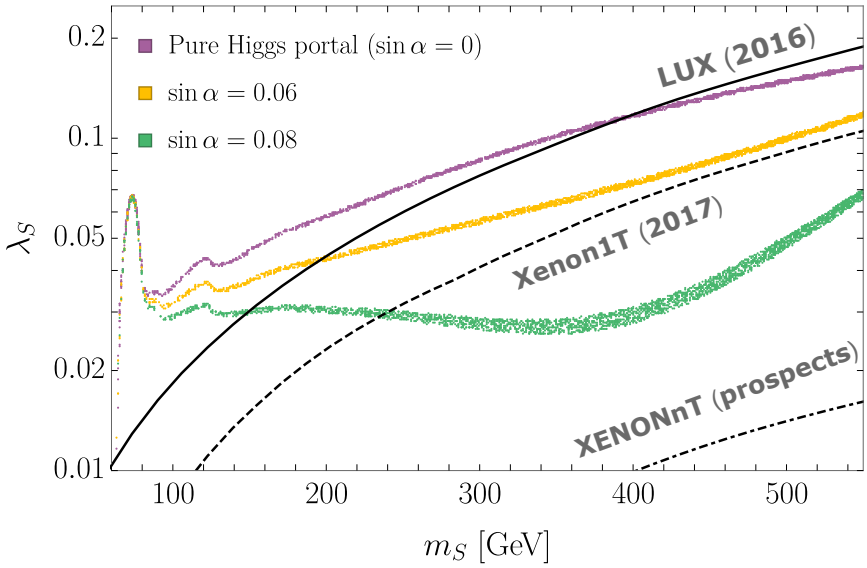

Figure 4.16: Regions corresponding to the observed dark matter relic abundance [108] in the $m_S - \lambda_S$ plane for several values of $\sin\alpha$. We have chosen $m_H = m_{\chi^{\pm\pm}} = m_{k^{\pm\pm}} =$ 800 GeV as a benchmark scenario. Current [109, 110] and future [111] exclusion bounds from direct detection experiments are also presented.

choice of hierarchies, $m_S < m_A < m_H$, the scalar S meets the previous requirement and therefore will be a DM candidate.

As a result of the parity symmetry, the scalars in the dark sector are not allowed to couple to the SM fermions. However, interactions of a pair of odd scalars with an even boson are not forbidden. This opens up new annihilation diagrams into gauge bosons, as we will see. The main annihilation channels are $SS \longrightarrow f\bar{f}, WW, ZZ, hh, kk$, provided the daughter particles are lighter than the DM candidate.

In the following, we will parametrise the interactions of the DM candidate with the SM Higgs boson and consider deviations from the pure Higgs portal scenario. In the Higgs portal scenario, the DM candidate is a singlet of $SU(2)_L$ and has no interactions with the gauge bosons. The main annihilation channels are shown in Figure 4.15. All of them are mediated by a s-channel SM Higgs exchange, except the hh channel, which can also be generated with a contact interaction. This simple model is very constrained by direct detection data for $m_S < 350 - 400$ GeV [112, 113], and has no flexibility for evading the bounds. Note that, when $\sin\alpha = 0$, the dark matter description of our model corresponds to the Higgs portal scenario. Indeed, the renormalizable interactions of the DM candidate, S, with the SM Higgs boson read

$$\mathcal{L} \supset -\frac{1}{2}\lambda_S S^2 \left(vh + \frac{1}{2}h^2\right), \tag{4.98}$$

where the Higgs portal coupling is given by

$$\lambda_S = \frac{1}{2}\Big[2\lambda_{\phi\sigma}\cos^2\alpha - \sqrt{2}\lambda_6 \sin 2\alpha + (\lambda_{\phi\chi} + \lambda'_{\phi\chi})\sin^2\alpha\Big]. \tag{4.99}$$

However, as we slowly turn on the mixing angle, new annihilation diagrams with gauge bosons in the final state start to open. These consist of contact interactions of the type $SSVV$ (with $V = W, Z$) whose strength depends on $g^2\sin^2\alpha$. When $\lambda_S > 0$, the new contact interactions interfere constructively with the original annihilation diagrams to gauge bosons of the pure Higgs portal scenario, and thus require smaller values of λ_S to reproduce the same dark matter relic abundance, as it scales with the cross section.

In Figure 4.16 we present curves of allowed dark matter relic density, $\Omega_{DM}h^2 = 0.12$ [108], in the $m_S - \lambda_S$ plane for several values of the mixing angle. Here, we have assumed $m_H = m_{\chi^{\pm\pm}} = m_{k^{\pm\pm}} = 800$ GeV and used the `MicrOMEGAs` package [114] to compute the relic abundance. Exclusion limits from current [109, 110] and future [111] direct detection experiments have also been plotted. The relevant parameters of direct detection are the mass of the dark matter candidate and the coupling constant λ_S. We see that the new contact interactions strongly enhance

the dark matter annihilations, even for small values of the mixing angle.

Finally, the case $\lambda_S < 0$, although not considered here, is perfectly allowed by the model. At first, all annihilations should still be purely dominated by Higgs portal diagrams. But as soon as the mixing angle is turned on, the situation changes. Because of the negative values of λ_S, the contact interaction diagrams will have a destructive interference relative to the Higgs portal diagrams with gauge bosons in the final state. When the gauge boson annihilation channels are strongly suppressed, the main contribution comes from the hh channel and λ_S can take even larger values than in the pure Higgs portal scenario, given that now there are fewer annihilations. The opposite case happens when the destructive interference is not strong enough and λ_S is allowed to take lower values, as in the case of $\lambda_S > 0$. However, more quantitative work in this direction is needed.

4.6 Some final considerations

The analysis of the effective Lagrangian approach suggests that the model would induce $0\nu\beta\beta$ and Majorana neutrino masses by new physics at the TeV scale. Moreover, the form of the neutrino mass matrix would be dictated by the hierarchy among the masses of the charged leptons. For this reason, the details of the oscillation parameters are described by an A1 texture zero that perfectly accommodates the most updated neutrino oscillation data. In addition, and despite predicting $M_{ee} \approx 0$, the model gives a sizeable $0\nu\beta\beta$ rate through a short-range mechanism, with the interesting possibility of an observation in the upcoming experiments. In fact, if a detection of $0\nu\beta\beta$ does happen, the measurement of the polarisation of the emitted electrons would help to discern this mechanism from the the standard neutrino exchange mechanism into left-handed electrons.

The analysis of the viability of the dark matter candidate showed that the mixing angle between the neutral scalars should be small for the sake of keeping the annihilation into gauge bosons through contact interactions under control. Moreover, limits on the oblique T parameter require the scalar masses to satisfy $|m_{\chi^{\pm\pm}} - m_H| < 100$ GeV, which implies that, for small mixing, the masses of those particles are also close to m_A and $m_{\chi^\pm}$. Finally, bounds on LFV processes, and in particular on $f_{\tau\tau}$, lead to a somewhat large value of μ_k.

In Table 4.2 we present benchmark values for the independent parameters of the model, as well as for some relevant quantities that are derived from these inputs. We have checked that these numbers satisfy all constraints from the low energy processes and experiments seeking for dark matter, as well as being able to accommodate neutrino oscillation data while generating a $0\nu\beta\beta$ rate large enough to be seen in

the upcoming rounds of experiments.

$m_{\chi^{\pm\pm}}$	$m_{k^{\pm\pm}}$	$\sin\alpha$	m_H	m_S	μ_κ	$\lvert f_{ee}\rvert$	$\lvert f_{\tau\tau}\rvert$	$\lvert f_{e\mu}\rvert$
800	800	0.08	800	200	20000	0.01	10^{-4}	0

$m_{\chi^{\pm}}$	m_A	I_β	I_ν	ϵ_3	$\lvert f_{e\tau}\rvert$	$\lvert f_{\mu\mu}\rvert$	$\lvert f_{\mu\tau}\rvert$
799	798	0.165	0.84	3.5×10^{-9}	0.12	0.03	1.7×10^{-3}

Table 4.2: Benchmark values for the input parameters (first row) and other relevant quantities (second row) calculated from the numbers of the first row. All parameters with dimensions of mass are in units of GeV.

Finally, the scalars of the model could have masses below the TeV scale, and could therefore be searched at colliders. In particular, $k^{\pm\pm}$ has interactions with the SM particles. This enables to probe its decay into light charged leptons in the LHC, which has been already investigated in the literature (see for instance Ref. [115]). On the other hand, $\chi^{\pm\pm}$ and $\chi^{\pm}$, despite being odd particles, can be explored through more exotic decay channels. For instance, $\chi^{\pm\pm}$ could decay into $k^{\pm\pm}$ plus missing energy. In such a case, the production pattern of the doubly-charged singlet is modified and consequently so is the LHC analysis. These possibilities will be explored in the next chapter, where we discuss LHC prospects for LNV scalars.

4.7 Summary

- Neutrinoless double beta decay and the generation of neutrino masses are very low energy processes and therefore they can be described by higher-dimension effective operators, within the framework of the SMEFT.

- In particular the RR dimension-nine operator induces $0\nu\beta\beta$ at tree level and neutrino masses at the two-loop level, with a new physics scale arising naturally at the TeV scale.

- In this chapter we have designed a model of neutrino masses that realises the RR dimension-nine effective operator, using the same local group of the Standard Model, with three new heavy scalars and a parity symmetry that splits the field content into a visible and a dark sector.

- We have computed the contributions given by the new diagrams to neutrino masses and the short-range mechanism of $0\nu\beta\beta$, in the gaugeless limit as well as in the unitary gauge.

- Both the rows and the columns of the neutrino mass matrix are proportional to the masses of the charged leptons, which translates to the following hierarchy among the elements of the neutrino mass matrix:

$$M_{ee}, M_{e\mu} \ll M_{e\tau}, M_{\mu\mu}, M_{\mu\tau}, M_{\tau\tau}.$$

  It follows that the predictions of the A1 pattern of two-zero textures can be applied to the model.

- Because $M_{ee} \approx 0$, the standard neutrino exchange source of $0\nu\beta\beta$ is very suppressed. However, we have found that upcoming $0\nu\beta\beta$ experiments can be sensitive to the short range mechanism provided the new scalars are lighter than around 15 TeV.

- Finally, we have discussed a benchmark point for the input parameters of the model, using constrains from electroweak precision data and lepton flavour violating processes along with an analysis of the viability of the DM candidate.

CHAPTER 5

LHC prospects for lepton number violating scalars

In previous chapters we discussed different extensions of the Standard Model that attempt to describe neutrino masses with the addition of exotic scalars. For instance, in Chapter 2 we described the seesaw type-II model, the simplest extension of the Standard Model generating Majorana neutrino masses, with the only inclusion of a new scalar triplet. In this context, the mass of the scalar could lie above the 10^8 GeV scale, well above the scope of current accelerators. However, it is only one of the three possible scalars that have renormalizable interactions with a lepton bilinear carrying a net lepton number.

The second possibility is a singly-charged scalar singlet. The Yukawa interaction with the lepton doublets requires the singlet to have a net lepton number. However, we cannot rely upon spontaneous symmetry breaking for breaking lepton number as the VEV of the singlet would also break the electromagnetic symmetry. So this Lagrangian alone is not sufficient to induce Majorana neutrino masses and we need more ingredients. There are several possibilities. Adding a second Higgs doublet leads to the Zee model [116], which generates neutrino masses at the one-loop level. In this case, lepton number violation is achieved by a trilinear interaction in the scalar sector. Although this model is interesting in many aspects, in its simplest version, it is incompatible with oscillation data (it predicts three-zero textures, which is ruled out by the experiments [117]).

The last scalar of this list is a doubly-charged singlet. But, as for the case of the singly-charged singlet, we cannot spontaneously break lepton number with this scalar alone. However, we can still use the doubly-charged singlet as the bedrock for the generation of neutrino masses, and there are lots of models following this approach. An interesting scenario, called Zee-Babu model, consists of simultaneously considering the two singlets [118, 119]. Then, as in the Zee model, lepton number

is broken by a trilinear term in the potential and neutrino masses are induced at the one-loop level. Another much more involved example was introduced in Chapter 4. Along with the doubly-charged singlet, this framework included two additional scalar multiplets and has a number of interesting phenomenological implications.

In contrast with the seesaw type-II model, models of loop-produced neutrino masses predict the scalar masses to lie in the TeV scale. This makes these scalars ideal candidates for being investigated at high-energy facilities. However, and although there are several searches for LNV scalars currently being performed at the LHC, none of them take into account the rich decay chains that these scalars would exhibit.

In this chapter we will study the possibility of probing at the LHC some of the scalars named above that are needed to break lepton number so that neutrinos can become massive.

5.1 Large Hadron Collider

Massive exotic particles typically exhibit very large decay rates. They are unstable and very rare in nature. Moreover, as they get larger masses they also become increasingly harder to produce in the laboratory. The most common technique to search for novel particles consists of accelerating known particles to very high kinetic energies and colliding them with other particles. The experiment is called a *collider* if its setup involves two beams of particles travelling in opposite direction at high velocities. Then, after the collision, the kinetic energy can be transformed into mass so that more massive particles could be produced. (Of course, the mass of the new particles cannot be larger than the total energy of the process.) For this reason, high-energy colliders are extremely useful tools for probing new exotic particles as well as to test the dynamics and the structure of matter.

Modern colliders can be categorised by shape and by the type of particles that each beam carries. Colliders can take either circular or linear shapes. In circular colliders, even though the rate of collision is very small, the beams can be used over and over, which translates into a rapid recollection of data. However, this type of accelerator suffers from energy losses from synchrotron radiation. Linear colliders have different properties. In fact, because of its straight shape there is no losses from synchrotron radiation (although it has other types of losses), but the collection of data is more demanding as the colliding particles cannot be reused.

Some colliders are based on beams of hadrons. The best feature of hadrons is that they are relatively heavy, which makes them easier to accelerate to large energies. On the negative side, they are compound particles and show more complicated collision

events. Other colliders utilise leptons, which give clean signals. Moreover, being elementary particles, initial states are well known. However, leptons are lighter than hadrons and therefore harder to accelerate to high energies. This is because losses from synchrotron radiation scales inversely with the fourth power of the mass of the travelling particle. The electron is 2000 times lighter than the proton, so that it losses energy 10^{13} times faster. For this reason, hadron colliders are usually more fitted for searching for new heavy particles, while lepton colliders are usually used for precision measurements of known particles.

Among all particle accelerators ever built, the Large Hadron Collider (LHC) is the most powerful one. Indeed, expectations for observing new particles are placed in the remarkable technological development that the LHC has achieved. It is a circular collider that (mainly) accelerates beams of protons with an energy of 6.5 TeV. In other words, collisions occur with a total centre of mass energy of 13 TeV. Although there are several experiments being conducted, the main two are CMS and ATLAS, which are design for general purposes. They typically search for new particles.

The detectors of these experiments include several layers that target different particles. An inner detector tracks charged particles, by curving them with a magnetic field, and plays an important role in identifying the particles and their collision point. A set of electromagnetic and hadronic calorimeters absorbs the energy of easily stopped particles, such as photons, light charged leptons and hadrons. Then, by sampling the form of the particle shower, they deduce the energy of the parent particle. The muon detectors, placed at the boundary of the experiments, make additional measurements of the momenta of highly penetrating muons. Finally, the magnetic systems trace the curvature of the path of the particles in order to measure their momentum.

Since the first collisions took placed in 2010, the LHC has collected an outstanding amount of data. Up until 2017, the total integrated luminosity jointly obtained by ATLAS and CMS was of 70 fb^{-1}. At the end of run 2, it increased to $\sim$ 270 fb^{-1}, counting 135 fb^{-1} for each experiment. An upgrade that will improve the potential of the LHC has already been started. The new phase will be called High-Luminosity LHC and it is expected to boost the luminosity by a factor of 10 in the upcoming years.

Before performing the actual experiments, with all the complications they involve, it is useful to study what we expect to see from the signal if the pursued particle exists in nature. This is done by means of computer simulations. There are several codes implementing each step; only those that we use are listed here. The first step is to implement the relevant particles and its interactions. This is done with the `FeynRules` package [120] that exports an UFO model. This file is then imported to `MadGraph` [121], which is able to generate both background and signal

events. Initial and final state radiation as well as parton showering and hadronisation is performed by `Pythia` [122, 123]. Finally, the events are selected and analyse with home-made routines based on `MadAnalysis` [124].

Throughout this chapter we will concentrate in the current phase of the LHC with 13 TeV of centre of mass energy and with the integrated luminosity so far collected, as well as with the luminosity expected in the near future. In the next section we present a search strategy containing several signal regions with light leptons in the final state, that will allow us to test scenarios of singly- and doubly-charged lepton number violating scalars.

5.2 Search strategy

In the following, we consider only electrons and muons as they show similar cut efficiencies at the LHC. Taus, with lower identification efficiency, are excluded of our analysis. Thus, throughout this chapter we will use the term *lepton* to denote exclusively electrons and muons. We define three orthogonal signal regions:

1. **SR1**, which contains events with two leptons in the final state.

2. **SR2**, with three leptons in the final state.

3. **SR3**, with four leptons in the final state.

The precise details of each signal region depend upon the analysis considered. For instance, in order to explore scenarios with doubly-charged scalars, the signal regions should contain leptons with the same sign. On the other hand, this requirement is somewhat more relaxed in the analyses of models with singly-charged scalars, for which the SR1 will consist of pairs of leptons with opposite sign.

In our search strategy we will make use of a set of three observables. First, every signal region considered here involves at least a pair of leptons. Then the following observable is useful:

1. The invariant mass of the lepton pair, $m_{\ell\ell}$.

Charged leptons are often accompanied by neutrinos, which we identify as sources of missing energy. Moreover, in more exotic decay channels, the particle that is being probed can be produced in association with particles belonging to a dark sector or with long-lived unstable particles; all these particles would escape the detectors. It is then natural to consider an observable that takes in consideration this missing energy:

2. The transverse mass of a lepton object L, defined as

$$m_T^2 = m_L^2 + 2(E_T^L E_T^{\text{miss}} - \vec{p}_T^{\,L} \cdot \vec{p}_T^{\,\text{miss}}), \tag{5.1}$$

where L can be a single lepton, $L = \ell$, and then all kinematic variables are defined as usual; or a lepton pair, in which case $L = \ell\ell$, $m_{\ell\ell}$ is the invariant mass above, $\vec{p}_T^{\,\ell\ell} = \vec{p}_T^{\,\ell_1} + \vec{p}_T^{\,\ell_2}$ and $E_T^{\ell\ell} = \sqrt{|\vec{p}_T^{\,\ell\ell}|^2 + m_{\ell\ell}^2}$.

Very often, the parent particle is produced in pairs, and then its decay will give two invisible particles. The following observable takes advantage of that scenario:

3. The stransverse mass, m_{T2}, defined as

$$m_{T2} = \min_{\vec{q}_{L1}^{\,\text{miss}} + \vec{q}_{L2}^{\,\text{miss}} = \vec{p}_T^{\,\text{miss}}} \left\{ \max \left[m_T(\vec{p}_T^{\,L1}, \vec{q}_{L1}^{\,\text{miss}}), m_T(\vec{p}_T^{\,L2}, \vec{q}_{L2}^{\,\text{miss}}) \right] \right\}, \tag{5.2}$$

with $m_T(\vec{p}_T^{\,X}, \vec{q}_X^{\,\text{miss}}) = \sqrt{m_X^2 + 2(E_T^X q_X^{\text{miss}} - \vec{p}_T^{\,X} \cdot \vec{q}_X^{\,\text{miss}})}$, where X denotes a visible particle, E_T^X and $\vec{p}_T^{\,X}$ its transverse energy and momentum, respectively, while $\vec{q}_X^{\,\text{miss}}$ is the part of the missing transverse momentum *associated* with X (and not the total missing energy). In general, we will be able to set $m_X = 0$ in the definition of m_T as all momenta will be much heavier than the lepton masses.

Throughout this chapter, $L1$ and $L2$ will be either a lepton or a lepton pair. In the upcoming sections we will explicitly discuss each case.

As for the signal regions, the exact definition of each observable depends on the analysis in consideration. We group the three observables together in the set $O = m_{\ell\ell}, m_T, m_{T2}$. It is interesting to note that the stransverse mass will be bounded from above by the mass of the parent particle. For the background, this implies that m_{T2} should show values below the mass of the top quark. Then, for values beyond the mass of the top quark, the distributions of m_{T2} will be dominated by the signal.

Finally, we will also consider the observable S_T, defined as the scalar sum of the p_T of all the leptons in the signal region. This observable will allow us to bin the variables in two dimensions. Indeed, for each signal region, we consider 81 different categories defined by $S_T > X$ and $O > Y$, with $X, Y = 100, ..., 900$ GeV, in steps of 100 GeV.

5.3 Application to searches of doubly-charged scalars

In this section we will apply the strategy to the case of searches for doubly-charged scalars within the framework of two different extensions of the Standard Model

describing Majorana neutrino masses[1]. In order to break lepton number in two units, these models introduce a doubly-charged scalar, $k^{\pm\pm}$, among with other new fields. To be precise, we will call $\chi^{\pm\pm}$, $h^{\pm}$ and S any additional doubly-charged, singly-charged or neutral scalar, respectively. Then, besides the production patterns and decay modes in which $k^{\pm\pm}$ directly couples to the SM particles, the doubly-charged scalar may also show new exotic decay channels. In the following we list the decay modes we consider. If not explicitly stated otherwise, $k^{\pm\pm}$ is produced in pairs through an s-channel mediated by neutral gauge bosons.

- $k^{\pm\pm} \longrightarrow \ell^{\pm}\ell^{\pm}$. This is a decay channel that very often appears in models of neutrino masses, like in seesaw type-II, Zee-Babu, or the three-loop model of Chapter 4. It is based on the renormalizable interaction $k^{\pm\pm}\ell^{\mp}\ell^{\mp}$ that gives $k^{\pm\pm}$ a net lepton number.

- $k^{\pm\pm} \longrightarrow W^{\pm}W^{\pm}$. This decay channel is present in models in which $k^{\pm\pm}$ is member of a non-trivial $SU(2)_L$ multiplet. For instance, in the seesaw type-II model of neutrino masses, $k^{\pm\pm}$ belongs to a triplet of $SU(2)_L$. In fact, when the VEV of the triplet is large enough, this decay channel is dominant.

- $k^{\pm\pm} \longrightarrow h^{\pm}h^{\pm}$, with $h^{\pm} \longrightarrow \ell^{\pm}\nu$. Again, the simplest model of neutrino masses showing this decay pattern is the Zee-Babu.

- $k^{\pm\pm} \longrightarrow h^{\pm}h^{\pm}$, with $h^{\pm} \longrightarrow W^{\pm}S$. Models in which $h^{\pm}$ and S belong to the same multiplet show this decay chain. Moreover, when the aforementioned multiplet is odd under a Z_2 parity symmetry[2], S is a dark matter particle and can therefore be treated as missing energy. The three-loop model of Chapter 4 is an example of this class of models.

- $\chi^{\pm\pm} \longrightarrow k^{\pm\pm}S$, with $k^{\pm\pm} \longrightarrow \ell^{\pm}\ell^{\pm}$. When the conditions of the previous decay channel are met, this decay mode also comes along. As a matter of fact, this decay channel enhances the production of $k^{\pm\pm}$ and hence the sensitivity to m_k. Finally, after being produced in association with S, the doubly-charged scalar can still decay through any of the channels above, but an analysis considering them goes beyond the scope of this study.

Of much interest are the possibilities opened up by the exotic interactions. Any dedicated search of doubly-charged scalars needs to take into consideration that the exotic decay channels will significantly change the signature of the observables. Indeed, in Figure 5.1 we show how much the distribution of the invariant mass of

[1] The work presented in this section was published by the author of this thesis and collaborators in Ref. [125]

[2] $k^{\pm\pm}$ should be even under Z_2, or otherwise this decay mode does not occur.

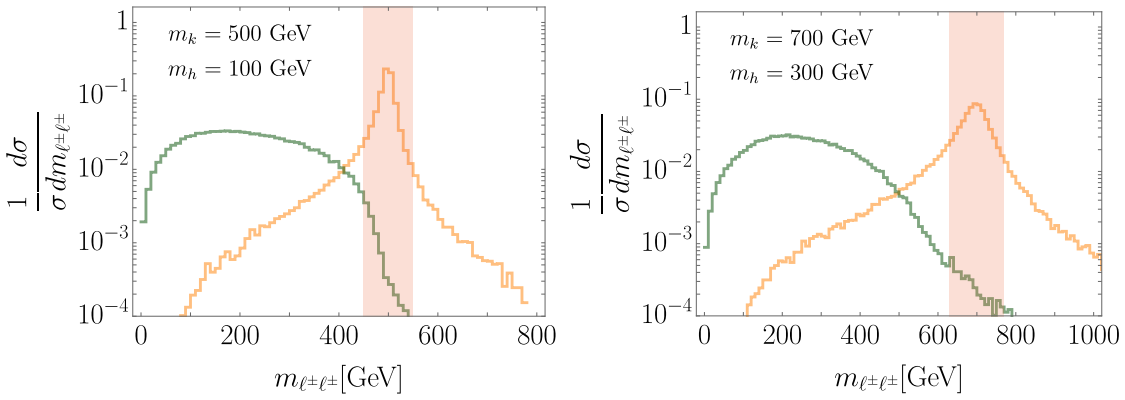

Figure 5.1: Distributions of the invariant mass of pair of same-sign leptons in events generated with $pp \longrightarrow kk$ followed by $k \longrightarrow \ell\ell$ (orange) and followed by $k \longrightarrow hh \longrightarrow \ell\ell\nu\nu$ (green). For illustration, we show in red the cut imposed by the experimental collaboration [129].

pairs of same-sign leptons might vary when considering the exotic decay pattern of the Zee-Babu model above.

Both ATLAS and CMS collaborations have performed searches of doubly-charged scalars [126–129]. These analyses have been inspired by the seesaw type-II model, and therefore look for the leptonic decay of $k^{\pm\pm}$ (orange curves in Figure 5.1). The reconstruction of the invariant mass of $k^{\pm\pm}$ in this class of models poses no difficulties. But as soon as more exotic decay modes are opened up, especially in the presence of missing energy, the distributions of the invariant mass starts to flatten. In this regard, more involved observables, as those listed in the previous section, may become useful to obtain information about the scalar that is being tested.

So, in the context of doubly-charged scalar searches, we will inclusively consider the set of observables described above, with the lepton pair being always of the same sign. Then, the invariant mass is constructed for every same-sign lepton pair. The transverse mass is also built for each same-sign lepton pair, as well as for the third lepton in SR2. Finally, in the SR1, the indices $L1$ and $L2$ in the definition of the stransverse mass stand for the harder and softer lepton, respectively. In the SR2, $L1$ corresponds to the vectorial sum of the two same-sign leptons, while $L2$ stands for the third lepton. In the SR3, $L1$ amounts for the vectorial sum of the two positive leptons and $L2$ for the vectorial sum of the negative ones.

5.3.1 Background for same-sign leptons

Taking into consideration the decay modes of $k^{\pm\pm}$ and the search strategy described above, we need to generate a multi-lepton background, whose events have at least two same-sign leptons. Although the estimation of the background is inspired in models of doubly-charged scalars, it is still useful for other LHC analyses containing

same-sign leptons. For instance, we will make use of it in the search we propose regarding singly-charged scalar singlets, as we will see in Section 5.4.

We generate the background events with `MadGraph 5` [121] at NLO in α_s, with parton showering performed by `Pythia 6` [122]. At generator level we impose the following cuts. Electrons (muons) are require to have $p_T^\ell > 20(10)$ GeV and $|\eta_\ell| < 2.5(2.6)$. Jets, defined to have $p_T^j > 20$ GeV and $|\eta_j| < 2.4$, are clustered using the anti-k_t algorithm [130] with $R = 0.4$. We have fixed the b-tagging efficiency to be 0.7 and the τ-tagging efficiency to 0.5. Furthermore, the correct estimation of the background depends upon the mis-identification of electrons. In Ref. [128] the charge mis-identification probability was parametrised by $P(|\eta_\ell|, p_T^\ell) = f(|\eta_\ell|)\sigma(p_T^\ell)$, where

$$f(x) = \begin{cases} 0.03 & \text{if } 0 < x < 0.4, \\ 0.04 & \text{if } 0.4 < x < 0.8, \\ 0.08 & \text{if } 0.8 < x < 1.1, \\ 0.15 & \text{if } 1.1 < x < 1.4, \\ 0.3 & \text{if } 1.5 < x < 1.7, \\ 0.6 & \text{if } 1.7 < x < 1.9, \\ 0.7 & \text{if } 1.9 < x < 2.1, \\ 1 & \text{if } 2.1 < x < 2.3, \\ 2 & \text{if } x > 2.3 \end{cases} \quad \text{and} \quad \sigma(x) = \begin{cases} 0.02 & \text{if } x < 70, \\ 0.035 & \text{if } 70 < x < 100, \\ 0.05 & \text{if } x > 100. \end{cases} \tag{5.3}$$

The following processes give sizeable contributions to the background: Drell-Yan, $t\bar{t}$, WZ, WW, ZZ, WWW, WWZ, WZZ, ZZZ, $t\bar{t}W$ and $t\bar{t}Z$. The Drell-Yan background was generated with $m_{\ell\ell} > 100$ GeV for the sake of reducing the running time of the simulation. In Table 5.1 we show the cross section and number of generated events for each process giving contributions to the background.

As said above, both ATLAS and CMS have performed searches of doubly-charged scalars in the context of the seesaw type-II model. We can make use of their results to check the validity of the background generated in this section. In Figure 5.2, we depict the minimum cross section on pair production of $k^{\pm\pm}$ followed by a leptonic decay with 100% branching ratio that can be excluded at the 95% CL (dashed black line) using our background. Then, we compare these values with the theoretical cross sections obtained with the seesaw type-II model (red line). The results are in very good agreement with those obtained by the experimental collaborations.

Finally, we have computed the number of background events in each of the categories of the signal regions defined above. In the following, we will see to what

Background	*Cross section* [pb]	*Simulated events*
Drell-Yan	220 ± 20	10^8
$t\bar{t}$	660 ± 70	10^8
WW	102 ± 4	10^7
WZ	45 ± 2	10^6
ZZ	13.6 ± 0.5	10^6
WWW	0.21 ± 0.01	10^6
WWZ	0.17 ± 0.01	10^6
WZZ	0.057 ± 0.004	10^6
ZZZ	0.014 ± 0.001	10^6
$t\bar{t}W$	0.59 ± 0.06	10^6
$t\bar{t}Z$	0.76 ± 0.09	10^6

Table 5.1: Backgrounds, cross sections and numbers of generated events.

extent the signal events of different models of doubly charged scalar singlets are compatible with this background.

5.3.2 Zee-Babu model

The Zee-Babu model is an extension of the Standard Model that generates neutrino masses at the one-loop level. It includes a doubly-charged scalar singlet, $k^{\pm\pm}$, along with a singly-charged scalar singlet, $h^{\pm}$. The singly-charged singlet is introduced in order to break lepton number in two units, which is needed for Majorana neutrino masses, by means of a trilinear interaction with the doubly-charged singlet. The

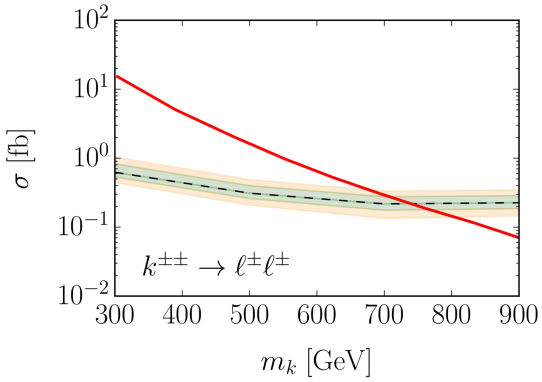

Figure 5.2: Bounds on the cross section (dashed black line) for an integrated luminosity $\mathcal{L} = 35$ fb^{-1} of the leptonic decay of $k^{\pm\pm}$. The green and orange regions show the 1σ and 2σ uncertainties. The theoretical cross section in the context of the seesaw type-II model (in which $k^{\pm\pm}$ is member of a $SU(2)_L$ triplet) is shown for reference (red line).

relevant piece of the Lagrangian reads

$$\mathcal{L}_{ZB} = g_{ab}\,\overline{e_a^c} e_b k^{\pm\pm} + f_{ab}\,\overline{\widetilde{\ell}_{La}}\ell_{Lb}h^+ - \mu\, k^{++}h^-h^- + h.c. \tag{5.4}$$

where f_{ab} is an antisymmetric matrix because of the $i\sigma_2$ factor in $\widetilde{\ell}_L$, while g_{ab} is symmetric. Finally, the trilinear coupling can be expressed in terms of a dimensionless parameter κ, defined by $\mu = \kappa\ \min(m_h, m_k)$, and which we take to be $\kappa < 4\pi$ due to naturalness arguments [105].

As the goal of the Zee-Babu model is to describe neutrino masses, the main constraints would be given by neutrino oscillation experiments. Both normal and inverted orderings are still allowed by current data [105]. In addition, we take into consideration the bounds from low energy processes. We proceed by selecting a particular benchmark set of values for the parameters in each neutrino mass ordering.

In NO, neutrino data demand $g_{ee} \sim g_{\mu\mu} \sim 0.1 \gg g_{e\mu}, g_{e\tau}, g_{\mu\tau}, g_{\tau\tau}$ and $f_{e\mu} \sim f_{e\tau} \sim f_{\mu\tau}/2$ [105]. Values of f around 0.01 satisfy bounds from $\mu \longrightarrow e\gamma$. Finally, the region $m_k < 2m_h$ is still allowed for $m_k > 600$ GeV if $\kappa < 5$. Values satisfying these constraints are shown in the first row of Table 5.2.

In IO, the parameter space in highly constrained for most of the values of the Majorana and Dirac phases [105]. In particular, the scalar masses are way beyond the reach of the LHC. However, in the small window in which the Dirac CP phase is around 180°, the bounds become more relaxed. The hierarchies among the Yukawa couplings become $g_{\tau\tau} \ll g_{\mu\tau} \sim g_{\mu\mu} \sim$ and $g_{e\mu}, g_{e\tau} < 0.1$. In the second row of Table 5.2 we present allowed values for the parameters.

	g_{ee}	$g_{e\mu}$	$g_{e\tau}$	$g_{\mu\mu}$	$g_{\mu\tau}$	$g_{\tau\tau}$	$f_{e\mu}$	$f_{e\tau}$	$f_{\mu\tau}$	κ
NO	0.1	0.001	0.001	0.1	0.001	0.001	0.01	0.01	0.02	5
IO	0.1	0.0001	0.0001	0.0001	0.1	0.0001	0.1	-0.1	0.01	5

Table 5.2: Benchmark values for the relevant parameters of the Zee-Babu model in the normal ordering (first row) and inverted ordering (second row) of neutrino masses.

Within the Zee-Babu model, the decay width of $k^{\pm\pm}$ into a pair of charged leptons is given by

$$\Gamma(k^{\pm\pm} \longrightarrow \ell_a^\pm \ell_b^\pm) = \frac{|g_{ab}|^2}{4\pi(1+\delta_{ab})} m_k. \tag{5.5}$$

As said above, $k^{\pm\pm}$ may also show more exotic decay modes. This translates into a signatures not yet explored experimentally. In the Zee-Babu model, $k^{\pm\pm}$ can decay

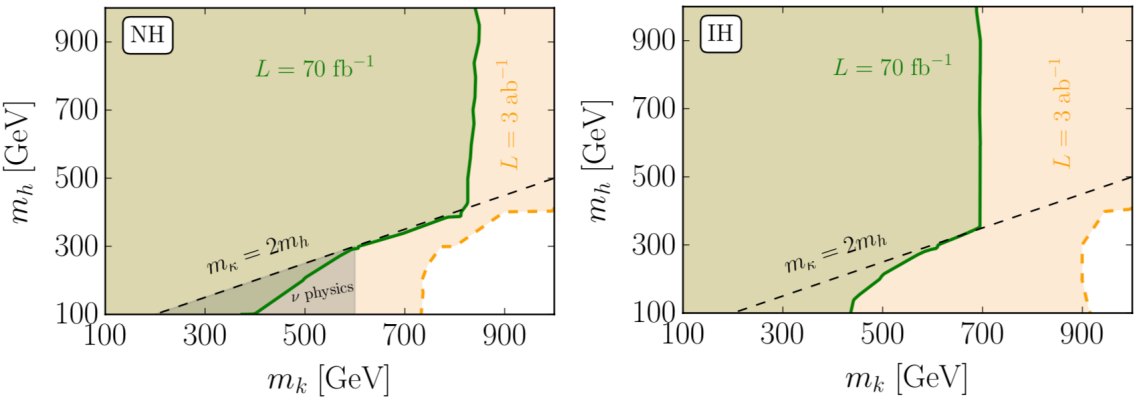

Figure 5.3: Excluded regions in the plane $m_k - m_h$ in the Zee-Babu model for normal ordering (left panel) and inverted ordering (right panel).

into a pair of $h^\pm$, following

$$\Gamma(k^{\pm\pm} \longrightarrow h^\pm h^\pm) = \frac{1}{8\pi}\left(\frac{\mu}{m_h}\right)^2 m_k \sqrt{1 - \frac{4m_h^2}{m_k^2}}, \tag{5.6}$$

which of course happens only for $m_k > 2m_h$. The subsequent decay $h^\pm \longrightarrow \ell_a^\pm \nu_b$ (where $a, b = e, \mu, \tau$) has a width that follows Eq. (5.5) but without the $1 + \delta_{ab}$ factor of identical particles, as the Yukawa coupling is antisymmetric (and ℓ and ν are different particles). For the hierarchy between Yukawa couplings in NO, this implies that $h^\pm$ decays into a lepton and a neutrino around 58% of the times, while the decay into a tau and a neutrino happens around 42% of the cases. Moreover, events with two, three and four leptons in the final state occur in 35%, 30% and 15% of the time. In the IO, the decay of $k^{\pm\pm}$ to a tau and a neutrino reduces down to around 25% of the cases. Thus we are safe to say that our search strategy captures most of the signal. Finally, for the benchmark points considered, the decay widths are small enough to make use of the narrow width approximation.

In order to set bounds on the scalar masses, we vary m_k and m_h between 100 and 1000 GeV and, for each pair of masses, we compute the efficiency ϵ of selecting events in each of the categories defined in Section 5.2. Then, the total number of signal events is given by

$$S = \sigma(pp \longrightarrow k^{++}k^{--}) \times \mathcal{L} \times \epsilon, \tag{5.7}$$

where $\mathcal{L}$ is the integrated luminosity. We compute the sensitivity for every category in each signal region. Out of it, we keep only the most sensitive category in SR1, SR2 and SR3. With this set of three independent categories, we compare the signal with the SM background. Using the CL_s method [131], we find the regions that can be

excluded at the 95 % CL in the $m_k - m_h$ plane[3]. Results are shown in Figure 5.3, for normal ordering (left panel) and inverted ordering (right panel). Two representative values of the luminosity were chosen. The green region delimits values that can be excluded with 70 fb^{-1}, that is, the luminosity collected by CMS and ATLAS together at the time this study was published. On the other hand, the orange region displays the results for $\mathcal{L} = 3000$ fb^{-1}, scheduled in the High-Luminosity phase of the LHC. The grey triangle is already excluded by neutrino oscillation data and low-energy constraints. We see that a mass of $k^{\pm\pm}$ as large as 1 TeV can be excluded in future analyses, in both leptonic and exotic decays.

5.3.3 Three-loop model

In the last chapter we have constructed a model that induces neutrino masses at the three-loop level. The foundation of this model was $k^{\pm\pm}$ and its interactions with the charged leptons. This interaction leads to the leptonic decay of $k^{\pm\pm}$, which is also present in the type-II seesaw model; in this case the search is analogous. But in order to generate neutrino masses and break lepton number in two units, the model also involved a scalar triplet with hypercharge +1 and a real scalar singlet, both odd under a Z_2 parity symmetry. Moreover, the real singlet and the neutral component of the triplet mix, leading to a dark neutral scalar S that show gauge interactions. This opens up the possibility for the last two exotic decays of $k^{\pm\pm}$ in the list of the beginning of Section 5.3. Indeed, $h^{\pm}$ is now member of a triplet and could decay into $SW^{\pm}$, via its gauge interactions. In addition, $k^{\pm\pm}$ can also be produced by a doubly-charged scalar $\chi^{\pm\pm}$, member of the triplet, and subsequently decay into charged leptons.

Following the same strategy, we may wonder what we can learn about $k^{\pm\pm}$ should these exotic decays exist in nature. We consider pair production of $k^{\pm\pm}$ with 100% decay branching ratio. We depict in Figure 5.4 the lowest cross section that can be excluded at the 95% CL (dashed black line) with an integrated luminosity of 35 fb^{-1}

[3]The CL$_s$ method is useful for excluding models in which the signal is small relative to the background. In those cases, the predictions of the signal+background model can be almost indistinguishable from those obtained with the background only hypothesis and we would lose experimental sensitivity. In order to remedy this situation, one could construct the statistic CL$_s$=CL$_{s+b}$/CL$_b$. Then, the signal hypothesis can be excluded at the 95% CL if CL$_s \leq 1 - 0.95$.

For a counting experiment with a single signal region, the statistic is simply:

$$\mathrm{CL}_s = 1 - \frac{\sum_{n=0}^{n_{obs}} \frac{e^{-(s+b)}(s+b)^n}{n!}}{\sum_{n=0}^{n_{obs}} \frac{e^{-b}b^n}{n!}}, \tag{5.8}$$

where s is the number of signal events, b is the expected background events, and n_{obs} is the number of events observed in the experiment. In the case that the analysis includes several signal regions, as in this section, the statistics can be computed with the `TLimits` routine of `ROOT` [132] which can also incorporate the uncertainties of the background.

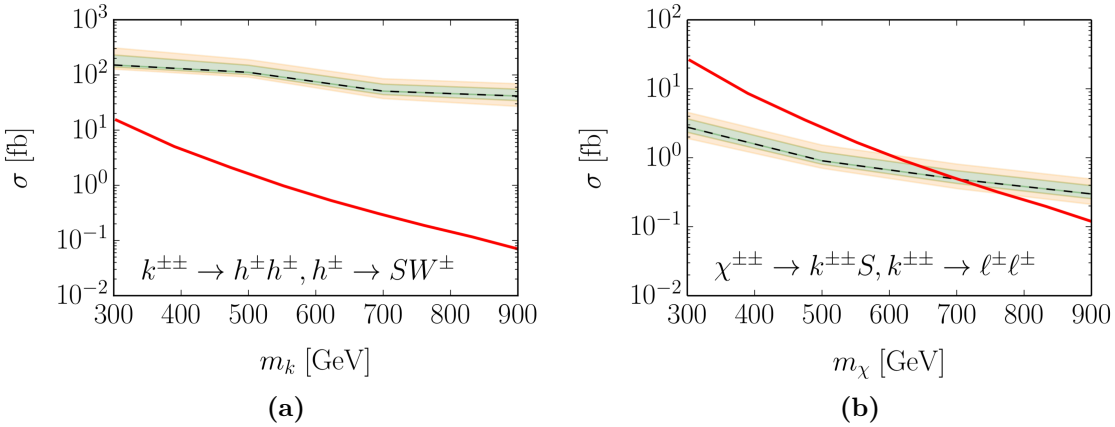

Figure 5.4: Bounds on the cross section (dashed black line) for an integrated luminosity $\mathcal{L} = 35$ fb^{-1} of (a) $k^{\pm\pm} \longrightarrow h^\pm h^\pm$ (with 100% branching ratio) followed by $h^\pm \longrightarrow SW^\pm$, and (b) $\chi^{\pm\pm} \longrightarrow k^{\pm\pm} S$ followed by the leptonic decay of $k^{\pm\pm}$. The green and orange regions show the 1σ and 2σ uncertainties. For the plot on the left, we have fixed $m_h = m_k/2.5$ and $m_S = m_h/2.5$; while, for the plot on the right, $m_k = m_S = m_\chi/2.5$. The theoretical cross section is shown for reference (red line).

for the two scenarios named above. As before, the green and yellow regions represent the 1σ and 2σ uncertainties. The theoretical cross section predicted by the three-loop model is also shown in red. From Subfigure 5.4a, we see that the decay channel with $SW^\pm$ in the final state remains inaccessible with the luminosity considered. However, the enhancement in the production of $k^{\pm\pm}$ through the exotic interaction with the triplet could imply interesting prospects, as seen in Subfigure 5.4b. Compare with the bounds assuming pair production of $k^{\pm\pm}$ alone. These exclusion limits can be inferred from Figure 5.2 after noting that, when $k^{\pm\pm}$ is a singlet, the production cross section is reduced down to be around half of that corresponding to $k^{\pm\pm}$ being member of a triplet. In that case, a m_k as large as $\sim 600 - 650$ GeV can be probed. On the other hand, a search that considers the exotic channel in Subfigure 5.4b could be able to exclude masses at around $m_k \sim 700$ GeV.

Finally, in Figure 5.5 we present the exclusion region in the $m_k - m_\chi$ plane, combining both production modes. In orange we depict the exclusion regions for which the decay mode to $\ell^\pm \ell^\pm$ saturates the branching ratio of $k^{\pm\pm}$; in green, $k^{\pm\pm}$ decays with 100% branching ratio to $\ell^\pm \tau^\pm$. The last decay mode is motivated in the context of the three-loop model of Chapter 4, in which $f_{e\tau}$ is much larger than the rest of the Yukawa couplings of the model (see Table 4.2). For this plot we have fixed $m_S = 200$ GeV, as suggested by the analysis of the DM candidate.

For $m_\chi < m_k + m_S$ only the channel with the pair production of $k^{\pm\pm}$ is present. We see that, in this region, masses could be probed up to $m_k \sim 650$ GeV if $\text{BR}(k^{\pm\pm} \longrightarrow \ell^\pm \ell^\pm) = 1$. In the case of $\text{BR}(k^{\pm\pm} \longrightarrow \ell^\pm \tau^\pm) = 1$, exclusion limits could be set at $m_k \sim 500$ GeV. More interestingly, when the exotic decay cascade is open the bounds can be improved with respect to those obtained when assuming

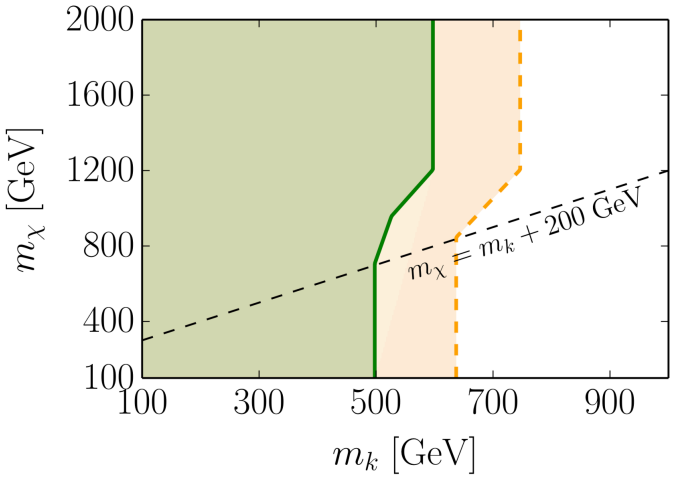

Figure 5.5: Exclusion regions in the context of the three-loop model. In orange we show a $k^{\pm\pm}$ decaying to $\ell^\pm\ell^\pm$ with 100% branching ratio along with a doubly-charged member of a scalar triplet, $\chi^{\pm\pm}$ decaying mostly to $k^{\pm\pm}$ and a neutral scalar S when kinematically possible; in green we show the same but with $k^{\pm\pm}$ decaying to $\ell^\pm\tau^\pm$ with 100% branching ratio. We have fixed $m_S = 200$ GeV.

the presence of $k^{\pm\pm}$ alone by around 100 GeV.

5.4 Application to searches of singly-charged scalars

We move on to applying the search strategy developed in Section 5.2 to tests of LNV singly-charged scalars, hereafter called $h^\pm$, with couplings to leptonic fields[4]. $h^\pm$ does not have renormalizable interactions with quarks; furthermore, we do not consider effective interactions either. Then, its production cross section will depend exclusively on the interactions with the gauge bosons and the leptons. In general, the leptonic interaction of $h^\pm$ would be with pairs of leptons of either chirality. Without adding right-handed neutrinos to the field content[5], two different combinations of chiralities arise:

$$\mathcal{O}_{LL} = \bar{\nu}_{La} e^c_{Lb} h^- + \text{h.c.} + ... \tag{5.11}$$

$$\mathcal{O}_{LR} = \bar{\nu}_{La} e_{Rb} h^+ + \text{h.c.} + ... \tag{5.12}$$

[4]The work presented here was first published by the author of this thesis and collaborators in Ref. [133].

[5]If we considered right-handed neutrinos there would be two additional operators, namely

$$\mathcal{O}_{RR} = \bar{\nu}_{Ra} e^c_{Rb} h^- + \text{h.c.} + ..., \tag{5.9}$$

$$\mathcal{O}_{RL} = \bar{\nu}_{Ra} e_{Lb} h^+ + \text{h.c.} + ..., \tag{5.10}$$

whose implementation would be equivalent to that of operators LL and LR, respectively.

In the context of renormalizable theories, the LL operator comes from gauge invariant leptonic interactions of either a weak singlet or a triplet, while the LR operator is realised when the interaction is with a doublet. Furthermore, both operators can also be generated within effective field theories in which the heavy states have been integrated out.

In the specific case of an $h^{\pm}$ singlet, the renormalizable Lagrangian describing its Yukawa interactions with leptons, like in the Zee-Babu model, is given by:

$$\mathcal{L}_{h^{\pm}}^{LL} = f_{ab}\bar{\ell}_{La}\ell_{Lb}^{c}h^{+} + h.c. \tag{5.13}$$

Again, the Yukawa coupling f_{ab} (with $a, b = e, \mu, \tau$) is antisymmetric. This interaction belongs to the LL category.

Alternatively, the LR interaction of the singlet to leptons can be realised at dimension five following the effective Lagrangian:

$$\mathcal{L}_{h^{\pm}}^{LR} = \frac{c_{ab}}{\Lambda}\left(\bar{\ell}_{La}\widetilde{\phi}\, e_{Rb}\, h^{+}\right) + h.c., \tag{5.14}$$

where c_{ab} encodes the information on new degrees of freedom, and Λ is the scale of new physics. After spontaneous symmetry breaking, we retrieve the operator LR in Eq. (5.12) and identify the coupling constant as $g_{ab} \equiv c_{ab}\frac{v}{\sqrt{2}\Lambda}$, where as usual $v \sim 246$ GeV is the SM VEV fixing the electroweak scale. Even for a c_{ab} of order 1, a new physics scale around the TeV will typically introduce a suppression factor.

In general, both f_{ab} and g_{ab} Yukawa couplings induce lepton flavour violation and hence show stringent bounds from lepton rare decay processes. These constraints can be summarised[6] by $|f_{e\mu}f_{\mu\tau}| \lesssim \mathcal{O}(10^{-2})$, $|f_{e\mu}f_{e\tau}| \lesssim \mathcal{O}(10^{-2})$ and $|f_{e\tau}f_{\mu\tau}| \lesssim \mathcal{O}(10^{-5})$. There are different ways to satisfy these bounds. For example, one could consider all coupling constants to be highly suppressed, so that the interactions to leptons are negligible. In fact, this is the approach followed in Ref. [136], where the antisymmetric Lagrangian is neglected and the interactions with leptons come from the dimension-five effective operator in Eq. (5.14). However, the authors of the aforementioned paper still consider only a small coupling scenario. Another possibility could be to set two of the couplings to zero and leave the remaining one unfixed. An aesthetic way to achieve this scenario would be imposing a global lepton number symmetry such as $L_i - L_j$, with $(i, j) = (e, \mu), (e, \tau)$ or (μ, τ), which leads to $f_{ij} \neq 0$ and $f_{ab} = 0$ for $ab \neq ij$. Then, the experimental bound would be automatically satisfied, even for the renormalizable interaction in Eq. (5.13). This will be the framework adopted in this analysis.

[6]These limits have been obtained using the analytic expressions in Ref. [105] with the most updated experimental results [134, 135] and considering a conservative value for the mass of the charged scalar of 100 GeV.

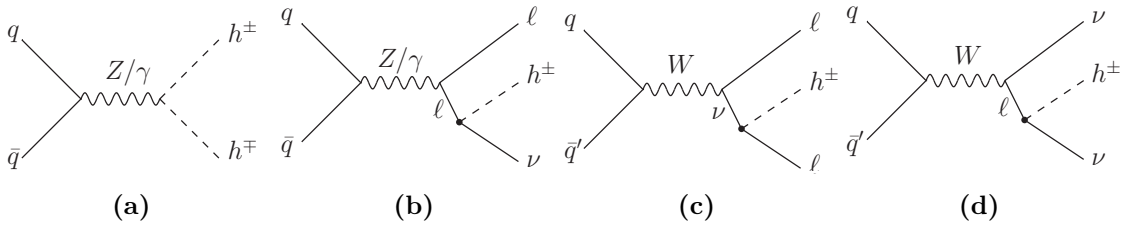

Figure 5.6: Feynman diagrams involved in the production of $h^\pm$: diagram (a) corresponds to pair production, (b)-(d) depict different single production modes. Diagrams (a) and (b) contribute to the 2ℓ+E_T^{miss} topology, while (c) and (d) lead to 3ℓ+E_T^{miss} and 1ℓ+E_T^{miss} topologies, respectively.

At leading order, $h^\pm$ can be pair-produced or single-produced, both possibilities in s-channel diagrams mediated by Z/γ, and Z, γ and W gauge bosons, respectively. Moreover, the singly production occurs when $h^\pm$ is radiated from an external lepton leg and in association with two charged leptons, one charged lepton and one neutrino, or two neutrinos. In Figure 5.6 we show the different production modes.

We assume that $h^\pm$ does not couple to quarks, so that the dominant decay channels are $h^+ \to \ell^+\nu_{\ell'}$, with $\ell, \ell' = e, \mu, \tau$. For the weak singlet with the renormalizable Lagrangian in Eq. (5.13) we necessarily have $\ell \neq \ell'$. This is no longer true when considering the LR effective interaction in Eq. (5.14), whose coupling constant g_{ab} has no preferred pattern of symmetry.

In summary, the discussed production modes with leptonic decay channels give three different final states:

1. Two opposite-sign leptons plus missing transverse energy, $2\ell + E_T^{\text{miss}}$ (diagrams a and b in Figure 5.6, with pair production and single production of $h^\pm$, respectively).

2. Three leptons plus missing energy, $3\ell + E_T^{\text{miss}}$, with single production of $h^\pm$ (diagram c).

3. One lepton plus missing energy, $1\ell + E_T^{\text{miss}}$, with single production of $h^\pm$ (diagram d).

In this analysis we focus on the first two, which are in principle more promising than the third one that contains just one lepton in the final state.

As said above, there are two contributions to the 2ℓ channel. The single production mode depends on the coupling of $h^\pm$ to leptons, while the production of pairs of $h^\pm$ is controlled by the gauge interactions. For this reason, the pair production mode is the main contribution for sufficiently small values of the coupling constant. In Figure 5.7 we consider the contribution of the pair production mode to the total cross section as a function of the coupling constant, for different masses of $h^\pm$. Indeed, for f below 0.1 we find that the pair production contribution is completely

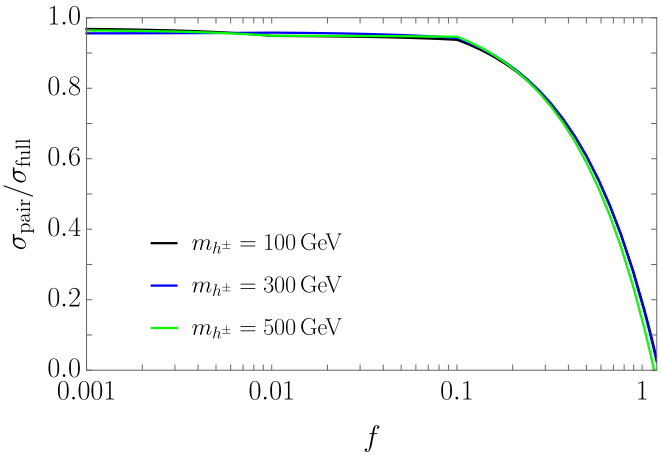

Figure 5.7: Contribution of the pair production mode ($\sigma_{\rm pair}$) to the cross section of the 2ℓ channel ($\sigma_{\rm full}$), for three selected masses of the singly-charged scalar.

dominant. On the other hand, the single production mode shows a cross section that grows with the coupling constant and becomes the leading contribution for $\mathcal{O}(f) = 1$. For in-between values, both contributions are competitive.

The 3ℓ channel is generated exclusively from the singly production diagram (c) in Figure 5.6. In contrast with the 2ℓ channel, a search strategy based on this channel would lose its sensitivity for decreasing values of the coupling constant. Following the discussion above, we separate the search strategy according to the strength of the leptonic interaction of $h^\pm$. For $f \gtrsim 0.1$ we focus on the 3ℓ channel, while for $f < 0.1$ we make use of the 2ℓ channel. In this manner, we not only retain the sensitivity regardless of the order of magnitude of the coupling f but we are also able to put the results obtained for the cross section in terms of f and/or $\text{BR}_{e+\mu} \equiv \text{BR}_e + \text{BR}_\mu$, the decay branching ratio of $h^\pm$ into electrons and muons. Indeed, for $\mathcal{O}(f) \leqslant 0.1$ the cross section of the 2ℓ channel is fully dominated by the pair production mode and then it can be written as

$$\sigma_{2\ell} = \sigma_{pp\to h^+h^-} \times \text{BR}^2_{e+\mu}, \tag{5.15}$$

The cross section of the 3ℓ channel is given by

$$\sigma_{3\ell}(f) = f^2 \times \sigma_{pp\to h^\pm\ell\ell}(f=1) \times \text{BR}_{e+\mu}, \tag{5.16}$$

where $\sigma_{pp\to h^\pm\ell\ell}(f=1)$ is the production cross section for $f = 1$.

Finally, we point out that the signal corresponding to the 2ℓ channel can be assumed to emerge from either the LL or LR operators, since they show the same signature. This is not the case for the 3ℓ channel, where the analysis based on the LR

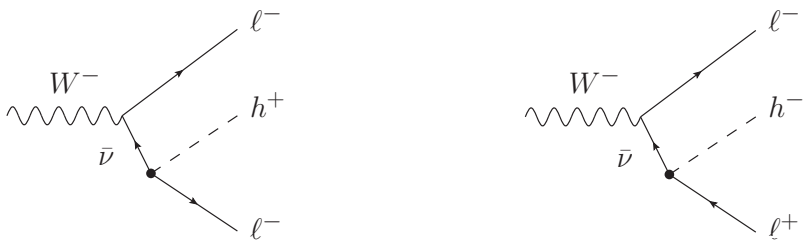

(a) LL interaction **(b)** LR interaction

Figure 5.8: Feynman diagrams representing the production of the charged scalar through the LL operator (panel a) and the LR operator (panel b).

interaction will report, to some extent, different results than the one considering the LL operator. In particular, the topology with the LR interaction shows a different configuration of the electric charges of the three leptonic fields in the final state (see Figure 5.8). For this reason, the observables will be constructed with leptons from different legs, and we expect the distributions to disagree from one scenario to the other.

5.4.1 Analysis in the two lepton channel

To start with, we focus on the search strategy in the 2ℓ channel, following the procedure of Section 5.2. The topology of the final state consists of two opposite-sign leptons and missing transverse energy. The relevant backgrounds are then Drell-Yan, $t\bar{t}$, WW, WZ, ZZ and tW. We generated all these background processes at leading order for a centre of mass energy of 13 TeV with `MadGraph_aMC@NLO 2.6` [121] and rescaled their cross sections with different K-factors to include the impact of QCD corrections. The parton shower and hadronisation were carried out with `PYTHIA 8` [123], while the detector response was simulated with `Delphes 3` [137]. In all the cases we impose the following set of cuts at generator level: $p_T^{\ell_1} > 25$ GeV, $p_T^{\ell_2} > 20$ GeV, $|\eta_\ell| < 2.5$, where ℓ_1 (ℓ_2) denotes the leading (sub-leading) lepton. Additionally, for the Drell-Yan process we set $m_{\ell^+\ell^-} > 100$ GeV in order to make the simulation more efficient. The information about the simulation of the different backgrounds is collected in Table 5.3.

Regarding the event generation for the signal, we use the package `FeynRules` [138] to implement the relevant interactions and write them in the UFO format [120]. In order to be conservative we do not apply any K-factor to the signal cross section. The rest of the simulation process proceeds in the same fashion as for the backgrounds. In particular, we demand the signal events to satisfy the same selection cuts at generator level as those imposed on the backgrounds. With the set of cuts imposed at generator level, the cross section at LO for producing pairs of $h^\pm$ is 5.5 fb, for $m_{h^\pm} = 200$ GeV.

Background	*Cross section (pb)*	*K-factor*	*Simulated events*
Drell-Yan	81	1.2	5.0×10^7
$t\bar{t}$	20	1.8	2.5×10^7
WW	4.9	1.5	3.0×10^6
WZ	2.0	1.4	1.0×10^6
ZZ	0.8	1.4	5.0×10^5
tW	4.2	0.9	1.5×10^6

Table 5.3: Main backgrounds along with their corresponding cross sections, the applied K-factors [139–148] and the number of simulated events used in the analysis of the 2ℓ-channel.

At the reconstruction level we select events with two opposite-sign leptons that satisfy the same set of cuts imposed at generator level. In addition, we demand the requirement $E_T^{\text{miss}} > 35$ GeV in order to reduce the Drell-Yan background which, unlike the signal, does not show large missing transverse energy.

We build the three observables of Section 5.2 with the lepton pair being of opposite sign. This choice makes straightforward the construction of $m_{\ell\ell}$ and m_T. In the case of the stransverse mass, the indices $L1$ and $L2$ stand for the harder and softer lepton, respectively. Again, we can safely set $m_X = 0$ in the definition of m_{T2} as all momenta are much heavier than the lepton masses.

By making use of these three variables along with the observable S_T, defined in Section 5.2, we build the 81 categories chosen in the search strategy. However, the distribution of m_{T2} exhibits an endpoint around $m_{h^\pm}$ as this variable is obtained from the transverse masses corresponding to the two leptons arising from the decay of h^+ and h^-. Therefore, the category with the lowest cut chosen for this observable (100 GeV) is not appropriate for values of $m_{h^\pm}$ around it. For this reason, we added 18 categories corresponding to $m_{T2} > 70$ GeV and $m_{T2} > 80$ GeV (with $S_T > X$ and $X = 100, ..., 900$ GeV).

We vary $m_{h^\pm}$ between 100 and 500 GeV in steps of 50 GeV. For each value of the mass and for each observable, we estimate the lower cross section that can be excluded with a luminosity of 300 fb^{-1} by looking for the category with the largest sensitivity, defined as $S/\sqrt{B}$. Exclusions for intermediate masses are obtained by linear interpolation. The results are shown in Figure 5.9. The sensitivity is driven by the m_{T2} categories in almost the whole range of masses considered. Below $m_{h^\pm} \sim 150$ GeV, its sensitivity worsens significantly and becomes similar to that achieved with the other observables around $m_{h^\pm} = 100$ GeV. In summary, with the m_{T2} categories it is possible to exclude cross sections ranging from ~ 30 fb to

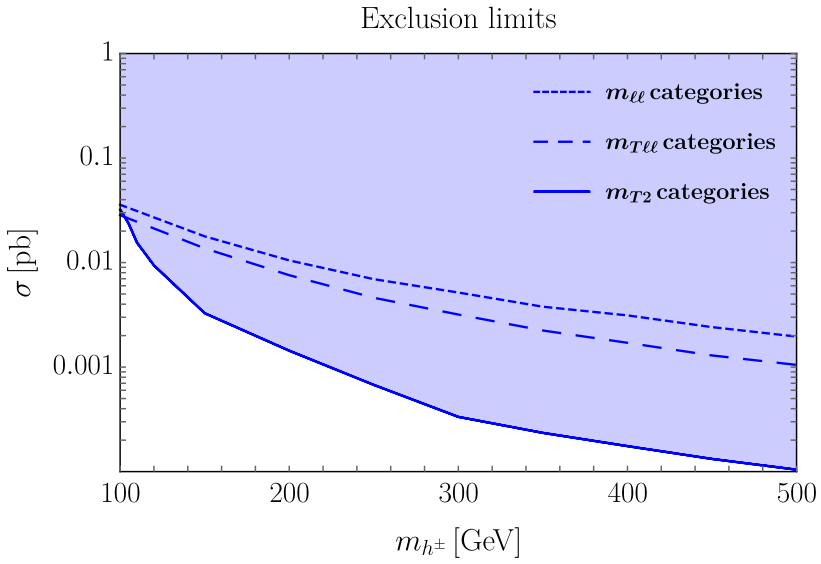

Figure 5.9: Bounds on the cross section of pair produced $h^\pm$ decaying into electrons and muons for a total integrated luminosity of 300 fb^{-1}.

0.1 fb for masses between 100 GeV and 500 GeV.

We can also interpret the results in terms of $\mathrm{BR}_{e+\mu}$, by considering the factorisation of the cross section in Eq. (5.15). In Figure 5.10 we display the limits obtained with the observable with the largest sensitivity (m_{T2}) for two representative values of the total integrated luminosity, $\mathcal{L} = 300\,\mathrm{fb}^{-1}$ and $3\,\mathrm{ab}^{-1}$. We see that $h^\pm$ decaying mostly to electrons and muons ($\mathrm{BR}_{e+\mu} \sim 0.9$) can be excluded up to 500 GeV with 300 fb^{-1}. When the luminosity is increased to 3 ab^{-1} this conclusion can be extended for branching ratios above 0.5. On the other hand, the sensitivity gap for $\mathrm{BR}_{e+\mu} < 0.3$ could be addressed with the tau decay channel because the exclusion limits in terms of BR_τ translate into an upper limit on $\mathrm{BR}_{e+\mu}$, given that $\mathrm{BR}_\tau = 1 - \mathrm{BR}_{e\mu}$. In fact, by combining our results with the exclusion reported in Ref. [136], based on the recasting of the analysis of Ref. [149], singlet $h^\pm$ with masses below $\sim$ 280 GeV can be excluded. A search strategy in the ditau channel more focused on the high-mass range could extend this exclusion, however this is beyond the scope of this work. Finally, an $h^\pm$ decaying fully into electrons and muons could be ruled out in all the considered mass range (100 GeV - 500 GeV) with a minimum luminosity of $\sim 192\,\mathrm{fb}^{-1}$. If a K-factor of 1.2 is applied to the signal[7], the minimum exclusion luminosity would reduce down to $\sim$ 133 fb^{-1}.

[7]This K-factor was obtained in Ref. [150] by considering the QCD corrections to pair production of right-handed sleptons, which have the same quantum numbers as the singly-charged scalar.

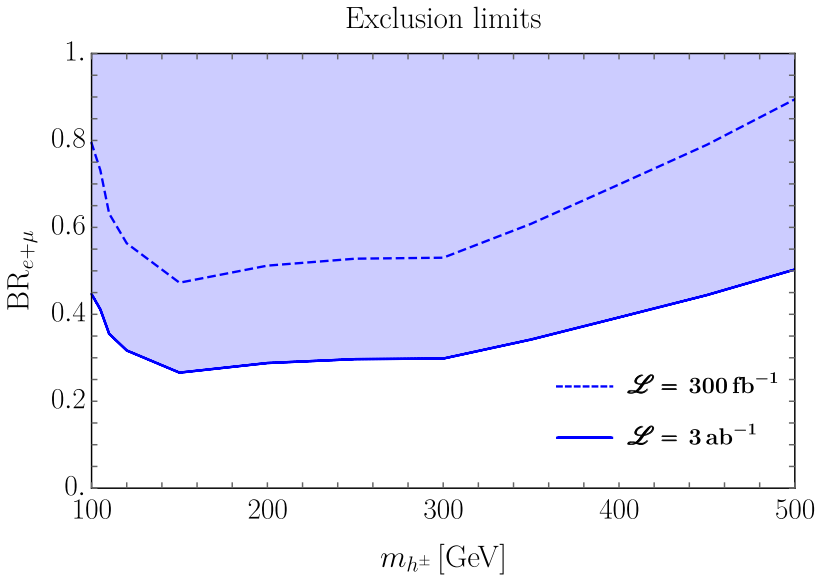

Figure 5.10: Bounds in the decay branching ratio of $h^\pm$ into electrons and muons obtained by using the m_{T2} categories with luminosities of 300 fb^{-1} (dashed line) and 3 ab^{-1} (solid line).

5.4.2 Analysis in the three lepton channel

Results with the LL operator

We move on to probe the large Yukawa coupling regime in the 3ℓ channel, with exactly two leptons of the same sign and one of opposite sign. We will make use of the background presented in Section 5.3.1, in which a number of events consistent with an integrated luminosity of 3 ab^{-1} was generated at $\sqrt{s} = 13$ TeV. Again, the relevant backgrounds consist of WZ, ZZ, WWW, WWZ, WZZ, ZZZ, ttW and ttZ. At the reconstruction level we demand leptons to pass the same cuts as those of the background generated in Section 5.3.1. We construct the following two observables:

1. $m_{\ell\ell}$, the invariant mass of the two same-sign leptons, and
2. the transverse mass of the same-sign lepton pair ($m_{T\ell\ell}$), as well as the one of the third lepton ($m_{T\ell}$).

We do not consider the observable m_{T2} since in this case, unlike in the 2ℓ channel, there is only one source of missing energy. Moreover, in Section 5.2 this observable was constructed taking $L1$ as the vectorial sum of the two same-sign leptons, while $L2$ was given by the third one. For this choice, m_X in the definition of m_{T2} (see Eq. (5.2)) cannot be neglected, as it corresponds to the invariant mass of the two same-sign leptons. This will be enough to make most $m_{\ell\ell}$ and m_{T2} categories almost identical.

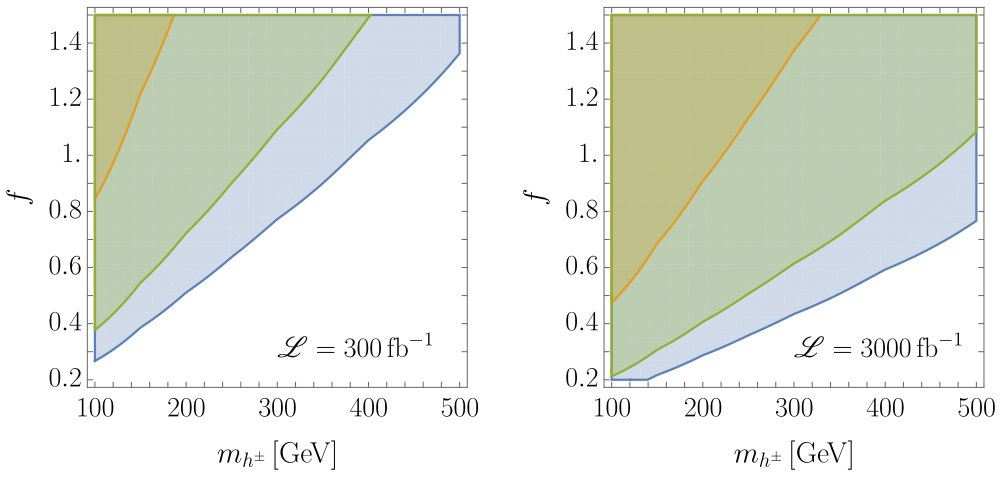

Figure 5.11: Exclusion limits at 95% CL on the Yukawa coupling of $h^\pm$ decaying into electrons and muons in the 3ℓ channel for a total integrated luminosity of 300 fb^{-1} (left panel) and 3 ab^{-1} (right panel). Colours correspond to: $\text{BR}_{e+\mu} = 0.1$ (orange), $\text{BR}_{e+\mu} = 0.5$ (green) and $\text{BR}_{e+\mu} = 1$ (blue).

Once again, we additionally consider the auxiliary observable S_T. Then, for each observable $O = m_{\ell\ell}$, m_T, we build 81 different categories with $O > X$ and $S_T > Y$, where $X, Y = 100, 200, ..., 900$ GeV. We remark that, contrary to the pair production channel, in this case there are two transverse masses and we demand both of them to simultaneously fulfil the selection cuts.

Regarding the signal events, we use the package `FeynRules` [120] to generate the UFO model [120] that implements the relevant interactions. In order to be consistent with the generation of background events in Section 5.3.1, we choose once again `MadGraph 5` [121] and then `PYTHIA 6` [151] for parton showering. We demand the signal events to satisfy the same selection cuts as the background.

We take $m_{h^\pm}$ to range between 100 and 500 GeV, in steps of 50 GeV. Because we are considering solely electrons and muons (plus missing transverse energy) in the final state, the production is such that only the coupling $f_{e\mu}$ is needed. Hereafter we set $f_{e\mu} = 1$ in all the simulations, as the results can be rescaled to any coupling strength following Eq. (5.16). For each observable and every value of $m_{h^\pm}$ we search for the category with the largest sensitivity, $S/\sqrt{B}$. By following this procedure, we compute the lowest cross section that can be excluded at the 95% CL. Again, exclusions for intermediate masses are obtained by linear interpolation. For $m_{h^\pm} \gtrsim 250$ GeV the sensitivity is slightly driven by m_T, while for lower values of the mass, the sensitivity of the transverse mass worsens due to the presence of an endpoint in its distribution around $m_{h^\pm}$. This makes the observable $m_{\ell\ell}$ the one with the best sensitivity in that region. The results are shown in Figure 5.11 for a total integrated luminosity of 300 fb^{-1} (left panel) and 3 ab^{-1} (right panel). Making use of Eq. (5.16), we plotted the coupling-mass plane for three different decay branch-

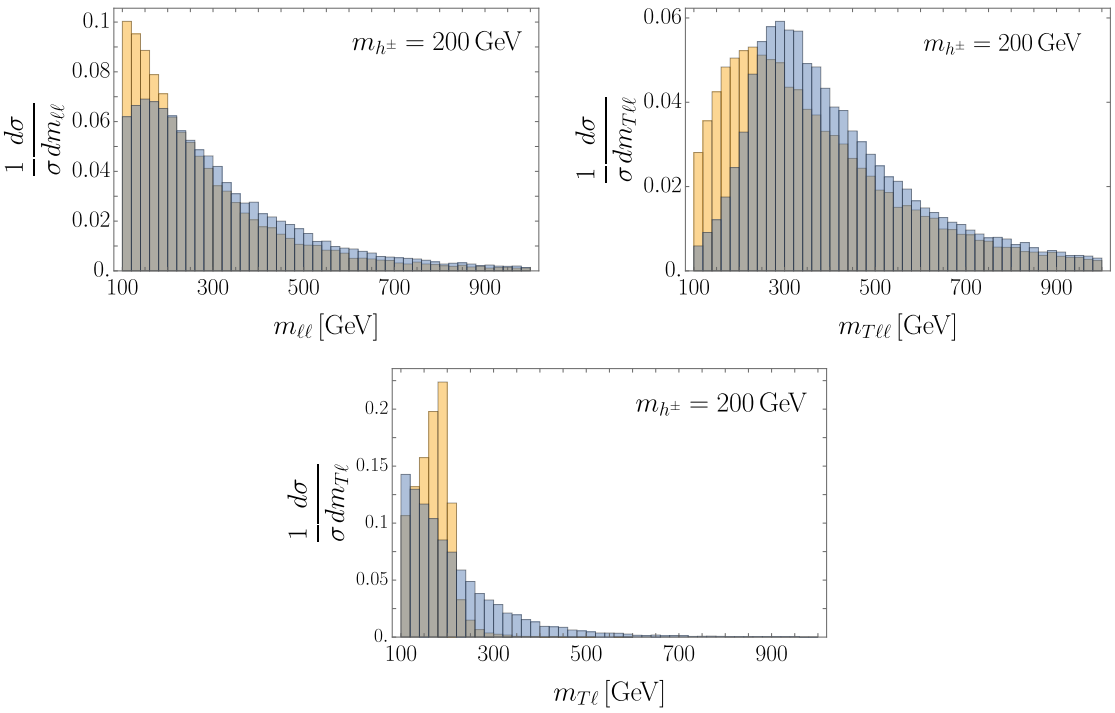

Figure 5.12: Top left panel: Invariant mass distribution of two same-sign leptons in events generated with the LL coupling (orange) and the LR interaction (blue), for $m_{h^\pm} = 200$ GeV. Top right panel: same as before but for the transverse mass distribution of two same-sign leptons. Bottom panel: same as before but for the transverse mass distribution of the single opposite-sign lepton.

ing ratios of the charged scalar, namely $\text{BR}_{e+\mu} = 0.1$ (orange), $\text{BR}_{e+\mu} = 0.5$ (green) and $\text{BR}_{e+\mu} = 1$ (blue). If $h^\pm$ decays only to electrons and muons, it is possible to exclude the entire range of studied masses for couplings larger than ~ 1.4 with a luminosity of 300 fb^{-1}. For the high luminosity phase, with 3 ab^{-1}, this limit could be extended to couplings as low as ~ 0.8. Additionally, smaller branching ratios become more accessible. For instance, $h^\pm$ with $\text{BR}_{e+\mu} = 0.5$ could be probed up to $m_{h^\pm} \sim 500$ GeV with a coupling ~ 1.1.

Results with the LR operator

As said above, the observables are now constructed with leptons coming from legs different than in the scenario with the LL operator. In Figure 5.12 we show several distributions in both frameworks, for a mass of 200 GeV. Notably and in contrast to the case of the LL interaction, $m_{T\ell}$ does not show an endpoint around $m_{h^\pm}$ since it is not built with the lepton arising from the decay of $h^\pm$. This feature could help to distinguish one scenario from the other. Additionally, while with the LL operator two diagrams contribute to the amplitude, there is only one diagram in the LR topology, making its production cross section typically one order of magnitude smaller. For instance, for a mass of 200 GeV and coupling ~ 1, the production

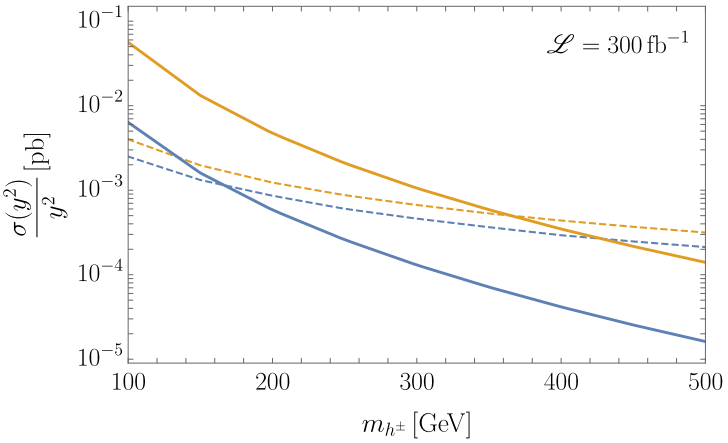

Figure 5.13: Bounds on the cross section of a $h^\pm$ singly-produced through the LR interaction (dashed blue line) and the LL operator (dashed orange line) for a luminosity of $\mathcal{L} = 300$ fb^{-1}, and decaying exclusively to electrons and muons. The theoretical cross section in the LR (solid blue line) and in the LL (solid orange line) case are also shown for reference. The coupling y represents the Yukawa couplings g (f) in the LR (LL) scenario.

cross section at LO in the context of the LL operator gives 4.7 fb, while for the LR operator it reads 0.5 fb.

In order to illustrate to what extent the change on the kinematic distributions impacts the results, let us assume that the Lagrangian in Eq. (5.12) preserves lepton flavour (that is, we only keep the diagonal elements) and redo the whole procedure, fixing the couplings $g_{ee} = g_{\mu\mu}$ for simplicity. Results for the LR operator are depicted in blue in Figure 5.13 for a luminosity of 300 fb^{-1}, in comparison to those obtained with the LL interaction in orange. The symbol y denotes the Yukawa coupling g (f) in the LR (LL) framework. Solid lines describe the theoretical cross section while dashed lines indicate the maximum cross section that can be probed at the given luminosity. The latter strongly depends on the acceptance of each category and observable. In the whole interval of study, the sensitivity for the LR operator is driven by $m_{\ell\ell}$, whose distribution is very similar to that of the LL interaction. Conversely, the theoretical cross section, as explained above, is typically one order of magnitude smaller. For this reason the exclusion limits will be weaker in this scenario and, for retrieving the same sensitivities that are obtained with the LL framework, larger couplings and/or luminosities are needed. In particular, a $h^\pm$ decaying exclusively to electrons and muons through the LR interaction can be excluded with a mass as large as ~ 170 GeV with a luminosity of 300 fb^{-1}, whereas this limit extends to ~ 370 GeV for the LL interaction.

5.5 Summary

- LNV scalars are relevant in models of Majorana neutrino masses. Some of these models induce the neutrino masses at the loop level, and therefore predict scalar masses at the TeV scale that can be probed at high-energy colliders in the near future. However, current searches do not take into consideration the rich production and decay patterns that these scalars would exhibit and therefore new dedicated searches are needed.
- We discussed a broad scope search strategy with three independent signal regions. Because these scalars have interactions with leptons, the signal regions contain events with two, three and four leptons in the final state.
- The search strategy considers three main observables. The importance of each observable depends on the kinematics of the signal studied.
- We proposed novel LHC searches of LNV singly- and doubly-charged scalars in model dependent and model independent frameworks.
- In order to estimate exclusion regions of the parameters in each scenario, signal events were simulated with the appropriate computational tools. Background events were also generated when needed.
- Results for the prospects for the Zee-Babu model and the three-loop model were found, as well as for the relevant parameters of a singly-charged scalar in a model independent framework.

CHAPTER 6

Probes of νSMEFT four-fermion operators

Under the assumption of the existence of a large energy gap between a given set of particles below the electroweak scale and new physics, the influence of the latter can be described by a tower of higher dimensional operators involving only the considered particles. These operators get increasingly suppressed by the scale of new physics as the order of the operators goes up; in this way, effects of operators of dimension six are less important than those of dimension five.

So far there has been only observation of the SM particles, so it is natural to consider an EFT involving only the SM field content. If we additional impose the SM gauge symmetry $SU(3)_C \times SU(2)_L \times U(1)_Y$ we get the SM effective field theory (SMEFT) [152]. In contrast with the Standard Model, global symmetries, like lepton or baryon number, can be broken by some of the effective operators. In fact, the dimension-five Weinberg operator generates a tree-level mass for neutrinos (see Chapter 2 for more details). Within this context, neutrinos are Majorana-type.

However, right-handed neutrinos, hereafter called N, are still an experimentally viable possibility (N is a sterile neutrino, and its observation could become extremely hard). In fact, if the SM neutrinos are Dirac particles and their right-handed component is N, the low energy physics is described by the SMEFT extended with N. Then the effective field theory considering both the SM field content along with the right-handed neutrino is simply called νSMEFT [153].

At dimension five, νSMEFT operators involving new right-handed neutrinos are just $(\bar{N}N^c)(\phi^\dagger\phi)$ and $(\bar{N}^c\sigma_{\mu\nu}N)B^{\mu\nu}$ [154] (in fact, should there be only one family of N, the second operator vanishes). The basis at dimension six, found in Ref. [155], consists of 16 operators conserving both lepton and baryon number, one operator breaking lepton number and two additional operators breaking lepton and baryon number. If we expand in flavour indices, the total number of operators

(restricting to lepton and baryon number conserving operators) rises up to 389 (1332) for one (three) family of right-handed neutrinos. Of course, this set of operators is an extension of the SMEFT, so they need to be added to those in order to constitute a complete basis of independent operators at a given dimension. Here we will consider only dimension-six operators that simultaneously conserve lepton and baryon number; these operators are listed in Table 6.1.

	Operator	*Notation*	*Operator*	*Notation*
SF	$(\overline{\ell_L}N)\widetilde{\phi}(\phi^\dagger\phi)$	$\mathcal{O}_{\ell N\phi}$ (+h.c.)		
	$(\overline{N}\gamma^\mu N)(\phi^\dagger i\overleftrightarrow{D_\mu}\phi)$	$\mathcal{O}_{\phi N}$	$(\overline{N}\gamma^\mu e_R)(\widetilde{\phi}^\dagger iD_\mu\phi)$	$\mathcal{O}_{\phi Ne}$ (+h.c.)
	$(\overline{\ell_L}\sigma_{\mu\nu}N)\widetilde{\phi}B^{\mu\nu}$	$\mathcal{O}_{NB}$ (+h.c.)	$(\overline{\ell_L}\sigma_{\mu\nu}N)\sigma_I\widetilde{\phi}W^{I\mu\nu}$	$\mathcal{O}_{NW}$ (+h.c.)
RRRR	$(\overline{N}\gamma_\mu N)(\overline{N}\gamma^\mu N)$	$\mathcal{O}_{NN}$		
	$(\overline{e_R}\gamma_\mu e_R)(\overline{N}\gamma^\mu N)$	$\mathcal{O}_{eN}$	$(\overline{u_R}\gamma_\mu u_R)(\overline{N}\gamma^\mu N)$	$\mathcal{O}_{uN}$
	$(\overline{d_R}\gamma_\mu d_R)(\overline{N}\gamma^\mu N)$	$\mathcal{O}_{dN}$	$(\overline{d_R}\gamma_\mu u_R)(\overline{N}\gamma^\mu e_R)$	$\mathcal{O}_{duNe}$ (+h.c.)
LLRR	$(\overline{\ell_L}\gamma_\mu\ell_L)(\overline{N}\gamma^\mu N)$	$\mathcal{O}_{\ell N}$	$(\overline{q_L}\gamma_\mu q_L)(\overline{N}\gamma^\mu N)$	$\mathcal{O}_{qN}$
LRRL	$(\overline{\ell_L}N)i\sigma_2(\overline{\ell_L}e_R)$	$\mathcal{O}_{\ell N\ell e}$ (+h.c.)	$(\overline{\ell_L}N)i\sigma_2(\overline{q_L}d_R)$	$\mathcal{O}_{\ell Nqd}$ (+h.c.)
	$(\overline{\ell_L}d_R)i\sigma_2(\overline{q_L}N)$	$\mathcal{O}_{\ell dqN}$ (+h.c.)	$(\overline{q_L}u_R)(\overline{N}\ell_L)$	$\mathcal{O}_{quN\ell}$ (+h.c.)

Table 6.1: Basis of dimension-six operators in the context of the νSMEFT [155]. Only operators that conserve lepton and baryon number are listed. Flavour indices are omitted for simplicity.

In this chapter we will find which νSMEFT operators are most constrained by current data with the aim of reporting the directions in which new physics might still be hidden[1]. To accomplish this task, we compare the new contributions, given by these operators, to several physical processes with the experimental data collected by the LHC and other experiments. We focus on four-fermion operators, which can be constrained by looking at searches for one lepton and missing energy at the LHC, monojet searches at the LHC and pion and tau decays. Moreover, operators involving third-generation quarks can receive stringent constraints from dedicated searches of rare top decays. We propose one such analysis.

Certain operators are left out of the present study as they involve only right-handed neutrinos ($\mathcal{O}_{NN}$), are better tested in lepton facilities (e.g. $\mathcal{O}^{ii}_{eN}$ or $\mathcal{O}^{13}_{uN}$) or give suppressed contributions (like the one-loop operators $\mathcal{O}_{NB}$ and $\mathcal{O}_{NW}$). For instance, when the SM neutrinos are Dirac-type and N their right-handed component, operators such as the last two are already strongly bounded by neutrino dipole moments measurements [157, 158]. For a Majorana N, these operators must

[1]The work presented here was published by the author of this thesis and collaborators in Ref. [156].

be also suppressed or they would strongly induce a decay into a SM neutrino and a photon [159]. Accordingly, we will only include the SF operators for completeness.

Finally, it is important to remark to which scenarios the analysis presented here applies. From a cosmological point of view, light sterile neutrinos are allowed by precise measurements of the primordial abundances at the time of Big Bang Nucleosynthesis (BBN) [160] (when the temperature of the thermal bath is $T_{\rm BBN} \sim$ MeV), unless new physics interactions enhances their interaction rate. Indeed, sterile neutrinos can only be produced by helicity flips of the left-handed neutrinos, which are suppressed because $m_\nu \ll T$. Then practically all neutrinos are left-handed, explaining the observed value of the effective number of relativistic species $N_{\rm eff} \approx 3$.

In the context of νSMEFT, the enhancements of the interaction rate are given by the four-fermion operators; the cross section of neutrino scatterings generated by these operators are proportional to $\sim T^2/\Lambda^4$, whereas the number density for relativistic particles is $\sim T^3$. At the end, the interaction rate is proportional to $\Gamma \sim T^5/\Lambda^4$. Then, the sterile neutrinos are in equilibrium with the thermal plasma when the interaction rate is larger than the expansion rate of the universe, which is proportional to $T^2_{\rm BBN}/m_P$, where $m_P \sim 10^{19}$ GeV is the Planck mass. Combining both expression, we obtain $\Lambda \lesssim (m_P T^3_{BBN})^{1/4} \sim 300$ GeV. This means that if Λ lies below the electroweak scale, N is in equilibrium at the BBN era and gives contributions to $N_{\rm eff}$ which, in turn, is bounded by observations of ^{4}He abundances. In short, for sterile neutrinos the scale of new physics described by the νSMEFT has to be above the electroweak scale. Further, in the particular case in which N is a Majorana neutrino, its mass is also constrained by measurements of $N_{\rm eff}$ made by the Planck collaboration [161]. In Ref. [162] it was found that the contribution of the right-handed neutrino to $N_{\rm eff}$ escapes the sensitivity of Planck's results when m_N is larger than about 10 MeV.

At the experiment level, when the leading contributions to the decay of a Majorana N are given by the four-fermion operators, N shows a three-body decay into two light jets and a charged lepton or missing energy, provided $m_N < m_W$. We can estimate its mean life to be $\tau_N \sim 256\pi^3\Lambda^4/m_N^5$. In the LHC, the radius of the cross section of the detectors is of around 10 meters, so that if N lives shorter than $\tau_N \approx 10$ [m]$/c \approx 10^{-8}$ s we will see its decaying products[2]. Plugging this limit into the formula of the mean life we find that N, when the scale of new physics is larger than the electroweak scale, can be considered for experimental purposes as a stable particle if $m_N < 0.1$ GeV.

To sum up, the combination of the previous constraints suggests that our study

[2]The signature of these processes can include displaced vertices [163, 164]. In that case, LHC dedicated searches, as proposed in Ref.[163], could be useful as they would have small SM background.

of the νSMEFT works when neutrinos are Dirac particles and the scale of the new physics is larger than the electroweak scale, or when neutrinos are of Majorana type with 0.01 GeV $\lesssim m_N \lesssim$ 0.1 GeV.

All throughout this study, we will focus on one family of N; results for more families are easily extrapolated. Finally, all collider simulations considered hereafter were made with `MadGraph 5` [121], parton showering was simulated using `Pythia 8` [123] and the reconstruction of jets, when necessary, was performed with `FastJet 3` [165]. Operators[3] in Table 6.1 were implemented with `FeynRules 2` [138].

6.1 Searches for one lepton and missing energy

In the last chapter we stated that the transverse mass is a good observable for measuring the signature of processes with sources of missing energy. Focusing on this observable, several searches for one lepton and missing energy has been done at the LHC. So in order to set bounds on the relevant operators giving $pp \longrightarrow \ell N$, we use the experimental information obtained by the ATLAS analysis of Ref. [166] based on 36 fb^{-1} of data collected at $\sqrt{s} = 13$ TeV. In that work, only events with exactly one light lepton were considered. When the lepton is an electron, the event is selected if $p_T > 65$ GeV and $E_{\text{miss}} > 65$ GeV. For muons, the selection cuts reduced down to be $p_T > 55$ GeV and $E_{\text{miss}} > 55$ GeV. Finally, the predicted SM background events along with the observed events are collected in several bins based on their values of the transverse mass, as shown in Table 6.2. Additionally, we compute the maximum number of signal events, s_{max}, that can be excluded at the 95% CL, using the CL$_s$ method [131]. As in Chapter 5, the CL$_s$ is implemented with the `TLimits` routine of `ROOT` [132] that takes into account the uncertainties of the background.

Although the experimental analysis provides with a large number of bins, we have chosen to work with only those that do not go too high in energy, in order to keep the effective theory valid at the TeV scale.

Searches for one tau and missing energy have been also carried out at the LHC. For our purposes, we recast the CMS analysis of Ref. [167] based on 35.9 fb^{-1} and a centre of mass energy of 13 TeV. In this case, the selection cuts consist of the requirement of a single hadronic tau with $p_T > 80$ GeV and $E_{\text{miss}} > 200$ GeV. Values of the predicted SM background events along with the observed number of events are collected in Table 6.3. Additionally, s_{max} is computed as before.

Operators giving new contributions are $\mathcal{O}_{quN\ell}$, $\mathcal{O}_{\ell dQN}$ and $\mathcal{O}_{\ell Nqd}$ (LRRL), $\mathcal{O}_{duNe}$

[3] We use the Fierz-transformed operator

$$\mathcal{O}_{\ell dqN} = \frac{1}{2}(\overline{q_L} d_R) i\sigma_2 (\overline{\ell_L} N) + \frac{1}{8}(\overline{q_L}\sigma_{\mu\nu} d_R) i\sigma_2 (\overline{\ell_L}\sigma^{\mu\nu} N), \tag{6.1}$$

with terms including scalar and tensor bilinears.

	$400-600$	$600-1000$	$1000-2000$ [GeV]
$\mathcal{A}_1$	7400 (4400)	12000 (7200)	16000 (9600)
$\mathcal{A}_2$	2100 (1300)	3600 (2200)	4700 (2800)
$\mathcal{A}_3$	-3500 (-2100)	-5600 (-3400)	-7700 (-4600)
$\mathcal{A}_4$	5.0 (3.0)	1.2 (0.73)	0.15 (0.089)
$\mathcal{A}_5$	360 (210)	210 (120)	79 (47)
SM	9700 ± 500 (6460 ± 330)	2010 ± 140 (1320 ± 90)	232 ± 24 (150 ± 13)
data	9551 (6772)	1931 (1392)	246 (177)
$s_{\max}$	791 (778)	213 (257)	67 (62)

Table 6.2: Coefficients in units of TeV^4 for $pp \to \ell N$ obtained upon recasting the experimental analysis of Ref. [166] for a luminosity of 36 fb^{-1}. Result are rounded to two significant figures. The numbers outside (inside) the parentheses correspond to the $\ell = e$ (μ) case.

	$0-500$	$500-1000$	>1000 [GeV]
$\mathcal{B}_1$	170	3600	10000
$\mathcal{B}_2$	40	990	3200
$\mathcal{B}_3$	-69	-1600	-4700
$\mathcal{B}_4$	0.33	1.0	0.15
$\mathcal{B}_5$	40	290	160
SM	1243 ± 160	485 ± 77	23.4 ± 6.2
data	1203	452	15
$s_{\max}$	258	125	12

Table 6.3: Coefficients in units of TeV^4 for $pp \to \tau N$ obtained upon recasting the experimental analysis of Ref. [167] for a luminosity of 35.9 fb^{-1}. Results are rounded to two significant figures. Note that Eq. 6.11 is obtained under the assumption $\sqrt{s} \gg m_W$, so $\mathcal{B}_{4,5}$ in the first bin should not be taken rigorously.

(RRRR), $\mathcal{O}_{\phi Ne}$ and $\mathcal{O}_{NW}$ (SR). The relevant pieces of the four-fermion operators giving contributions to $pp \longrightarrow \ell N$, are

$$\text{LRRL}: \begin{cases} \mathcal{O}_{quN\ell} \supset (\bar{d}_L u_R)(\bar{N}_R e_L) \\ \mathcal{O}_{\ell Nqd} \supset -(\bar{e}_L N_R)(\bar{u}_L d_R) \\ \mathcal{O}_{\ell dqN} \supset -(\bar{e}_L d_R)(\bar{u}_L N_R) \end{cases} \qquad \text{RRRR}: \left\{ \mathcal{O}_{duNe} \supset (\bar{d}_R \gamma_\mu u_R)(\bar{N} \gamma^\mu e_R) \right. . \tag{6.2}$$

Operators including the same fields, such as $\mathcal{O}_{\ell dQN}$ and $\mathcal{O}_{\ell Nqd}$, can produce interferences. Operators from different classes can still give interferences, but they

are chirality suppressed and we do not consider them here.

In order to test the impact of these operators we need to compute the cross section obtained with every one of them. For instance, the first operator in the previous list gives the following amplitude

$$\mathcal{M} = \frac{\alpha_{quN\ell}}{\Lambda^2}[u(u)P_R\bar{v}(d)][v(\ell)P_R\bar{u}(N)], \tag{6.3}$$

where as usual u and v are the spinors satisfying the Dirac equation. The squared sum of the amplitude reads

$$\begin{aligned}\overline{\Sigma}|\mathcal{M}|^2 &= \frac{\alpha_{quN\ell}^2}{3\cdot 4\Lambda^4}\mathrm{Tr}[\not{p}_u P_R \not{p}_d] \times \mathrm{Tr}[\not{p}_\ell P_R \not{p}_N] \\ &= \frac{\alpha_{quN\ell}^2}{48\Lambda^4} 4(p_u p_d) 4(p_\ell p_N) \\ &= \frac{\alpha_{quN\ell}^2}{12\Lambda^4} s^2,\end{aligned} \tag{6.4}$$

where the factor of 1/3 in the first line is because we are summing over the three color states of $u\bar{d}$. In the last step we put the products of momenta in terms of Lorentz invariant quantities[4]. Finally, the invariant differential cross section can be expressed as

$$\frac{d\sigma}{dt} = \frac{1}{16\pi s^2}\overline{\Sigma}|\mathcal{M}|^2, \tag{6.7}$$

so that the contribution of the operator $\mathcal{O}_{quN\ell}$ to the differential cross section is

$$\frac{d\sigma}{dt} = \frac{1}{192\pi s^2}\frac{\alpha_{quN\ell}^2}{\Lambda^4} s^2. \tag{6.8}$$

As said, the operators $\mathcal{O}_{\ell Nqd}^{i11}$ and $\mathcal{O}_{\ell dqN}$ involve the same fields and hence interfere. The amplitude is

$$\mathcal{M} = \frac{\alpha_{\ell Nqd}}{\Lambda^2}[v(e)P_R\bar{u}(N)(u(u)P_R\bar{v}(d)] + \frac{\alpha_{\ell dqN}}{\Lambda^2}[v(e)P_R\bar{v}(d)(u(u)P_R\bar{u}(N)], \tag{6.9}$$

[4]We are going to set all momenta in terms of the Mandelstam variables

$$\begin{aligned} s &= (p_u + p_d)^2 = (p_\ell + p_N)^2 \simeq 2(p_u p_d) \simeq 2(p_\ell p_N), \\ t &= (p_u - p_N)^2 = (p_\ell - p_d)^2 \simeq -2(p_u p_N) \simeq -2(p_d p_\ell), \\ u &= (p_u - p_\ell)^2 = (p_N - p_d)^2 \simeq -2(p_u p_\ell) \simeq -2(p_d p_N), \end{aligned} \tag{6.5}$$

for vanishing masses. This also implies

$$s + t + u = 0. \tag{6.6}$$

and then

$$\begin{aligned}\overline{\Sigma}|\mathcal{M}|^2 &= \frac{1}{12\Lambda^4}[4\alpha^2_{\ell Nqd}(p_e p_N)(p_u p_d) + 4\alpha^2_{\ell dqN}(p_e p_d)(p_u p_N) \\ &+ 4\alpha_{\ell Nqd}\,\alpha_{\ell dqN}((p_e p_N)(p_u p_d) + (p_e p_d)(p_N p_u) - (p_e p_u)(p_u p_N))] \\ &= \frac{1}{12\Lambda^4}[\alpha^2_{\ell Nqd}\,s^2 + \alpha^2_{\ell dqN}\,t^2 + \alpha_{\ell Nqd}\,\alpha_{\ell dqN}(t^2+s^2-u^2)] \\ &= \frac{1}{12\Lambda^4}(\alpha^2_{\ell Nqd}\,s^2 + \alpha^2_{\ell dqN}\,t^2 - 2\alpha_{\ell Nqd}\,\alpha_{\ell dqN}\,st),\end{aligned} \tag{6.10}$$

where in the last step we have used Eq. (6.6). From here the differential cross section is straightforward to calculate.

In the same manner, contributions for the rest of the operators are computed. In particular, those obtained with the last two operators are a little more subtle as they generate s-channel diagrams mediated by a W gauge boson. For these operators we use the approximation $\sqrt{s} \gg M_W$.

To summarise, the modification to the differential cross section coming from this set of operators is

$$\begin{aligned}\frac{d\sigma}{dt}(u\bar{d} \to \ell_i^+ N) = \frac{1}{192\pi\Lambda^4 s^2}\Bigg\{ &\left[(\alpha^{11i}_{quN\ell})^2 + 4(\alpha^{11i}_{duNe})^2 + (\alpha^{i11}_{\ell Nqd})^2\right]s^2 \\ &4\left[4(\alpha^{11i}_{duNe})^2 + (\alpha^{i11}_{\ell dqN})^2\right]t^2 + 2\left[4(\alpha^{11i}_{duNe})^2 - \alpha^{i11}_{\ell Nqd}\alpha^{11i}_{\ell dqN}\right]st \\ &+ 4(\alpha^i_{\phi Ne})^2 m_W^2 \frac{t^2}{s^2} - 32(\alpha^i_{NW})^2 m_W^2\left(\frac{t^2}{s}+t\right)\Bigg\},\end{aligned} \tag{6.11}$$

where the index $i = 1$ (2) corresponds to electrons (muons). Moreover, we are only considering the first quark family. Although it is true that the same operators for the second family can give contributions with no interferences with those of the first-family operators, the bounds obtained with them are expected to be one order of magnitude smaller because of the smaller parton distribution functions.

As seen, the differential cross section in Eq. (6.11) is parametrised in terms of some functions of the invariant variables. The operator coefficients are then grouped according to their dependence upon these functions. Contributions from operators of the same group will give the same distributions. For this reason we can also parametrise the number of signal events obtained for each group in terms of some coefficients $\mathcal{A}_i$:

$$\begin{aligned}N = \frac{1}{\Lambda^4}\Bigg\{ &\left[(\alpha^{11i}_{quN\ell})^2 + 4(\alpha^{11i}_{duNe})^2 + (\alpha^{i11}_{\ell Nqd})^2\right]\mathcal{A}_1 + \left[4(\alpha^{11i}_{duNe})^2 + (\alpha^{i11}_{\ell dqN})^2\right]\mathcal{A}_2 \\ &+ 2\left[4(\alpha^{11i}_{duNe})^2 - \alpha^{i11}_{\ell Nqd}\,\alpha^{i11}_{\ell dqN}\right]\mathcal{A}_3 + (\alpha^i_{\phi Ne})^2\mathcal{A}_4 + (\alpha^i_{NW})^2\mathcal{A}_5\Bigg\}.\end{aligned} \tag{6.12}$$

	$690-740$	$740-790$	$790-840$	$840-900$	$900-960$ [GeV]
$\mathcal{C}_1$	210	170	130	130	94
$\mathcal{C}_2$	97	78	59	53	39
$\mathcal{C}_3$	320	250	180	170	130
SM	526 ± 14	325 ± 12	223 ± 9	169 ± 8	107 ± 6
data	557	316	233	172	101
$s_{\max}$	82	40	44	35	21

Table 6.4: Coefficients in units of TeV^4 for $pp \to N\overline{N}g(q)$ obtained upon recasting the experimental analysis of Ref. [168] for a luminosity of 35.9 fb^{-1}. Results are rounded to two significant figures.

These coefficients are bin-dependent and have to be computed by simulation using the same selection criteria as the experimental analysis considered. As for the distributions, contributions for operators within each group give the same number of events. For instance, we can compute the value of $\mathcal{A}_1$ by only switching on $\alpha_{quN\ell}^{11i}$ and with $\alpha_{duNe}^{11i} = \alpha_{\ell Nqd}^{i11} = 0$. Results for each coefficient and for each bin are collected in Table 6.2. Values for muons (in parentheses) are estimated to be a factor of 0.6 smaller because of the harder muon trigger and identification efficiency.

Finally, we repeat this procedure for the same operators but with taus instead of light leptons. The number of signal events is obtained from Eq. (6.12) by changing the label i (corresponding to $i = e, \mu$) to '3' (which refers to taus). In addition, the coefficients $\mathcal{A}_i$ are renamed as $\mathcal{B}_i$. We report our results in Table 6.3.

Later on, we will set bounds on the effective operators by demanding that the number of signal events N is not larger than $s_{\max}$.

6.2 Monojet searches at the LHC

Here, we recast the CMS analysis of Ref. [168] with collisions performed at $\sqrt{s} = 13$ TeV corresponding to a luminosity of 35.9 fb^{-1}, and focusing on the missing transverse energy. Candidate events are required to show $E_{\text{miss}} > 250$ GeV, at least one hard jet with $p_T > 250$ GeV and no isolated leptons. Like in the previous section, we give numbers of background events, data events and $s_{\max}$. They are listed in Table 6.4.

Operators giving contributions to monojets processes are $\mathcal{O}_{uN}$, $\mathcal{O}_{dN}$, $\mathcal{O}_{qN}$ and $\mathcal{O}_{\phi N}$. However, we are not considering the last one since its cross section decreases at

large energies. For this reason, we focus only on the following four-fermion operators:

$$\text{RRRR}: \begin{cases} \mathcal{O}_{uN} = (\bar{u}_R \gamma_\mu u_R)(\bar{N}\gamma^\mu N) \\ \mathcal{O}_{dN} = (\bar{d}_R \gamma_\mu d_R)(\bar{N}\gamma^\mu N) \end{cases} \text{LLRR}: \mathcal{O}_{qN} = (\bar{q}_L \gamma_\mu q_L)(\bar{N}\gamma^\mu N) = (\bar{d}_L \gamma_\mu d_L + \bar{u}_L \gamma_\mu u_L)(\bar{N}\gamma^\mu N) \tag{6.13}$$

Further, we do not consider interferences among $\mathcal{O}_{qN}$ and any of the RRRR operators since they are chirality suppressed. Under these considerations, the number of signal events, in terms of the coefficients $\mathcal{C}_i$, is

$$N = \frac{1}{\Lambda^4}[(\alpha_{uN}^{11})^2 \mathcal{C}_1 + (\alpha_{dN}^{11})^2 \mathcal{C}_2 + (\alpha_{qN}^{11})^2 \mathcal{C}_3]. \tag{6.14}$$

We report our findings in Table 6.4.

6.3 Pion decays

Operators giving contributions to pion decays are exactly the same as those of semileptonic searches in Section 6.1. In particular, $\mathcal{O}_{quN\ell}$ and $\mathcal{O}_{\ell Nqd}$ give scalar form factors, while $\mathcal{O}_{duNe}$ and $\mathcal{O}_{\phi Ne}$ vector form factors. Finally $\mathcal{O}_{\ell dqN}$, after the corresponding Fierz transformation, leads to a tensor form factor which is hard to estimate. For this reason we do not consider $\mathcal{O}_{\ell dqN}$ here. With this discussion in mind, the matrix elements read:

$$\begin{aligned} \mathcal{M}(\pi^- \to \ell_i^- \overline{N}) = \frac{1}{\Lambda^2} \overline{u(p_{\ell_i})} \Big\{ & \langle 0|V^\mu|\pi^-\rangle \left[\left(\alpha_{duNe}^{11i} + \alpha_{\phi Ne}^{i} \right) \gamma_\mu \right] \\ & + \langle 0|S|\pi^-\rangle \left(\alpha_{quN\ell}^{11i} - \alpha_{\ell Nqd}^{i11} \right) \Big\} P_R v(p_N)\,. \end{aligned} \tag{6.15}$$

We point out that $\mathcal{O}_{NW}$ gives the following contribution to the amplitude:

$$\mathcal{M}_{\mathcal{O}_{NW}} = \frac{2\sqrt{2}}{\Lambda^2} \alpha_{NW}^{i} \left[\overline{u(p_{\ell_i})} \frac{\left(\gamma_\mu \not{q} - q_\mu\right)}{M_W} P_R v(p_N) \right], \tag{6.16}$$

where $q = p_{\ell_i} + p_N$ is the momentum of the exchanged W gauge boson. But because we are in the limit $q \ll M_W$, we can safely neglect this contribution.

The corresponding scalar and vector form factors are:

$$\langle 0|S|\pi^-\rangle = f_\pi \frac{m_\pi^2}{m_u + m_d}, \qquad \text{and} \qquad \langle 0|V^\mu|\pi^-\rangle = f_\pi q^\mu, \tag{6.17}$$

with $f_\pi \simeq 131$ MeV. Then, using the equations of motion for the Dirac spinors

$\overline{u(p_{\ell_i})}(\not{p}_\ell - m_\ell)$ and $(\not{p}_N + m_N)v(p_N)$, we obtain:

$$\mathcal{M}(\pi^- \to \ell_i^- \overline{N}) = \frac{f_\pi}{\Lambda^2}\left(m_{\ell_i}\left(\alpha_{duNe}^{11i} + \alpha_{\phi Ne}^{i}\right) + \frac{m_\pi^2}{m_u + m_d}\left(\alpha_{quN\ell}^{11i} - \alpha_{\ell Nqd}^{i11}\right)\right)[\overline{u(p_{\ell_i})}P_R v(p_N)]. \tag{6.18}$$

In order to arrive to this expression we have neglected the term proportional to the mass of N, which in any case, needs to be $m_N < m_\pi \approx 139$ MeV. From here it is straightforward to compute the decay rate:

$$\Gamma(\pi^- \to \ell_i^- \overline{N}) = \frac{f_\pi^2 m_\pi}{16\pi\Lambda^4}\left(1 - \frac{m_{\ell_i}^2}{m_\pi^2}\right)^2\left[m_{\ell_i}\left(\alpha_{duNe}^{11i} + \alpha_{\phi Ne}^{i}\right) + \frac{m_\pi^2}{m_u + m_d}\left(\alpha_{quN\ell}^{11i} - \alpha_{\ell Nqd}^{i11}\right)\right]^2. \tag{6.19}$$

Finally, we will use the experimental values [4] of the decay width into electrons:

$$\Gamma(\pi \longrightarrow e + \text{inv}) = (310 \pm 1) \times 10^{-23}\ \text{GeV}, \tag{6.20}$$

and muons:

$$\Gamma(\pi \longrightarrow \mu + \text{inv}) = (25279 \pm 5) \times 10^{-21}\ \text{GeV}. \tag{6.21}$$

In order to set bounds on the corresponding operators we require that the new contributions to pion decays, given by Eq. (6.19), are smaller than twice the experimental error.

6.4 Tau decays

In order to further put constraints on the operators of the νSMEFT framework, we use the measured values of the tau decay width into electrons or muons and missing energy. The most updated experimental results [4] are

$$\Gamma(\tau \longrightarrow e + \text{inv}) = (4.03 \pm 0.02) \times 10^{-13}\ \text{GeV}, \tag{6.22}$$

and

$$\Gamma(\tau \longrightarrow \mu + \text{inv}) = (3.93 \pm 0.02) \times 10^{-13}\ \text{GeV}. \tag{6.23}$$

As in the case of the pion decays, we will demand the new contributions to the decay width to be smaller than two standard deviations.

Operators giving contributions to leptonic tau decays are

$$\begin{aligned}
&\text{RRRR}: \mathcal{O}_{eN}^{i3} = (\overline{\ell_{iR}}\gamma_\mu \tau_R)(\overline{N}\gamma^\mu N)\,,\\
&\text{LLRR}: \mathcal{O}_{\ell N}^{i3} = (\overline{\nu_{iL}}\gamma_\mu \nu_{\tau L})(\overline{N}\gamma^\mu N) + \boldsymbol{(\overline{\ell_{iL}}\gamma_\mu \tau_L)(\overline{N}\gamma^\mu N)}\,,\\
&\text{LRRL}: \begin{cases}
\mathcal{O}_{\ell N\ell e}^{ii3} = \boldsymbol{(\overline{\nu_{iL}}N)(\overline{\ell_{iL}}\tau_R)} - \boldsymbol{(\overline{\ell_{iL}}N)(\overline{\nu_{iL}}\tau_R)} + h.c.\,,\\
\mathcal{O}_{\ell N\ell e}^{i3i} = \boldsymbol{(\overline{\nu_{iL}}N)(\overline{\tau_L}\ell_{iR})} - (\overline{\ell_{iL}}N)(\overline{\nu_{\tau L}}\ell_{iR}) + h.c.\,,\\
\mathcal{O}_{\ell N\ell e}^{3ii} = (\overline{\nu_{\tau L}}N)(\overline{\ell_{iL}}\ell_{iR}) - \boldsymbol{(\overline{\tau_L}N)(\overline{\nu_{iL}}\ell_{iR})} + h.c.\,,\\
\mathcal{O}_{\ell N\ell e}^{i33} = (\overline{\nu_{iL}}N)(\overline{\tau_L}\tau_R) - \boldsymbol{(\overline{\ell_{iL}}N)(\overline{\nu_{\tau L}}\tau_R)} + h.c.\,,\\
\mathcal{O}_{\ell N\ell e}^{3i3} = \boldsymbol{(\overline{\nu_{\tau L}}N)(\overline{\ell_{iL}}\tau_R)} - (\overline{\tau_L}N)(\overline{\nu_{iL}}\tau_R) + h.c.\,,\\
\mathcal{O}_{\ell N\ell e}^{33i} = \boldsymbol{(\overline{\nu_{\tau L}}N)(\overline{\tau_L}\ell_{iR})} - \boldsymbol{(\overline{\tau_L}N)(\overline{\nu_{\tau L}}\ell_{iR})} + h.c..
\end{cases}
\end{aligned} \tag{6.24}$$

In the SR category, the relevant loop operators are $\mathcal{O}^i_{\phi Ne}$, $\mathcal{O}^3_{\phi Ne}$, $\mathcal{O}^i_{NW}$, $\mathcal{O}^3_{NW}$. When there are more that one term, only those in boldface are relevant. As before, only operators within the same class can give interferences.

Using the operators from this list we can see that the invisible piece of the leptonic decay of the tau can be composed of the following combination of neutrinos: $N\bar{N}$, $N\bar{\nu}_i$, $N\bar{\nu}_\tau$, $\bar{N}\nu_i$ and $\bar{N}\nu_\tau$. It is important to note that we need to separate those channels in which the light neutrino can have either light-lepton flavour or tau flavour. Indeed, $\tau \longrightarrow \ell_i \nu_\tau \bar{N}$ will be generated by the contact interactions that correspond to the effective operators along with additional diagrams with a $W\tau\bar{\nu}_\tau$ SM vertex. Similarly, $\tau \longrightarrow \ell_i \bar{\nu}_i N$ is generated by a point-like diagram as well as by a diagram that includes the $W\ell_i\bar{\nu}_i$ SM vertex. This is no longer true for $N\bar{\nu}_\tau$ and $\bar{N}\nu_i$, because the LNV vertex $W\tau\bar{\nu}_i$ is not present in the Standard Model. With these considerations in mind, we list the decay rates obtained for the relevant operators.

For instance, the operator $\mathcal{O}^{ii3}_{\ell N\ell e}$ is the only one giving contributions to the decay mode $\tau \longrightarrow \ell_i \nu_i \bar{N}$. Its matrix element reads

$$\mathcal{M} = \frac{\alpha^{ii3}_{\ell N\ell e}}{\Lambda^2}\Big\{[\bar{u}(\nu)P_R v(N)][\bar{u}(e)P_R u(\tau)] - [\bar{u}(e)P_R v(N)][\bar{u}(\nu)P_R u(\tau)]\Big\}. \tag{6.25}$$

Then the spin averaged squared amplitude is

$$\begin{aligned}
\overline{\Sigma}|\mathcal{M}|^2 &= \frac{1}{2}\frac{(\alpha^{ii3}_{\ell N\ell e})^2}{\Lambda^4}[\mathrm{Tr}(\not{p}_\nu \not{p}_N P_L)\mathrm{Tr}(\not{p}_e \not{p}_\tau P_L) + \mathrm{Tr}(\not{p}_e \not{p}_N P_L)\mathrm{Tr}(\not{p}_\nu \not{p}_\tau P_L)\\
&\quad - \mathrm{Tr}(\not{p}_\nu \not{p}_N \not{p}_e \not{p}_\tau P_L) - \mathrm{Tr}(\not{p}_e \not{p}_N \not{p}_\nu \not{p}_\tau P_L)]\\
&= \frac{2(\alpha^{ii3}_{\ell N\ell e})^2}{\Lambda^4}(p_\nu p_e)(p_N p_\tau).
\end{aligned} \tag{6.26}$$

The final state is a three-body phase space. We can make use of the Lorentz-invariant

variables $s_{ij} = (p_i + p_j)^2 = (p_\tau - p_k)^2$ with $i \neq j \neq k$ that satisfy $s_{12} + s_{13} + s_{23} = m_\tau^2$ for $m_\tau \gg m_N, m_\nu, m_{\ell_i}$. In this limit, the kinematic variables are simply:

$$\begin{aligned} s_{12} &= 2(p_e p_N) = s - 2(p_\tau p_\nu), \\ s_{13} &= 2(p_e p_\nu) = s - 2(p_\tau p_N), \\ s_{23} &= 2(p_N p_\nu) = s - 2(p_\tau p_e). \end{aligned} \tag{6.27}$$

So that

$$\overline{\Sigma}|\mathcal{M}|^2 = \frac{(\alpha^{ii3}_{\ell N \ell e})^2}{\Lambda^4} \frac{s_{13}(s - s_{13})}{2}. \tag{6.28}$$

Finally, the decay width can be expressed in terms of the invariant kinematic variables:

$$\Gamma = \frac{1}{256\pi^3 s^{3/2}} \int ds_{23} \int ds_{23}\, \overline{\Sigma}|\mathcal{M}|^2. \tag{6.29}$$

The integration limits are

$$0 \leq s_{13} \leq s \qquad \text{and} \qquad 0 \leq s_{23} \leq s - s_{13}. \tag{6.30}$$

At the end, the decay width obtained with this operator is

$$\Gamma(\tau \to \ell_i \overline{N} \nu_i) = \frac{m_\tau^5}{6144\pi^3\Lambda^4} (\alpha^{ii3}_{\ell N \ell e})^2. \tag{6.31}$$

Following an analogous procedure we compute the rest of the leptonic decay width of tau. Special attention needs to be paid in those cases where interferences are present, as for $\mathcal{O}_{\phi Ne}$ with $\mathcal{O}_{NW}$, $\mathcal{O}^{i3i}_{\ell N \ell e}$ with $\mathcal{O}^{3ii}_{\ell N \ell e}$ and $\mathcal{O}^{i33}_{\ell N \ell e}$ with $\mathcal{O}^{3i3}_{\ell N \ell e}$. Here, we list the rest of our results:

$$\Gamma(\tau \to \ell_i \overline{N} N) = \frac{m_\tau^5}{1536\pi^3\Lambda^4} \left[(\alpha^{i3}_{eN})^2 + (\alpha^{i3}_{\ell N})^2 \right], \tag{6.32}$$

$$\Gamma(\tau \to \ell_i \overline{N} \nu_i) = \frac{m_\tau^5}{6144\pi^3\Lambda^4} (\alpha^{ii3}_{\ell N \ell e})^2, \tag{6.33}$$

$$\begin{aligned} \Gamma(\tau \to \ell_i \overline{\nu_i} N) = \frac{m_\tau^5}{6144\pi^3\Lambda^4} \Bigg[& (\alpha^{i3i}_{\ell N \ell e})^2 + (\alpha^{3ii}_{\ell N \ell e})^2 - \alpha^{i3i}_{\ell N \ell e} \alpha^{3ii}_{\ell N \ell e} + 4(\alpha^3_{\phi Ne})^2 \\ & + \frac{64}{5} \frac{m_\tau^2}{m_W^2} (\alpha^3_{NW})^2 + 8\sqrt{2} \frac{m_\tau}{m_W} \alpha^3_{\phi Ne} \alpha^3_{NW} \Bigg], \end{aligned} \tag{6.34}$$

$$\begin{aligned} \Gamma(\tau \to \ell_i \overline{N} \nu_\tau) = \frac{m_\tau^5}{6144\pi^3\Lambda^4} \Bigg[& (\alpha^{i33}_{\ell N \ell e})^2 + (\alpha^{3i3}_{\ell N \ell e})^2 - \alpha^{i33}_{\ell N \ell e} \alpha^{3i3}_{\ell N \ell e} + 4(\alpha^i_{\phi Ne})^2 \\ & + \frac{24}{5} \frac{m_\tau^2}{m_W^2} (\alpha^i_{NW})^2 - 2\sqrt{2} \frac{m_\tau}{m_W} \alpha^{3i3}_{\ell N \ell e} \alpha^i_{NW} \Bigg], \end{aligned} \tag{6.35}$$

$$\Gamma(\tau \to \ell_i \overline{\nu_\tau} N) = \frac{m_\tau^5}{6144\pi^3\Lambda^4} (\alpha^{33i}_{\ell N \ell e})^2. \tag{6.36}$$

6.5 Top quark decays

Operators that give contributions to top quark decays are listed below:

$$\begin{aligned}
&\text{RRRR}: \mathcal{O}^{33i}_{duNe} = (\overline{b_R}\gamma_\mu t_R)(\overline{N}\gamma^\mu \ell_{iR}) + h.c.\,,\\
&\text{LRRL}: \begin{cases}
\mathcal{O}^{i33}_{\ell dqN} = \boldsymbol{\frac{1}{2}(\overline{t_L} b_R)(\overline{\ell_{iL}} N)} - \frac{1}{2}(\overline{b_L} b_R)(\overline{\nu_{iL}} N)\\
\qquad\qquad + \boldsymbol{\frac{1}{8}(\overline{t_L}\sigma_{\mu\nu} b_R)(\overline{\ell_{iL}}\sigma^{\mu\nu} N)} - \frac{1}{8}(\overline{b_L}\sigma_{\mu\nu} b_R)(\overline{\nu_{iL}}\sigma^{\mu\nu} N) + h.c.\,,\\
\mathcal{O}^{i33}_{\ell Nqd} = (\overline{\nu_{iL}} N)(\overline{b_L} b_R) - \boldsymbol{(\overline{\ell_{iL}} N)(\overline{t_L} b_R)} + h.c.\,,\\
\mathcal{O}^{33i}_{quN\ell} = (\overline{t_L} t_R)(\overline{N}\nu_{iL}) + \boldsymbol{(\overline{b_L} t_R)(\overline{N}\ell_{iL})} + h.c.
\end{cases}
\end{aligned} \tag{6.37}$$

As before, whenever there are more than one term, only those in boldface are relevant. From this list, only operators $\mathcal{O}^{i33}_{\ell dqN}$ and $\mathcal{O}^{i33}_{\ell Nqd}$ produce interferences. Using the same calculation techniques of previous sections, we compute the contribution of these effective operators to the partial decay width of the top quark into $b\ell N$:

$$\Gamma(t \to b\ell_i^+ N) = \frac{m_t^5}{6144\pi^3\Lambda^4}\left[4(\alpha^{33i}_{duNe})^2 + (\alpha^{33i}_{quN\ell})^2 + (\alpha^{i33}_{\ell dqN})^2 + (\alpha^{i33}_{\ell Nqd})^2 - \alpha^{i33}_{\ell dqN}\alpha^{i33}_{\ell Nqd}\right]. \tag{6.38}$$

The particle data group lists the top quark total decay width to be $\Gamma(t) = 1.42^{+0.19}_{-0.15}$ GeV [4]. Then, for the purpose of setting bounds on these operators, we could proceed as in previous sections and demand the new contributions to top quark decays to be smaller than twice the experimental error. However, the results obtained in this manner are rather weak. For instance, in the case of $\mathcal{O}^{33i}_{quN\ell}$ we would find $\alpha < 640$ (with $\Lambda = 1$ TeV) and $\Lambda > 40$ GeV (with $\alpha = 1$).

On the other hand, we could try to constrain these operators using the information regarding the partial decay width. Experimental values of $\Gamma(t \longrightarrow b\ell + \text{inv})$ and their uncertainties reported in the literature are obtained with the assumption that the signature of the charged lepton and the neutrino reconstructs a W gauge boson. This is no longer (always) true in the context of νSMEFT, in which the invisible part of the new contributions corresponds to N. Under these circumstances, we cannot make use of the experimental results from existing analyses to set bounds on the effective operators in Eq. (6.38). New physics could still be hidden in these operators, and new dedicated studies must be performed in order to test this possibility. Here, we propose one such analysis.

In passing, it is interesting to note that, despite the νSMEFT framework is built respecting the gauge symmetries of the Standard Model, invariance under accidental symmetries is no longer a requirement. Accordingly, the following flavour-violating

operators are to be considered:

$$\mathcal{O}_{uN}^{13} = (\overline{\boldsymbol{u_R}}\boldsymbol{\gamma_\mu}\boldsymbol{t_R})(\overline{\boldsymbol{N}}\boldsymbol{\gamma^\mu}\boldsymbol{N})\,, \tag{6.39}$$

$$\mathcal{O}_{qN}^{13} = (\overline{\boldsymbol{u_L}}\boldsymbol{\gamma_\mu}\boldsymbol{t_L})(\overline{\boldsymbol{N}}\boldsymbol{\gamma^\mu}\boldsymbol{N}) + (\overline{d_L}\gamma_\mu b_L)(\overline{N}\gamma^\mu N)\,, \tag{6.40}$$

$$\mathcal{O}_{quN\ell}^{13i} = (\overline{\boldsymbol{u_L}}\boldsymbol{t_R})(\overline{\boldsymbol{N}}\boldsymbol{\nu_{iL}}) + (\overline{d_L}t_R)(\overline{N}\ell_{iL}) + h.c.\,, \tag{6.41}$$

$$\mathcal{O}_{quN\ell}^{31i} = (\overline{\boldsymbol{t_L}}\boldsymbol{u_R})(\overline{\boldsymbol{N}}\boldsymbol{\nu_{iL}}) + (\overline{b_L}u_R)(\overline{N}\ell_{iL}) + h.c. \tag{6.42}$$

and likewise for second generation quarks. These operators do not interfere and produce the following decay widths:

$$\Gamma(t \to u\overline{N}N) = \frac{m_t^5}{1536\pi^3\Lambda^4}\left[(\alpha_{uN}^{13})^2 + (\alpha_{qN}^{13})^2\right], \tag{6.43}$$

$$\Gamma(t \to u\overline{\nu_i}N) = \frac{m_t^5}{6144\pi^3\Lambda^4}(\alpha_{quN\ell}^{13i})^2\,, \tag{6.44}$$

$$\Gamma(t \to u\overline{N}\nu_i) = \frac{m_t^5}{6144\pi^3\Lambda^4}(\alpha_{quN\ell}^{31i})^2\,. \tag{6.45}$$

However, this type of operators, for which the signature corresponds to one light jet + two sources of missing energy, are hard to probe at hadron colliders, as the original centre of mass energy of the interacting partons is not fixed. These operators are better suited for being tested in lepton colliders, in which not only the transverse but also the longitudinal component of the missing momentum is measured.

6.5.1 Prospects for $t \longrightarrow b\ell N$ at the LHC

At the LHC, top quarks are either singly-produced through weak interactions or produced in pairs via the strong interactions. We concentrate in the latter. Top quarks are too heavy to hadronise and quickly decay into $W^\pm b$ in the 99.9% of the cases. In the next step of the decay chain, the W gauge boson decays into pairs of quarks or into a lepton and a neutrino. Accordingly, we can categorise the final states of the pair of top quarks as follows:

- Fully hadronic. The two W decay hadronically into $q\bar{q}$. The final state is $b\bar{b}$+ 4 light jets with BR = 4/9. This decay mode has no sources of missing energy, shows the largest branching ratio but it also has a lot of QCD background contamination.

- Fully leptonic. The two W decay into a charged lepton and a neutrino. The final state is composed of a pair of b quarks, a pair of charged leptons and a pair of neutrinos. This decay mode happens 1/9 of the time. In the opposite case of the fully hadronic decay channel, this decay mode is the cleanest, but has the smallest branching ratio. Furthermore, there are two sources of

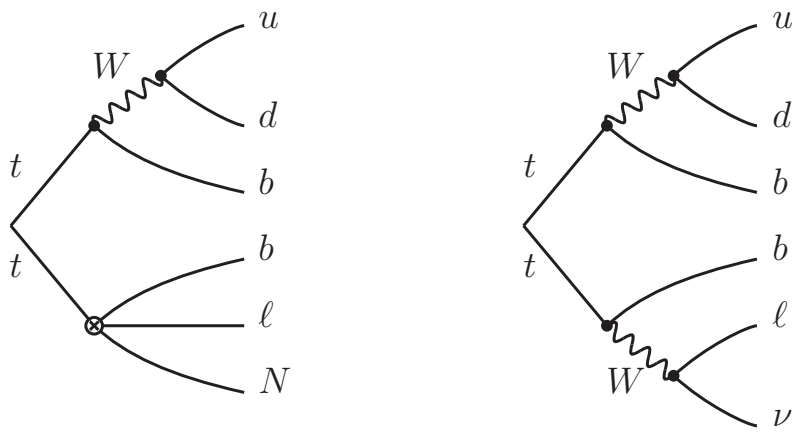

Figure 6.1: Semileptonic top decays in the νSMEFT (subfigure a) and in the Standard Model (subfigure b).

missing energy.

- Semileptonic. Finally, one W decays into pairs of light jets and the other W into a charged lepton and a neutrino. In this case, the final state exhibits a pair of b-jets, a pair of light jets, a charged lepton and a single source of missing energy. The branching ratio is 4/9 although it drops to $\approx 1/3$ if we consider only light leptons (tau leptons are hard to reconstruct and are often omitted, as in our study). Its features lie between those of the previous decay modes. In particular, it has a very small QCD background and a considerable large branching ratio.

Here we will focus on the semileptonic decay of pairs of top quarks in the LHC, which will allow us to set bounds on the operators $\mathcal{O}_{duNe}$, $\mathcal{O}_{\ell dqN}$, $\mathcal{O}_{\ell Nqd}$ and $\mathcal{O}_{qu\ell N}$. Indeed, these operators generate a topology with a top quark decaying hadronically as in the Standard Model, while the other decays into a lepton and one source of missing energy through the effective vertex (see diagram (a) in Figure 6.1). This is exactly the same final state as that of the semileptonic decay of the pair of top quarks within the Standard Model (diagram (b) in Figure 6.1). However, in the νSMEFT framework the charged lepton and the neutrino do not reconstruct a W gauge boson and this implies a new signal so far not studied.

In order to study the LHC prospects for this new signal, we start by generating background and signal events at $\sqrt{s} = 14$ TeV using the NNPDF23LO PDF set [169]. The background consists of the SM semileptonic $t\bar{t}$ decay channel. We focus on muons in the final state, while assuming that the analysis considering electrons is similar. Events are generated at leading order (with a $t\bar{t}$ cross section of 605.2 pb) and rescale them with a K-factor of ~ 1.63. This K-factor is obtained with a cross section at NNLO of 984.5 pb for $m_t = 172.5$ GeV [170].

At the generator level, we demand events to have $p_T(j, b, \ell) > 15, 15, 10$ GeV, $\eta(j, b, \ell) < 5, 3, 3$, $\Delta R(jj, bb, bj, j\ell, \ell\ell) > 0.3$ and $\Delta R(\ell\ell) > 0.2$. We reconstruct the jets with `FastJet 3` [165] making use of the anti-k$_t$ algorithm [130] with $R = 0.4$. Further requirements include $p_t(j) > 30$ GeV, $|\eta(b)| < 2.5$. In the case of leptons we demand $p_T > 10$ GeV and $\eta < 2.5$. b-jets are tagged with an efficiency of 0.7 and reconstructed by requiring B mesons to be at $\Delta R < 0.2$ of a jet. We additionally consider a 10% (1%) probability of a c quark (a light lepton) to be mis-identified as a b-jet. Finally, we define a charged lepton to be isolated when within a cone of size $\Delta R = 0.2$ there is a hadronic activity smaller than 10% of its p_T.

We require events to have exactly two b-tagged jets, one isolated lepton and at least two light jets, out of which we will consider only the two hardest ones.

First, we reconstruct the hadronic top mass, that is, the mass of the top quark that decays hadronically. For this, the ingredients we need are two light jets, reconstructing the hadronic W boson (M_W^{had}), along with one b-tagged jet. However, there are two of them. So, subsequently, we reconstruct hadronic top masses twice, one for each of the b-jets. From these two variables, we only keep the one that is closer to the actual top mass (taken to be 172.5 GeV); accordingly, we simply call it the hadronic top mass, m_t^{had}. The b-tagged jet best reconstructing the hadronic top mass is then assigned to the hadronic top (thus, hereafter it will be called b_t), while the remaining b-jet belongs to the leptonic top decay cascade (b_ℓ). Finally, we keep only those events for which the reconstructed hadronic top mass and the reconstructed hadronic W mass lie within 40 GeV and 30 GeV of the top quark and W masses, respectively.

Next, we reconstruct the leptonic top. In this case, we have a b-jet, a charged lepton and N. In order to accomplish our task, we need the kinematic information about these three objects. However, in proton colliders, like the LHC, the longitudinal component of the momentum of the neutrino is not accessible[5]. In the Standard Model, the leptonic decay of the top quark is mediated by the W gauge boson. Then, typically we would find p_z^ν by solving for the fixed value of M_W:

$$M_W^2 = m_\ell^2 + 2(E_\ell E_\nu - \vec{p}_T^{\,\ell} \cdot \vec{p}_T^{\,\text{miss}} - p_z^\ell p_z^\nu), \tag{6.46}$$

where $E_\nu = \sqrt{(E_T^{\text{miss}})^2 + (E_z^\nu)^2}$. This is a quadratic equation in p_z^ν and therefore it has two solutions. With each of them, the leptonic top mass is finally reconstructed

[5]Indeed, for a single neutrino only the transverse momentum can be computed. In a given collider the beams travel along one axis, so that the transverse momentum before the collision is zero. After the collision, the momentum is conserved and by measuring the transverse momentum of the visible particles one can infer the transverse component of the momentum of the neutrino. This exact method can be followed in lepton colliders, in which the kinematics of the collision is well-known, to obtain the longitudinal motion of the neutrino. However, in proton colliders this is no longer true, as there is no control of the momenta carried by the colliding quarks.

twice. The leptonic top mass that agrees best with the hadronic top mass is kept. However, within the νSMEFT framework the leptonic top decay is governed by the contact interactions given by the different effective operators. We could try to proceed in the same fashion as in the Standard Model, but it turns out that now the charged lepton-neutrino system does not originate from the W gauge boson so that we are not able to use the fixed value of M_W to solve the quadratic equation in p_z^ν. Here we find p_z^ν by solving for the quadratic equation for the leptonic top mass which, as before, we take to be equal to 172.5 GeV. With the two solutions of the quadratic equation, we reconstruct the invariant mass of the lepton-neutrino system. Note that for the background this invariant mass is indeed a distribution of the W mass, but for the signal this is no longer true. By making use of this feature we can check to what extent the signal is compatible with the background. Accordingly, we show the distribution of these variables in Figure 6.2, for both the signal and the SM background. We have called these variables $m_W^{\ell,1}$ and $m_W^{\ell,2}$, where '1' and '2' refer to the '+' and '-' solutions of the quadratic equation. Only those solutions with positive discriminant have been kept. At the end, the subsequent selection cuts, including trigger, isolation and analysis cuts give an efficiency of 4.4% and 4.7% for the signal and the background, respectively.

From Figure 6.2, we see that the signal and background distributions of $m_W^{\ell,1}$ and $m_W^{\ell,2}$ are very similar. Therefore and in order to extract the maximum amount of information from data, we perform a multivariate analysis based on a simple machine learning boosted decision tree classifier (BDT), which is no more than a forest of decision trees, using the TMVA environment [171]. We consider the following observables as inputs: the four-momentum of the lepton and that of the b_ℓ-jet, the transverse missing momentum along with the transverse missing energy, m_W^{had}, $m_W^{\ell,1}$ and $m_W^{\ell,2}$, m_t^{had}, $\Delta R_{b_\ell b_h}$, $\Delta R_{b_\ell j_{1,2}}$, $\Delta R_{\ell,b_h}$ and $\Delta R_{\ell,j_{1,2}}$. Because BDTs algorithms are prone to suffer from overtraining, we have checked that the Kolmogorov-Smirnov statistic test does not fall below the critical value of 0.01 [172]. We find that the most discriminating observables are $m_W^{\ell,1}$ and $m_W^{\ell,2}$. In Figure 6.3 we show the distributions of the BDT variable for the signal and the background.

In order to avoid the systematic uncertainties, we consider the asymmetry variable defined for every bin of the BDT as

$$A = \frac{N_{right} - N_{left}}{N_{right} + N_{left}}, \tag{6.47}$$

where N_{right} (N_{left}) counts the number of events to the left (right) of the given bin (the bin itself is included in the count of N_{right}). The systematic uncertainties are common to both N_{right} and N_{left} and thus cancel in this ratio. We compute the asymmetry for the total number of events of signal+background and background

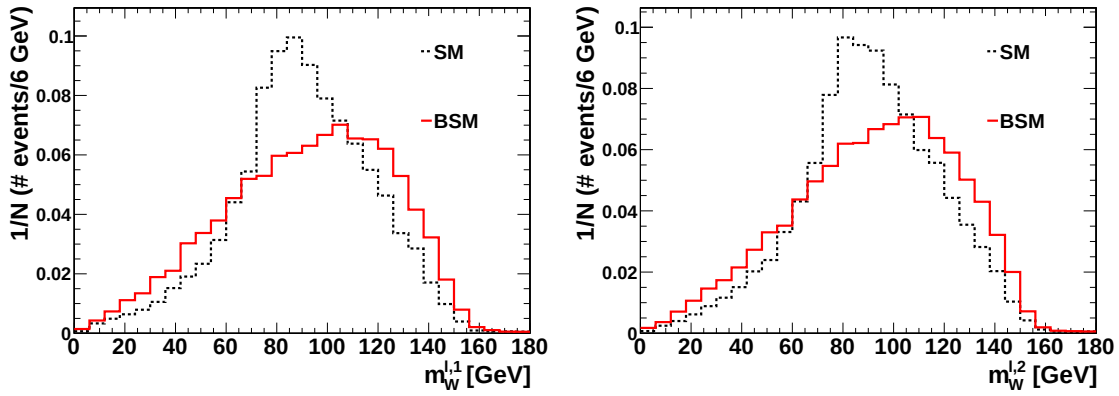

Figure 6.2: Reconstructed W-boson mass for the signal (solid red) and background (dashed black). Here 1 (2) refers to the '+' ('−') solution of the neutrino p_z to the quadratic equation for the invariant mass of the leptonic top. The signal was generated with a BR$(t \longrightarrow b\mu N) = 10^{-6}$.

alone, in each bin of the BDT variable. Then we look at the bin with the largest $|A_{s+b} - A_b|$ separation. In Figure 6.4 we depict the $|A_{s+b} - A_b + 1\sigma|$ distance in units of the standard deviation of A_b, as a function of the branching ratio of the exotic top decay. For the sake of providing a more straightforward readability, we show three curves, for which the 1σ, 2σ and 3σ bounds on BR$(t \longrightarrow b\ell N)$ can be obtained from where the intersection with the abscissa axis occurs. From the left panel, we find that branching ratios as low as $\sim 2 \times 10^{-4}$ could be probed at the High Luminosity phase of the LHC at $\sqrt{s} = 14$ TeV with an integrated luminosity of 3 ab^{-1}. The expected bounds in the long run, at $\sqrt{s} = 27$ TeV with $\mathcal{L} = 10^{-1}$ ab, are also shown in the right panel[6]. For this case, the limits would be improved by a factor of ~ 4.

Finally, we can use the 95% CL bounds on the branching ratio of the exotic top decay obtained in this subsection to set limits on α and Λ. Indeed, this is easily done by plugging the 2σ values of BR$(t \longrightarrow b\ell N)$ in the expressions for the top quark partial decay width found in Eq. (6.38) (with the total decay width of the top quark being $\Gamma_{total} \simeq 1.41$ GeV [4]) and solving for α (or Λ).

6.6 Global analysis

In this section we put together the results and find bounds on the parameters of the four-fermion effective operators, namely the Wilson coefficients α and the scale of new physics Λ. In every case, we look for the maximum value of α assuming $\Lambda = 1$ TeV. Similarly, we constraint the minimum value of Λ by assuming $\alpha = 1$. As said before, in order to keep the validity of the EFT under control, we restrain to

[6] At this centre of mass energy, the $t\bar{t}$ cross section at LO is 3813 pb.

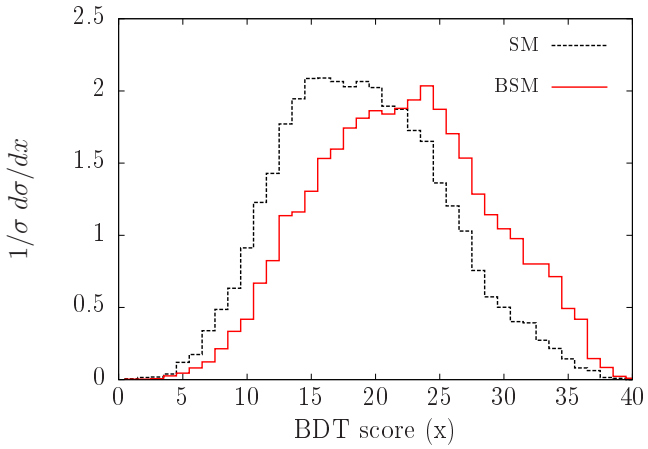

Figure 6.3: BDT score variable for the signal (red line) and the background (black line).

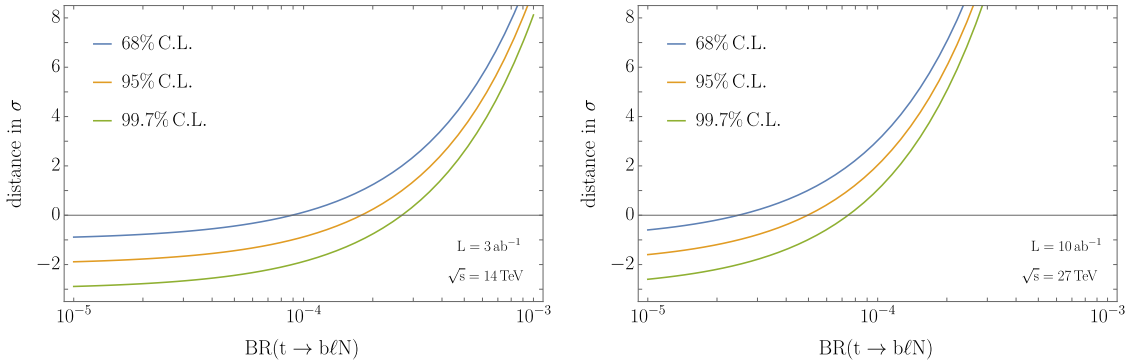

Figure 6.4: Number of standard deviations between the BDT asymmetry for the signal + background and the asymmetry for the background alone as a function of the exotic top decay mode branching ratio. Left panel corresponds to $\sqrt{s} = 14$ TeV and $\mathcal{L} = 3$ ab^{-1}; while the right panel refers to $\sqrt{s} = 27$ TeV and $\mathcal{L} = 10$ ab^{-1}.

bins with energies below 1 TeV, although, in some cases, bins with larger energies could give improved bounds.

We start with the LHC searches. Regarding one light lepton and missing energy analyses, limits from operators $\mathcal{O}^{11i}_{quN\ell}$ and $\mathcal{O}^{11i}_{duNe}$ are easy to compute, as these operators show no interferences with any other operator. For each bin in Table 6.2 we compute the bounds on α and Λ by demanding the number of signal events to be equal to $s_{\max}$. Finally, we keep the limit from the m_T bin giving the most stringent result. For $\ell + E_{miss}$ this bin is $[600 - 1000]$ GeV. The remaining two operators, i.e. $\mathcal{O}^{i11}_{\ell Nqd}$ and $\mathcal{O}^{i11}_{\ell dqN}$, produce interferences, which are treated with marginalisation. This process consists of finding the value of the marginalised operator that minimise the total number of signal events, plugging in this expression and finally solving the resulting one-dimensional equation. Likewise, this process is repeated for the other operator. As before, the most constraining m_T bin is $[600 - 1000]$ GeV. All bounds for $\ell = \mu$ are less restrictive as the LHC study of Ref. [166] shows a weaker sensitivity

to final states with muons, as seen in Table 6.2.

Bounds from $\tau + E_{\text{miss}}$ searches follow an analogous procedure. As before, we consider operators $\mathcal{O}^{113}_{quN\ell}$ and $\mathcal{O}^{113}_{duNe}$, along with those that produce interferences, $\mathcal{O}^{311}_{\ell Nqd}$ and $\mathcal{O}^{311}_{\ell dqN}$. In all cases, the m_T bin giving the hardest bound is $[500 - 1000]$ GeV.

When $m_N < m_\pi \approx 139$ MeV[7], we can use pion decays to further improve the bounds on the corresponding operators. We see that (neglecting the m_ℓ term) the split between the bounded values of the Wilson coefficients of $\mathcal{O}^{11i}_{quN\ell}$ and $\mathcal{O}^{i11}_{\ell Nqd}$ is rather small:

$$\alpha^{11i}_{quN\ell} - \alpha^{i11}_{\ell Nqd} = \Lambda^2 \sqrt{\frac{16\pi(m_u + m_d)^2 \times 2\Delta\Gamma(\pi \to e + \text{inv})}{f_\pi^2 m_\pi^5}} \approx 2 \times 10^{-4}, \tag{6.48}$$

for $\Lambda = 1$ TeV. We can use this result to improve the bounds on the less constrained of these two operators. With $\ell + E_{\text{miss}}$ searches we have found $\alpha^{11i}_{quN\ell} < 0.133$ and $\alpha^{i11}_{\ell Nqd} < 0.25$. Using pion decays, the bounds regarding the parameter $\alpha^{i11}_{\ell Nqd}$ can be improved by a factor of 1.9 (1.8) for electrons (muons). However, here we report the most conservative limit.

In the case of monojets searches, we can set limits on the operators $\mathcal{O}^{11}_{uN}$, $\mathcal{O}^{11}_{dN}$ and $\mathcal{O}^{11}_{qN}$. There is no interference, which makes the computation straightforward. For the three operators, the most restraining bounds are found with the E_{miss} bin $[740 - 790]$ GeV.

Tau decays are useful for constraining several operators. In particular, bounds from $\mathcal{O}^{i3}_{eN}$, $\mathcal{O}^{i3}_{\ell N}$, $\mathcal{O}^{ii3}_{\ell N\ell e}$ and $\mathcal{O}^{33i}_{\ell N\ell e}$ are straightforward to compute, while $\mathcal{O}^{3ii}_{\ell N\ell e}$ with $\mathcal{O}^{3i3}_{\ell N\ell e}$ and $\mathcal{O}^{i33}_{\ell N\ell e}$ with $\mathcal{O}^{3i3}_{\ell N\ell e}$ produce interferences. We marginalise these operators in the same way as before. This set of operators, but involving the first and second lepton families instead of the third (for instance $\mathcal{O}^{12}_{eN}$ and $\mathcal{O}^{12}_{\ell N}$), could give contributions to muon decays. In that case, they modify the Fermi constant for which reason special care has to be taken in computing their bounds. We leave this computation for future work.

Finally, there are several operators giving new contributions to rare top decays. Moreover, these searches would be the only way to probe these operators. We have seen that using the top quark total decay width leads to weak constrains. Indeed, we would find

$$\mathcal{O}^{33i}_{quN\ell}: \qquad \alpha < 640 \text{ or } \Lambda > 40 \text{ GeV}, \tag{6.49}$$

$$\mathcal{O}^{33i}_{duN\ell}: \qquad \alpha < 320 \text{ or } \Lambda > 55 \text{ GeV}, \tag{6.50}$$

$$\mathcal{O}^{i33}_{\ell dqN} \text{ and } \mathcal{O}^{i33}_{\ell Nqd}: \qquad \alpha < 740 \text{ or } \Lambda > 35 \text{ GeV}. \tag{6.51}$$

[7]This is always true for Dirac neutrinos as well as for Majorana neutrinos in the range of masses considered in this work (see the introduction of this chapter).

Thus, these directions remain very unconstrained and further exploration for new physics is needed. New dedicated top quark searches could be useful in this regard. In order to evaluate the bounds, we proceed in the same manner as before, but using the LHC prospects obtained in Subsection 6.5.1. Bounds on operators $\mathcal{O}_{dune}^{33i}$ and $\mathcal{O}_{quN\ell}^{33i}$ are straightforward to calculate, while $\mathcal{O}_{\ell dqN}^{i33}$ and $\mathcal{O}_{\ell Nqd}^{i33}$ give interferences and we need to marginalise. We see that bounds achieved with dedicated searches would be significantly improved in around an order of magnitude, relative to the those obtained with the measurement of the top quark total decay width.

We report all our findings in Figure 6.5 (see Table 6.5 for the actual numbers).

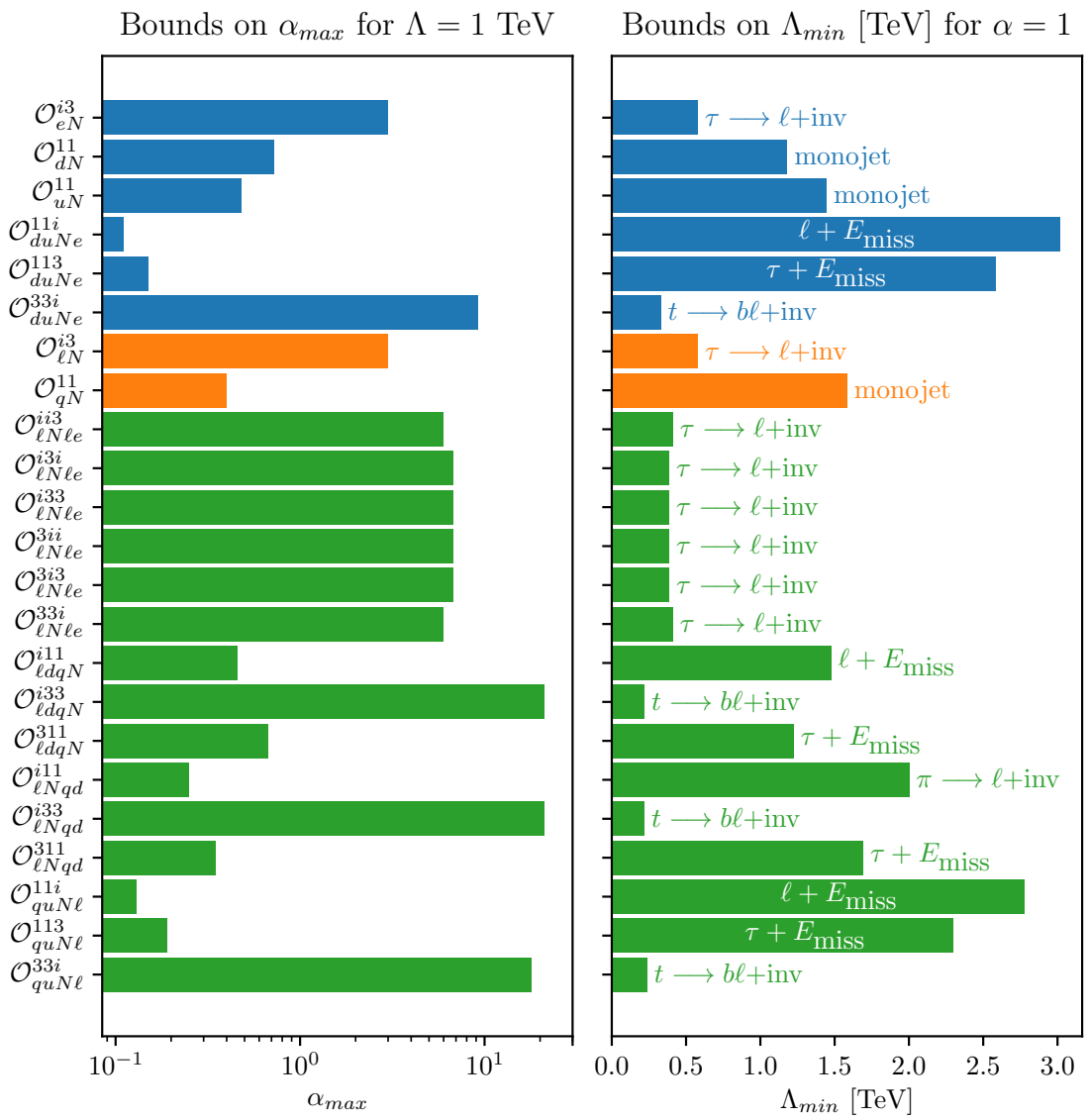

Figure 6.5: Bounds on the four-fermion effective operators in the νSMEFT framework. Left panel: upper bounds on α assuming $\Lambda = 1$ TeV. Right panel: lower bounds on Λ assuming $\alpha = 1$. Colours correspond to categories RRRR (blue), LLRR (orange) and LRRL (green). Here ℓ stands for an electron. Bounds for $\ell = \mu$ are obtained to be practically identical.

	Operator	$\alpha_{\max}$ for $\Lambda = 1$ TeV	$\Lambda_{\min}$ [TeV] for $\alpha = 1$	*Observable*
RRRR	$\mathcal{O}_{eN}^{i3}$	3.0 (2.9)	0.58 (0.59)	$\tau \to \ell + \text{inv}$
	$\mathcal{O}_{dN}^{11}$	0.72	1.2	monojet
	$\mathcal{O}_{uN}^{11}$	0.48	1.4	monojet
	$\mathcal{O}_{duNe}^{11i}$	0.11 (0.16)	3.0 (2.5)	$\ell + E_{\text{miss}}$
	$\mathcal{O}_{duNe}^{113}$	0.15	2.6	$\tau + E_{\text{miss}}$
	$\mathcal{O}_{duNe}^{33i}$	9.2 (9.2)	0.33 (0.33)	$t \to b + \text{inv}$
LLRR	$\mathcal{O}_{\ell N}^{i3}$	3.0 (2.9)	0.58 (0.59)	$\tau \to \ell + \text{inv}$
	$\mathcal{O}_{qN}^{11}$	0.40	1.6	monojet
LRRL	$\mathcal{O}_{\ell N\ell e}^{ii3}$	6.0 (5.9)	0.41 (0.41)	$\tau \to \ell + \text{inv}$
	$\mathcal{O}_{\ell N\ell e}^{i3i}$	7.6 (7.6)	0.36 (0.36)	$\tau \to \ell + \text{inv}$
	$\mathcal{O}_{\ell N\ell e}^{i33}$	7.6 (7.6)	0.36 (0.36)	$\tau \to \ell + \text{inv}$
	$\mathcal{O}_{\ell N\ell e}^{3ii}$	7.6 (7.6)	0.36 (0.36)	$\tau \to \ell + \text{inv}$
	$\mathcal{O}_{\ell N\ell e}^{3i3}$	7.6 (7.6)	0.36 (0.36)	$\tau \to \ell + \text{inv}$
	$\mathcal{O}_{\ell N\ell e}^{33i}$	6.0 (5.9)	0.41 (0.41)	$\tau \to \ell + \text{inv}$
	$\mathcal{O}_{\ell dqN}^{i11}$	0.46 (0.66)	1.5 (1.2)	$\ell + E_{\text{miss}}$
	$\mathcal{O}_{\ell dqN}^{i33}$	21 (21)	0.22 (0.22)	$t \to b\ell + \text{inv}$
	$\mathcal{O}_{\ell dqN}^{311}$	0.67	1.2	$\tau + E_{\text{miss}}$
	$\mathcal{O}_{\ell Nqd}^{i11}$	0.25 (0.36)	2.0 (1.7)	$\pi \to \ell + \text{inv}$
	$\mathcal{O}_{\ell Nqd}^{i33}$	21 (21)	0.22 (0.22)	$t \to b\ell + \text{inv}$
	$\mathcal{O}_{\ell Nqd}^{311}$	0.35	1.7	$\tau + E_{\text{miss}}$
	$\mathcal{O}_{quN\ell}^{11i}$	0.13 (0.19)	2.8 (2.3)	$\ell + E_{\text{miss}}$
	$\mathcal{O}_{quN\ell}^{113}$	0.19	2.3	$\tau + E_{\text{miss}}$
	$\mathcal{O}_{quN\ell}^{33i}$	18 (18)	0.23 (0.23)	$t \to b\ell + \text{inv}$

Table 6.5: Maximum (minimum) value of α (Λ) assuming $\Lambda = 1$ TeV ($\alpha = 1$) for the four-fermion operators. The last column indicates the most constraining observable. Numbers refer to $\ell = e$, while numbers inside parentheses correspond to $\ell = \mu$.

6.7 Summary

- The effective field theory with the same gauge symmetries and the same field content as the Standard Model is called SMEFT. If neutrinos are Dirac particles, one needs to extend the field content by adding a right-handed neutrino. In this case, the effective theory is called νSMEFT.

- The non-renormalizable operators of the νSMEFT will induce new contributions to several physical processes. Among the different possibilities, of special interest are the dimension-six four-fermion operators.

- We have computed new physics contributions to searches of one lepton and missing energy, monojets searches, pion decays, tau decays and top quarks decays coming from these operators.

- By comparing the new contributions given by the four-fermion operators with experimental data we have set bounds on several of these operators.

- Results obtained in this chapter are valid when neutrinos are Dirac particles and the scale of new physics is beyond the electroweak scale, or when neutrinos are Majorana particles with 0.01 GeV $\lesssim m_N \lesssim$ 0.1 GeV.

- By using the current experimental data regarding the processes listed above, we have set bounds on the maximum (minimum) values of α (Λ) assuming $\Lambda = 1$ TeV ($\alpha = 1$) corresponding to the four-fermion effective operators of the νSMEFT.

- Unconstrained operators could still hide new physics and therefore must be explored.

- In particular, operators giving contributions to rare top decays receive weak constrains from measurements of top quark total decay widths.

- However, the new contributions to leptonic top quark decays show final states that do not reconstruct the W gauge boson. For this reason, dedicated analyses must be implemented to study their signature. Here, we have proposed a search strategy for this aim.

Conclusions

For a long time neutrinos were thought to be massless. This prejudice was supported by insufficient experimental information. The discovery of neutrino oscillations completely changed this paradigm. In the pages that layout this thesis we tried to address several topics related to the non-vanishing neutrino masses.

The Standard Model does not provide a mechanism for generating neutrino masses; new pieces are to be added for this purpose. Physicists have designed a great amount of models but without a more complete experimental knowledge about the neutrino mixing parameters they work somewhat blindly. Here, we have compared the available oscillation data with patterns of the neutrino mass matrix. These patterns can be induced by new symmetries or by the dynamics of the underlying theory. In particular, we have revisited the case of two-zero textures for Majorana neutrinos using a purely numerical method. This technique not only needs no previous algebraic work, but also allows to compare the viability among different textures in terms of their χ^2 and the available parameter space. More importantly, it gives predictions of the unknown parameters and can be used to study the stability of the results when the constraints are approximate. Our findings indicate that the most promising textures are those of class A. Textures of class B, in both mass orderings, show a very constrained parameter space, with the phases mostly fixed to a given value. Finally, texture C-NO requires $\sin^2\theta_{23} = 0.5$, which could be incompatible with data in the near future, fixed values of the Majorana phases and relative large values of the mass of the lightest neutrino ($m_\ell \gtrsim 0.1$ eV). Texture C-IO relaxes its predictions respect to those of C-NO; however, current data gives a great preference of normal ordering over inverted ordering. Furthermore, we have checked that, if the constraints are relaxed, the main predictions of the textures remain while the parameter space is enlarged. Finally, excluded textures are also revisited. In particular, texture F1-NO could show interesting prospects when the constraint is only approximate.

Another fundamental aspect of neutrino masses that needs to be clarified before the generation of neutrino masses can be properly described concerns whether they are Dirac or Majorana type. The main difference is that the latter implies lepton

number violation, which can be tested in experiments looking for neutrinoless double beta decay. If one designs a model of Majorana neutrino masses that make use of the predictions of texture A, it will also imply that the standard neutrino exchange mechanism of neutrinoless double beta decay is highly suppressed (because texture A demands $(M_\nu)_{ee} \approx 0$). However, this mechanism needs not be the main source of neutrinoless double beta decay for there could be additional short-range mechanisms that are based on the exchange of new heavy lepton number violating fields. In this thesis we have presented a three-loop neutrino mass model that leads to the above features. In particular, we have found that neutrinoless double beta decay could be observed in the near future should the masses of the new fields be in the TeV scale. Moreover, the model could receive constraints from processes with lepton flavour violation, electroweak precision data and dark matter searches.

Many models of Majorana neutrino masses, like the one described above, are based on explicit lepton number symmetry breaking. For this aim, they typically introduce new heavy scalars that couple to leptons. Moreover, these scalars could be embedded in larger multiplets or have interactions with neutrinos, which would translate into enhancements of the production pattern, and into decay modes with missing energy. Current LHC searches of doubly-charged and singly-charged scalars do not take these considerations into account. Accordingly, we have presented a broad scope search strategy with several signal regions and based on several observables with the purpose of studying the signatures of these scalars.

First, we have applied the search strategy to the case of doubly-charged scalars, with special attention given to the Zee-Babu model and the three-loop model presented in this thesis. We have generated the relevant background regarding events with two, three and four leptons, all of which have at least two leptons with the same sign. Our findings report that future analyses could probe both leptonic and exotic decays of doubly-charged scalars in the context of the Zee-Babu model. In particular, masses as large as 1 TeV could be excluded in the near future. Moreover, models with additional scalar multiplets show an enhancement of the production mode of the doubly-charged scalar. We have found that, in the particular case of the three-loop model, bounds on the mass of the doubly-charged scalar, obtained by considering the enlarged production, would be more stringent than those obtained with the standard pair production mode by around ~ 100 GeV.

Then, we have studied singly-charged scalars, decaying into a light charged lepton and a neutrino. These scalars can be pair-produced or singly produced in association with two charged leptons, two neutrinos or a charged lepton and a neutrino. Moreover, the single-production cross section depends on the Yukawa coupling of the scalar with the leptons. Subsequently, we have divided the analysis in two signal regions with two charged leptons and three charged leptons, respectively. The

former can be applied only when Yukawa couplings are small, while the former is more relevant in the regime of large Yukawa coupling. For the signal region with two leptons, we have shown that the branching ratio vs mass plane can be better tested in the near future using our search strategy than with those previously considered in the literature. On the other hand, the three lepton signal region has not been considered prior to this work. Our results indicate that masses up to 500 GeV can be probed in the High-Luminosity phase of the LHC, for Yukawa couplings as low as ~ 0.8 when the decay branching ratio into electrons and muons is saturated.

The last topic we have addressed is related to the effective field theory of the Standard Model extended with right-handed neutrinos, which is the appropriate description of low energy physics when neutrinos are Dirac particles. Here, we have focused on four-fermion operators and computed the contributions they give to several processes. After comparing with experimental data, we have set bounds on the parameters of several of these operators. The unconstrained operators can hide new physics and therefore it is necessary to probe them for new physics. New strategies need to be designed to this aim. Accodingly, we have proposed one such analysis for signatures of rare top decays not yet studied at high-energy colliders.

References

[1] M. Goldhaber, L. Grodzins, and A. W. Sunyar. "Helicity of Neutrinos". In: *Phys. Rev.* 109 (3 Feb. 1958), pp. 1015–1017. DOI: 10.1103/PhysRev.109.1015. URL: https://link.aps.org/doi/10.1103/PhysRev.109.1015.

[2] S. S. Gershtein and Ya. B. Zeldovich. "Meson corrections in the theory of beta decay". In: *Zh. Eksp. Teor. Fiz.* 29 (1955). [,80(1955)], pp. 698–699.

[3] M. L. Perl et al. "Evidence for anomalous lepton production in e^+e^- annihilation". In: 35.22 (Dec. 1975), pp. 1489–1492. DOI: 10.1103/PhysRevLett.35.1489.

[4] M Tanabashi et al. "Review of Particle Physics, 2018". In: *Phys. Rev. D* 98.3 (2018), 030001. 1898 p. DOI: 10.1103/PhysRevD.98.030001. URL: http://cds.cern.ch/record/2636832.

[5] S. L. Glashow. "Partial Symmetries of Weak Interactions". In: *Nucl. Phys.* 22 (1961), pp. 579–588. DOI: 10.1016/0029-5582(61)90469-2.

[6] Peter W. Higgs. "Broken symmetries, massless particles and gauge fields". In: *Phys. Lett.* 12 (1964), pp. 132–133. DOI: 10.1016/0031-9163(64)91136-9.

[7] Peter W. Higgs. "Broken Symmetries and the Masses of Gauge Bosons". In: *Phys. Rev. Lett.* 13 (16 Oct. 1964), pp. 508–509. DOI: 10.1103/PhysRevLett.13.508. URL: https://link.aps.org/doi/10.1103/PhysRevLett.13.508.

[8] F. Englert and R. Brout. "Broken Symmetry and the Mass of Gauge Vector Mesons". In: *Phys. Rev. Lett.* 13 (9 Aug. 1964), pp. 321–323. DOI: 10.1103/PhysRevLett.13.321. URL: https://link.aps.org/doi/10.1103/PhysRevLett.13.321.

[9] G. S. Guralnik, C. R. Hagen, and T. W. B. Kibble. "Global Conservation Laws and Massless Particles". In: *Phys. Rev. Lett.* 13 (20 Nov. 1964), pp. 585–587. DOI: 10.1103/PhysRevLett.13.585. URL: https://link.aps.org/doi/10.1103/PhysRevLett.13.585.

[10] T. W. B. Kibble. "Symmetry breaking in nonAbelian gauge theories". In: *Phys. Rev.* 155 (1967). [,165(1967)], pp. 1554–1561. DOI: 10.1103/PhysRev.155.1554.

[11] Steven Weinberg. "A Model of Leptons". In: *Phys. Rev. Lett.* 19 (1967), pp. 1264–1266. DOI: 10.1103/PhysRevLett.19.1264.

[12] S. L. Glashow, J. Iliopoulos, and L. Maiani. "Weak Interactions with Lepton-Hadron Symmetry". In: *Phys. Rev. D* 2 (7 Oct. 1970), pp. 1285–1292. DOI: 10.1103/PhysRevD.2.1285. URL: https://link.aps.org/doi/10.1103/PhysRevD.2.1285.

[13] Gerard 't Hooft. "Renormalization of Massless Yang-Mills Fields". In: *Nucl. Phys.* B33 (1971), pp. 173–199. DOI: 10.1016/0550-3213(71)90395-6.

[14] Murray Gell-Mann. "A Schematic Model of Baryons and Mesons". In: *Phys. Lett.* 8 (1964), pp. 214–215. DOI: 10.1016/S0031-9163(64)92001-3.

[15] G Zweig. *An SU_3 model for strong interaction symmetry and its breaking; Version 1*. Tech. rep. CERN-TH-401. Geneva: CERN, Jan. 1964. URL: http://cds.cern.ch/record/352337.

[16] G Zweig. "An SU_3 model for strong interaction symmetry and its breaking; Version 2". In: CERN-TH-412 (Feb. 1964). Version 1 is CERN preprint 8182/TH.401, Jan. 17, 1964, 80 p. URL: http://cds.cern.ch/record/570209.

[17] H. Fritzsch, Murray Gell-Mann, and H. Leutwyler. "Advantages of the Color Octet Gluon Picture". In: *Phys. Lett.* 47B (1973), pp. 365–368. DOI: 10.1016/0370-2693(73)90625-4.

[18] David J. Gross and Frank Wilczek. "Ultraviolet Behavior of Non-Abelian Gauge Theories". In: *Phys. Rev. Lett.* 30 (26 June 1973), pp. 1343–1346. DOI: 10.1103/PhysRevLett.30.1343. URL: https://link.aps.org/doi/10.1103/PhysRevLett.30.1343.

[19] H. David Politzer. "Reliable Perturbative Results for Strong Interactions?" In: *Phys. Rev. Lett.* 30 (26 June 1973), pp. 1346–1349. DOI: 10.1103/PhysRevLett.30.1346. URL: https://link.aps.org/doi/10.1103/PhysRevLett.30.1346.

[20] G. Danby et al. "Observation of High-Energy Neutrino Reactions and the Existence of Two Kinds of Neutrinos". In: *Phys. Rev. Lett.* 9 (1962), pp. 36–44. DOI: 10.1103/PhysRevLett.9.36.

[21] M. L. Perl et al. "Evidence for Anomalous Lepton Production in $e^+ - e^-$ Annihilation". In: *Phys. Rev. Lett.* 35 (22 Dec. 1975), pp. 1489–1492. DOI: 10.1103/PhysRevLett.35.1489. URL: https://link.aps.org/doi/10.1103/PhysRevLett.35.1489.

[22] S. Schael et al. "Precision electroweak measurements on the Z resonance". In: *Phys. Rept.* 427 (2006), pp. 257–454. DOI: 10.1016/j.physrep.2005.12.006. arXiv: hep-ex/0509008 [hep-ex].

[23] K. Kodama et al. "Observation of tau neutrino interactions". In: *Phys. Lett.* B504 (2001), pp. 218–224. DOI: 10.1016/S0370-2693(01)00307-0. arXiv: hep-ex/0012035 [hep-ex].

[24] Georges Aad et al. "Observation of a new particle in the search for the Standard Model Higgs boson with the ATLAS detector at the LHC". In: *Phys. Lett.* B716 (2012), pp. 1–29. DOI: 10.1016/j.physletb.2012.08.020. arXiv: 1207.7214 [hep-ex].

[25] Nicola Cabibbo. "Unitary Symmetry and Leptonic Decays". In: *Phys. Rev. Lett.* 10 (12 June 1963), pp. 531–533. DOI: 10.1103/PhysRevLett.10.531. URL: https://link.aps.org/doi/10.1103/PhysRevLett.10.531.

[26] Makoto Kobayashi and Toshihide Maskawa. "CP Violation in the Renormalizable Theory of Weak Interaction". In: *Prog. Theor. Phys.* 49 (1973), pp. 652–657. DOI: 10.1143/PTP.49.652.

[27] M. Tanabashi et al. "Review of Particle Physics". In: *Phys. Rev. D* 98 (3 Aug. 2018), p. 030001. DOI: 10.1103/PhysRevD.98.030001. URL: https://link.aps.org/doi/10.1103/PhysRevD.98.030001.

[28] Steven Weinberg. "Baryon- and Lepton-Nonconserving Processes". In: *Phys. Rev. Lett.* 43 (21 Nov. 1979), pp. 1566–1570. DOI: 10.1103/PhysRevLett.43.1566. URL: https://link.aps.org/doi/10.1103/PhysRevLett.43.1566.

[29] B. Grzadkowski et al. "Dimension-Six Terms in the Standard Model Lagrangian". In: *JHEP* 10 (2010), p. 085. DOI: 10.1007/JHEP10(2010)085. arXiv: 1008.4884 [hep-ph].

[30] Yi Liao and Xiao-Dong Ma. *Renormalization Group Evolution of Dimension-seven Baryon- and Lepton-number-violating Operators*. 2016. arXiv: 1607.07309 [hep-ph].

[31] Landon Lehman and Adam Martin. "Hilbert Series for Constructing Lagrangians: expanding the phenomenologist's toolbox". In: *Phys. Rev.* D91 (2015), p. 105014. DOI: 10.1103/PhysRevD.91.105014. arXiv: 1503.07537 [hep-ph].

[32] Brian Henning et al. "Hilbert series and operator bases with derivatives in effective field theories". In: *Commun. Math. Phys.* 347.2 (2016), pp. 363–388. DOI: 10.1007/s00220-015-2518-2. arXiv: 1507.07240 [hep-th].

[33] Landon Lehman and Adam Martin. "Low-derivative operators of the Standard Model effective field theory via Hilbert series methods". In: *JHEP* 02 (2016), p. 081. DOI: 10.1007/JHEP02(2016)081. arXiv: 1510.00372 [hep-ph].

[34] Brian Henning et al. "2, 84, 30, 993, 560, 15456, 11962, 261485, ...: Higher dimension operators in the SMEFT". In: *JHEP* 08 (2017). [Erratum: JHEP09,019(2019)], p. 016. DOI: 10.1007/JHEP09(2019)019, 10.1007/JHEP08(2017)016. arXiv: 1512.03433 [hep-ph].

[35] K. Abe et al. "Solar neutrino results in Super-Kamiokande-III". In: *Phys. Rev.* D83 (2011), p. 052010. DOI: 10.1103/PhysRevD.83.052010. arXiv: 1010.0118 [hep-ex].

[36] K. Abe et al. "Atmospheric neutrino oscillation analysis with external constraints in Super-Kamiokande I-IV". In: *Phys. Rev.* D97.7 (2018), p. 072001. DOI: 10.1103/PhysRevD.97.072001. arXiv: 1710.09126 [hep-ex].

[37] M. G. Aartsen et al. "Determining neutrino oscillation parameters from atmospheric muon neutrino disappearance with three years of IceCube DeepCore data". In: *Phys. Rev.* D91.7 (2015), p. 072004. DOI: 10.1103/PhysRevD.91.072004. arXiv: 1410.7227 [hep-ex].

[38] D. Adey et al. "Measurement of the Electron Antineutrino Oscillation with 1958 Days of Operation at Daya Bay". In: *Phys. Rev. Lett.* 121.24 (2018), p. 241805. DOI: 10.1103/PhysRevLett.121.241805. arXiv: 1809.02261 [hep-ex].

[39] G. Bak et al. "Measurement of Reactor Antineutrino Oscillation Amplitude and Frequency at RENO". In: *Phys. Rev. Lett.* 121.20 (2018), p. 201801. DOI: 10.1103/PhysRevLett.121.201801. arXiv: 1806.00248 [hep-ex].

[40] Y. Abe et al. "Improved measurements of the neutrino mixing angle θ_{13} with the Double Chooz detector". In: *JHEP* 10 (2014). [Erratum: JHEP02,074(2015)], p. 086. DOI: 10.1007/JHEP02(2015)074, 10.1007/JHEP10(2014)086. arXiv: 1406.7763 [hep-ex].

[41] K. Abe et al. "Measurement of neutrino and antineutrino oscillations by the T2K experiment including a new additional sample of ν_e interactions at the far detector". In: *Phys. Rev.* D96.9 (2017). [Erratum: Phys. Rev.D98,no.1,019902(2018)], p. 092006. DOI: 10.1103/PhysRevD.96.092006,10.1103/PhysRevD.98.019902. arXiv: 1707.01048 [hep-ex].

[42] P. Adamson et al. “Measurement of Neutrino and Antineutrino Oscillations Using Beam and Atmospheric Data in MINOS”. In: *Phys. Rev. Lett.* 110.25 (2013), p. 251801. DOI: 10.1103/PhysRevLett.110.251801. arXiv: 1304.6335 [hep-ex].

[43] M. A. Acero et al. “New constraints on oscillation parameters from ν_e appearance and ν_μ disappearance in the NOvA experiment”. In: *Phys. Rev.* D98 (2018), p. 032012. DOI: 10.1103/PhysRevD.98.032012. arXiv: 1806.00096 [hep-ex].

[44] Valencia-Globalfit. http://globalfit.astroparticles.es/. 2018.

[45] Tsutomu Yanagida. “Horizontal gauge symmetry and masses of neutrinos”. In: *Conf. Proc. C* 7902131 (1979). Ed. by Osamu Sawada and Akio Sugamoto, pp. 95–99.

[46] Murray Gell-Mann, Pierre Ramond, and Richard Slansky. “Complex Spinors and Unified Theories”. In: *Conf. Proc. C* 790927 (1979), pp. 315–321. arXiv: 1306.4669 [hep-th].

[47] Rabindra N. Mohapatra and Goran Senjanovic. “Neutrino Mass and Spontaneous Parity Nonconservation”. In: *Phys. Rev. Lett.* 44 (1980), p. 912. DOI: 10.1103/PhysRevLett.44.912.

[48] Carlo Giunti and T. Lasserre. “eV-scale Sterile Neutrinos”. In: *Ann. Rev. Nucl. Part. Sci.* 69 (2019), pp. 163–190. DOI: 10.1146/annurev-nucl-101918-023755. arXiv: 1901.08330 [hep-ph].

[49] A. Diaz et al. *Where Are We With Light Sterile Neutrinos?* 2019. arXiv: 1906.00045 [hep-ex].

[50] J. Schechter and J.W.F. Valle. “Neutrino Masses in SU(2) x U(1) Theories”. In: *Phys. Rev. D* 22 (1980), p. 2227. DOI: 10.1103/PhysRevD.22.2227.

[51] J. Schechter and J. W. F. Valle. “Neutrino decay and spontaneous violation of lepton number”. In: *Phys. Rev. D* 25 (3 Feb. 1982), pp. 774–783. DOI: 10.1103/PhysRevD.25.774. URL: https://link.aps.org/doi/10.1103/PhysRevD.25.774.

[52] George Lazarides, Q. Shafi, and C. Wetterich. “Proton Lifetime and Fermion Masses in an SO(10) Model”. In: *Nucl. Phys. B* 181 (1981), pp. 287–300. DOI: 10.1016/0550-3213(81)90354-0.

[53] Rabindra N. Mohapatra and Goran Senjanovi ć. “Neutrino masses and mixings in gauge models with spontaneous parity violation”. In: *Phys. Rev. D* 23 (1 Jan. 1981), pp. 165–180. DOI: 10.1103/PhysRevD.23.165. URL: https://link.aps.org/doi/10.1103/PhysRevD.23.165.

[54] C. Wetterich. "Neutrino Masses and the Scale of B-L Violation". In: *Nucl. Phys. B* 187 (1981), pp. 343–375. DOI: 10.1016/0550-3213(81)90279-0.

[55] J. Schechter and J. W. F. Valle. "Neutrinoless Double beta Decay in SU(2) x U(1) Theories". In: *Phys. Rev. D* 25 (11 June 1982), pp. 2951–2954. DOI: 10.1103/PhysRevD.25.2951. URL: https://link.aps.org/doi/10.1103/PhysRevD.25.2951.

[56] Thomas Schwetz, Mariam Tortola, and J. W. F. Valle. "Where we are on θ_{13}: addendum to 'Global neutrino data and recent reactor fluxes: status of three-flavour oscillation parameters'". In: *New J. Phys.* 13 (2011), p. 109401. DOI: 10.1088/1367-2630/13/10/109401. arXiv: 1108.1376 [hep-ph].

[57] K. Abe et al. *Constraint on the Matter-Antimatter Symmetry-Violating Phase in Neutrino Oscillations*. 2019. arXiv: 1910.03887 [hep-ex].

[58] Andre de Gouvea, Boris Kayser, and Rabindra N. Mohapatra. "Manifest CP Violation from Majorana Phases". In: *Phys. Rev.* D67 (2003), p. 053004. DOI: 10.1103/PhysRevD.67.053004. arXiv: hep-ph/0211394 [hep-ph].

[59] Guido Altarelli and Ferruccio Feruglio. "Discrete Flavor Symmetries and Models of Neutrino Mixing". In: *Rev. Mod. Phys.* 82 (2010), pp. 2701–2729. DOI: 10.1103/RevModPhys.82.2701. arXiv: 1002.0211 [hep-ph].

[60] Hajime Ishimori et al. "Non-Abelian Discrete Symmetries in Particle Physics". In: *Prog. Theor. Phys. Suppl.* 183 (2010), pp. 1–163. DOI: 10.1143/PTPS.183.1. arXiv: 1003.3552 [hep-th].

[61] Zhi-zhong Xing and Zhen-hua Zhao. "A review of - flavor symmetry in neutrino physics". In: *Rept. Prog. Phys.* 79.7 (2016), p. 076201. DOI: 10.1088/0034-4885/79/7/076201. arXiv: 1512.04207 [hep-ph].

[62] Shivani Gupta, Anjan S. Joshipura, and Ketan M. Patel. "How good is μ-τ symmetry after results on non-zero θ_{13}?" In: *JHEP* 09 (2013), p. 035. DOI: 10.1007/JHEP09(2013)035. arXiv: 1301.7130 [hep-ph].

[63] Zhen-hua Zhao. "Breakings of the neutrino $\mu - \tau$ reflection symmetry". In: *JHEP* 09 (2017), p. 023. DOI: 10.1007/JHEP09(2017)023. arXiv: 1703.04984 [hep-ph].

[64] Paul H. Frampton, Sheldon L. Glashow, and Danny Marfatia. "Zeroes of the neutrino mass matrix". In: *Phys. Lett.* B536 (2002), pp. 79–82. DOI: 10.1016/S0370-2693(02)01817-8. arXiv: hep-ph/0201008 [hep-ph].

[65] Walter Grimus et al. "Symmetry realization of texture zeros". In: *Eur. Phys. J.* C36 (2004), pp. 227–232. DOI: 10.1140/epjc/s2004-01896-y. arXiv: hep-ph/0405016 [hep-ph].

[66] Walter Grimus and Luis Lavoura. "On a model with two zeros in the neutrino mass matrix". In: *J. Phys.* G31.7 (2005), pp. 693–702. DOI: 10.1088/0954-3899/31/7/014. arXiv: hep-ph/0412283 [hep-ph].

[67] R. González Felipe and H. Serôdio. "Abelian realization of phenomenological two-zero neutrino textures". In: *Nucl. Phys.* B886 (2014), pp. 75–92. DOI: 10.1016/j.nuclphysb.2014.06.015. arXiv: 1405.4263 [hep-ph].

[68] W. Rodejohann and Michael A. Schmidt. "Flavor symmetry L(mu) - L(tau) and quasi-degenerate neutrinos". In: *Phys. Atom. Nucl.* 69 (2006), pp. 1833–1841. DOI: 10.1134/S1063778806110056. arXiv: hep-ph/0507300 [hep-ph].

[69] M. Hirsch et al. "Predictive flavour symmetries of the neutrino mass matrix". In: *Phys. Rev. Lett.* 99 (2007), p. 151802. DOI: 10.1103/PhysRevLett.99.151802. arXiv: hep-ph/0703046 [HEP-PH].

[70] Shun Zhou. "Update on two-zero textures of the Majorana neutrino mass matrix in light of recent T2K, Super-Kamiokande and NOνA results". In: *Chin. Phys.* C40.3 (2016), p. 033102. DOI: 10.1088/1674-1137/40/3/033102. arXiv: 1509.05300 [hep-ph].

[71] Di Zhang. "A modular A_4 symmetry realization of two-zero textures of the Majorana neutrino mass matrix". In: *Nucl. Phys.* B952 (2020), p. 114935. DOI: 10.1016/j.nuclphysb.2020.114935. arXiv: 1910.07869 [hep-ph].

[72] Satoru Kaneko et al. *New Approach to Texture-zeros with S_3 symmetry - Flavor Symmetry and Vacuum Aligned Mass Textures* -. 2007. arXiv: hep-ph/0703250 [hep-ph].

[73] E. I. Lashin and N. Chamoun. "The One-zero Textures of Majorana Neutrino Mass Matrix and Current Experimental Tests". In: *Phys. Rev.* D85 (2012), p. 113011. DOI: 10.1103/PhysRevD.85.113011. arXiv: 1108.4010 [hep-ph].

[74] K. N. Deepthi, Srinu Gollu, and R. Mohanta. "Neutrino mixing matrices with relatively large θ_{13} and with texture one-zero". In: *Eur. Phys. J.* C72 (2012), p. 1888. DOI: 10.1140/epjc/s10052-012-1888-2. arXiv: 1111.2781 [hep-ph].

[75] Deirdre Black et al. "Complementary Ansatz for the neutrino mass matrix". In: *Phys. Rev.* D62 (2000), p. 073015. DOI: 10.1103/PhysRevD.62.073015. arXiv: hep-ph/0004105 [hep-ph].

[76] Madan Singh. "The Texture One Zero Neutrino Mass Matrix With Vanishing Trace". In: *Adv. High Energy Phys.* 2018 (2018), p. 2863184. DOI: 10.1155/2018/2863184. arXiv: 1803.10735 [hep-ph].

[77] G. C. Branco et al. "Removing ambiguities in the neutrino mass matrix". In: *Phys. Lett.* B562 (2003), pp. 265–272. DOI: 10.1016/S0370-2693(03)00572-0. arXiv: hep-ph/0212341 [hep-ph].

[78] Harald Fritzsch, Zhi-zhong Xing, and Shun Zhou. "Two-zero Textures of the Majorana Neutrino Mass Matrix and Current Experimental Tests". In: *JHEP* 09 (2011), p. 083. DOI: 10.1007/JHEP09(2011)083. arXiv: 1108.4534 [hep-ph].

[79] Amol Dighe and Narendra Sahu. *Texture zeroes and discrete flavor symmetries in light and heavy Majorana neutrino mass matrices: a bottom-up approach*. 2008. arXiv: 0812.0695 [hep-ph].

[80] nufit. www.nu-fit.org. 2019.

[81] Ivan Esteban et al. "Global analysis of three-flavour neutrino oscillations: synergies and tensions in the determination of θ_{23}, δ_{CP}, and the mass ordering". In: *JHEP* 01 (2019), p. 106. DOI: 10.1007/JHEP01(2019)106. arXiv: 1811.05487 [hep-ph].

[82] K. Abe et al. "Atmospheric neutrino oscillation analysis with external constraints in Super-Kamiokande I-IV". In: *Physical Review D* 97.7 (Apr. 2018). ISSN: 2470-0029. DOI: 10.1103/physrevd.97.072001. URL: http://dx.doi.org/10.1103/PhysRevD.97.072001.

[83] Julien Alcaide, Jordi Salvado, and Arcadi Santamaria. "Fitting flavour symmetries: the case of two-zero neutrino mass textures". In: *JHEP* 07 (2018), p. 164. DOI: 10.1007/JHEP07(2018)164. arXiv: 1806.06785 [hep-ph].

[84] F. Feroz, M. P. Hobson, and M. Bridges. "MultiNest: an efficient and robust Bayesian inference tool for cosmology and particle physics". In: *Mon. Not. Roy. Astron. Soc.* 398 (2009), pp. 1601–1614. DOI: 10.1111/j.1365-2966.2009.14548.x. arXiv: 0809.3437 [astro-ph].

[85] F. Feroz et al. "Importance Nested Sampling and the MultiNest Algorithm". In: (2013). DOI: 10.21105/astro.1306.2144. arXiv: 1306.2144 [astro-ph.IM].

[86] A. Gando et al. "Search for Majorana Neutrinos near the Inverted Mass Hierarchy Region with KamLAND-Zen". In: *Phys. Rev. Lett.* 117.8 (2016). [Addendum: Phys. Rev. Lett.117,no.10,109903(2016)], p. 082503. DOI: 10.1103/PhysRevLett.117.109903, 10.1103/PhysRevLett.117.082503. arXiv: 1605.02889 [hep-ex].

[87] Ivan Esteban et al. “Updated fit to three neutrino mixing: exploring the accelerator-reactor complementarity”. In: *JHEP* 01 (2017), p. 087. DOI: 10.1007/JHEP01(2017)087. arXiv: 1611.01514 [hep-ph].

[88] Sunny Vagnozzi et al. “Unveiling ν secrets with cosmological data: neutrino masses and mass hierarchy”. In: *Phys. Rev.* D96.12 (2017), p. 123503. DOI: 10.1103/PhysRevD.96.123503. arXiv: 1701.08172 [astro-ph.CO].

[89] Claudia Hagedorn, Jörn Kersten, and Manfred Lindner. “Stability of texture zeros under radiative corrections in see-saw models”. In: *Phys. Lett.* B597 (2004), pp. 63–72. DOI: 10.1016/j.physletb.2004.06.094. arXiv: hep-ph/0406103 [hep-ph].

[90] M. Goeppert-Mayer. “Double Beta-Disintegration”. In: *Phys. Rev.* 48 (6 Sept. 1935), pp. 512–516. DOI: 10.1103/PhysRev.48.512. URL: https://link.aps.org/doi/10.1103/PhysRev.48.512.

[91] H. V. Klapdor-Kleingrothaus. “Double beta decay and neutrino mass: The Heidelberg-Moscow experiment”. In: *Prog. Part. Nucl. Phys.* 32 (1994), pp. 261–280. DOI: 10.1016/0146-6410(94)90024-8.

[92] Stefan. Schonert et al. “The GERmanium Detector Array (GERDA) for the search of neutrinoless beta beta decays of Ge-76 at LNGS”. In: *Nucl. Phys. Proc. Suppl.* 145 (2005). [,242(2005)], pp. 242–245. DOI: 10.1016/j.nuclphysbps.2005.04.014.

[93] M. Auger et al. “The EXO-200 detector, part I: Detector design and construction”. In: *JINST* 7 (2012), P05010. DOI: 10.1088/1748-0221/7/05/P05010. arXiv: 1202.2192 [physics.ins-det].

[94] A. Piepke. “KamLAND: A reactor neutrino experiment testing the solar neutrino anomaly”. In: *Nucl. Phys. Proc. Suppl.* 91 (2001). [,99(2001)], pp. 99–104. DOI: 10.1016/S0920-5632(00)00928-2.

[95] F. Granena et al. “NEXT, a HPGXe TPC for neutrinoless double beta decay searches”. In: (2009). arXiv: 0907.4054 [hep-ex].

[96] Francisco del Aguila et al. “Effective Lagrangian approach to neutrinoless double beta decay and neutrino masses”. In: *JHEP* 06 (2012), p. 146. DOI: 10.1007/JHEP06(2012)146. arXiv: 1204.5986 [hep-ph].

[97] Julien Alcaide, Dipankar Das, and Arcadi Santamaria. “A model of neutrino mass and dark matter with large neutrinoless double beta decay”. In: *JHEP* 04 (2017), p. 049. DOI: 10.1007/JHEP04(2017)049. arXiv: 1701.01402 [hep-ph].

[98] Mattias Blennow et al. “Neutrinoless double beta decay in seesaw models”. In: *JHEP* 07 (2010), p. 096. DOI: 10.1007/JHEP07(2010)096. arXiv: 1005.3240 [hep-ph].

[99] Frank F. Deppisch, Martin Hirsch, and Heinrich Pas. “Neutrinoless Double Beta Decay and Physics Beyond the Standard Model”. In: *J. Phys.* G39 (2012), p. 124007. DOI: 10.1088/0954-3899/39/12/124007. arXiv: 1208.0727 [hep-ph].

[100] J. Suhonen and O. Civitarese. “Weak-interaction and nuclear-structure aspects of nuclear double beta decay”. In: *Phys. Rept.* 300 (1998), pp. 123–214. DOI: 10.1016/S0370-1573(97)00087-2.

[101] A. S. Barabash. “Double beta decay experiments”. In: *Phys. Part. Nucl.* 42 (2011), pp. 613–627. DOI: 10.1134/S1063779611040022. arXiv: 1107.5663 [nucl-ex].

[102] Michael E. Peskin and Tatsu Takeuchi. “New constraint on a strongly interacting Higgs sector”. In: *Phys. Rev. Lett.* 65 (8 Aug. 1990), pp. 964–967. DOI: 10.1103/PhysRevLett.65.964. URL: https://link.aps.org/doi/10.1103/PhysRevLett.65.964.

[103] Michael E. Peskin and Tatsu Takeuchi. “Estimation of oblique electroweak corrections”. In: *Phys. Rev. D* 46 (1 July 1992), pp. 381–409. DOI: 10.1103/PhysRevD.46.381. URL: https://link.aps.org/doi/10.1103/PhysRevD.46.381.

[104] Max Baak and Roman Kogler. “The global electroweak Standard Model fit after the Higgs discovery”. In: *Proceedings, 48th Rencontres de Moriond on Electroweak Interactions and Unified Theories: La Thuile, Italy, March 2-9, 2013*. [,45(2013)]. 2013, pp. 349–358. arXiv: 1306.0571 [hep-ph].

[105] Juan Herrero-Garcia et al. “The Zee–Babu model revisited in the light of new data”. In: *Nucl. Phys.* B885 (2014), pp. 542–570. DOI: 10.1016/j.nuclphysb.2014.06.001. arXiv: 1402.4491 [hep-ph].

[106] C Patrignani et al. “Review of Particle Physics, 2016-2017”. In: *Chin. Phys. C* 40.10 (2016), 100001. 1808 p. DOI: 10.1088/1674-1137/40/10/100001. URL: http://cds.cern.ch/record/2241948.

[107] J. Adam et al. “New constraint on the existence of the $\mu^+ \to e^+\gamma$ decay”. In: *Phys. Rev. Lett.* 110 (2013), p. 201801. DOI: 10.1103/PhysRevLett.110.201801. arXiv: 1303.0754 [hep-ex].

[108] P. A. R. Ade et al. “Planck 2013 results. XVI. Cosmological parameters”. In: *Astron. Astrophys.* 571 (2014), A16. DOI: 10.1051/0004-6361/201321591. arXiv: 1303.5076 [astro-ph.CO].

[109] Andi Tan et al. “Dark Matter Results from First 98.7 Days of Data from the PandaX-II Experiment”. In: *Phys. Rev. Lett.* 117.12 (2016), p. 121303. DOI: 10.1103/PhysRevLett.117.121303. arXiv: 1607.07400 [hep-ex].

[110] E. Aprile et al. “First Dark Matter Search Results from the XENON1T Experiment”. In: *Phys. Rev. Lett.* 119.18 (2017), p. 181301. DOI: 10.1103/PhysRevLett.119.181301. arXiv: 1705.06655 [astro-ph.CO].

[111] E. Aprile et al. “Physics reach of the XENON1T dark matter experiment”. In: *JCAP* 1604.04 (2016), p. 027. DOI: 10.1088/1475-7516/2016/04/027. arXiv: 1512.07501 [physics.ins-det].

[112] Huayong Han and Sibo Zheng. “New Constraints on Higgs-portal Scalar Dark Matter”. In: *JHEP* 12 (2015), p. 044. DOI: 10.1007/JHEP12(2015)044. arXiv: 1509.01765 [hep-ph].

[113] Miguel Escudero et al. “Toward (Finally!) Ruling Out Z and Higgs Mediated Dark Matter Models”. In: *JCAP* 1612 (2016), p. 029. DOI: 10.1088/1475-7516/2016/12/029. arXiv: 1609.09079 [hep-ph].

[114] G. Belanger et al. “micrOMEGAs 3: A program for calculating dark matter observables”. In: *Comput. Phys. Commun.* 185 (2014), pp. 960–985. DOI: 10.1016/j.cpc.2013.10.016. arXiv: 1305.0237 [hep-ph].

[115] Georges Aad et al. “Search for doubly-charged Higgs bosons in like-sign dilepton final states at $\sqrt{s} = 7$ TeV with the ATLAS detector”. In: *Eur. Phys. J.* C72 (2012), p. 2244. DOI: 10.1140/epjc/s10052-012-2244-2. arXiv: 1210.5070 [hep-ex].

[116] A. Zee. “A Theory of Lepton Number Violation, Neutrino Majorana Mass, and Oscillation”. In: *Phys. Lett.* 93B (1980). [Erratum: Phys. Lett.95B,461(1980)], p. 389. DOI: 10.1016/0370-2693(80)90349-4, 10.1016/0370-2693(80)90193-8.

[117] Madan Singh, Gulsheen Ahuja, and Manmohan Gupta. “Revisiting the texture zero neutrino mass matrices”. In: *PTEP* 2016.12 (2016), 123B08. DOI: 10.1093/ptep/ptw180. arXiv: 1603.08083 [hep-ph].

[118] A. Zee. “Quantum Numbers of Majorana Neutrino Masses”. In: *Nucl. Phys.* B264 (1986), pp. 99–110. DOI: 10.1016/0550-3213(86)90475-X.

[119] K. S. Babu. “Model of ’Calculable’ Majorana Neutrino Masses”. In: *Phys. Lett.* B203 (1988), pp. 132–136. DOI: 10.1016/0370-2693(88)91584-5.

[120] Celine Degrande et al. "UFO - The Universal FeynRules Output". In: *Comput. Phys. Commun.* 183 (2012), pp. 1201–1214. DOI: 10.1016/j.cpc.2012.01.022. arXiv: 1108.2040 [hep-ph].

[121] J. Alwall et al. "The automated computation of tree-level and next-to-leading order differential cross sections, and their matching to parton shower simulations". In: *JHEP* 07 (2014), p. 079. DOI: 10.1007/JHEP07(2014)079. arXiv: 1405.0301 [hep-ph].

[122] Torbjörn Sjöstrand, Leif Lönnblad, and Stephen Mrenna. *PYTHIA 6.2 Physics and Manual*. 2001. arXiv: hep-ph/0108264 [hep-ph].

[123] Torbjörn Sjöstrand et al. "An Introduction to PYTHIA 8.2". In: *Comput. Phys. Commun.* 191 (2015), pp. 159–177. DOI: 10.1016/j.cpc.2015.01.024. arXiv: 1410.3012 [hep-ph].

[124] Eric Conte, Benjamin Fuks, and Guillaume Serret. "MadAnalysis 5, A User-Friendly Framework for Collider Phenomenology". In: *Comput. Phys. Commun.* 184 (2013), pp. 222–256. DOI: 10.1016/j.cpc.2012.09.009. arXiv: 1206.1599 [hep-ph].

[125] Julien Alcaide, Mikael Chala, and Arcadi Santamaria. "LHC signals of radiatively-induced neutrino masses and implications for the Zee–Babu model". In: *Phys. Lett.* B779 (2018), pp. 107–116. DOI: 10.1016/j.physletb.2018.02.001. arXiv: 1710.05885 [hep-ph].

[126] Georges Aad et al. "Search for new phenomena in events with three charged leptons at $\sqrt{s} = 7$ TeV with the ATLAS detector". In: *Phys. Rev.* D87.5 (2013), p. 052002. DOI: 10.1103/PhysRevD.87.052002. arXiv: 1211.6312 [hep-ex].

[127] Georges Aad et al. "Search for anomalous production of prompt same-sign lepton pairs and pair-produced doubly charged Higgs bosons with $\sqrt{s} = 8$ TeV pp collisions using the ATLAS detector". In: *JHEP* 03 (2015), p. 041. DOI: 10.1007/JHEP03(2015)041. arXiv: 1412.0237 [hep-ex].

[128] *Search for doubly-charged Higgs bosons in same-charge electron pair final states using proton-proton collisions at* $\sqrt{s} = 13\,\text{TeV}$ *with the ATLAS detector*. Tech. rep. ATLAS-CONF-2016-051. Geneva: CERN, Aug. 2016. URL: https://cds.cern.ch/record/2206133.

[129] *A search for doubly-charged Higgs boson production in three and four lepton final states at* $\sqrt{s} = 13$ TeV. Tech. rep. CMS-PAS-HIG-16-036. Geneva: CERN, 2017. URL: https://cds.cern.ch/record/2242956.

[130] Matteo Cacciari, Gavin P. Salam, and Gregory Soyez. "The anti-k_t jet clustering algorithm". In: *JHEP* 04 (2008), p. 063. DOI: 10.1088/1126-6708/2008/04/063. arXiv: 0802.1189 [hep-ph].

[131] A L Read. "Modified frequentist analysis of search results (the CL_s method)". In: CERN-OPEN-2000-205 (2000). DOI: 10.5170/CERN-2000-005.81. URL: http://cds.cern.ch/record/451614.

[132] R. Brun and F. Rademakers. "ROOT: An object oriented data analysis framework". In: *Nucl. Instrum. Meth.* A389 (1997), pp. 81–86. DOI: 10.1016/S0168-9002(97)00048-X.

[133] Julien Alcaide and Nicolás I. Mileo. "LHC sensitivity to singly-charged scalars decaying into electrons and muons". In: (2019). arXiv: 1906.08685 [hep-ph].

[134] A. M. Baldini et al. "Search for the lepton flavour violating decay $\mu^+ \to e^+\gamma$ with the full dataset of the MEG experiment". In: *Eur. Phys. J.* C76.8 (2016), p. 434. DOI: 10.1140/epjc/s10052-016-4271-x. arXiv: 1605.05081 [hep-ex].

[135] Bernard Aubert et al. "Searches for Lepton Flavor Violation in the Decays $\tau^\pm \to e^\pm\gamma$ and $\tau^\pm \to \mu^\pm\gamma$". In: *Phys. Rev. Lett.* 104 (2010), p. 021802. DOI: 10.1103/PhysRevLett.104.021802. arXiv: 0908.2381 [hep-ex].

[136] Qing-Hong Cao et al. "Searching for Weak Singlet Charged Scalar at the Large Hadron Collider". In: *Phys. Rev.* D97.11 (2018), p. 115036. DOI: 10.1103/PhysRevD.97.115036. arXiv: 1711.02113 [hep-ph].

[137] J. de Favereau et al. "DELPHES 3, A modular framework for fast simulation of a generic collider experiment". In: *JHEP* 02 (2014), p. 057. DOI: 10.1007/JHEP02(2014)057. arXiv: 1307.6346 [hep-ex].

[138] Adam Alloul et al. "FeynRules 2.0 - A complete toolbox for tree-level phenomenology". In: *Comput. Phys. Commun.* 185 (2014), pp. 2250–2300. DOI: 10.1016/j.cpc.2014.04.012. arXiv: 1310.1921 [hep-ph].

[139] Massimiliano Grazzini et al. "W^+W^- production at the LHC: fiducial cross sections and distributions in NNLO QCD". In: *JHEP* 08 (2016), p. 140. DOI: 10.1007/JHEP08(2016)140. arXiv: 1605.02716 [hep-ph].

[140] Fabrizio Caola et al. "QCD corrections to W^+W^- production through gluon fusion". In: *Phys. Lett.* B754 (2016), pp. 275–280. DOI: 10.1016/j.physletb.2016.01.046. arXiv: 1511.08617 [hep-ph].

[141] Georges Aad et al. "Measurement of the ZZ Production Cross Section in pp Collisions at $\sqrt{s} = 13$ TeV with the ATLAS Detector". In: *Phys. Rev. Lett.* 116.10 (2016), p. 101801. DOI: 10.1103/PhysRevLett.116.101801. arXiv: 1512.05314 [hep-ex].

[142] Massimiliano Grazzini et al. "$W^{\pm}Z$ production at hadron colliders in NNLO QCD". In: *Phys. Lett.* B761 (2016), pp. 179–183. DOI: 10.1016/j.physletb.2016.08.017. arXiv: 1604.08576 [hep-ph].

[143] Radja Boughezal et al. "Color singlet production at NNLO in MCFM". In: *Eur. Phys. J.* C77.1 (2017), p. 7. DOI: 10.1140/epjc/s10052-016-4558-y. arXiv: 1605.08011 [hep-ph].

[144] Valentin Ahrens et al. "Precision predictions for the $t\bar{t}$ production cross section at hadron colliders". In: *Phys. Lett.* B703 (2011), pp. 135–141. DOI: 10.1016/j.physletb.2011.07.058. arXiv: 1105.5824 [hep-ph].

[145] Michał Czakon, Paul Fiedler, and Alexander Mitov. "Total Top-Quark Pair-Production Cross Section at Hadron Colliders Through $O(\alpha_S^4)$". In: *Phys. Rev. Lett.* 110 (2013), p. 252004. DOI: 10.1103/PhysRevLett.110.252004. arXiv: 1303.6254 [hep-ph].

[146] Qing-Hong Cao. "Demonstration of One Cutoff Phase Space Slicing Method: Next-to-Leading Order QCD Corrections to the tW Associated Production in Hadron Collision". In: (2008). arXiv: 0801.1539 [hep-ph].

[147] Stefano Frixione et al. "Single-top hadroproduction in association with a W boson". In: *JHEP* 07 (2008), p. 029. DOI: 10.1088/1126-6708/2008/07/029. arXiv: 0805.3067 [hep-ph].

[148] Nikolaos Kidonakis. "Theoretical results for electroweak-boson and single-top production". In: *PoS* DIS2015 (2015), p. 170. DOI: 10.22323/1.247.0170. arXiv: 1506.04072 [hep-ph].

[149] CMS Collaboration. *Search for pair production of tau sleptons in* $\sqrt{s} = 13$ TeV *pp collisions in the all-hadronic final state*. Tech. rep. CMS-PAS-SUS-17-003. 2017. URL: http://cds.cern.ch/record/2273395.

[150] Benjamin Fuks et al. "Revisiting slepton pair production at the Large Hadron Collider". In: *JHEP* 01 (2014), p. 168. DOI: 10.1007/JHEP01(2014)168. arXiv: 1310.2621.

[151] Torbjorn Sjostrand, Stephen Mrenna, and Peter Z. Skands. "PYTHIA 6.4 Physics and Manual". In: *JHEP* 05 (2006), p. 026. DOI: 10.1088/1126-6708/2006/05/026. arXiv: hep-ph/0603175 [hep-ph].

[152] W. Buchmuller and D. Wyler. "Effective Lagrangian Analysis of New Interactions and Flavor Conservation". In: *Nucl. Phys.* B268 (1986), pp. 621–653. DOI: 10.1016/0550-3213(86)90262-2.

[153] Francisco del Aguila et al. "Heavy Majorana Neutrinos in the Effective Lagrangian Description: Application to Hadron Colliders". In: *Phys. Lett.* B670 (2009), pp. 399–402. DOI: 10.1016/j.physletb.2008.11.031. arXiv: 0806.0876 [hep-ph].

[154] Alberto Aparici et al. "Right-handed neutrino magnetic moments". In: *Phys. Rev.* D80 (2009), p. 013010. DOI: 10.1103/PhysRevD.80.013010. arXiv: 0904.3244 [hep-ph].

[155] Yi Liao and Xiao-Dong Ma. "Operators up to Dimension Seven in Standard Model Effective Field Theory Extended with Sterile Neutrinos". In: *Phys. Rev.* D96.1 (2017), p. 015012. DOI: 10.1103/PhysRevD.96.015012. arXiv: 1612.04527 [hep-ph].

[156] Julien Alcaide et al. "Probes of the Standard Model effective field theory extended with a right-handed neutrino". In: *JHEP* 08 (2019), p. 031. DOI: 10.1007/JHEP08(2019)031. arXiv: 1905.11375 [hep-ph].

[157] B. C. Canas et al. "Updating neutrino magnetic moment constraints". In: *Phys. Lett.* B753 (2016). [Addendum: Phys. Lett.B757,568(2016)], pp. 191–198. DOI: 10.1016/j.physletb.2016.03.078,10.1016/j.physletb.2015.12.011. arXiv: 1510.01684 [hep-ph].

[158] O. G. Miranda et al. "Probing neutrino transition magnetic moments with coherent elastic neutrino-nucleus scattering". In: *JHEP* 07 (2019), p. 103. DOI: 10.1007/JHEP07(2019)103. arXiv: 1905.03750 [hep-ph].

[159] Lucia Duarte, Javier Peressutti, and Oscar A. Sampayo. "Majorana neutrino decay in an Effective Approach". In: *Phys. Rev.* D92.9 (2015), p. 093002. DOI: 10.1103/PhysRevD.92.093002. arXiv: 1508.01588 [hep-ph].

[160] Ryan Cooke et al. "Precision measures of the primordial abundance of deuterium". In: *Astrophys. J.* 781.1 (2014), p. 31. DOI: 10.1088/0004-637X/781/1/31. arXiv: 1308.3240 [astro-ph.CO].

[161] Planck Collaboration et al. *Planck 2018 results. VI. Cosmological parameters.* 2018. arXiv: 1807.06209 [astro-ph.CO].

[162] Miguel Escudero. "Neutrino decoupling beyond the Standard Model: CMB constraints on the Dark Matter mass with a fast and precise $N_{\rm eff}$ evaluation". In: *JCAP* 1902 (2019), p. 007. DOI: 10.1088/1475-7516/2019/02/007. arXiv: 1812.05605 [hep-ph].

[163] Juan C. Helo, Martin Hirsch, and Sergey Kovalenko. "Heavy neutrino searches at the LHC with displaced vertices". In: *Phys. Rev.* D89 (2014). [Erratum: Phys. Rev.D93,no.9,099902(2016)], p. 073005. DOI: 10.1103/PhysRevD.89.073005,10.1103/PhysRevD.93.099902. arXiv: 1312.2900 [hep-ph].

[164] Georges Aad et al. "Search for massive, long-lived particles using multitrack displaced vertices or displaced lepton pairs in pp collisions at $\sqrt{s} = 8$ TeV with the ATLAS detector". In: *Phys. Rev.* D92.7 (2015), p. 072004. DOI: 10.1103/PhysRevD.92.072004. arXiv: 1504.05162 [hep-ex].

[165] Matteo Cacciari, Gavin P. Salam, and Gregory Soyez. "FastJet User Manual". In: *Eur. Phys. J.* C72 (2012), p. 1896. DOI: 10.1140/epjc/s10052-012-1896-2. arXiv: 1111.6097 [hep-ph].

[166] Morad Aaboud et al. "Search for a new heavy gauge boson resonance decaying into a lepton and missing transverse momentum in 36 fb^{-1} of pp collisions at $\sqrt{s} = 13$ TeV with the ATLAS experiment". In: *Eur. Phys. J.* C78.5 (2018), p. 401. DOI: 10.1140/epjc/s10052-018-5877-y. arXiv: 1706.04786 [hep-ex].

[167] Albert M Sirunyan et al. "Search for a W' boson decaying to a τ lepton and a neutrino in proton-proton collisions at $\sqrt{s} = 13$ TeV". In: *Phys. Lett.* B792 (2019), pp. 107–131. DOI: 10.1016/j.physletb.2019.01.069. arXiv: 1807.11421 [hep-ex].

[168] A. M. Sirunyan et al. "Search for new physics in final states with an energetic jet or a hadronically decaying W or Z boson and transverse momentum imbalance at $\sqrt{s} = 13$ TeV". In: *Phys. Rev.* D97.9 (2018), p. 092005. DOI: 10.1103/PhysRevD.97.092005. arXiv: 1712.02345 [hep-ex].

[169] Richard D. Ball et al. "Parton distributions with LHC data". In: *Nucl. Phys.* B867 (2013), pp. 244–289. DOI: 10.1016/j.nuclphysb.2012.10.003. arXiv: 1207.1303 [hep-ph].

[170] Michal Czakon and Alexander Mitov. "Top++: A Program for the Calculation of the Top-Pair Cross-Section at Hadron Colliders". In: *Comput. Phys. Commun.* 185 (2014), p. 2930. DOI: 10.1016/j.cpc.2014.06.021. arXiv: 1112.5675 [hep-ph].

[171] A. Hoecker et al. *TMVA - Toolkit for Multivariate Data Analysis*. 2007. arXiv: physics/0703039 [physics.data-an].

[172] David Ciupke. "Study of BDT Training Configurations with an Application to the $Z/H \longrightarrow \tau\tau \longrightarrow ee$ Analysis". In: (2012).